

AB689 618

RRI

RIVERSIDE RESEARCH INSTITUTE

RECEIVED  
FEB 12 1968  
RIVERSIDE RESEARCH INSTITUTE

RECEIVED FEB 12 1968  
RIVERSIDE RESEARCH INSTITUTE

RECEIVED FEB 12 1968  
CLEARINGHOUSE  
FOR INFORMATION ON  
INFORMATION SECURITY

225

# **DISCLAIMER NOTICE**

**THIS DOCUMENT IS THE BEST  
QUALITY AVAILABLE.**

**COPY FURNISHED CONTAINED  
A SIGNIFICANT NUMBER OF  
PAGES WHICH DO NOT  
REPRODUCE LEGIBLY.**

# RIVERSIDE RESEARCH INSTITUTE

632 West 125th Street / New York, New York 10027 / 212 UUniversity 5-5000

October 15, 1968

POWER SPECTRAL MEASUREMENTS  
BY THE DIFFRACTION OF COHERENT LIGHT  
TECHNICAL REPORT T-1/006-1-00

By

H. Stark

Prepared for

Director  
Advanced Research Projects Agency  
Washington, D. C. 20301

Contract No. F19628-68-C-0084  
ARPA Order No. 1088

## ABSTRACT

The theory and technique of estimating power spectral densities by Fraunhofer diffraction are investigated analytically and experimentally. A technique for estimating the spectral density is developed by which the estimate is independent of changing light levels in the diffraction system. It is shown that the estimated spectrum is biased and in the case of a rectangular aperture, the error can be written in terms of the Hilbert transforms of the spectrum. The variability of the estimate is computed and the ratio of the variance to square mean is shown to approach unity for large apertures, indicating the need for smoothing by additional filtering. Reasonable bounds on the bandwidth of the scanning filter are established theoretically. The experimental results are found consistent with the theoretical evaluations.

Techniques for reducing the zero-order light level are investigated. It is found that the use of large, apodised apertures are useful in estimating the spectrum at low frequencies. The application of a half-wave phase grating for measuring the spectrum of grain-noise at DC is investigated theoretically and experimentally. A serious limitation to measuring the grain-noise at DC is the presence of residual phase noise.

The spectral densities of several common photographic films are experimentally determined and compared with models of grain-noise and total film-noise. It is found that a modified form of the overlapping circular grain model of film-grain noise furnishes an excellent fit to the measured spectra. The range of Silberstein's quantum theory of photographic exposure is experimentally explored. An analysis of grain-noise in the presence of signal indicates that film-noise cannot be regarded as additive or multiplicative.

## TABLE OF CONTENTS

	<u>Title</u>	<u>Page</u>
	<u>ABSTRACT</u>	iii
1.	<u>INTRODUCTION</u>	1
	1.1 General	1
	1.2 Investigations and Contributions	3
	1.3 Review of Film Noise-Measurements	9
2.	<u>BASIC RELATIONS</u>	17
	2.1 Complex Transmittance	17
	2.2 Spatial Random Processes	22
	2.3 Power Spectra	25
	2.4 Spectral Measurements by Diffraction	26
	2.5 Spectral Measurements of the Real Processes $\{t(x,y)\}$ and $\{\psi(x,y)\}$	36
3.	<u>MEASUREMENTS OF POWER SPECTRA WITH FINITE         SYSTEMS</u>	41
	3.1 Effect of a Finite Aperture; Astig- matic Systems	41
	3.2 Effect of a Finite Aperture; Ordinary Systems	46
	3.3 Two-Dimensional Hilbert Transforms	50
	3.4 The Bias Error in the Apparent Spec- trum, $\tilde{W}(u,v)$	53
	3.5 Spatial Filtering	56
	3.6 Effect of the Scanning Slit	61
4.	<u>FILM NOISE MODELS</u>	68
	4.1 General	68
	4.2 Models of Photographic Granularity	73
	4.3 Models for Total Film Noise	81
5.	<u>VARIANCE OF POWER SPECTRUM ESTIMATE</u>	89
	5.1 Formula for the Variance	89
	5.2 Derivation of Eq. (5.1-3)	90

TABLE OF CONTENTS (Cont'd.)

	<u>Title</u>	<u>Page</u>
6.	<u>EXPERIMENTAL TECHNIQUES AND APPARATUS</u>	100
6.1	Description of Measurement Equipment	100
6.2	Measurement Technique and Calibration	111
6.3	Determination of Film-Noise Parameters	120
6.4	Reduction of Zero-Order Sidelobes by Aperture Shaping	123
6.5	Use of Magnification in Power Spectra Measurements	129
7.	<u>EXPERIMENTAL RESULTS</u>	138
7.1	Reduction of Film Noise with a Liquid Gate	138
7.2	Experimental Determination of the Effects of the Aperture and Scanning Filter	139
7.3	Measurements of the Spectra of Film Grain Noise	150
7.4	Measurements of the Spectra of Total Noise	169
7.5	Spectra of Magnified Grain Noise and Frequency Response of Optical System	177
<u>APPENDIX A:</u> Film-Grain Noise in the Presence of Signal		184
<u>APPENDIX B:</u> Suppression of the Zero-Order Light at DC		190
<u>REFERENCES</u>		211

## LIST OF FIGURES

<u>Figure No.</u>	<u>Title</u>	<u>Page</u>
2.1-1	Illustrating the Complex Transmittance of an Object	19
2.1-2	The Domain of the Complex Transmittance $R(x,y)$	21
2.4-1	Coherent Optical System	27
2.4-2	Optical Systems for Measuring Power Spectra	30
2.4-3	Diagram for Evaluating the Integral in Eq. (2.4-14)	33
3.1-1	Effect of Finite Aperture on Covariance Estimate	47
3.2-1	Illustrating the Function $h(\alpha, \beta)$ of Eq. (3.2-3) for a Rectangular Aperture of Width $W$ and Length $L$	49
3.5-1	Spatial Filter Characteristics Required for Filtering Power Spectrum	60
3.5-2	Optical System for Spatial Filtering of the Measured Spectrum	62
3.6-1	Illustrating the Distorting Effect of a Scanning Slit on Two Different Spectra	65
4.1-1	Illustrating the Action of a Liquid Gate in Reducing Noise Due to Random Thickness Variations	69
4.1-2	Maximum Allowable Variation of Film Thickness (Rayleigh Limit Criterion)	71
4.2-1	Random Checkerboard Model of Film Grains	74

## LIST OF FIGURES (Cont'd.)

<u>Figure No.</u>	<u>Title</u>	<u>Page</u>
4.2-2	Theoretical Point Aperture Microdensitometer Trace of Random Checkerboard Model of Film Grains	76
4.2-3	Overlapping Circular-Grain Model of Photographic Film	79
4.2-4	Normalized Power Spectrum of Grain Noise as Computed for the Overlapping Circular-Grain Model	82
4.2-5	Variation of Power Spectrum at Zero Spatial Frequency with Average Amplitude Transmittance	83
5.2-1	Diagram Showing the Field of Integration for Eq. (5.2-10) with the Transformation of Eq. (5.2-11)	94
5.2-2	The Integrand of Eq. (5.2-18)	97
6.1-1	Schematic Diagram of Coherent Optical System	101
6.1-2	The Coherent Optical System Used in the Experiments	103
6.1-3	Filtering and Collimation of the Laser Beam	104
6.1-4	Spreader Lens Assembly	105
6.1-5	Gate and Collimated Region	107
6.1-6	Scanning - Mechanism Assembly	108
6.1-7	Schematic Representation of System for Measurement of Back-Focal Plane Light Intensity	109
6.1-8	Automatic Recording Microdensitometer	110

LIST OF FIGURES (Cont'd.)

<u>Figure No.</u>	<u>Title</u>	<u>Page</u>
6.1-9	Intensity Transmittance Measurements with a Microdensitometer	112
6.1-10	Microscope and Camera Assembly	113
6.2-1	Scattered-Light Level of Optical System	116
6.2-2	Illustrating Power Spectrum Measurement Technique	117
6.4-1	Envelope of Diffraction Patterns for 3 Apertures (Theoretical)	127
6.4-2	Gaussian Apertures for Sidelobe Suppression	128
6.5-1	The Effect of Linear Magnification	131
6.5-2	Normalized Frequency Responses for Systems Free of Geometrical Aberrations	135
6.5-3	Imaging of Granularity Through an Incoherent Optical System	136
7.1-1	Focal-Plane Light Intensity Distribution Along x' Axis for Clear System	140
7.1-2	Focal-Plane Light Intensity Distribution Along x' Axis When System is Loaded with Film Without Phase Compensation	141
7.1-3	Focal-Plane Light Intensity Distribution Along x' Axis When System is Loaded with Film with Partial Phase Compensation	142
7.1-4	Focal Plane Light Intensity Distribution Along x' Axis When System is Loaded with Film with Optimum Phase Compensation	143

LIST OF FIGURES (Cont'd.)

<u>Figure No.</u>	<u>Title</u>	<u>Page</u>
7.2-1	Effect of Aperture Shapes on the Measurement of the Power Spectrum of Grain Noise	145
7.2-2	Influence of Aperture on Power Spectrum Measurements	148
7.2-3	Influence of Scanning Filter on Power Spectrum Measurement	149
7.3-1	Grain Structure of Photographic Film Viewed at Three Levels of Magnification	152
7.3-2	Power Spectrum of Grain Noise of Royal-X Pan Compared with Theoretical Models	153
7.3-3	Power Spectrum of Grain Noise of Kodak 2479 Compared with Theoretical Models	154
7.3-4	Power Spectrum of Grain Noise of Kodak 2475 Developed in D <sub>19</sub> , Compared with Theoretical Models	155
7.3-5	Power Spectrum of Grain Noise of Kodak 2475 Developed in Dektol, Compared with Theoretical Models	156
7.3-6	Variation of Grain Noise with Amplitude Transmittance for Kodak 2475	162
7.3-7	Variation of Spectrum at DC with Amplitude Transmittance (Extrapolated from Measurements)	163
7.3-8	Variation of Grain Noise with Amplitude Transmittance for Royal-X Pan Exposed on Kodak 2496	165
7.3-9	Variation of Grain Size with Average Amplitude Transmittance	166

LIST OF FIGURES (Cont'd.)

<u>Figure No.</u>	<u>Title</u>	<u>Page</u>
7.3-10	Two-Sided Power Spectrum of Isotropic Noise	168
7.3-11	Power Spectra of Non-Isotropic Grain Noise	170
7.4-1	Experimental Relationship Between the Real and Complex Transmittance of Film (Kodak 2496)	172
7.4-2	Experimental Relationship Between the Real and Complex Transmittance of Film (Kodak 2475)	173
7.4-3	Power Spectrum of Total Noise Compared with Grain Noise (Kodak 2475)	175
7.4-4	Power Spectrum of Total Noise at Peak Grain Noise (Kodak 2475)	176
7.4-5	Anomalous Behavior of Dense Film (Kodak 2475)	178
7.5-1	Measured Average Frequency Response of Wollensak "Raptar" Enlarging Lens used in White Light	181
7.5-2	Spectrum of Granularity Magnified Box Compared with Spectrum of Original Granularity	183
A-1	Theoretical Point Aperture Microdensitometer Trace of Random Checkerboard Model	186
B-1	Half-Wave Retardation Plate: Amplitude and Phase Characteristics	191
B-2	Diffraction Pattern of Half-Wave Retardation Plate (Theoretical)	192
B-3	Log Diffraction Pattern of Half-Wave Plate (Theoretical)	193

LIST OF FIGURES (Cont'd.)

<u>Figure No.</u>	<u>Title</u>	<u>Page</u>
B-4	Self-Correlation Function of Half-Wave Plate of Area $A = LW$	195
B-5	Laboratory Built Half-Wave Plate and Mount	198
B-6	Experimentally Obtained Diffraction Pattern of Half-Wave Plate	200
B-7	Fourier-Plane Photographs Illustrating Use of Phase Grating with a Square Aperture	201
B-8	Fourier-Plane Photographs Illustrating Use of Phase Grating with a Diamond Aperture	202
B-9	Measurement of Film Noise at Origin of Kodak 2479 Developed in D-19	208
B-10	Measurement of Film Noise at Origin of Bleached Kodak 2479	209

## 1. INTRODUCTION

### 1.1 GENERAL

The research described in this thesis has been concerned with the theoretical and experimental aspects of power density measurements by diffraction. The theoretical design considerations and the experimental techniques that evolved from the study furnish a procedure by which the power spectrum of translucent objects can be obtained. Because of the outstanding role played in modern optical systems by photographic film, it was chosen as the subject of the experimental investigation. The motivation for measuring film noise spectra is a consequence of the following recent developments, described below.

The discovery of the laser as a powerful source of coherent light has enabled the construction of optical signal processing and filtering systems which offer significant advantages over their electronic counterparts in certain applications. These advantages stem from the following properties of coherent optical systems:

- (1) The two dimensions available in optical systems, offer an additional degree of freedom over electronic systems.
- (2) Coherent optical systems can be made to generate successive Fourier transform pairs by simply adding lenses.
- (3) Independent control over the amplitude and phase of spatial filters is easily effected and implies that a wide variety of filter functions can be synthesized (Cutrona, et al., 1960).

In these systems, the filters and the storage media are almost always photographic transparencies.

Another activity which was given fresh impetus because of the development of the laser is waveform reconstruction imaging or holography (Gabor 1948, Gabor 1951, Stroke 1966). In holography, the waveform recording media are generally photographic transparencies.

A fundamental limitation in the performance of both optical signal processing and wavefront reconstruction systems is the noise introduced by the photographic film (Goodman 1967).

The noise produced by photographic film results from two causes: (1) the turbidity of the emulsion and (2) the variations in the optical path length in the cross section of the transparency. The turbidity is a consequence of the suspension of microscopic silver grains in the emulsion. These grains produce random amplitude fluctuations in light and this effect is known as grain noise. The randomness of the optical path length, which results from variations in the thickness and refractive index of the emulsion, produces phase errors in coherent light. This effect is similar to that produced by random imperfection in lenses (Rowe 1966).

Both of these effects can be described conveniently by defining a complex transmittance of a transparency as the ratio of the complex amplitudes of the transmitted to incident light. The complex transmittance,  $R(x,y)$ , can be written as the product of a real amplitude transmittance  $t(x,y)$  representing the grain noise and a complex exponential phase term representing the phase noise.

The power spectrum of a photographic transparency furnishes an excellent way of describing the noise characteristics of the transparency. In optical correlators, where the signal-to-noise ratio is approximately inversely proportional to the power spectrum of the transparency noise, knowledge of the power spectrum is useful for obvious reasons.

The possibility of spectral density measurements by diffraction has been recognized earlier (Shack, et al., 1961). The advantages offered by this method are a consequence of the following:

- (1) The entire three-dimensional sample is involved simultaneously. A large volume is thus simultaneously analyzed instead of a single trace.
- (2) The spectrum can be obtained directly without any intermediate operations and with high resolution.
- (3) The spectrum can be obtained for positive and negative frequencies. This is useful in detecting non-isotropic noise.
- (4) The diffraction method offers the possibility of measuring the spectra of colloids, turbid fluids, etc. for which the application of standard techniques is difficult.

#### 1.2 INVESTIGATIONS AND CONTRIBUTIONS

The conclusions enumerated in this section relate to a coherent optical spectral analyzer which in simplest form consists of a coherent source, two lenses, an aperture, a slit capable of scanning in a plane and the object to be analyzed which must be able to transmit light. The coherent source which in practice is a laser, generates a spherical beam which is collimated (made parallel) by a lens and incident through an aperture on the object located in the front focal plane of the second lens. The light transmitted by the object is passed through a second lens which, according to Fraunhofer diffraction theory, produces a back focal plane field proportional to the two-dimensional Fourier transform of the front focal plane field. The scanning slit, which is a spatial-frequency bandpass filter, enables a small portion of the focal plane field to impinge on a photomultiplier tube which generates a current proportional

to the power of the beam transmitted by the slit. The total back focal plane field is the sum of the field produced by the diffraction by the aperture and the field produced by the random transmittance of the object. The latter generates phase-front perturbations through the injection of random phases and amplitudes resulting from inhomogeneities in the body of the object.

With the above as a background, the theoretical investigation led to the following results:

(1) The expected value of the field generated by the random transmittance of the object in the back focal plane of the second lens will be a reasonable, albeit, biased, estimate of the spectral density of the transmittance, provided that the aperture dimensions are large compared with the maximum correlation intervals of interest.

(2) There are two contributions to the bias, both resulting from the use of a finite aperture. Measurements made with an aperture of transverse dimension  $D$  cannot furnish information about correlation intervals greater than  $D$ . This produces what might be called a truncation error and represents a loss of information. Even when  $D$  is large enough to include all significant correlation intervals, there is still a contribution to the bias because the optical system cannot resolve spectral components in the power spectrum to better than  $D^{-1}$ . This represents a resolution limitation and contributes to the bias. In the absence of a truncation error, the effects of finite resolution can be negated by further filtering and thus do not constitute a loss of information.

When a rectangular aperture is used, the bias error can be shown to be directly proportional to the partial derivatives of the Hilbert transforms of the true power spectrum and inversely proportional to the dimensions of the aperture (Eq. (3.4-11)), provided that the truncation error is zero. If the

truncation error is not zero, the above is still true provided that the true spectrum is replaced by the spectrum of the truncated process.

(3) Under wide-sense stationary Gaussian circumstances, the variance of the spectral density estimator as obtained by diffraction was derived for a rectangular aperture. It was found that the variance depends on the average transmittance of the sample, the true power spectrum of the process, the transverse spatial frequencies in the back focal plane and the aperture dimensions. For a large aperture, the ratio of the standard deviation to the mean becomes unity everywhere except at the origin. This result shows that the estimate of the spectral density has much variability which must be reduced by means other than enlarging the aperture.

Control of the variability of the power spectrum estimator is best effected by the scanning filter which has the effect of averaging the back focal plane field over frequency. The best choice of slit requires a compromise between stability and resolution. For an aperture of length  $L$  and maximum significant correlation interval  $\alpha_{\max}$  (it is assumed that  $L \gg \alpha_{\max}$ ), reasonable bounds on the width,  $d$ , of the slit are furnished by

$$\frac{\lambda f}{L} < d < \frac{\lambda f}{\alpha_{\max}}$$

where

$\lambda$  = wavelength of the radiation

$f$  = focal length of lens

(4) With the random checkerboard configuration as a basis for representing the granularity of photographic film, it was shown that the grain noise cannot be treated as uncorrelated additive or multiplicative noise.

(5) The principal interference with the observation of the spectrum comes from the zero-order light which represents the diffraction by the aperture. Apodisation by aperture shaping may be used to reduce the sidelobe level of the zero-order for selected directions in the back focal plane, without significantly contributing to the bias of the measured spectrum. The peak of the zero-order occurs at the origin and can be many orders of magnitude above the spectral density, hence, not allowing its observation there. A null in the zero-order at the origin can be generated by using odd-symmetric aperture functions, the simplest being the one-cycle phase grating. The effect of using this grating on the measurement of the spectrum is to decrease the frequency resolution by approximately a factor of two.

The experimental phase of the research was restricted to measurements on photographic film, but the techniques which were used could be applied equally well to other translucent objects.

The major aims of this phase of the research were (1) the development of techniques by which reliable and accurate spectral density measurements could be made, (2) the verification of several theoretical results and (3) the measurement of the properties of film noise and a comparison of these with theoretical predictions where possible. Specifically, the following experimental results were obtained:

(1) A technique was developed by which the estimate of the power spectrum of film grain noise could be obtained directly and continuously with high reliability down to frequencies very near the origin. In the case of total film noise, i.e., the noise resulting when random amplitude and phase effects are both present, the technique enabled the observation of the noise to frequencies as low as 5 cycles/mm. The technique offered several advantages, including ease of calibration directly in units of  $\text{mm}^2$  and furnishing results which were independent both of

system-scattered light and changes in the light level of the system.

(2) The dependence of the spectral estimate on system parameters such as aperture size, shape and bandwidth of the scanning slit was experimentally obtained and the results were found to be consistent with theoretical predictions. It was found that the general shape of the average spectral estimate was relatively independent of aperture shape, provided that the aperture dimensions were large compared with the largest significant correlation intervals of the film noise process. The size and shape of the aperture did influence the variability of the estimate in a way which was theoretically predicted, namely that the variance was reduced for high spatial frequencies and large apertures.

Although increasing the aperture size reduced the variability, it was found that best control over the variability could be effected by increasing the bandwidth of the scanning slit. The bandwidth ultimately used corresponded to a slit size well within the theoretical bounds given earlier.

(3) Apodisation by aperture shaping was found to be a useful technique for reducing the zero-order light. The degree of sidelobe suppression was not as great as that theoretically predicted, primarily because the aperture shape did not reduce the component of light scattered from lenses, reflections, etc.

A half-cycle phase grating was built with the object of reducing the zero-order light at the origin in order to measure the spectrum there. The performance of the grating corresponded closely to theory and the feasibility of its use in power spectral measurements at the origin was firmly established.

(4) Good agreement was found between the measured spectrum and the theoretical spectrum of the 3-parameter overlapping

circular grain (OCG) model which includes the effect of the film gelatin. The 2-parameter OCG model and the random checkerboard (RC) models furnished power spectra which were somewhat higher than the measured spectrum, hence enabling S/N estimations based on these models to be on the "safe" side. A serious drawback of the RC model is that it does not have isotropic statistics and hence, the goodness of fit depends on the orientation of the model "grains."

The measurements enabled the determination of the parameters of these models. The knowledge of these parameters proved useful in determining additional information about the relation of film granularity structure to average transmittance and the effect of developer on grain size.

The variation of the grain noise spectra with average amplitude transmittance was experimentally determined for two film types. In each case, the maximum was observed in the spectrum when the average transmittance was near 0.6. The existence and location of such a maximum are predicted by both the RC and OCG models.

Examination of the spectrum of non-isotropic film grain noise was found to be a useful technique for detecting directional anomalies such as granularity streaking.

(4) Measurements indicated that the total noise of film was a low-frequency phenomena. Typically, the total noise decreased to one-half its maximum value in a frequency span one-fifth that of grain noise. At the origin, the total noise was much larger than the grain noise - an order of magnitude not being unusual.

The magnitude of the complex transmittance was found to vary linearly with the average amplitude transmittance. This result furnished the variance of the random phase within the framework of a model which assumes independence between amplitude and phase and Gaussian statistics for the latter.

(5) Spectral density measurements can be used to determine the frequency response of optical systems because the transition from object to image in optics is equivalent to the action of a linear filter. In addition, imaging and magnification with high-resolution optics can be used to obtain the spectrum over extended frequencies without generating unsuitably large diffraction angles. Experiments designed to demonstrate the feasibility of these techniques were performed with a measure of success.

### 1.3 REVIEW OF FILM-NOISE MEASUREMENTS

Photographic granularity of grain noise has been a subject of intense investigation for at least fifty years. Contributions have come from scientific workers in many fields, including chemistry, physics, mathematics and engineering. A great and diverse fund of knowledge is scattered in the literature in several languages and many journals. The investigator can at best only hope to refer to those works which occupy, in his opinion, salient positions in the continuing investigation of this subject.

One of the earliest attempts to view photographic granularity as a random process was the work by Silberstein in 1922. Silberstein viewed the grain-development process from a quantum-mechanical viewpoint. According to his theory, the probability that a silver-halide grain becomes exposed (i.e., is ultimately reduced to metallic silver) is a function of two numbers: (1) the probability  $\epsilon$  that a photon incident upon a grain is absorbed by the grain, and (2) the quantum threshold  $m$  which is the number of photons required to make a grain developable (Silberstein 1922). Silberstein later amended his theory to include, in any emulsion, grains of varying quantum sensitivities (Silberstein 1941). The Silberstein theory was experimentally justified by Trivelli and Righter (Trivelli & Righter 1922).

Attempts to measure photographic granularity through micro-densitometer traces date back to 1932 [Mees and James(1)\*1966]. Attempts at evaluating these traces did not occur until the following year, when it was observed that the random optical density of uniformly exposed film was in good agreement with the Gaussian probability law [Mees and James(2),(3),(4) 1966]. However, it was expected and ultimately verified that the variance of the optical density,  $\sigma_D^2$ , varies with the scanning aperture. Bricout found a variation approximately as  $d^{0.8}$ , where  $d$  is the aperture diameter. These results limited the usefulness of using  $\sigma_D^2$  alone as a measure of granularity.

In 1935, a theoretical study based on the examination of three sets of assumptions about the nature of photographic transparencies led to a new measure of granularity called the Selwyn granularity coefficient or, simply, the Selwyn granularity. The assumptions leading to this new measure were the following: (1) the number of grains within a scanning aperture is a random sample from a binomial distribution and the optical density is strictly proportional to the number of grains in the aperture; (2) the emulsion can be described as an aggregate of elementary cubes that consist of opaque silver grains or transparent gelatin; and (3) the density distribution involves only one parameter in addition to the area of the scanning spot, densities of adjacent neighboring areas are uncorrelated and fluctuations of density are small. Consideration of these assumptions led to the conclusion that the observed variance is inversely proportional to the square root of the scanning area and therefore, that the product of the two must be a constant [Mees and James (5) 1956]. The Selwyn granularity is defined by

$$S = (2a)^{1/2} \sigma_D$$

---

\* Number in parenthesis refers to reference cited in the work by C.E.K. Mees and T. H. James. See 2 references at end.

where  $\sigma_D$  = observed variance, and  $a$  = area of the scanning aperture.

Experimental attempts to verify the above led to mixed results. Departures from the square-root law were observed by several workers (Bricout, van Kreveld, Debot) and in one case [Mees and James(6) 1966], it was found that the square-root law fitted experimental observations quite well if observations were made on the transmittance  $T$  instead of the density  $D$  ( $D = \log_{10} 1/T$ ).

Careful studies on granularity revealed that the Selwyn measure for granularity was a function of optical density and failed for both very small and very large apertures (Jones & Higgins 1946). Furthermore, it was found that the Selwyn coefficient did not always produce results that corresponded to subjective visual evaluation. To eliminate the latter, the Selwyn measure was modified to give way to a syzygetic Selwyn granularity coefficient. This measure attempts to duplicate the effect of granularity on retinal receptors (Jones & Higgins 1947). To obtain the syzygetic coefficient, granularity is measured in terms of the magnification for which the average density difference between two microdensitometer apertures attain a certain value.

With the advent of more rapid and accurate instruments, the Selwyn granularity was measured for a number of samples as functions of both the density and the square root of scanning area (Higgins & Stultz 1959). The results may be summarized as follows: in general, the granularity increases with density (or decreases with transmittance). For an aperture in the range between 7 and 200 microns, the Selwyn coefficient is fairly constant. Above 200 microns,  $S$  increases quite sharply with the square root of the aperture. Results for apertures smaller than 7 microns are not available.

Granularity has been linked to entropy. If the entropy, H, of a transparency is defined by

$$H = -T \log_2 T - (1-T) \log_2 (1-T)$$

where T is the intensity transmittance, then it has been shown that the function H vs T closely follows the subjective impressions of "graininess" as a function of transmittance (O'Neill 1958).

During the nineteen-fifties, the mathematical tools of communication theory were applied to grain-noise analysis. The usefulness of autocorrelation methods in studying granularity became apparent (Fellgett 1953). The relation of Selwyn's granularity measure to the characteristics of the autocorrelation function was investigated by H. J. Zweig (Zweig 1956), who computed autocorrelation functions from microdensitometer traces and found that the size of the scanning aperture had a profound influence on the shape of the autocorrelation curve. By varying the diameter of the scanning aperture from 6 microns to 50 microns, Zweig obtained for the same sample very peaked autocorrelation functions with significant autocorrelation intervals never larger than 8 microns in the case of the 6 micron aperture to almost flat autocorrelation curves with significant intervals extending to 20 microns in the case of the 50-micron aperture.

Reciprocal relationships between the autocorrelation function and the Selwyn granularity were derived (Marriage & Pitts 1956). In a widely quoted paper, R. C. Jones argued that the only fully adequate way to describe the granularity of photographic materials is by means of the noise power spectrum (R. C. Jones 1955).

The power spectrum of the film grain noise goes beyond any previous measure in that it leads to the solution of

many of the signal-to-noise problems that arise in connection with the detection of signals on photographic transparencies. The power spectrum can easily be related to the Selwyn coefficients.

A very common technique for measuring the power spectrum of the grain noise consists of scanning a uniformly exposed sample of film with a microdensitometer and passing the electrical output of the densitometer through a narrow band-pass filter. The spectrum may then be explored by varying the center frequency of the pass band. This technique has been applied to obtain the spectra of various transparencies (Jones 1955, Doerner 1961, Steel 1966).

The method just described has several disadvantages. Since this technique really measures the power spectrum of the electrical noise signal produced by the microdensitometer, a relation between the electrical noise spectrum and the grain-noise spectrum must be established. The general relation as computed by R. C. Jones (Jones 1955) depends upon the relative velocity between the film sample and the densitometer, the shape and size of the aperture, the frequency response of the densitometer, and the noise spectrum. It is not generally possible to determine the grain-noise spectrum from the electrical spectrum except for certain densitometer apertures. The spectra obtained by this method tend to show a characteristic droop which reflects the filtering action of the aperture and not any property of the random noise process. Also, for reasons that probably pertain to the electrical system, very low spatial frequencies (<1 line/mm) are usually not investigated with the above method.

With the advent of lasers, high-intensity coherent optical systems became useful as signal processing and filtering systems. The two-dimensional Fourier transforming property of lenses could be exploited. Successive linear operations of

an integral-transform nature could be implemented by simply adding additional lenses to a system. In a basic paper, Cutrona showed that most of the filtering and signal processing operations performed by electronic equipment could be duplicated by using elements of coherent optical systems (Cutrona 1960). Electro-optical spectrum analyzers using the Debye-Sears effect were constructed and proved useful in processing and spectrum analyzing electrical signals (Lambert 1965).

With respect to film-grain noise, it was discovered that when a photographic transparency was placed in the collimated region of a coherent optical system, scattered light appeared in the back focal plane of the Fourier transforming lens. Explained in terms of Fraunhofer diffraction theory, the scattered light was adjudged to be the spectral distribution of granularity (Shack, et al. 1961, Leith 1962, Thiry 1963). It thus appeared that the spectrum of grain noise could be measured by diffraction techniques. Attempts to measure the scattered light intensity proved to be a difficult task chiefly because the diffracted source light (often called the zero-order light), was several orders of magnitude more intense than the light of interest.

One technique, which in principle could reduce the sidelobe level of the zero-order light, would be to weight the aperture with an absorbing pupil function (Jacquinot 1966). However, the fabrication of accurately controlled pupil functions is a difficult task, and such pupil functions would themselves be granular transparencies. An indirect technique involving a combination of diffraction, spatial filtering and imaging can be used to measure the light scattered by the grains in a transparency (Leith 1962). This method involves a three-step operation in which the combined zero-order light and scattered light is spatially filtered in the frequency plane and then re-imaged on a fixed photocell. According to the author, if the bandpass

region of the spatial filter is appropriately chosen, the zero order light can be displaced from the region where the scattered light is being measured. Unfortunately, this technique involves such low light levels that a reasonably wide spatial filter must be used. A wide spatial filter implies observing a smoothed version of the scattered light variation and the fine structure in the scattered light is consequently lost.

Attempts to measure grain-scattered light by observing the perturbation in the diffraction pattern of a very small circular aperture were made using incoherent light sources (Thiry 1963). A combination of diffraction and electronics techniques enabled Burckhardt to measure the scattered light from holographic plates down to 200 lines/millimeter. Data were not obtained for spatial frequencies lower than 200 lines/mm (Burckhardt 1967).

In addition to the noise resulting from the granularity of a transparency, a coherent optical system will also sense noise resulting from random phase misalignments in the complex light amplitude emerging from such a transparency. The random phases result from variations in both the thickness of the transparency and the refractive index of the medium. It has been shown that in order to stay within the Rayleigh limit (maximum optical path difference across aperture  $\leq \lambda/4$ ) the transparency must be inserted in a liquid gate whose refractive index is equal to the refractive index of the transparency (Ingalls 1960).

Several theoretical models exist for describing the grain distribution in an emulsion (O'Neill 1963, Picinbono 1955, Savelli 1958). Some of these models have been used to predict signal-to-noise ratios in wavefront reconstruction imaging (Goodman 1967). Two commonly used theoretical models are the overlapping circular grain model and the random-checkerboard

model. The former is the more realistic of the two and models the grains as opaque disks which may overlap. If a point is covered by a disk, the transmittance of the point is zero and if the point is not covered by a disk, the transmittance is unity. The random-checkerboard model is the two-dimensional extension of the random binary waveform in electrical engineering. Comparisons between the theoretical models and experimental data have led to mixed results (Jones 1955).

## 2. BASIC RELATIONS

In this chapter the basic equations relating to the measurement of power spectra by the diffraction of coherent light are derived for ordinary and astigmatic optical systems. Ordinary optical systems perform two-dimensional operations while the astigmatic systems considered here are one-dimensional. Astigmatic optical systems are simulated in practice by using cylindrical instead of spherical lenses and scanning along a specific axis instead of in a plane. Both ordinary and astigmatic optical systems are assumed to be free from geometrical aberrations.

### 2.1 COMPLEX TRANSMITTANCES

A convention that appears in the literature on coherent optics (Born and Wolf 1964) and is used here is the following: A wave of the form

$$e(x,y,z,t) = A(x,y) \cos [\beta z - \omega t + \gamma(x,y)] \quad (2.1-1)$$

is denoted as the complex function  $E(x,y)e^{j(\beta z - \omega t)}$  where

$$E(x,y) = A(x,y) e^{j\gamma(x,y)} \quad (2.1-2)$$

$E(x,y)$  is commonly called the complex amplitude of a coherent light wave. The other symbols have the following meanings:

- $A(x,y)$  real amplitude, a function of  $(x,y)$
- $\omega$  temporal radian frequency of the wave
- $\beta$  = the propagation constant =  $2\pi/\lambda$
- $\lambda$  the wavelength of the wave in the medium

$z$  = the axis of propagation, also the position  
of the wavefront

$t$  = time parameter

$\gamma(x,y)$  = the relative phase, a function of  $(x,y)$

$j = \sqrt{-1}$

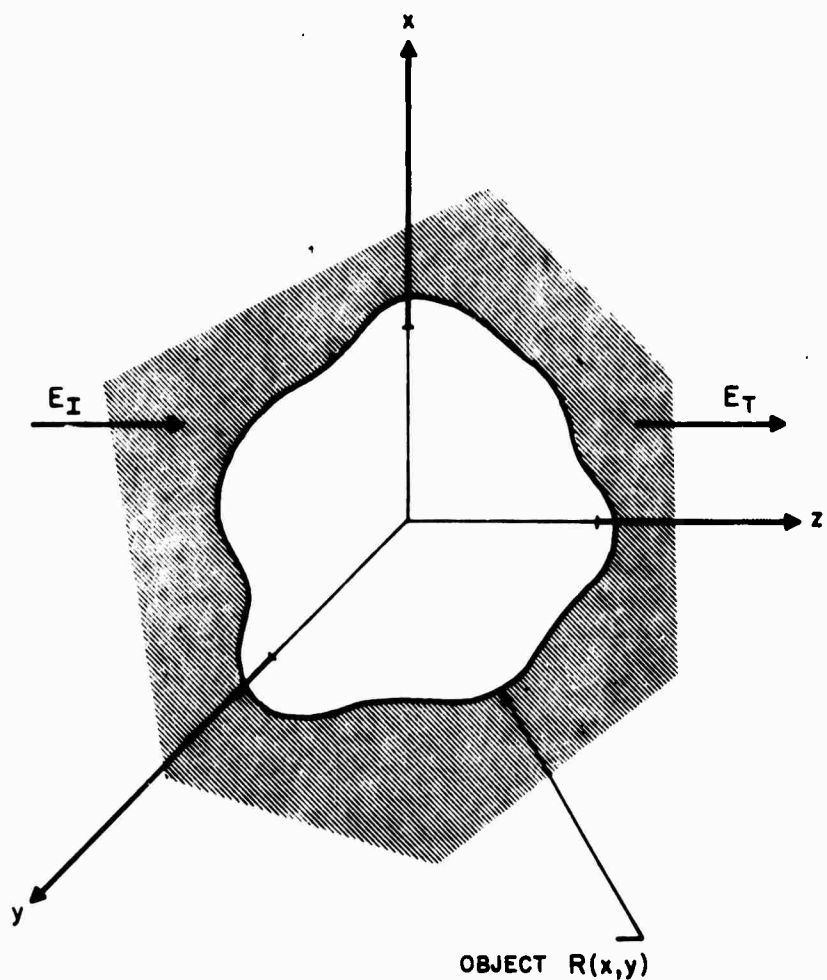
The principal motivation for adopting the representation of Eq. (2.1-1) of a wave is that (i) all the significant features of the optical systems considered here are time invariant, (ii) the notation is very useful when defining the complex transmittance of an object, and (iii) all physical sensors sense the power or energy in a wave and these quantities are proportional to the time average of  $e^2$  or  $E(x,y)E^*(x,y)$  where \* denotes conjugate. In the following work, the intensity associated with a wave of complex amplitude  $E(x,y)$  is defined as

$$I(x,y) = |E(x,y)|^2 \quad (2.1-3)$$

A transparent or semi-transparent object illuminated by an incident coherent light wave as shown in Fig. 2.1-1 will generally alter the amplitude and phase of the light as the latter passes through the object. The effect of the object on the transmission of light is conveniently described by defining a complex transmittance of the object by the ratio of the transmitted to incident light. The complex transmittance, denoted as  $R(x,y)$  is then given by

$$R(x,y) = \frac{E_T(x,y)}{E_I(x,y)} \quad (2.1-4)$$

where  $E_I(x,y)$  and  $E_T(x,y)$  denote incident and transmitted light respectively. When  $\arg R(x,y) = 0$ , the transmittance is purely an amplitude transmittance and is denoted by  $t(x,y)$ .



$$R(x, y) = \frac{E_T(x, y)}{E_I(x, y)}$$

A-006-1-00-0027

FIG.2.1-1 ILLUSTRATING THE COMPLEX TRANSMITTANCE OF AN OBJECT

More generally, both amplitude and phase are affected and it is convenient to write

$$R(x,y) = t(x,y) e^{j\psi(x,y)} \quad (2.1-5)$$

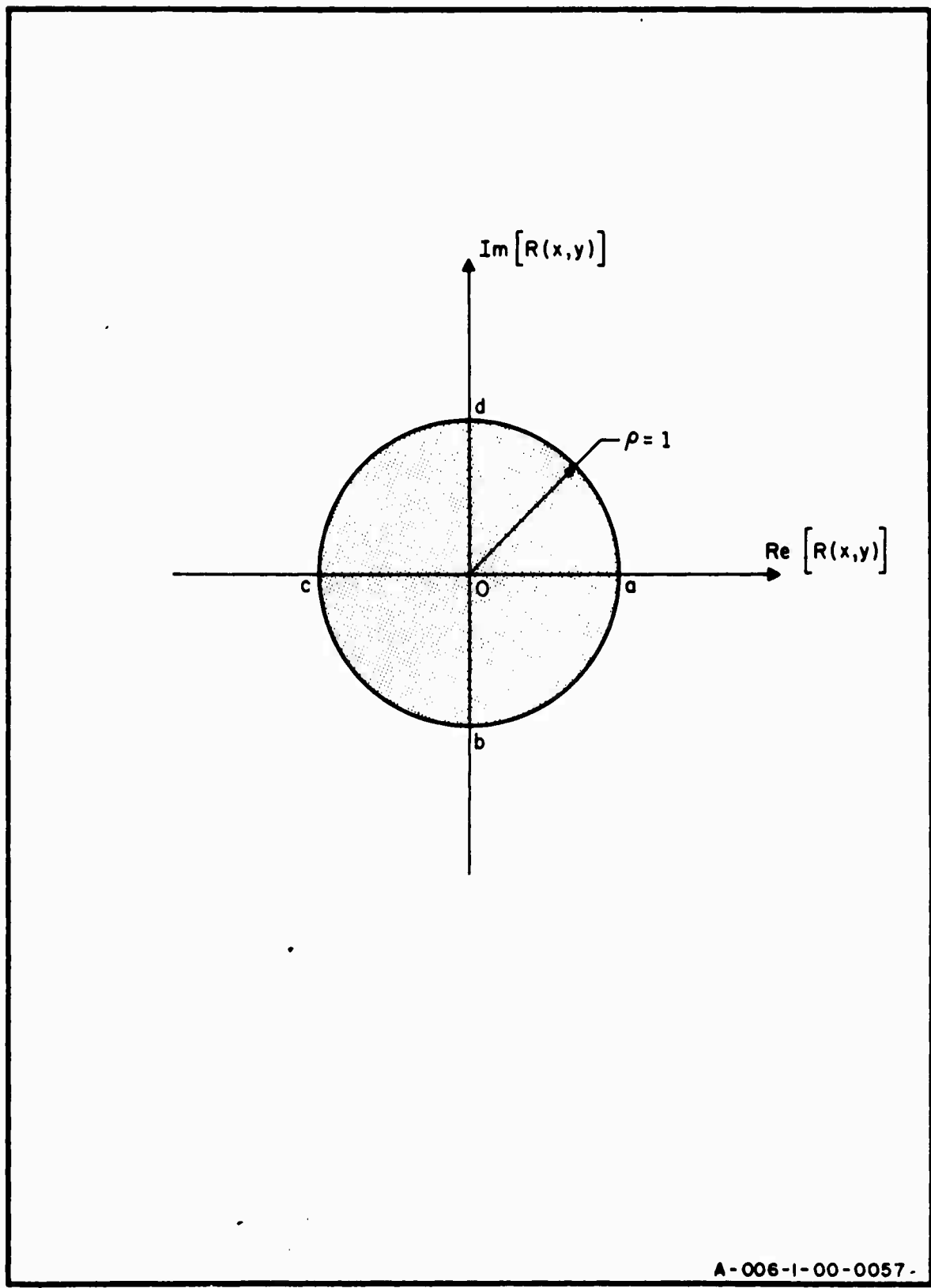
Observe that  $t(x,y)$  is a real number such that  $0 \leq t(x,y) \leq 1$  and  $\psi(x,y)$  is a real number resulting from variations in the optical path length across the object. If the thickness of the object at  $(x,y)$  is  $\sigma(x,y)$  then the phase retardation  $\psi(x,y)$  at  $(x,y)$  when the object is assumed immersed in air is given by

$$\psi(x,y) = (2\pi/\lambda) (n-1) \sigma(x,y) \quad (2.1-6)$$

where  $n$  is the index of refraction of the object.

The values of  $R(x,y)$  may be represented by points on or within a circle of unit radius in the complex plane, as shown in Fig. 2.1-2. When  $\arg R(x,y) = 0$ , implying a uniform phase retardation over the entire object, the domain of  $R(x,y)$  is the segment Oa. When the object has a uniform amplitude transmittance with varying phase, the range of  $R(x,y)$  consists of points lying on a circle concentric and within the unit circle.

In many physical situations, the complex transmittance of an object is a randomly varying quantity, the randomness being inherent in  $t(x,y)$ ,  $\psi(x,y)$  or both. To cite some examples, consider the situation that arises when uniformly exposed photographic film is inserted into a liquid gate whose refractive index is equal to that of the film's; the optical path length at all points is the same and the relative phase is zero. The granularity of the film, however, produces random amplitude fluctuations in the transmitted light. In this case  $R(x,y) = t(x,y)$ , and the latter can be considered as a real random variable for any point  $(x,y)$ . On the other hand,



A-006-I-00-0057-

FIG. 2.I-2 THE RANGE OF THE COMPLEX TRANSMITTANCE  $R(x,y)$

a thin lens with random surface imperfections produces only a random phase shift  $\psi(x,y)$  while maintaining  $t(x,y)$  at essentially unity (Rowe 1966). Finally, photographic film which is not in a liquid gate contains random variations in both  $t(x,y)$  and  $\psi(x,y)$ . The random variables,  $R(x,y)$  and  $t(x,y)$  do not have zero mean. For subsequent work, it is convenient to define the auxiliary random variables  $r(x,y)$  and  $\tau(x,y)$  as follows

$$\begin{aligned} r(x,y) &= R(x,y) - R_o \\ \tau(x,y) &= t(x,y) - t_o \end{aligned} \quad (2.1-7)$$

where  $R_o = \langle R(x,y) \rangle$  and  $t_o = \langle t(x,y) \rangle$  and  $\langle \cdot \rangle$  denotes expectation. Clearly  $\langle r(x,y) \rangle = \langle \tau(x,y) \rangle = 0$ .

## 2.2 SPATIAL RANDOM PROCESSES

Any point in the  $xy$  plane can be considered as a vector with initial point at the origin and terminus at the point. Such a point can be defined by either the pair  $(x,y)$  or the vector  $\vec{s} = x\hat{i}_x + y\hat{i}_y$  where  $\hat{i}_x$  and  $\hat{i}_y$  are orthogonal unit vectors parallel to the coordinate axes. When  $\vec{s}$  is any given vector,  $R(\vec{s})$  is the random variable describing the complex transmittance at  $\vec{s}$ . Note that  $R(\vec{s})$  is a scalar function of the vector  $\vec{s}$ . When  $\vec{s}$  is used to index  $R$ , a collection of random variables is formed, one for each point in the plane. This collection of random variables constitutes the random process  $\{R(\vec{s})\}$ . A similar argument holds for  $\{t(\vec{s})\}$  and  $\{\psi(\vec{s})\}$ .

In all of the present work, the complex process  $\{R(\vec{s})\}$  and the real processes  $\{t(\vec{s})\}$  and  $\{\psi(\vec{s})\}$  are assumed to be wide sense stationary. This requires that

$$(1) \quad \langle R(\vec{s}) \rangle = R_o \text{ independent of } \vec{s} \quad (2.2-1)$$

$$\begin{aligned} (2) \quad \langle R(\vec{s} + \vec{\ell}) R^*(\vec{s}) \rangle &\equiv \phi_R(\vec{s} + \vec{\ell}, \vec{s}) \\ &= \phi_R(\vec{\ell}) \end{aligned} \quad (2.2-2)$$

i.e., the autocorrelation function of  $\{R(\mathbf{s})\}$  is only a function of the difference of the two vectors, and

$$(2.2-3) \quad \langle |R(\mathbf{s})|^2 \rangle < \infty$$

The covariance of  $\{R(\mathbf{s})\}$  is the autocorrelation function of  $\{r(\mathbf{s})\}$  and is given by

$$\phi_r(\ell) = \phi_R(\ell) - |R_0|^2 \quad (2.2-4)$$

From the definition of  $\phi_R(\ell)$ , it follows that  $\phi_R(\ell) = \phi_R^*(-\ell)$ . Hence, in rectangular coordinates, there results

$$\phi_R(\alpha, \beta) = \phi_R^*(-\alpha, -\beta) \quad (2.2-5)$$

from which it follows that

$$\phi_R(\alpha, -\beta) = \phi_R^*(-\alpha, \beta)$$

$$\phi_R(-\alpha, \beta) = \phi_R^*(\alpha, -\beta)$$

In certain physical situations, it is reasonable to assume that the covariance function  $\phi_r(\ell)$  is a function only of the magnitude of  $\ell$ , i.e., the covariance function is a function of a scalar. In this case the statistics are independent of the direction of the coordinate axes and the covariance depends only on the distance from the origin of the  $\alpha, \beta$  coordinate axes. Hence, one may write for this special process,

$$\phi_r(\alpha, \beta) = \phi_r^+(\rho) \quad \text{where } \rho = (\alpha^2 + \beta^2)^{1/2} \quad (2.2-6)$$

---

<sup>+</sup> The symbol  $\phi$  will be used throughout to denote correlation or covariance functions. A subscript will be added only when there is a need to differentiate among various processes.

and since

$$\phi_r(\alpha, \beta) = \phi_r(-\alpha, -\beta) = \phi_r^*(\alpha, \beta) \quad (2.2-7)$$

the covariance function  $\phi_r(\alpha, \beta)$  is a real function. When the covariance may be written as a function of the single argument  $\rho$  as in Eq. (2.2-6), the random process is said to be isotropic. The covariance of an isotropic process possesses circular symmetry in the sense that the loci of constant  $\phi_r(\rho)$  are circles about the origin.

When the spatial random process is the noise associated with uniformly exposed film, it is reasonable to assume that the process is stationary. The statistical properties of the granularity and surface corrugations are the same from one portion of the film to another (Jones 1955).

There is far less justification for assuming on an a-priori basis that film noise is isotropic. This is equivalent to assuming that there is no preferred direction on the surface of the film - that film noise is not streaked in any particular direction. That the isotropic noise condition may indeed be unjustified can be seen from the fact that when emulsion is spread on the film base, there is a likelihood that the granularity acquires a directional character, related to the direction in which the emulsion is spread on the film base.

The questions concerning the isotropy of film noise and for that matter, any other spatial noise process may be resolved by examination of the power spectrum of the process. Before dealing with this problem, it is noteworthy that in the case of film noise, the process  $\{t(x,y)\}$  is closely associated with the granularity of the film (the dichotomous state of grains), while the noise process  $\{\psi(x,y)\}$  is primarily a consequence

of the surface irregularities of the emulsion, which randomize the optical path length and produce random phase errors in coherent light. More will be said about film noise in Chapter 4.

### 2.3 POWER SPECTRA

The two-dimensional spectral density of a stationary random process is the Fourier transform of its covariance  $\phi(\alpha, \beta)$ . Thus if  $W(u, v)$  denotes the spectral density,

$$W(u, v) = \int_{-\infty}^{+\infty} \int_{-\infty}^{+\infty} \phi(\alpha, \beta) e^{-j2\pi(u\alpha+v\beta)} d\alpha d\beta \quad (2.3-1)$$

where  $u$  and  $v$  are the transverse frequencies of the "frequency domain."

The power spectrum is a real function of the arguments  $u, v$ . This is easily seen by considering the conjugate of Eq. (2.3-1) and using the fact that  $\phi^*(\alpha, \beta) = \phi(-\alpha, -\beta)$ .  $W(-u, v)$  is given by

$$\begin{aligned} W(-u, v) &= \int_{-\infty}^{+\infty} \int_{-\infty}^{+\infty} \phi(\alpha, \beta) e^{-j2\pi(-u\alpha+v\beta)} d\alpha d\beta \\ &= \int_{-\infty}^{+\infty} \int_{-\infty}^{+\infty} \phi(-\alpha, \beta) e^{-j2\pi(u\alpha+v\beta)} d\alpha d\beta \end{aligned} \quad (2.3-2)$$

Since  $\phi(-\alpha, \beta)$  is not generally equal to  $\phi(\alpha, \beta)$ , it may be concluded from the uniqueness property of the Fourier transform that  $W(-u, v)$  is not equal to  $W(u, v)$ . An identical argument can be applied to show that  $W(u, v)$  is not equal to  $W(u, -v)$ .

An exception occurs in the isotropic case, for which  
 $\phi(\alpha, \beta) = \phi(\sqrt{\alpha^2 + \beta^2}) = \phi(r)$ . Let

$$\begin{aligned} \alpha &= r \cos \theta \\ \beta &= r \sin \theta \\ u &= w \cos \zeta \\ v &= w \sin \zeta \end{aligned} \quad (2.3-3)$$

Equation (2.3-1) may then be written as

$$w(w \cos \zeta, w \sin \zeta) = 2\pi \int_0^\infty \phi(r) J_0(2\pi wr) r dr \equiv W(w) \quad (2.3-4)$$

Clearly in the isotropic case,  $w(u, v)$  is an even function with respect to both arguments.

Equation (2.3-4) is recognized as the Hankel transform of  $\phi(r)$ . Hence

$$\phi(r) = 2\pi \int_0^\infty W(w) J_0(2\pi rw) w dw \quad (2.3-5)$$

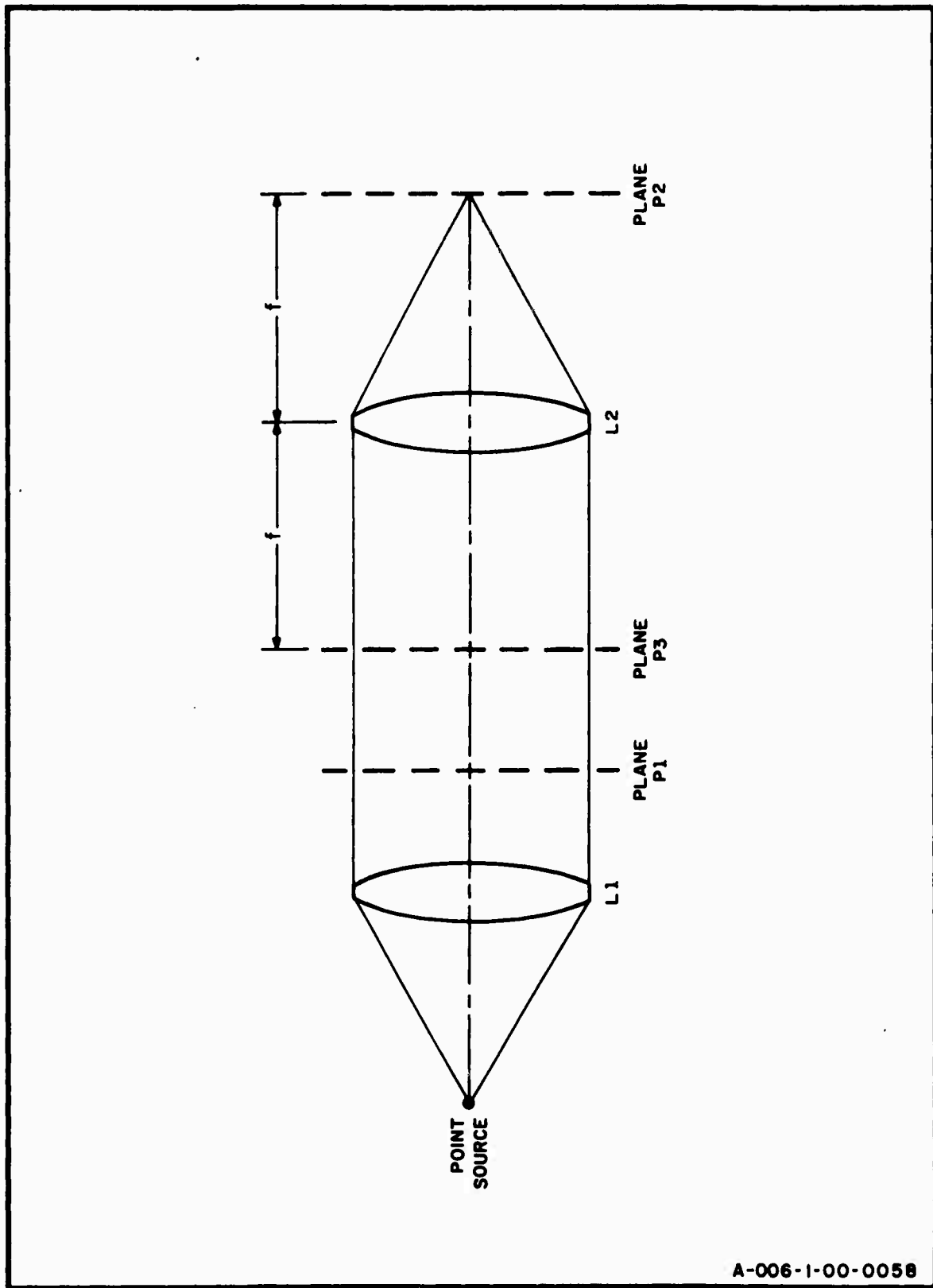
## 2.4 SPECTRAL MEASUREMENTS BY DIFFRACTION

Consider the system shown in Fig. 2.4-1. The source of light is a monochromatic\* coherent point source, meaning that the relative phases of the light at any two points in the optical system are invariant with respect to time. If the light in plane P1 (P1 being any plane between L1 and L2) is denoted by  $E(x, y)$  and the light in plane P2 is given by  $E_f(x', y')$ , then by application of the Fresnel-Kirchhoff diffraction integral, it may be shown that \*\* (Born and Wolf 1964)

---

\* This requires that the source has been on for all time.

\*\* With the usual assumptions about small diffraction angles.



A-006-1-00-0058

FIG.2.4-1 COHERENT OPTICAL SYSTEM

$$E_f(x', y') = C \iint_A E(x, y) e^{-j(2\pi/\lambda f)(xx' + yy')} dx dy \quad (2.4-1)$$

where       $x, y$     coordinates in plane P1  
 $x', y'$     coordinates in plane P2  
 $C$  = a complex number with phase dependence on  
 $x', y'$   
 $\lambda$  = wavelength of light in free space  
 $f$  = focal length of the lens  
 $A$  = surface of aperture  
 $P_1$  = any plane between  $L_1$  and  $L_2$

When  $P_1$  coincides with the front focal plane ( $P_3$ ) of the lens,  $C$  is independent of  $x'$  and  $y'$ . However, in the work presented here, the phase of  $C$  is of no interest and only the magnitude of  $C$ , denoted by  $K$ , is required for the calibration of experimentally obtained data.

It is convenient to define the transverse spatial frequencies  $u, v$  by

$$\begin{aligned} u &= x'/\lambda f \\ v &= y'/\lambda f \end{aligned} \quad (2.4-2)$$

Spatial frequencies have the units of cycles per unit distance. A convention that sometimes appears in the literature is to ascribe units of "lines" per millimeter to  $u$  and  $v$ . Plane  $P_2$  is referred to as the frequency domain. For the work here it is most convenient to express the light in  $P_2$  in terms of the frequencies  $(u, v)$ , giving

$$E_f(u, v) = K \iint_A E(x, y) e^{-j2\pi(ux+vy)} dx dy \quad (2.4-3)$$

It will now be demonstrated that with properly chosen parameters, the system shown in Fig. 2.4-2a can be used to measure the power spectral density of the complex process  $\{R(x,y)\}$  associated with the transparency  $T$ . If the total power of the coherent beam is  $J$ , the complex amplitude of the coherent wave  $E_I(x,y)$  incident upon the object  $T$  is given by

$$E_I(x,y) = \left(\frac{J}{LW}\right)^{\frac{1}{2}} \text{rect} \frac{x}{L} \text{rect} \frac{y}{W}, \quad (2.4-4)$$

where  $L$  and  $W$  are the aperture dimensions, and

$$\begin{aligned} \text{rect } \xi &= 1 \quad |\xi| \leq 1/2 \\ &= 0 \quad \text{otherwise} \end{aligned} \quad (2.4-5)$$

The light  $E_T(x,y)$  transmitted by the object is given by

$$E_T(x,y) = E_I(x,y) R(x,y), \quad (2.4-6)$$

and the light  $E_f(u,v)$  in the  $uv$  plane is, according to Eq. (2.4-3), given by

$$E_f(u,v) = K \iint_A E_T(x,y) e^{-j2\pi(ux+vy)} dx dy, \quad (2.4-7)$$

where the aperture surface comprises a rectangle of area  $LW$ . From Parseval's theorem,

$$\int_{-\infty}^{\infty} \int_{-\infty}^{\infty} |E_f(u,v)|^2 du dv = K^2 \int_{-\infty}^{+\infty} \int_{-\infty}^{+\infty} |E_T(x,y)|^2 dx dy \quad (2.4-8)$$

Substituting the expressions for  $u$  and  $v$  in terms of  $x'$  and  $y'$ , Eq. (2.4-2) gives

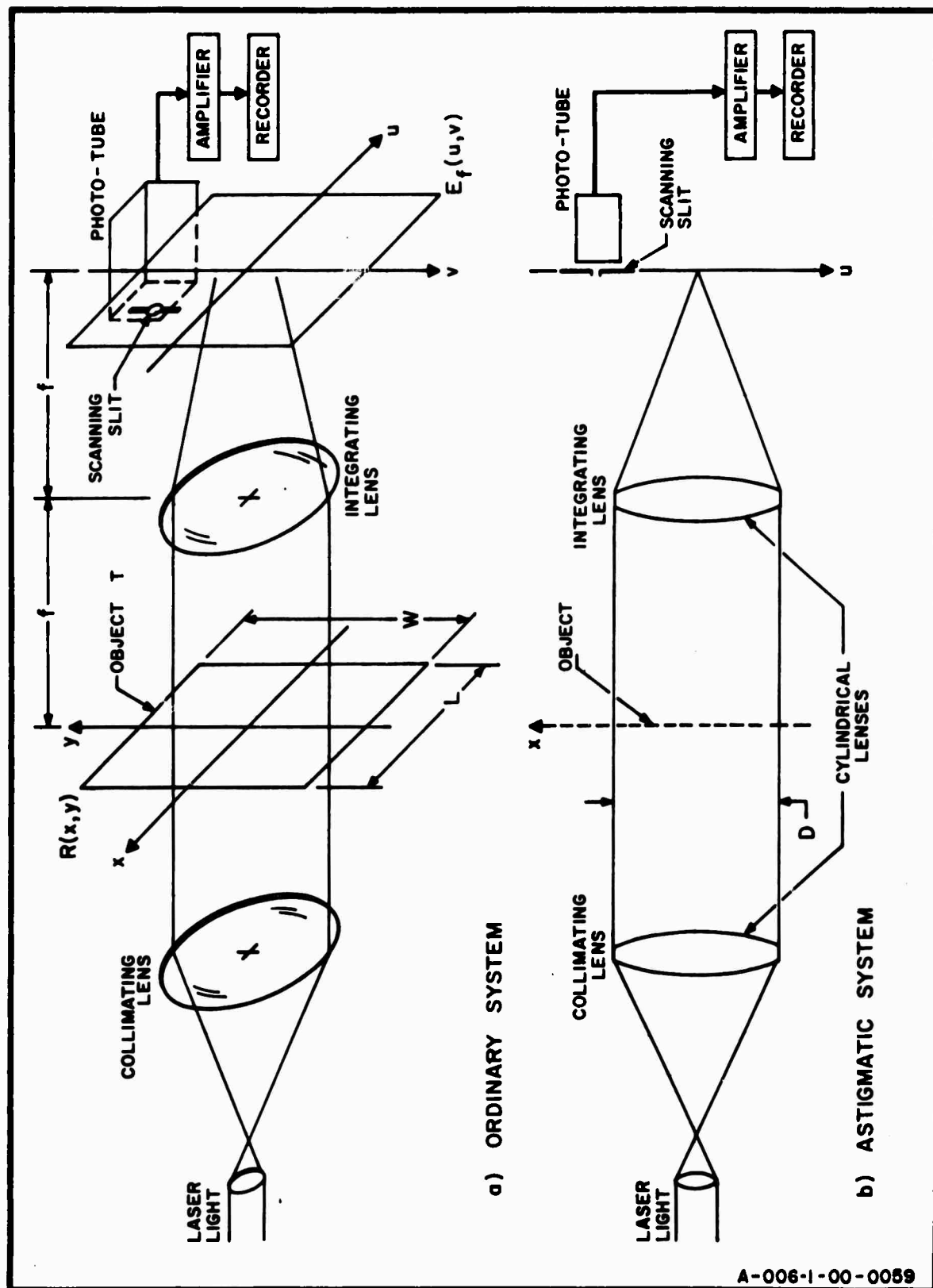


FIG.2.4-2 OPTICAL SYSTEMS FOR MEASURING POWER SPECTRA

$$\begin{aligned}
 (1/\lambda f)^2 & \int_{-\infty}^{+\infty} \int_{-\infty}^{+\infty} |E_f(x'/\lambda f, y'/\lambda f)|^2 dx' dy' \\
 & = K^2 \int_{-\infty}^{+\infty} \int_{-\infty}^{+\infty} |E_T(x, y)|^2 dx dy
 \end{aligned} \tag{2.4-9}$$

However, if the lens is lossless, the integrals

$$\begin{aligned}
 \int_{-\infty}^{+\infty} \int_{-\infty}^{+\infty} |E_f(x'/\lambda f, y'/\lambda f)|^2 dx' dy' \quad \text{and} \\
 \int_{-\infty}^{+\infty} \int_{-\infty}^{+\infty} |E_T(x, y)|^2 dx dy
 \end{aligned}$$

must be equal since they represent the total power on each side of the integrating lens L2. Hence,

$$K = 1/\lambda f \tag{2.4-10}$$

and the light amplitude in the uv plane is given

$$E_f(u, v) = 1/\lambda f \left( \frac{J}{LW} \right)^{\frac{1}{2}} \iint_A R(x, y) e^{-j2\pi(ux+vy)} dx dy \tag{2.4-11}$$

where from Eq. (2.1-7)

$$R(x, y) = R_o + r(x, y) \quad R_o \equiv \langle R(x, y) \rangle$$

The intensity in the uv plane is given

$$I'_f(u, v) = E_f(u, v) E_f^*(u, v) \tag{2.4-12}$$

Observe that  $I'_f(u, v)$  is a random variable; its expected value is

$$\begin{aligned}
 \langle I'_f(u, v) \rangle & = \frac{JLW}{\lambda f^2} |R_o|^2 (\text{sinc}^2 Lu) (\text{sinc}^2 Lv) \\
 & + \langle I'_n(u, v) \rangle.
 \end{aligned} \tag{2.4-13}$$

where

$$\text{sinc } x = \frac{\sin \pi x}{\pi x}$$

The term  $\langle I'_{n'}(u,v) \rangle$  is the contribution of the noise and is given by

$$\begin{aligned} \langle I'_{n'}(u,v) \rangle &= \frac{J}{\lambda f LW} \int_{-L/2}^{L/2} \int_{-W/2}^{W/2} \int_{-L/2}^{L/2} \int_{-W/2}^{W/2} \phi_r(x-\xi, y-\eta) \\ &\quad e^{-j2\pi [u(x-\xi) + v(y-\eta)]} dx dy d\xi d\eta \end{aligned} \quad (2.4-14)$$

With the transformation

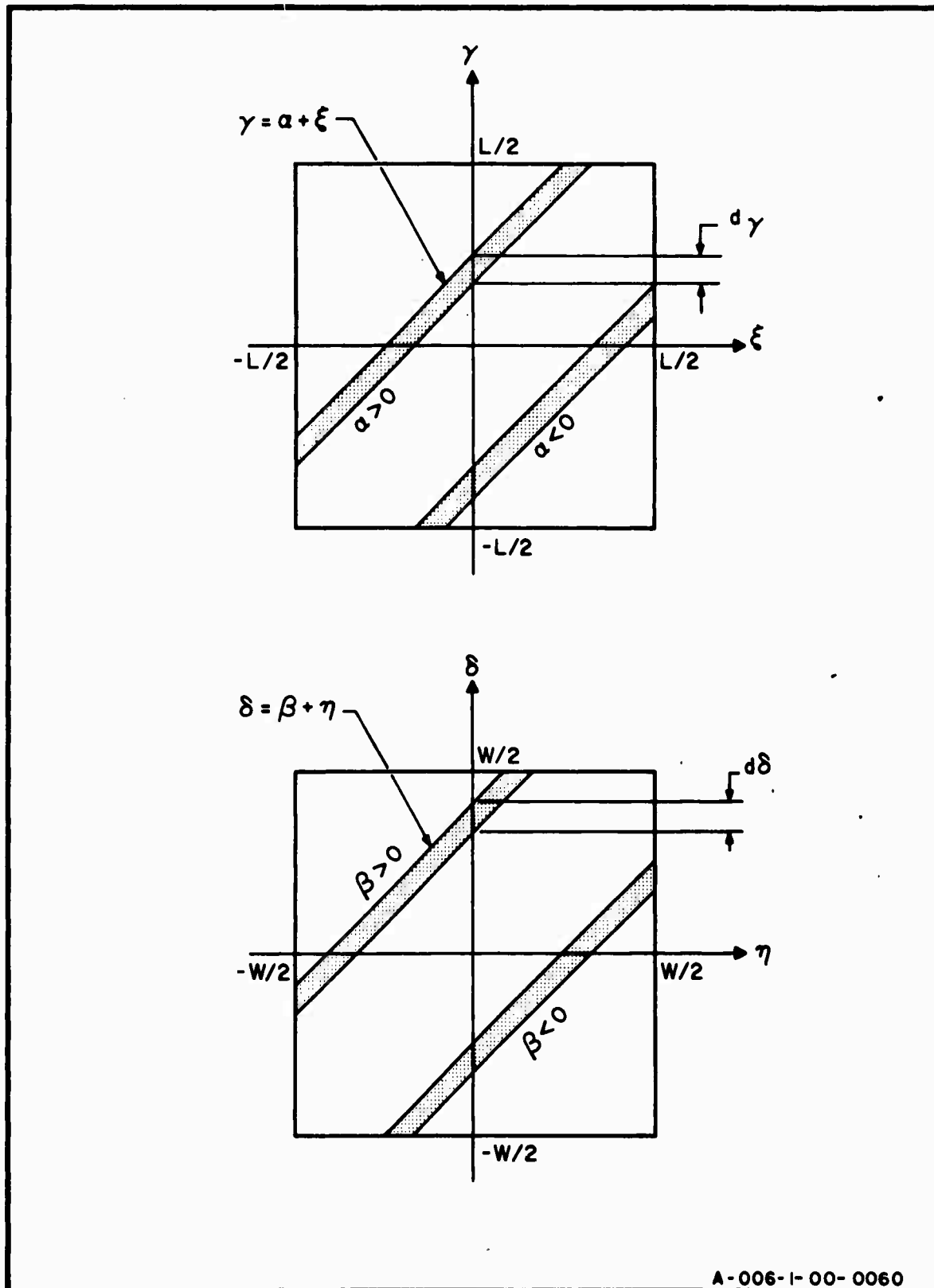
$$\begin{aligned} \alpha &= x - \xi \\ \beta &= y - \eta \\ \gamma &= x \\ \delta &= y \end{aligned} \quad (2.4-15)$$

the integral  $\langle I'_{n'}(u,v) \rangle$  can be reduced to a double integral. The Jacobian of the transformation is

$$J \left( \frac{\alpha, \beta, \gamma, \delta}{x, y, \xi, \eta} \right) = 1 \quad (2.4-16)$$

and the region of integration is a four-dimensional cube which can be described as follows: With  $\alpha$  and  $\beta$  fixed, the limits of integration on  $\gamma$  and  $\delta$  are (Fig. 2.4-3)

for $\alpha > 0$	$\alpha - L/2 \leq \gamma \leq L/2$
for $\alpha < 0$	$-L/2 \leq \gamma \leq \alpha + L/2$
for $\beta > 0$	$\beta - W/2 \leq \delta \leq W/2$
for $\beta < 0$	$-W/2 \leq \delta \leq \beta + W/2$



A-006-I-00-0060

FIG. 2.4-3 DIAGRAM FOR EVALUATING THE INTEGRAL IN EQUATION (2.4-14)

The limits of integration on  $\alpha$  and  $\beta$  are

$$\begin{array}{c} -L \leq \alpha \leq L \\ -W \leq \beta \leq W \end{array}$$

If the relative average noise intensity is defined by

$$\langle I_n(u, v) \rangle = \frac{\langle I_n(u, v) \rangle}{J/\gamma^2 f^2} \quad (2.4-17)$$

then

$$\begin{aligned} \langle I_n(u, v) \rangle &= 2 \int_0^L \int_0^W (1 - \alpha/L) (1 - \beta/W) f(\alpha, \beta, u, v) d\alpha d\beta \\ &+ \int_0^L \int_{-W}^0 (1 - \alpha/L) (1 + \beta/W) f(\alpha, \beta, u, v) d\alpha d\beta \\ &+ \int_{-L}^0 \int_0^W (1 - \alpha/L) (1 - \beta/W) f(\alpha, \beta, u, v) d\alpha d\beta \\ &+ \int_{-L}^0 \int_{-W}^0 (1 + \alpha/L) (1 + \beta/W) f(\alpha, \beta, u, v) d\alpha d\beta \end{aligned} \quad (2.4-18)$$

where

$$f(\alpha, \beta, u, v) = \phi_r(\alpha, \beta) e^{-j2\pi(\alpha u + \beta v)}$$

Using  $\phi_r(\alpha, \beta) = \phi_r^*(-\alpha, -\beta)$  and  $\phi_r(\alpha, -\beta) = \phi_r^*(-\alpha, \beta)$ , we can write Eq. (2.4-18) as

$$\begin{aligned} \langle I_n(u, v) \rangle &= 2 \int_0^L \int_0^W (1 - \alpha/L) (1 - \beta/W) \operatorname{Re}[f(\alpha, \beta, u, v) \\ &+ f(\alpha, -\beta, u, v)] d\alpha d\beta \end{aligned} \quad (2.4-19)$$

$$\begin{aligned}
&= \int_{-L}^{+L} \int_{-W}^{+W} \phi_r(\alpha, \beta) e^{-j2\pi(u\alpha+v\beta)} d\alpha d\beta \\
&- 2 \int_0^L \int_0^W (\alpha/L + \beta/W - \alpha\beta/LW) \operatorname{Re}[f(\alpha, \beta, u, v) \\
&\quad + f(\alpha, -\beta, u, v)] d\alpha d\beta \quad (2.4-20)
\end{aligned}$$

Hence, in the limit as  $L$  and  $W$  become arbitrarily large, we obtain

$$\begin{aligned}
\lim_{L, W \rightarrow \infty} I_n(u, v) &= w_r(u, v) \\
&- \lim_{L, W \rightarrow \infty} \int_0^L \int_0^W (\alpha/L + \beta/W - \alpha\beta/LW) \\
&\cdot \operatorname{Re}[f(\alpha, \beta, u, v) + f(\alpha, -\beta, u, v)] d\alpha d\beta \quad (2.4-21)
\end{aligned}$$

If the magnitude of the covariance  $\phi_r(\alpha, \beta)$  tends to zero at a rate greater than  $|\alpha\beta|^{-(1+\lambda)}$ , where  $\lambda > 0$ , in the region where  $\alpha$  is greater than some  $\alpha_m$  and  $\beta$  is greater than some  $\beta_m$ , the second term of Eq. (2.4-21) becomes zero and

$$\lim_{L, W \rightarrow \infty} I_n(u, v) = w_r(u, v). \quad (2.4-22)$$

When the covariance function is zero or negligible at all points outside a region which is small compared with the area of the aperture, an excellent approximation to an estimation of  $w_r(u, v)$  may be obtained with a finite aperture. The effect of finite apertures on the measurement of spectral densities is investigated in Chapter 3.

The astigmatic system shown in Fig. 2.4-2b can be used for obtaining one-dimensional spectral densities. If the

length of the aperture is  $D$ , the relative average light intensity as a function of  $u$  is given by

$$\langle I_f(u) \rangle = D |R_o|^2 \operatorname{sinc}^2 uD + \langle I_n(u) \rangle \quad (2.4-23)$$

where  $\langle I_n(u) \rangle$  is the relative noise intensity given by

$$\langle I_n(u) \rangle = 1/D \int_{-D/2}^{+D/2} \int_{-D/2}^{+D/2} \phi_r(x-t) e^{-j2\pi u(x-t)} dx dt \quad (2.4-24)$$

With  $\gamma = x - t$  and  $\beta = x$ , Eq. (2.4-24) can be written as the single integral

$$\begin{aligned} \langle I_n(u) \rangle &= 2 \int_0^D (1 - \alpha/D) \operatorname{Re}(\phi_r(\alpha) e^{-j2\pi u\alpha}) d\alpha \\ &- \int_{-D}^{+D} \phi_r(\alpha) e^{-j2\pi u\alpha} d\alpha \\ &- 2 \int_0^D \alpha/D \operatorname{Re}(\phi_r(\alpha) e^{-j2\pi u\alpha}) d\alpha \end{aligned} \quad (2.4-25)$$

If there exists an interval  $[-\alpha_M, \alpha_M]$  such that for all  $|\alpha| > \alpha_M$ ,  $|\phi(\alpha)|$  tends to zero at least as fast as  $\alpha^{-(1+\lambda)}$  where  $\lambda > 0$ , then

$$\lim_{D \rightarrow \infty} I_n(u) = \int_{-\infty}^{+\infty} \phi_r(\alpha) e^{-j2\pi u\alpha} d\alpha = w(u). \quad (2.4-26)$$

## 2.5 SPECTRAL MEASUREMENTS OF THE REAL PROCESSES $\{t(x,y)\}$ AND $\{\psi(x,y)\}$

When an object with complex transmittance  $R(x,y) = t(x,y) e^{j\psi(x,y)}$  is inserted into a liquid gate with refractive

index matched to the refractive index of the object, the optical path length for the coherent wave is constant across the aperture and the relative phase  $\psi(x,y) = 0$ . Hence,  $R(x,y) = t(x,y)$ , where  $t(x,y)$  is a real random variable with range

$$0 < t(x,y) < 1 \quad (2.5-1)$$

$$\langle t(x,y) \rangle = t_o$$

When a liquid gate is used in the system shown in Fig. (2.4-1), the relative light intensity in the uv plane is

$$I(u,v) \approx LW t_o^2 \operatorname{sinc}^2 uL \operatorname{sinc}^2 vW$$

$$+ 1/LW \int_{-L/2}^{L/2} \int_{-W/2}^{W/2} \int_{-L/2}^{L/2} \int_{-W/2}^{W/2} \phi_\tau(x-\xi, y-\eta)$$

$$\epsilon^{-j2\pi u(x-\xi)+v(y-\eta)} dx dy d\xi d\eta \quad (2.5-2)$$

where

$$\phi_\tau(x-\xi, y-\eta) = \langle (t(x,y) - t_o) (t(\xi, \eta) - t_o) \rangle \quad (2.5-3)$$

$$= \langle \tau(x,y) \tau(\xi, \eta) \rangle$$

If the aperture dimensions are very large compared with the largest intervals over which the random process has significant correlation then to a very good approximation

$$\langle I(u,v) \rangle \approx LW t_o^2 \operatorname{sinc}^2 uL \operatorname{sinc}^2 vW + W_\tau(u,v) \quad (2.5-4)$$

where  $W_r(u,v)$  is the power spectrum of the process  $\{\tau(x,y)\}$ .

The direct measurement of the power spectrum of the process  $\{\psi(x,y)\}$  is not so easily obtained. The reason for this is that it is generally not possible to relate the power spectrum  $W_r(u,v)$  directly to the spectra of  $\{\tau(x,y)\}$  and  $\{\psi(x,y)\}$  even if  $\{\tau(x,y)\}$  and  $\{\psi(x,y)\}$  are independent random processes. To see this, observe that the spectra  $W_\tau(u,v)$  and  $W_\psi(u,v)$ , of  $\{\tau(x,y)\}$  and  $\{\psi(x,y)\}$ , respectively, depend only on the second moments of  $\{\tau(x,y)\}$  and  $\{\psi(x,y)\}$ , while  $W_r(u,v)$  normally depends on all the moments of  $\{\psi(x,y)\}$ . When  $\{\psi(x,y)\}$  and  $\{\tau(x,y)\}$  are independent, it follows that

$$R(x,y) = t(x,y) e^{j\psi(x,y)} = t_0 e^{j\psi(x,y)} + \tau(x,y) e^{j\psi(x,y)}$$

and

(2.5-5)

$$\langle R(x,y) \rangle = R_0 = t_0 M_{\psi_{xy}}(1) \quad (2.5-6)$$

where  $M_{\psi_{xy}}(1) = e^{j\psi(x,y)}$  is the characteristic function of  $\psi(x,y)$ . Since

$$r(x,y) = \tau(x,y) e^{j\psi(x,y)} + t_0 [e^{j\psi(x,y)} - M_{\psi_{xy}}(1)], \quad (2.5-7)$$

the covariance  $\phi_r(x-\xi, y-\eta)$  is given by

$$\begin{aligned} \phi_r(x-\xi, y-\eta) &= \phi_\tau(x-\xi, y-\eta) M_{\psi_{xy}}(\xi, \eta) (1, -1) \\ &\quad + t_0^2 [M_{\psi_{xy}}(\xi, \eta) (1, -1) - M_{\psi_{\xi\eta}}(-1) M_{\psi_{xy}}(1)] \end{aligned} \quad (2.5-8)$$

where  $M_{\psi_{xy}}(\cdot, \cdot)$  is the joint characteristic function of  $\psi(x,y), \psi(\xi,\eta)$  and is given by

$$M_{\psi_{xy}}(\cdot, \cdot) = \langle e^{j[\gamma_1 \psi(x,y) + \gamma_2 \psi(\xi,\eta)]} \rangle \quad (2.5-9)$$

Now  $M_{\psi_{xy}}(1, -1)$  can be expressed as

$$M_{\psi_{xy}}(1, -1) = \sum_{k=0}^{\infty} \langle [\psi(x,y) - \psi(\xi,\eta)]^k \rangle \frac{j^k}{k!} \quad (2.5-10)$$

which clearly indicates the dependence of  $\phi_r(x-\xi, y-\eta)$  on all the moments of  $\psi(x,y)$ .

In the special case where the phase errors are small, a possibility, for example, when the matching liquid in a film gate has a refractive index slightly different from the refractive index of the transparency, and  $\{t(x,y)\}$  and  $\{\psi(x,y)\}$  are independent processes, there results

$$\begin{aligned} & \langle t(x,y) t(\xi, \eta) e^{j[\psi(x,y) - \psi(\xi, \eta)]} \rangle \\ & \approx [t_o^2 + \phi_\tau(x-\xi, y-\eta)] \cdot [1 - \phi_\psi(0,0) \\ & \quad + \phi_\psi(x-\xi, y-\eta)] \end{aligned}$$

where  $\phi_\psi(x-\xi, y-\eta) = \langle \psi(x,y) \psi(\xi, \eta) \rangle$ . Hence the relative light intensity in the uv plane is given by

$$\begin{aligned} \langle I(u,v) \rangle & \approx t_o^2 [1 - \phi_\psi(0,0)] LW \operatorname{sinc}^2 uL \operatorname{sinc}^2 vW \\ & + [1 - \phi_\psi(0,0)] w_\tau(u,v) + w_\tau * w_\psi \\ & + t_o^2 w_\psi(u,v) \end{aligned}$$

where the asterisk denotes convolution. Thus in addition to the attenuated zero-order light, the average light intensity contains terms that are proportional to the spectra of  $\{-(x,y)\}$  and  $\{\psi(x,y)\}$  and their convolution. The presence of the convolution term prevents the direct measurement of  $\{W_\psi(u,v)\}$  even if  $W(u,v)$  is known from an independent measurement. More will be said about the random processes  $\{\psi(x,y)\}$  and  $\{t(x,y)\}$  when discussing theoretical models of film noise in Chapter 1.

### 3. MEASUREMENTS OF POWER SPECTRA WITH FINITE SYSTEMS

In the previous chapter it was shown that a diffraction system with an infinite object plane aperture produces in the uv plane a light-intensity distribution whose average provides an unbiased estimate of the power spectrum of a random process. Spectral density measurements with a real system always entail the use of finite apertures and scanning slits. The principal effects of these components are to reduce the sensitivity of the system and to bias the estimates of the true spectral density.

It is generally desirable to make spectral density measurements with large-aperture systems. A large aperture reduces the bias of the measurement, allows the observation of correlation effects over large intervals, and improves the ratio of scattered spectral light to unwanted zero-order light.

If the power spectrum were available in the uv plane, then ideally the scanning slit should be an infinitely small pinhole. Such a pinhole would faithfully transmit the power spectrum to a photomultiplier tube. However, in practice, the light intensity is an observation upon a random variable whose expected value approximates the true spectrum. Hence some smoothing is desirable. The ideal slit in this case is a slit which is large enough to smooth the random fluctuations in the light intensity yet not so large as to smooth significant changes or peaks in the power spectrum.

#### 3.1 EFFECT OF A FINITE APERTURE; ASTIGMATIC SYSTEMS

The relative noise intensity given in Eq. (2.4-25) and obtained with a one-dimensional diffraction system can be written as

$$\begin{aligned}
 \langle I_n(u) \rangle &= \int_{-D}^{+D} \left(1 - \frac{|\alpha|}{D}\right) \phi(\alpha) e^{-j2\pi u \alpha} d\alpha \\
 &= \int_{-\infty}^{+\infty} \left(1 - \frac{|\alpha|}{D}\right) \text{rect } \alpha/2D \phi(\alpha) e^{-j2\pi u \alpha} d\alpha \\
 &\equiv \tilde{W}(u)
 \end{aligned} \tag{3.1-1}$$

where  $\phi(\alpha)$  is the covariance of the process,  $\text{rect } \alpha/2D$  is defined by Eq. (2.4-5), and  $W(u)$  is the system-generated power spectrum or apparent power spectrum of the random process. The Fourier transform of Eq. (3.1-1) is the convolution of the true power spectrum and the Fourier transform of the triangular function

$$h(\gamma) = \left(1 - \frac{|\alpha|}{D}\right) \text{rect } \alpha/2D \tag{3.1-2}$$

Hence,

$$\tilde{W}(u) = D \int_{-\infty}^{+\infty} W(\zeta) \text{sinc}^2(u - \zeta)D d\zeta \tag{3.1-3}$$

where

$$\text{sinc}^2 x = \left( \frac{\sin \pi x}{\pi x} \right)^2 \tag{3.1-4}$$

and  $D \text{sinc}^2 uD$  is the Fourier transform of  $h(\alpha)$ . Equation (3.1-4) clearly describes the effect of the finite aperture of the spectrum.  $\tilde{W}(u)$  is the result of averaging over frequency the spectrum  $W(\zeta)$  with weights proportional to  $H(u - \zeta) = D \text{sinc}^2(u - \zeta)D$ . In the terminology of communication theory (Blackman & Tukey 1958),  $H(u)$  is the spectral window corresponding to the spatial lag window  $h(\alpha)$ . From Eq. (3.1-3) it is seen that  $\tilde{W}(u)$  is a biased estimate of  $W(u)$ . The degree of bias

depends on  $D$  and on  $W(u)$ . For large apertures the significant averaging over frequency is confined to frequencies near  $u$ , and  $W(u)$  would be expected to be a better replica of  $W(u)$  than if small apertures were used, for which the averaging would extend over a large frequency spread. Since over 90° of the area of  $\text{sinc}^2(u-\zeta)D$  lies under the main lobe and the largest sidelobe (the first) is 13 db below the peak of the main lobe, most of the averaging is done over the frequency interval  $-1/D \leq u - \zeta \leq 1/D$ . Nevertheless, the contributions of the sidelobes are undesirable since they involve frequencies "far" removed from  $u = \zeta$  and thus tend to distort the spectrum. The problem of confining the smoothing to the main lobe is tantamount to finding a function with a low sidelobe response and a reasonably narrow main lobe. This problem has been extensively treated by several authors (Dolph 1946, Jacquinot and Roizen-Dossier 1966). In optics, sidelobe reduction can be achieved by apodisation. Apodisation may be accomplished by using either light-absorbing aperture functions (also called pupil functions) or contoured apertures. Advantages and drawbacks of the methods are discussed in Chapter 6.

In the measurement of power spectra by diffraction, a principal reason for apodising is to reduce the zero-order diffracted light of the aperture, i.e., the term that always appears with  $\langle I_n(u) \rangle$  or  $\langle I_n(u,v) \rangle$  as in Eqs. (2.4-23) or (2.4-13). This unwanted light must be suppressed if observations are to be made on the power spectrum.

When it may be presumed that the least distance over which there are significant changes in  $W(u)$  are small compared to  $1/D$ , the form of  $W(u)$  is essentially reproduced in  $\tilde{W}(u)$ . When  $D$  is made arbitrarily large,

$$\lim_{D \rightarrow \infty} D \text{sinc}^2 uD = \begin{cases} \infty & u = 0 \\ 0 & u \neq 0 \end{cases}$$

and

$$\lim_{D \rightarrow \infty} \tilde{W}(u) = \int_{-\infty}^{+\infty} W(\zeta) \delta(u - \zeta) d\zeta = W(u)$$
(3.1-5)

The bias introduced by a finite aperture is the difference between  $W(u)$  and  $\tilde{W}(u)$ . It will now be shown that the bias depends on the Hilbert transform of  $W(u)$ . Since  $\phi^*(-\alpha) = \phi(\alpha)$ , it follows that

$$W(u) = \int_{-\infty}^{+\infty} \phi(\alpha) e^{-j2\pi u\alpha} d\alpha = \int_{-\infty}^{+\infty} \phi^*(\alpha) e^{+j2\pi u\alpha} d\alpha$$
(3.1-6)

The truncated spectrum  $W^D(u)$  is defined by

$$W^D(u) = \int_{-D}^{+D} \phi(\alpha) e^{-j2\pi u\alpha} d\alpha$$
(3.1-7)

and the truncation error  $\sigma(u, D)$  is defined by

$$\sigma(u, D) = W(u) - W^D(u) = 2\operatorname{Re} \int_D^\infty \phi^*(\alpha) e^{+j2\pi u\alpha} d\alpha$$
(3.1-8)

where  $\sigma(u, \infty) = 0$ . The Hilbert transform of  $W^D(u)$  is given by

$$\begin{aligned} \hat{W}^D(u) &= \int_0^D \phi^*(\alpha) e^{j(2\pi u\alpha - \pi/2)} d\alpha \\ &\quad + \int_{-D}^0 \phi^*(\alpha) e^{j(2\pi u\alpha + \pi/2)} d\alpha \\ &= 2\operatorname{Re} \int_0^D (-j) e^{j2\pi u\alpha} \phi^*(\alpha) d\alpha \end{aligned}$$
(3.1-9)

where  $\hat{\cdot}$  denotes the Hilbert transform.

Hence from Eqs. (2.4-25), (3.1-7), and (3.1-9) there results

$$\hat{w}(u) = w^D(u) - \frac{1}{2\pi D} \frac{d}{du} \hat{w}^D(u) \quad (3.1-10)$$

and the bias is given by

$$w(u) - \hat{w}(u) = \sigma(u, D) + \frac{1}{2\pi D} \frac{d}{du} (\hat{w}(u) - \hat{\sigma}(u, D)) \quad (3.1-11)$$

Equation (3.1-11) shows that the error in measuring the spectrum results from two effects. First, observe that  $\hat{w}(u)$  is independent of  $D$  and therefore  $\frac{1}{2\pi D} \frac{d}{du} \hat{w}(u)$  decreases inversely with increasing  $D$ . This error could be called the resolution error since it is independent of the truncation of  $\phi(\alpha)$ . The terms involving  $\sigma(u, D)$  and  $\frac{d}{du} [\hat{\sigma}(u, D)]$  are truncation errors since they vanish when  $D$  is chosen large enough to include all the correlation intervals of the random process. For example, suppose that  $\phi(\alpha)$  is zero (or at least negligibly small) outside an interval  $A$ , centered at the origin with  $A < 2D$ . Then the limits in Eq. (3.1-7) can be changed to  $(-\infty, \infty)$  and  $\sigma(u, D) = 0$  for all  $u$ . In this case there is no contribution to the bias from truncation although there is still a bias due to the resolution error. In the spatial domain the bias is manifested as a nonuniform attenuation of  $\phi(\alpha)$ . This may be seen as follows. The Fourier transform of Eq. (3.1-3) gives

$$\tilde{\phi}(\alpha) = \phi(\alpha) h(\alpha) \quad (3.1-12)$$

where

$$h(\alpha) = (1 - \frac{|\alpha|}{D}) \text{rect} \frac{\alpha}{2D}$$

indicating that  $\phi(\alpha)$  can be recovered from the apparent covariance  $\tilde{\phi}(\alpha)$  from the inverse operation

$$\phi(\alpha) = \tilde{\phi}(\alpha) h^{-1}(\alpha) \quad (3.1-13)$$

This situation is shown in Fig. 3.1-1a.

When the truncation error is not zero,  $\phi(\alpha)$  cannot be recovered from  $\tilde{\phi}(\alpha)$  since there is no information about the covariance for intervals greater than D. This situation is shown in Fig. 3.1-1b.

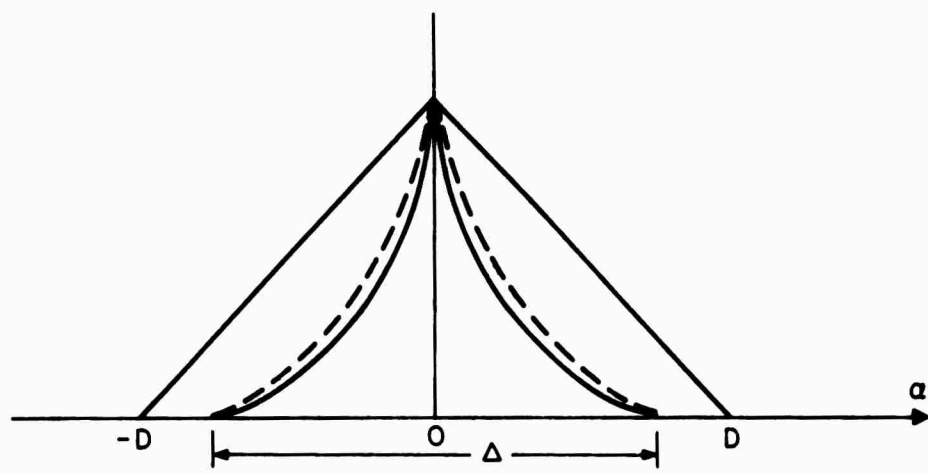
### 3.2 EFFECT OF A FINITE APERTURE; ORDINARY SYSTEMS

The situation in two dimensions is essentially a direct extension of the one-dimensional case. Equation (2.4-18) can be written as

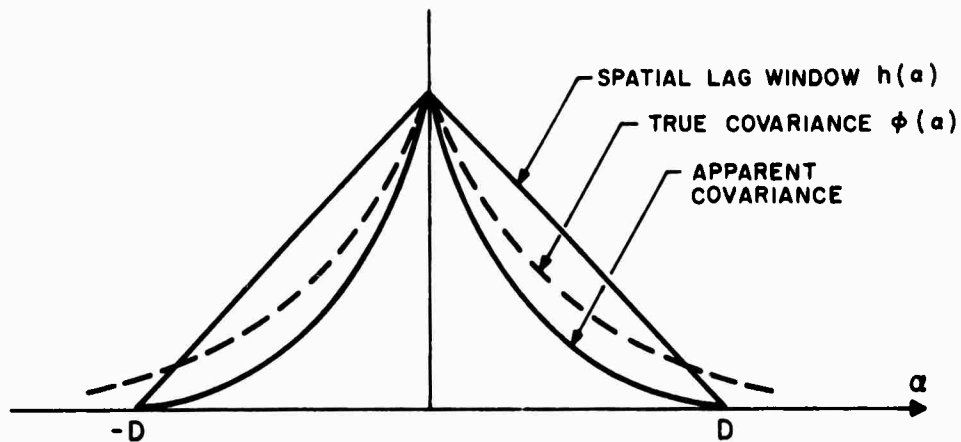
$$\begin{aligned} \langle I_n(u, v) \rangle &= \int_{-\infty}^{+\infty} \int_{-\infty}^{+\infty} (1 - \frac{|\alpha|}{L}) \text{rect} \frac{\alpha}{2L} (1 - \frac{|\beta|}{W}) \text{rect} \frac{\beta}{2W} \\ &\quad \cdot \phi(\alpha, \beta) e^{-j2\pi (u\alpha + v\beta)} d\alpha d\beta \\ &= \tilde{W}(u, v) \end{aligned} \quad (3.2-1)$$

where  $\phi(\alpha, \beta)$  is the covariance of the two-dimensional random process,  $\tilde{W}(u, v)$  is the apparent spectrum, and all other quantities have been defined earlier. Two-dimensional Fourier transforms have properties similar to one-dimensional transforms (Sneddon 1951). Thus, the above may be written as the convolution of the true spectrum  $W(u, v)$  and  $H(u, v) = LW \text{sinc}^2 uL \cdot \text{sinc}^2 vW$ . This gives

$$\begin{aligned} \tilde{W}(u, v) &= W(u, v) * H(u, v) \\ &= LW \int_{-\infty}^{+\infty} \int_{-\infty}^{+\infty} W(\zeta, \eta) \text{sinc}^2(u - \zeta) L \text{sinc}^2(v - \eta) W d\zeta d\eta \end{aligned} \quad (3.2-2)$$



a) DISTORTION OF THE COVARIANCE IN ABSENCE OF A TRUNCATION ERROR



b) DISTORTION OF THE COVARIANCE IN PRESENCE OF A TRUNCATION ERROR

A-006-1-00-0061

FIG.3.1-1 EFFECT OF FINITE APERTURE (WIDTH=D) ON COVARIANCE ESTIMATE

The apparent covariance,  $\tilde{\phi}(\alpha, \beta) = F^{-1} \{ \tilde{W}(u, v) \}$  is, from Eq. (3.2-1),

$$\begin{aligned}\tilde{\phi}(\alpha, \beta) &= (1 - \frac{|\alpha|}{L})(1 - \frac{|\beta|}{W}) \operatorname{rect} \frac{\alpha}{2L} \operatorname{rect} \frac{\beta}{2W} \phi(\alpha, \beta) \\ &\equiv h(\alpha, \beta) \phi(\alpha, \beta)\end{aligned}\quad (3.2-3)$$

When  $\phi(\alpha, \beta)$  is non-negative,  $\tilde{\phi}(\alpha, \beta)$  is always less than  $\phi(\alpha, \beta)$  except at nulls and the point  $\alpha = \beta = 0$ , where  $\tilde{\phi}(0, 0) = \phi(0, 0)$ . Hence,

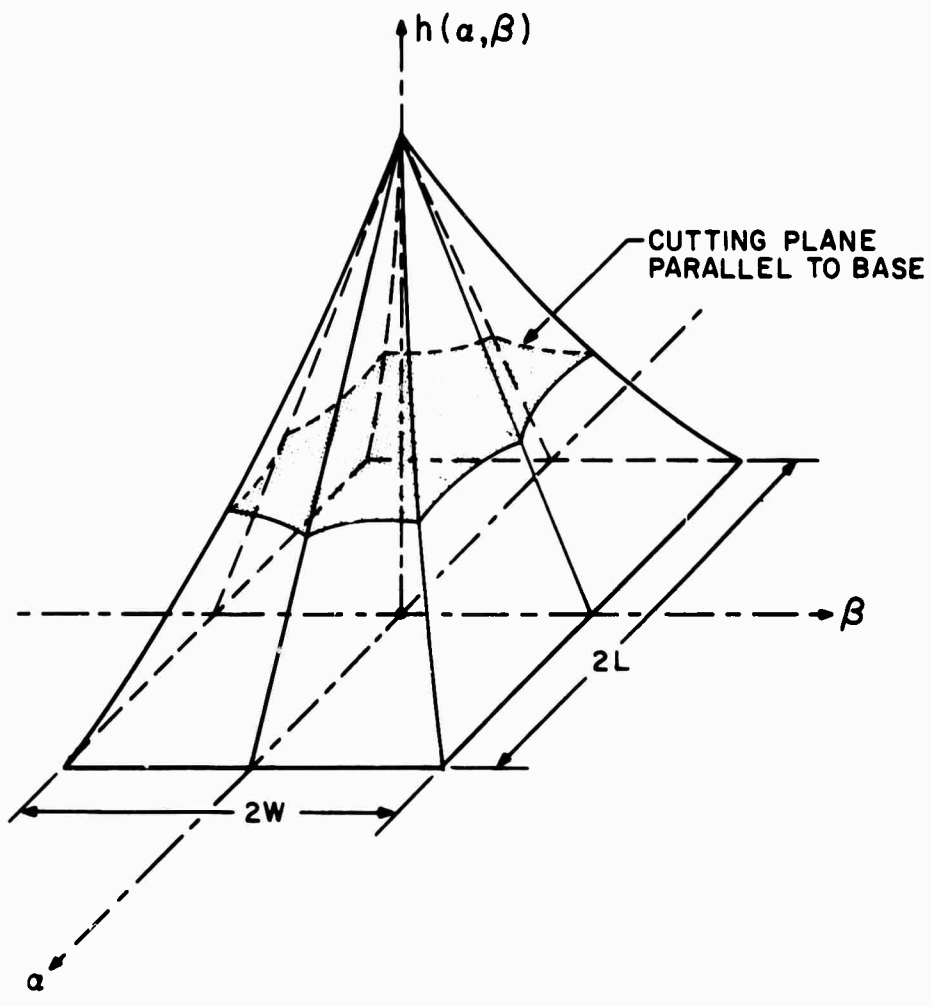
$$\int_{-\infty}^{+\infty} \int_{-\infty}^{+\infty} \tilde{W}(u, v) du dv = \int_{-\infty}^{+\infty} \int_{-\infty}^{+\infty} W(u, v) du dv \quad (3.2-4)$$

The function  $h(\alpha, \beta)$  is shown in Fig. 3.2-1 and is a pyramid of height unity and with base dimensions  $2L$  and  $2W$ . If  $\phi(\alpha, \beta)$  is zero for all points outside the base of  $h(\alpha, \beta)$ , that is, for points  $|\alpha| > L$ ,  $|\beta| > W$ , then by analogy with the one-dimensional results, there is no truncation error and the true spectrum can be recovered from the measured spectrum by digital-computer filtering. For example,  $W(u, v)$  can be obtained from

$$W(u, v) = F \left\{ \frac{F^{-1} \{ \tilde{W}(u, v) \}}{h(\alpha, \beta)} \right\} \quad |\alpha| < L, |\beta| < W \quad (3.2-5)$$

Optical spatial filtering of  $\tilde{W}(u, v)$  is investigated in Sec. (3.5).

From Eq. (3.2-2) it can be seen that  $L$  and  $W$  must both be large for  $\tilde{W}(u, v)$  to be a reasonable replica of  $W(u, v)$ . Thus, for example as an extreme case, if only  $L$  is large while  $W$  is small,  $\tilde{W}(u, v)$  would be given by



$$\tilde{\phi}(\alpha, \beta) = h(\alpha, \beta) \phi(\alpha, \beta)$$

WHERE

$\tilde{\phi}(\alpha, \beta)$  = EXPERIMENTALLY GENERATED COVARIANCE

$\phi(\alpha, \beta)$  = TRUE COVARIANCE OF PROCESS

A-006-1-00-0062

FIG. 3.2-1 ILLUSTRATING THE FUNCTION  $h(\alpha, \beta)$  OF EQUATION (3.2-3) FOR A RECTANGULAR APERTURE OF WIDTH W AND LENGTH L

$$\begin{aligned}\tilde{W}(u,v) &\approx W \int_{-\infty}^{+\infty} \int_{-\infty}^{+\infty} w(\zeta, \eta) \delta(u-\zeta) \operatorname{sinc}^2(v-\eta) W d\zeta d\eta \\ &\approx W \int_{-\infty}^{+\infty} w(u, \eta) d\eta\end{aligned}\quad (3.2-6)$$

where it has been assumed that over the frequencies for which  $w(\zeta, \eta)$  is not negligible,  $W \operatorname{sinc}^2(v-\eta) W$  is essentially constant. With both  $L$  and  $W$  arbitrarily large

$$\begin{aligned}\tilde{W}(u,v) &\approx \int_{-\infty}^{+\infty} w(\zeta, \eta) \delta(u-\zeta) \delta(v-\eta) d\zeta d\eta \\ &= W(u,v)\end{aligned}\quad (3.2-7)$$

The effect of the aperture function  $H(u,v)$  is to average the true spectrum over frequencies centered about  $u = \zeta$  and  $v = \eta$  with weights proportional to  $H(u-\zeta, v-\eta)$ . If  $L^{-1}$  and  $W^{-1}$  are small compared with the least distances by which  $W(u,v)$  changes by any significant amount,  $\tilde{W}(u,v)$  will be a reasonably good replica of  $W(u,v)$ . The degree of bias is again a function of the truncation and resolution errors. Before computing the bias error,  $W(u,v) - \tilde{W}(u,v)$ , it is convenient to introduce some transforms which, by direct analogy with the ordinary Hilbert transform, will be referred to as two-dimensional Hilbert transforms.

### 3.3 TWO-DIMENSIONAL HILBERT TRANSFORMS

This section is a brief digression from the main work of this chapter. In what follows, certain Hilbert transform-type integrals are derived for functions of two variables. The results of this section will be used in the following section to derive the bias in the system-generated spectrum  $\tilde{W}(u,v)$ .

The notation used in this section is unrelated to the notation used elsewhere in this chapter. Thus, for example, the reader should refrain from associating  $(\alpha, \beta)$  with the spatial "lag" domain and  $(u, v)$  with the spatial frequency domain.

Although the Hilbert transform has been used in Sec. 3.1, it is best to begin this section with its formal definition. The ordinary Hilbert transform of a function  $x(\alpha)$  is defined as the Cauchy principal value (C.P.V.) of the integral

$$\hat{x}(\alpha) = (1/\pi) \int_{-\infty}^{+\infty} \frac{x(\lambda)}{\alpha - \lambda} d\lambda \quad (3.3-1)$$

where  $\hat{x}(\alpha)$  denotes the Hilbert transform of  $x(\alpha)$  (Titchmarsh 1948). The function  $x(\alpha)$  can be recovered from  $\hat{x}(\alpha)$  by the C.P.V. of the integral

$$x(\alpha) = (-1/\pi) \int_{-\infty}^{+\infty} \frac{\hat{x}(\lambda)}{\alpha - \lambda} d\lambda \quad (3.3-2)$$

If  $X(u)$  denotes the Fourier transform of  $x(\alpha)$  and  $Y(u)$  denotes the Fourier transform of  $\hat{x}(\alpha)$ , then

$$\begin{aligned} Y(u) &= -jX(u) & u > 0 \\ &= +jX(u) & u < 0 \end{aligned} \quad (3.3-3)$$

The substitution of Eq. (3.3-1) into Eq. (3.3-2) gives

$$x(\alpha) = (-1/\pi^2) \int_{-\infty}^{+\infty} d\lambda x(\lambda) \int_{-\infty}^{+\infty} \frac{d\zeta}{(\lambda - \zeta)(\zeta - \alpha)} \quad (3.3-4)$$

Hence,

$$(-1/\pi^2) \int_{-\infty}^{+\infty} \frac{d\zeta}{(\lambda - \zeta)(\zeta - \alpha)} = \delta(\lambda - \alpha) \quad (3.3-5)$$

Consider now the C.P.V. about  $\alpha = \zeta$  and  $\beta = \eta$  of the following integrals

$$\hat{x}(\alpha, \beta) = (1/\pi^2) \int_{-\infty}^{+\infty} \int_{-\infty}^{+\infty} \frac{x(\zeta, \eta)}{(\alpha - \zeta)(\beta - \eta)} d\zeta d\eta \quad (3.3-6)$$

$$g(\alpha, \beta) = (1/\pi^2) \int_{-\infty}^{+\infty} \int_{-\infty}^{+\infty} \frac{\hat{x}(\zeta, \eta)}{(\alpha - \zeta)(\beta - \eta)} d\zeta d\eta \quad (3.3-7)$$

Define the following quantities ( $F \{ \cdot \}$  = Fourier transform)

$$L(u, v) = F \left\{ \frac{1}{\pi^2 \alpha \beta} \right\}$$

$$X(u, v) = F \{ x(\alpha, \beta) \}$$

$$Y(u, v) = F \{ \hat{x}(\alpha, \beta) \}$$

$$G(u, v) = F \{ g(\alpha, \beta) \}.$$

For  $L(u, v)$  there results

$$\begin{aligned} L(u, v) &= (1/\pi^2) \int_{-\infty}^{+\infty} \int_{-\infty}^{+\infty} e^{-j2\pi(u\alpha+v\beta)} \frac{d\alpha d\beta}{\alpha \beta} \\ &= (1/j\pi) \int_{-\infty}^{+\infty} \frac{\sin 2\pi u\alpha}{\alpha} d\alpha \cdot 1/j\pi \int_{-\infty}^{+\infty} \frac{\sin 2\pi v\beta}{\beta} d\beta \end{aligned} \quad (3.3-8)$$

Since

$$\begin{aligned} (1/j\pi) \int_{-\infty}^{+\infty} \frac{\sin tx}{x} dx &= -j \quad t > 0 \\ &= +j \quad t < 0 \end{aligned} \quad (3.3-9)$$

it follows that

$$\begin{aligned} L(u,v) &= -1 & uv &> 0 \\ &= +1 & uv &< 0 \end{aligned} \quad (3.3-10)$$

If the Fourier transform is taken of both sides of Eqs. (3.3-6) and (3.3-7), then

$$Y(u,v) = X(u,v) L(u,v) \quad (3.3-11)$$

$$G(u,v) = Y(u,v) L(u,v) \quad (3.3-12)$$

Hence  $G(u,v) = X(u,v) L^2(u,v) = X(u,v)$ , and it is established that

$$x(\alpha, \beta) = g(\alpha, \beta) \quad (3.3-13)$$

This result could also have been achieved by direct substitution of Eq. (3.3-6) into Eq. (3.3-7) and using Eq. (3.3-5).

Equations (3.3-6) and (3.3-7) are the two-dimensional analogs of Eqs. (3.3-1) and (3.3-2) and hence  $\hat{x}(\alpha, \beta)$  can be viewed as the two-dimensional Hilbert transform of  $x(\alpha, \beta)$ . For what follows it is also useful to define the quantities  $\hat{x}_\alpha(\alpha, \beta)$  and  $\hat{x}_\beta(\alpha, \beta)$  by

$$\hat{x}_\alpha(\alpha, \beta) = (1/\pi) \int_{-\infty}^{+\infty} \frac{x(\alpha, \beta)}{\alpha - \zeta} d\zeta \quad (3.3-14)$$

$$\hat{x}_\beta(\alpha, \beta) = (1/\pi) \int_{-\infty}^{+\infty} \frac{x(\alpha, \beta)}{\beta - \zeta} d\zeta \quad (3.3-15)$$

### 3.4 THE BIAS ERROR IN THE APPARENT SPECTRUM $\tilde{W}(u,v)$

The results of the previous chapter enable the writing of the two-dimensional Hilbert transform of the true power spectrum  $W(u,v)$  as

$$\hat{W}(u, v) = -2 \int_0^{\infty} \int_0^{\infty} \operatorname{Re} [f(\alpha, \beta, u, v) - f(\alpha, -\beta, u, v)] d\alpha d\beta \quad (3.4-1)$$

where

$$f(\alpha, \beta, u, v) = \phi(\alpha, \beta) e^{-j2\pi(u\alpha+v\beta)}$$

Assuming that differentiating inside the integral sign is permitted,\* there results

$$\frac{1}{(2\pi)^2 LW} \frac{\partial^2 \hat{W}(u, v)}{\partial u \partial v} = 2 \int_0^{\infty} \int_0^{\infty} \frac{\alpha \beta}{LW} \operatorname{Re} [f(\alpha, \beta, u, v) + f(\alpha, -\beta, u, v)] d\alpha d\beta \quad (3.4-2)$$

In deriving Eq. (3.4-1) use was made of the fact that  $W(u, v)$  could be written as

$$W(u, v) = \int_{-\infty}^{+\infty} \int_{-\infty}^{+\infty} \phi^*(\alpha, \beta) e^{j2\pi(u\alpha+v\beta)} d\alpha d\beta \quad (3.4-3)$$

Similarly,

$$\frac{1}{2\pi L} \frac{\partial \hat{W}_u(u, v)}{\partial u} = 2 \int_0^{\infty} \int_0^{\infty} \frac{\alpha}{L} \operatorname{Re} [f(\alpha, \beta, u, v) + f(\alpha, -\beta, u, v)] d\alpha d\beta \quad (3.4-4)$$

---

\* This requires that the integrand in Eq. 3.4-1 has sectionally continuous partial derivatives with respect to  $u, v$  and the integrals in Eqs. (3.4-1) and (3.4-2) converge uniformly (Courant, Vol III, "Differential and Integral Calculus.")

and

$$\frac{1}{2\pi W} \frac{\partial \hat{W}_v(u, v)}{\partial v} = 2 \int_0^\infty \int_0^\infty \frac{\beta}{W} \operatorname{Re} [f(\alpha, \beta, u, v) + f(\alpha, -\beta, u, v)] d\alpha d\beta \quad (3.4-5)$$

where

$$\hat{W}_u(u, v) = (1/\pi) \int_{-\infty}^{+\infty} \frac{w(\zeta, v)}{u - \zeta} d\zeta \quad (3.4-6)$$

and

$$\hat{W}_v(u, v) = (1/\pi) \int_{-\infty}^{+\infty} \frac{w(u, \zeta)}{v - \zeta} d\zeta \quad (3.4-7)$$

Let the truncated spectrum  $w^{(L, W)}(u, v)$  and the truncation error  $\sigma(u, v, L, W)$  be defined by

$$w^{(L, W)}(u, v) \equiv \int_{-L}^L \int_{-W}^W \phi(\alpha, \beta) e^{-j2\pi(u\alpha+v\beta)} d\alpha d\beta \quad (3.4-8)$$

$$\sigma(u, v, L, W) \equiv w(u, v) - w^{(L, W)}(u, v) \quad (3.4-9)$$

Then Eq. (2.4-20) can be written with  $\langle I_n(u, v) \rangle \equiv \tilde{w}(u, v)$ , as

$$\begin{aligned} \tilde{w}(u, v) &= w^{(L, W)}(u, v) - \frac{1}{2\pi L} \frac{\partial}{\partial u} \hat{W}_u^{(L, W)}(u, v) \\ &\quad - \frac{1}{2\pi W} \frac{\partial}{\partial v} \hat{W}_v^{(L, W)}(u, v) \\ &\quad + \frac{1}{(2\pi)^2 LW} \frac{\partial^2}{\partial u \partial v} \hat{W}^{(L, W)}(u, v) \end{aligned} \quad (3.4-10)$$

When Eq. (3.4-1) is used, the bias  $W(u,v) - \tilde{W}(u,v)$  can be written as

$$\begin{aligned}
 W(u,v) - \tilde{W}(u,v) &= \frac{1}{2\pi L} \frac{\partial}{\partial u} \hat{W}_u(u,v) + \frac{1}{2\pi L} \frac{\partial}{\partial v} \hat{W}_v(u,v) \\
 &- \frac{1}{(2\pi)^2 LW} \frac{\partial^2}{\partial u \partial v} \hat{W}(u,v) \\
 &+ \text{terms involving the truncation error,} \\
 &\quad \text{its derivatives and transforms.}
 \end{aligned}$$

(3.4-11)

It may be seen from Eq. (3.4-8) that the truncation error is identically zero for all  $u,v$  if  $\phi(\alpha,\beta)$  is zero outside a region bounded by  $|\alpha| > L$ ,  $|\beta| > W$ . In this situation, the only remaining error in the measurement of  $\tilde{W}(u,v)$  is the resolution error which, in principle at least, can be corrected to yield  $W(u,v)$ . The spatial filtering of  $\tilde{W}(u,v)$  or  $W(u,v)$ , as the case may be, is discussed next.

### 3.5 SPATIAL FILTERING

When the truncation error is insignificant compared with the resolution error, the bias in the measured spectrum may be eliminated by further processing. This is implied by Eq. (3.2-5) which is, perhaps, the way a digital computer might proceed. In this section, the feasibility of spatial filtering is considered, and it is shown that direct spatial filtering is not physically realizable.

Consider a one-dimensional system first. The true covariance  $\phi(\tau)$  is given by

$$\phi(\tau) = g(\tau) \tilde{\phi}(\tau) \quad (3.5-1)$$

where

$$g(\alpha) = \begin{cases} (1 - \frac{|\alpha|}{D})^{-1} & |\alpha| < D \\ 0 & \text{otherwise} \end{cases} \quad (3.5-2)$$

and it is assumed that  $\phi(\alpha) = 0$  or is insignificant for  $|\alpha| > D$ . If  $G(u)$  denotes the Fourier transform of  $g(\alpha)$ , then the Fourier transform of Eq. (3.5-1) gives

$$W(u) = G(u) * \tilde{W}(u) \quad (3.5-3)$$

This operation can be performed optically in the frequency plane by collecting  $\tilde{W}(u)$  through a filter with intensity transmission function  $G(u)$  and integrating over the  $u$  domain with a photomultiplier tube. In order for the operation expressed in Eq. (3.5-3) to have any physical significance,  $G(u)$  should satisfy the following three conditions:

- (i)  $\lim_{u \rightarrow \infty} G(u) = 0$
- (ii)  $G(u)$  should be real  $-\infty < u < \infty$
- (iii)  $G(u) \geq 0 \quad -\infty < u < \infty$  (3.5-4)

Condition (i) requires that any degree of accuracy in reconstructing  $W(u)$  can be achieved by using a filter of finite dimensions. Conditions (ii) and (iii) reflect the fact that  $\tilde{W}(u)$  and  $W(u)$  are intensities and therefore are nonnegative, real quantities.

That  $G(u)$  satisfies condition (i) is easily demonstrated by the Riemann-Lebesgue lemma which states that if a function  $x(\alpha)$  is integrable on  $[\alpha, \beta]$ , then

$$\lim_{u \rightarrow \infty} \int_a^b x(\alpha) \cos 2\pi u\alpha d\alpha = 0 \quad (3.5-5)$$

Since  $(1 - \frac{|\alpha|}{D})^{-1}$  is integrable on  $[0, \Delta]$  for  $\Delta < D$ , it follows that

$$\lim_{u \rightarrow \infty} 2 \int_0^{\Delta} \frac{\cos 2\pi u \alpha}{1 - |\alpha|/D} d\alpha = 0$$

The function  $g(\alpha)$  is real and even. This requires that  $G(u)$  be a real function of  $u$ . Finally, to test condition (iii), observe that at  $u = 1/2\Delta$ ,

$$\begin{aligned} G(1/2\Delta) &= 2D \int_0^{\pi} \frac{\cos \beta d\beta}{\pi\lambda - \beta} \\ &= 2D \int_0^{\pi/2} \cos \beta \left[ \frac{1}{\pi\lambda - \beta} - \frac{1}{\pi(\lambda-1) + \beta} \right] d\beta \end{aligned} \quad (3.5-6)$$

where  $\lambda = D/\Delta$ . In the interval  $[0, \pi/2]$ ,  $\cos \beta > 0$ . Now  $G(1/2\Delta)$  will be negative if  $1/(\pi(\lambda-1) + \beta) > 1/(\pi\lambda - \beta)$  for all  $\beta$  in  $[0, \pi/2]$ ; however, this will be true if  $2\beta/\pi < 1$  for all  $\beta$  in  $[0, \pi/2]$ . Clearly this is so, proving that  $G(1/2\Delta) < 0$ . Hence,  $G(u)$  violates condition (iii) and cannot correspond to a physically realizable filter.

The function  $G(u)$  can be written in terms of tabulated functions (Jahnke & Emde 1945) as follows:

$$\begin{aligned} G(u) &= D \cos 2\pi uD [Ci(2\pi uD) - Ci(2\pi uD\Gamma)] \\ &\quad + D \sin 2\pi uD [Si(2\pi uD) - Si(2\pi uD\Gamma)] \end{aligned} \quad (3.5-7)$$

where

$$Ci(x) = - \int_x^{\infty} \frac{\cos \zeta}{\zeta} d\zeta \quad (3.5-8)$$

$$Si(x) = \int_0^x \frac{\sin \zeta}{\zeta} d\zeta$$

and  $\Gamma = 1 - \Delta/D < 1$ .

$G(u)$  is plotted in Fig. 3.5-1.

The analog of Eq. (3.5-1) in two dimensions is

$$\phi(\alpha, \beta) = g(\alpha, \beta) \tilde{\phi}(\alpha, \beta)$$

where

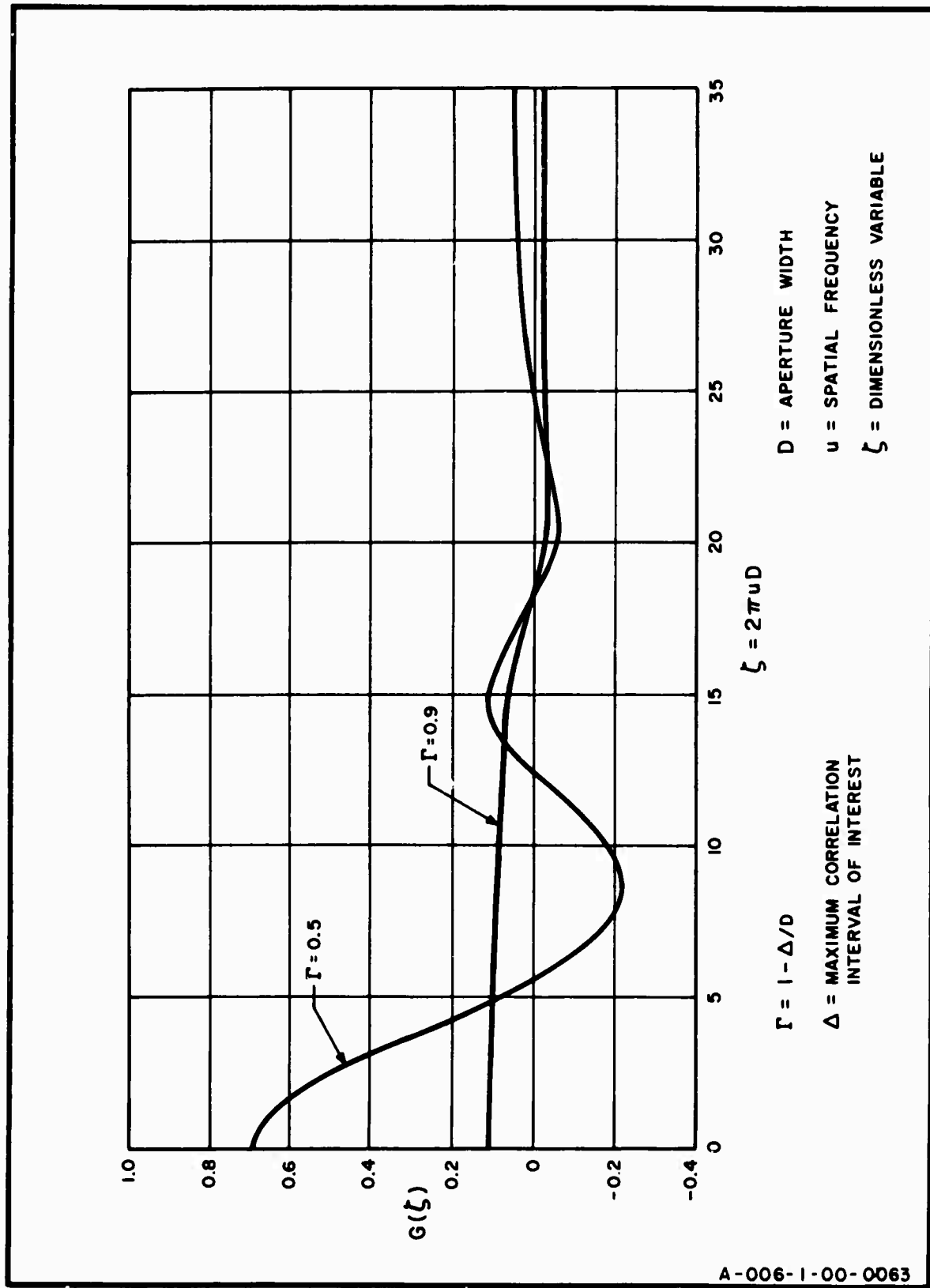
$$h(\alpha, \beta) = \left(1 - \frac{|\alpha|}{L}\right) \left(1 - \frac{|\beta|}{W}\right) \text{ for } |\alpha| < L, \\ |\beta| < W \\ = 0 \quad \text{otherwise.} \quad (3.5-9)$$

The function  $g(\alpha, \beta)$  which would rectify the distortion is

$$g(\alpha, \beta) = [h(\alpha, \beta)]^{-1} \quad \begin{matrix} |\alpha| < \Delta_1 < L \\ |\beta| < \Delta_2 < W \end{matrix} \\ . \quad (3.5-10)$$

where  $\Delta_1$  and  $\Delta_2$  are intervals beyond which  $\phi(\alpha, \beta) = 0$ .  
Clearly if  $G(u, v) = F\{g(\alpha, \beta)\}$ , then

$$G(u, v) = \int_{-\infty}^{+\infty} \int_{-\infty}^{+\infty} g(\alpha, \beta) e^{-j2\pi(u\alpha+v\beta)} d\alpha d\beta \\ = G(u) G(v). \quad (3.5-11)$$



A-006-1-00-0063

FIG. 3.5-1 SPATIAL FILTER CHARACTERISTICS REQUIRED FOR FILTERING POWER SPECTRUM

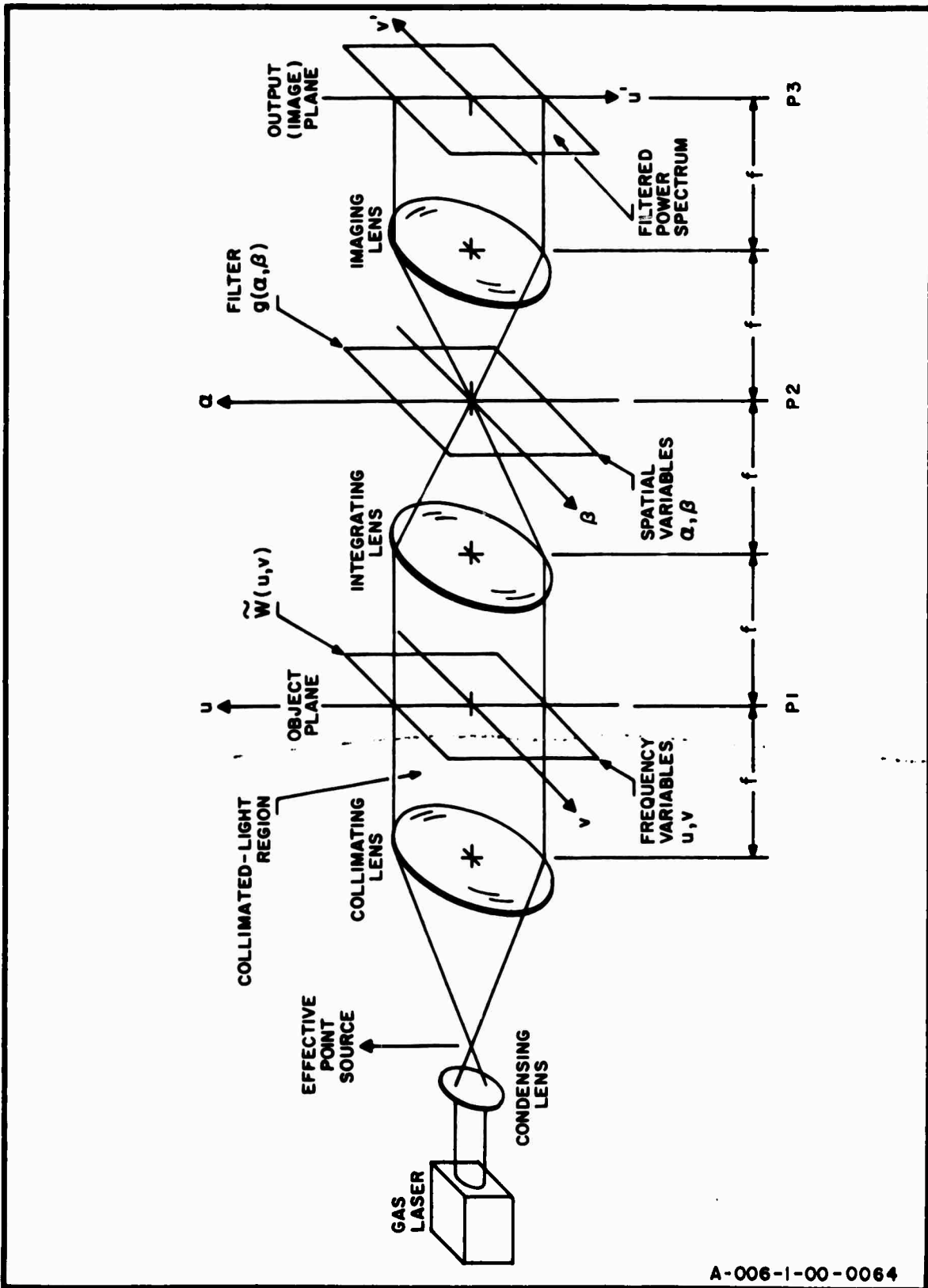
But the properties of  $G(u)$  have been determined in the one-dimensional analysis, where it was found that  $G(u)$  could not correspond to the space transmission function of a physically realizable filter. Therefore  $G(u,v)$  is not physically realizable.

An optical filtering technique for reducing the resolution inherent in  $\tilde{W}(u)$  when the sample of data is small and the effective aperture is limited by the sample and not by the lens is the following. Let  $\tilde{W}(u)$  be recorded on low-noise film so as to let the average amplitude transmittance of the film be proportional to  $\tilde{W}(u)$ , i.e.,  $t(u) = k\tilde{W}(u)$ , where  $t(u)$  denotes the amplitude transmittance and  $k$  is some constant. If this transparency is placed in the aperture of the optical system shown in Fig. 3.5-2, then the Fourier transform of  $t(u)$  is proportional to  $\phi(\alpha)$ , and a filter in the Fourier transform plane ( $P_2$ ) with transmittance  $g(\alpha)$  will yield a light-amplitude variation proportional to  $\phi(\alpha)$ . In plane ( $P_3$ ), the Fourier transform  $W(u)$  of  $\phi(\alpha)$  is obtained.

The method described above has several drawbacks. First, a very low-noise film such as a Lippmann emulsion type (Mees and James 1966) is required for storing  $\tilde{W}(u)$ . This film must also be linear over a dynamic range sufficient to accommodate the significant variations in  $\tilde{W}(u)$ . Finally, if the sample from which  $\tilde{W}(u)$  was obtained is very small, a large aperture may be required for good results.

### 3.6 EFFECT OF THE SCANNING SLIT

Consider a scanning aperture (henceforth called a slit to avoid confusion with the object-plane aperture) which together with a photomultiplier tube, amplifier, and recording device enables the recording of the light-intensity distribution at any point  $(x',y')$  in the frequency plane. Recall that any



A-006-1-00-0064

FIG. 3.5-2 OPTICAL SYSTEM FOR THE SPATIAL FILTERING OF THE MEASURED SPECTRUM  $\tilde{W}(u,v)$

point in the frequency plane corresponds to spatial frequencies  $u = x'/\lambda f$ ,  $v = y'/\lambda f$  [see Eq. (2.4-2) and Sec. 2.4]. If the slit is a rectangular hole of width  $b$  and length  $h$ , the total illumination received by the photomultiplier tube through the slit is obtained by integration, and the current in the photomultiplier tube when the center of the slit is at  $(x', y')$  is given by

$$i = k \int_{y'-b/2}^{y'+b/2} \int_{x'-h/2}^{x'+h/2} I(\xi, \eta) d\xi d\eta \quad (3.6-1)$$

where

$I(\xi, \eta)$  = light intensity at  $(\xi, \eta)$

$k$  = gain of the photomultiplier tube

$i$  = current

Equation (3.6-1) can be written as

$$i = k \int_{-\infty}^{+\infty} \int_{-\infty}^{+\infty} I(x' - \xi, y' - \eta) g'(\xi, \eta) d\xi d\eta \quad (3.6-2)$$

where the function  $g'(\xi, \eta)$  is given by

$$g'(\xi, \eta) = \text{rect} \frac{\xi}{h} \text{ rect} \frac{\eta}{b} \quad (3.6-3)$$

and is the ratio of the transmitted intensity to incident intensity at the point  $(\xi, \eta)$ . The coordinates  $(\xi, \eta)$  are defined with respect to an origin at the center of the slit. Since scanning takes place in the frequency plane, it is convenient to write  $g'(\xi, \eta)$  in terms of spatial frequencies. Hence, with  $u' = \xi/\lambda f$  and  $v' = \eta/\lambda f$ , one may write

$$\begin{aligned}
 g(u', v') &= 1, \quad -\frac{h}{2\lambda f} < u' < \frac{h}{2\lambda f} \\
 &\quad -\frac{b}{2\lambda f} < v' < \frac{b}{2\lambda f} \\
 &= 0 \text{ otherwise}
 \end{aligned} \tag{3.6-4}$$

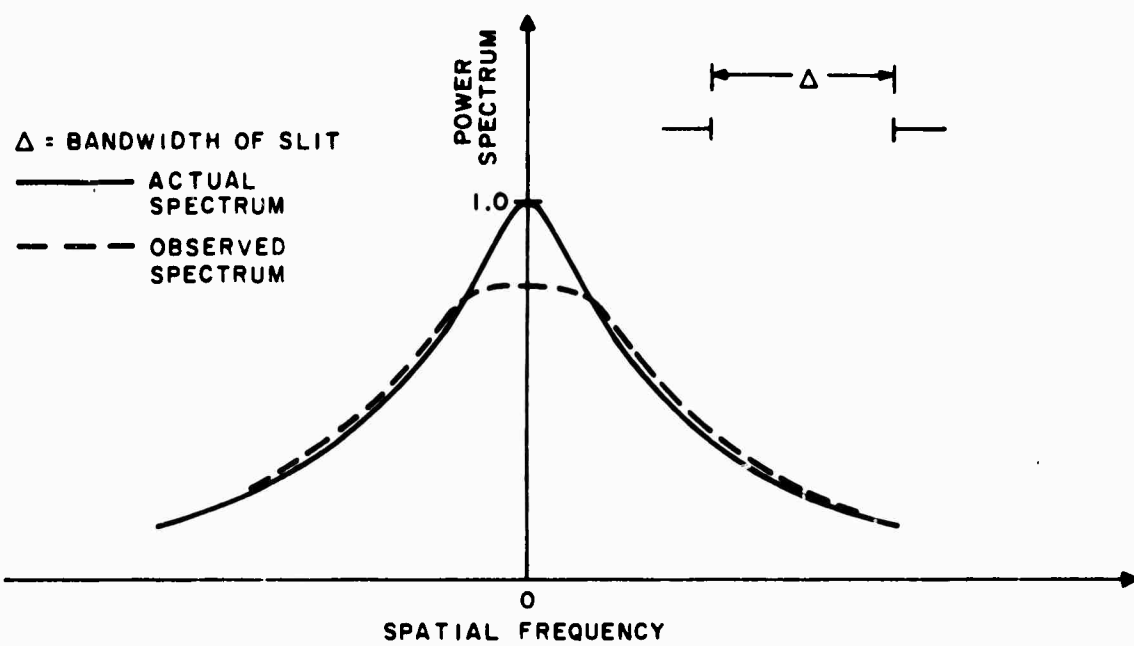
For any given light intensity  $I(u, v)$ , the light intensity observed through the slit can be defined by

$$I_o(u, v) = \frac{(\lambda f)^2}{A_s} \int_{-\infty}^{+\infty} \int_{-\infty}^{+\infty} I(u', v') g(u-u', v-v') du' dv' \tag{3.6-5}$$

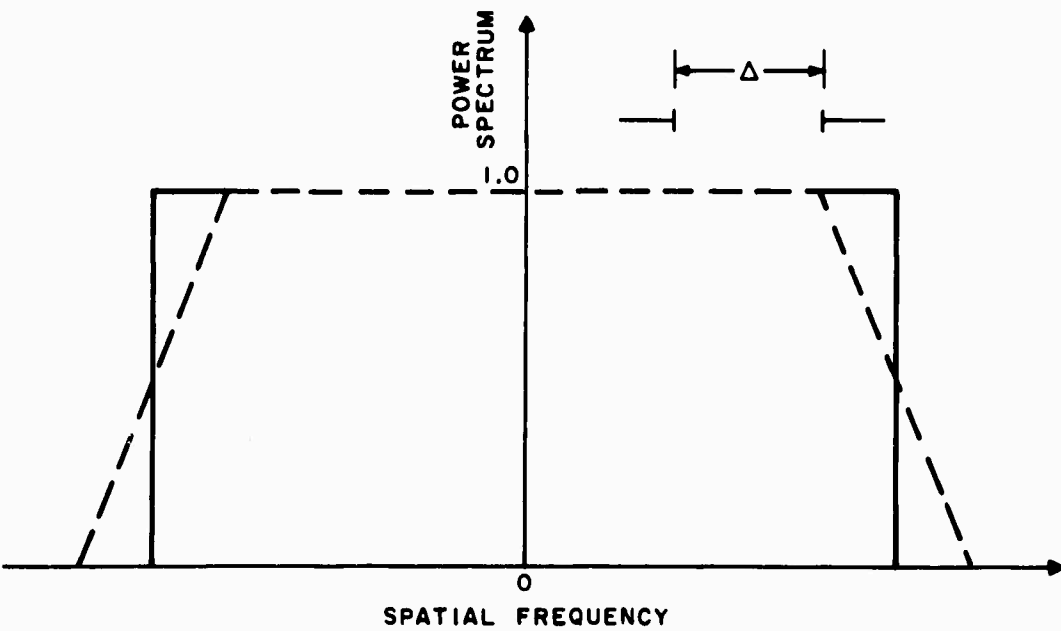
where

$$\begin{aligned}
 I_o(u, v) &= \text{observed intensity at } (u, v) \\
 I(u', v') &= \text{intensity at } (u', v') \\
 g(u-u', v-v') &= \text{the filter function of the slit centered at } u = u', v = v' \\
 A_s &= \text{area of slit} \\
 \frac{A_s}{(\lambda f)^2} &= \text{"area" of slit in units of spatial frequency}
 \end{aligned}$$

The slit produces an averaging effect which causes blurring by masking high-frequency components in the distribution  $I(u, v)$  (see Fig. 3.6-1). Clearly, the best way to minimize blurring is to use the smallest possible slit consistent with the sensitivity of the photomultiplier tube. In the limit when  $k \rightarrow \infty$  and  $h$  and  $b$  become zero, blurring will vanish and  $I_o(u, v) = I(u, v)$ . When, however, the problem is to estimate the spectral density of a random process, there are considerations other than blurring that dictate a good choice of scanning slit. When spectral density measurements are made with the



(a)



(b)

A - 321-S-0499

FIG. 3.6-1 ILLUSTRATING THE DISTORTING EFFECT OF A SCANNING SLIT ON TWO DIFFERENT SPECTRA

system of Fig. 2.4-2, the light intensity in the  $uv$  plane is an estimate of  $W(u,v)$  and hence subject to variability. The stability of the estimate will decrease with decreasing slit size since the averaging takes place over fewer spatial-frequency-resolution cells. Hence, from the viewpoint of stability, too small a slit is undesirable. Observe also that a small slit implies a narrow-bandpass filter. The narrower the band, the greater is the frequency-resolving capability of the scanner. However, the apparent spectrum  $\tilde{W}(u,v)$  is an averaged version of the true spectrum  $W(u,v)$ , the averaging occurring over frequency intervals of the order of  $1/L$  for the "u" frequencies and  $1/W$  for the "v" frequencies [ $1/L$  and  $1/W$  are approximately the half-power widths of the function  $H(u,v)$  defined by Eq. (3.2-2)]. Hence, it would be wasteful to demand resolving capabilities far in excess of  $1/L$  and  $1/W$  since this would furnish unstable estimates.

The above considerations illustrate that stability may be increased at the expense of frequency resolution and vice versa. Since stability improves with increasing slit size, the problem of what constitutes an appropriate upper bound on slit size must be considered. Clearly, it is undesirable to let the bandwidth of the slit be greater than the smallest frequency intervals over which the spectral density changes by a significant amount. For a one-dimensional process, consider a data sample large enough to contain information about all correlation intervals  $\alpha$  such that  $|\alpha| < \alpha_{\max}$ , where  $\alpha_{\max}$  is the longest correlation distance of interest. The least distance over which  $W(u)$  will change by a significant amount is then of the order of  $\alpha_{\max}^{-1}$ . Hence, the one-dimensional slit of assumed width  $d$ , should satisfy

$$\frac{d}{\lambda f} < \alpha_{\max}^{-1} \quad (3.6-6)$$

By way of illustration, consider the measurement of isotropic grain noise with a system for which  $\lambda = 6328 \text{ \AA}$  (He-Ne laser),  $f = 1 \text{ meter}$ , and  $L = W = 60 \text{ mm}$ . Then assuming that  $\alpha_M = \beta_M = 1000 \text{ microns}$  (which is very large and leaves room for considerable "clumping" - see Sec. 4.1) a reasonable guide as to the width  $d$  would be furnished by

$$\frac{\lambda f}{L} < d < \frac{\lambda f}{\alpha_{\max}} \quad (3.6-7)$$

which gives approximately

$$10 \text{ microns} < d < 600 \text{ microns.}$$

The problem of obtaining a stable estimate is best determined by experimentation. It may turn out that very stable estimates of  $W(u,v)$  are obtained with even a 5-micron slit. Or else perhaps frequency resolution in excess of what was planned may have to be sacrificed to obtain reasonable stability.

The effect of slit on the covariance may be illustrated as follows. From Eq. (3.6-5) it follows that the observed spectrum  $W_o(u,v)$  is related to the apparent spectrum  $\tilde{W}(u,v)$  by

$$W_o(u,v) = \frac{(\lambda f)^2}{A_s} \int_{-\infty}^{+\infty} \int_{-\infty}^{+\infty} \tilde{W}(u',v') g(u-u',v-v') du dv \quad (3.6-8)$$

The Fourier transform of the above gives

$$\phi_o(a,b) = \tilde{\phi}(a,b) \operatorname{sinc} \frac{ah}{\lambda f} \operatorname{sinc} \frac{bb}{\lambda f}$$

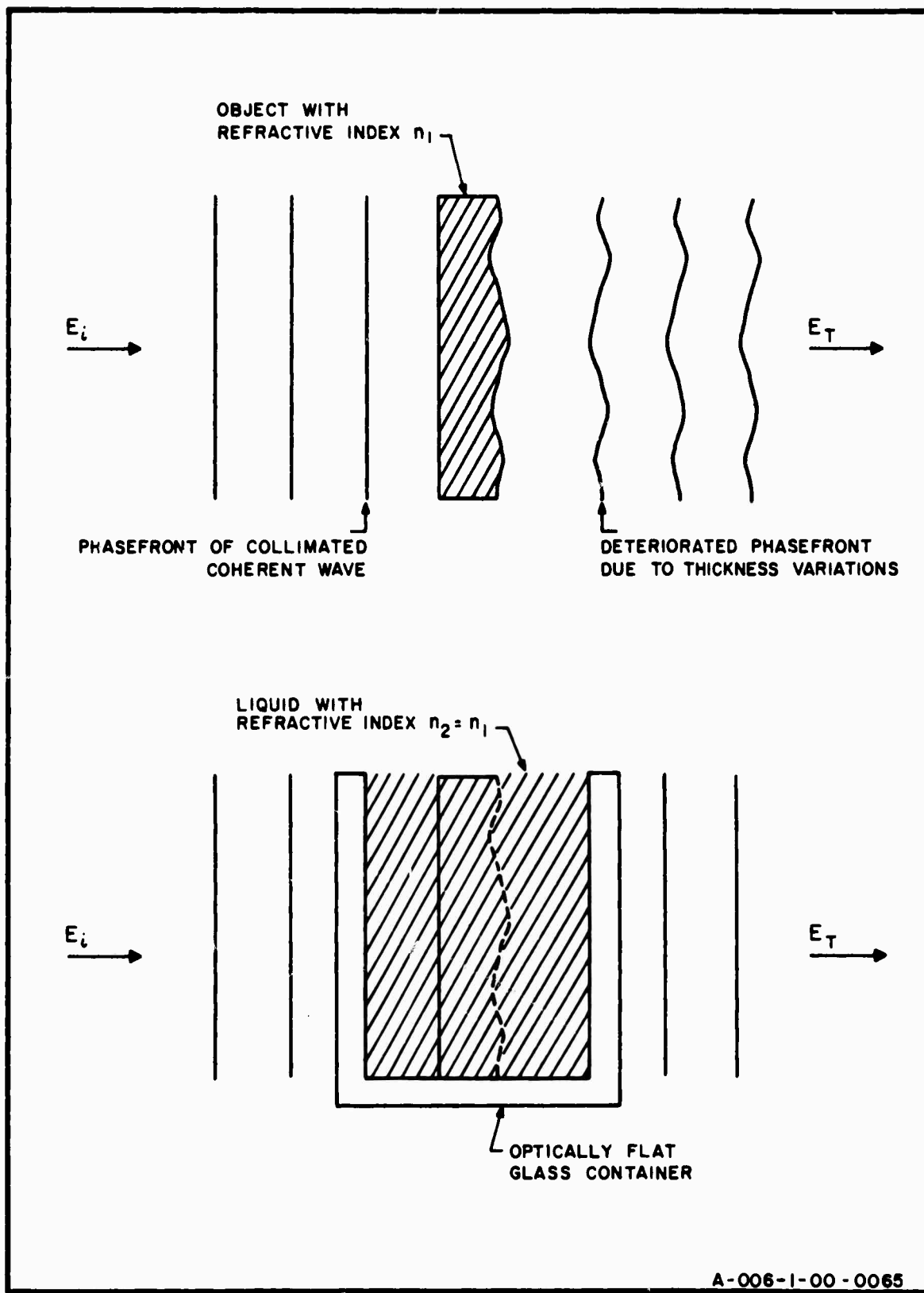
which shows how the blurring affects the correlation function. Clearly, if  $h \ll \lambda f / \alpha_{\max}$  and  $b \ll \lambda f / \beta_{\max}$ , the blurring is negligible since the sinc functions are almost constant over regions for which there is significant correlation.

#### 4. FILM-NOISE MODELS

The experimental work in this thesis concerns the measurement of the power spectra of film noise. Results are included for both  $\{t(x,y)\}$  and  $\{R(x,y)\}$ . In this chapter, the properties of existing and proposed film-noise models are discussed.

##### 4.1 GENERALITIES

As stated earlier, in many optical signal-processing and wavefront reconstruction systems, the fundamental limitation to high performance is film noise. Very often, predictions of achievable signal-to-noise ratios of such systems take into account film grain noise only since the phase noise can be significantly reduced by using so-called liquid gates (Thiry 1963). A liquid gate consists of two optically flat glass sections containing between them a liquid whose refractive index is chosen to be equal to that of the object which is to be immersed in the gate. Ideally, the optical path length across any point in the aperture is then a constant for all ray trajectories and the phase fluctuations resulting from random optical path length differences vanish (Fig. 4.1-1). When optical path length differences are due to variations in the refractive index of the film emulsion or when the object is of a compound nature, that is, made up of several materials, the liquid gate can reduce but not eliminate phase errors. The relative contributions of film thickness irregularities and variations of refractive index to the phase deterioration of a quasi-coherent beam has been measured for photographic film, for which it has been shown that thickness irregularities are the chief sources of phase noise (Ingalls 1960).



A-006-1-00-0065

FIG. 4.1-1 ILLUSTRATING THE ACTION OF A LIQUID GATE IN REDUCING NOISE DUE TO RANDOM THICKNESS VARIATIONS

As a measure of what constitutes acceptable variations in the optical path length, that is, variations not sufficiently large to deteriorate the phase front of a coherent beam significantly, the Rayleigh limit may be employed. This criterion specifies that optical path differences no more than one-quarter of the wavelength of light are permissible over the active aperture. Hence, for film\* immersed in air and coherently illuminated in an optical system employing a He-Ne laser ( $6328 \text{ \AA}$ ), the maximum allowable variation in film thickness is

$$\Delta T_{\max} = \frac{\lambda}{4(n_f - 1)} \approx .00032\text{-mm}$$

which is a very small variation.

When film with refractive index  $n_1$  is immersed in a liquid gate with refractive index  $n_2$ , the Rayleigh limit is given by

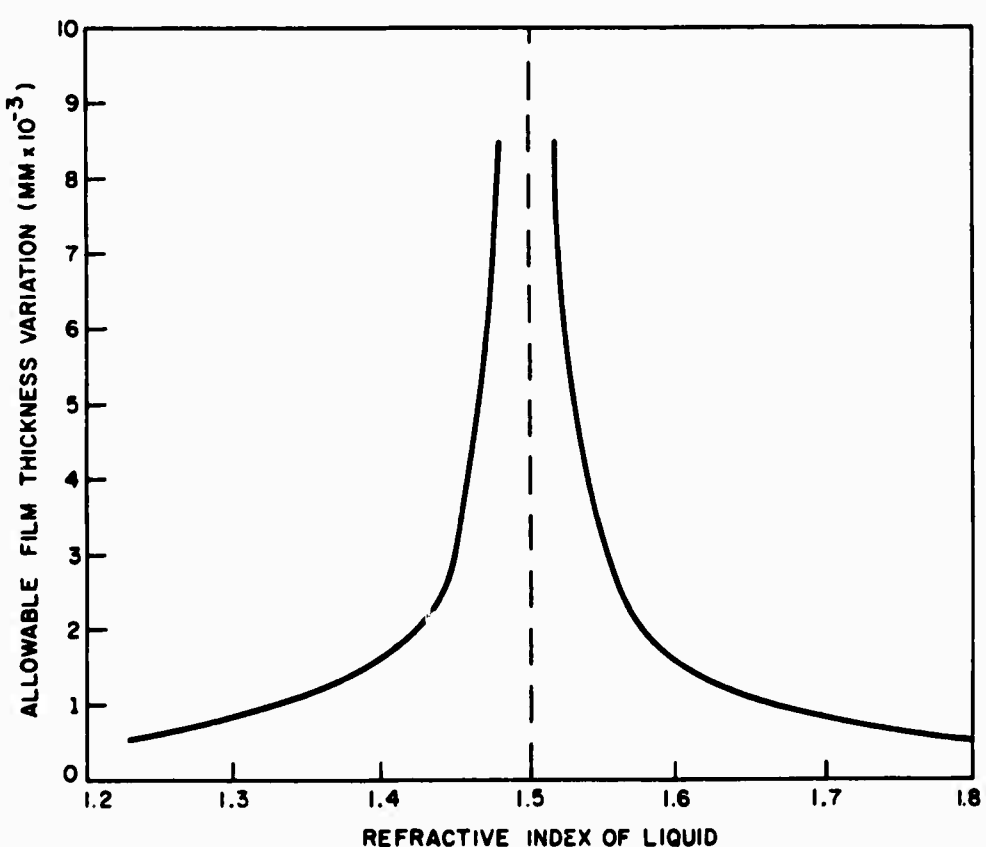
$$\Delta T_{\max} = \frac{\lambda}{4 |n_2 - n_1|}$$

A plot of the Rayleigh allowable film-thickness variations vs immersion-liquid index, for  $\lambda = 6328 \text{ \AA}$  and film with refractive index of 1.5, is given in Fig. 4.1-2.

In the next section several models of film granularity are discussed. These models are highly simplified and their use in signal-to-noise predictions is at best a first-order approximation to the problem. Real grain structure is very complicated. Photomicrographs have shown that developed grains rarely have the shape of the undeveloped grains, which are halide crystals of definite and regular shape. The developed silver grains are either twisted filaments of silver or, usually, masses of such filaments. Even for uniformly exposed film, the density of grains is not uniform throughout the emulsion, the number of developed grains being most numerous near the

---

\* A refractive index of 1.5 for film is assumed.



REFRACTIVE INDEX OF FILM = 1.5  
 $\lambda = 6328 \text{ \AA}$

A-006-1-00-0066

FIG. 4.1-2 MAXIMUM ALLOWABLE VARIATION OF FILM THICKNESS (RAYLEIGH LIMIT CRITERION)

outer surface of the emulsion and decreasing with increasing displacement from the surface. The distribution in depth depends on such features as the concentration of the silver halide, the size of the grains, the thickness of the emulsion and the composition of the developer (Mees & James 1966).

Formerly, it had been considered that the grain is the unit of photographic action and that a grain develops independently depending on its quantum efficiency (the probability,  $\epsilon$ , that a photon incident upon the grain is absorbed by that grain) and on the minimum number of photons  $m$  required to make a grain developable. Subject to the assumption of Poisson-distributed photon arrivals, the probability that a given grain with parameter  $(\epsilon, m)$  becomes opaque during development is then given by (Silberstein 1922, Goodman 1967)

$$P(t = 0) = \sum_{k=m}^{\infty} \frac{(\epsilon E_T A_g / \hbar \omega)^k}{k!} \exp^{-\epsilon E_T A_g / \hbar \omega} \quad (4.1-1)$$

where

$E_T$  = total exposure (energy density) to which the grain is subjected

$\hbar$  = Planck's constant divided by  $2\pi$

$f$  = frequency of the radiation

$\omega$  =  $2\pi f$

$A_g$  = the area of the grain

However, as early as 1922 it was found that certain grains develop by virtue of their contact with developed grains and that the process may repeat several times, ultimately forming a clump whose size may be many times the size of a single grain. This phenomenon is called clumping and may be aggravated by certain developers, notably those that contain hydrazine (Trivelli, et.al. 1922).

If grains were to develop independently, then the covariance function would be expected to be zero for correlation intervals greater than the length of the longest grains. When clumping is present, this is not the case however; the clumping may be viewed as a random process with a Markov-type component, namely the state of a grain depending in some degree on the state (developed or undeveloped) of an adjacent grain. When clumping is widespread, the length of significant correlation intervals increases the amplitude of the low-frequency components of the spectral density.

The author has no knowledge of stochastic grain models designed to include the statistics of clumping.

#### 4.2 MODELS OF PHOTOGRAPHIC GRANULARITY

##### A. The Random Checkerboard Model

The random checkerboard model is shown in Fig. 4.2-1. The transparency is assumed to be composed of square cells, each of length  $\lambda$  and arranged in parallel rows and columns. A given cell is assumed to be either perfectly opaque, corresponding to a grain that has been developed, or perfectly transparent, corresponding to a grain that has remained undeveloped. Whether or not a grain has been developed depends on (1) the sensitivity of the grain, (2) the energy incident on the grain during exposure, and (3) the degree to which the photographic plate has been processed.

Let the transparency be uniformly exposed. In the random checkerboard model, the grains are assumed to develop independently so that the probability that a given grain is opaque is independent of the state of adjacent grains. The amplitude transmittance of the transparency may be written as

$$t(x,y) = t_o + \tau(x,y) \quad t_o = \langle t(x,y) \rangle \quad (4.2-1)$$

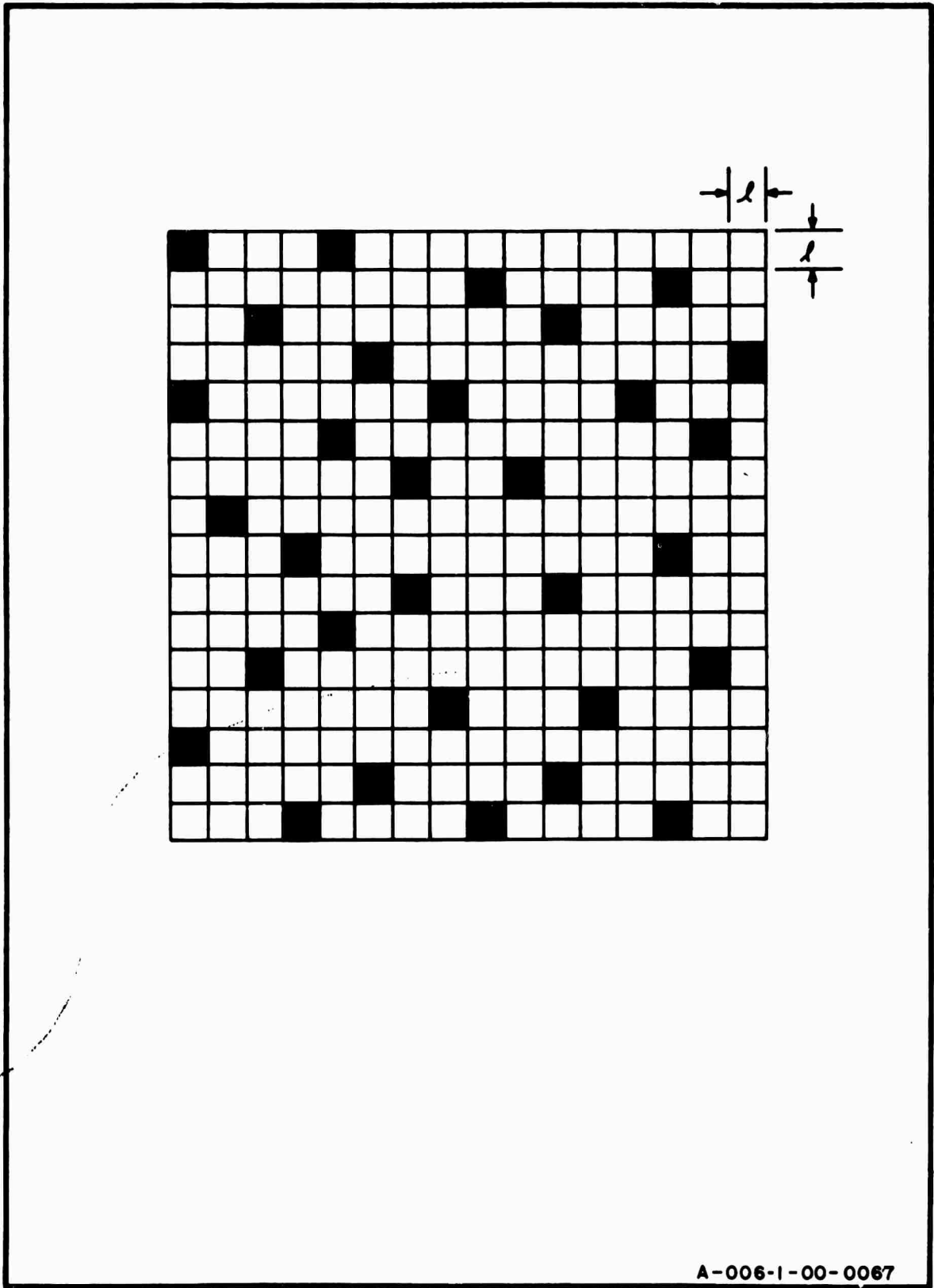


FIG. 4.2-1 RANDOM CHECKERBOARD MODEL OF FILM GRAINS

and a typical sample function is shown in Fig. 4.2-2. The process  $\{t(x,y)\}$  is a two-dimensional analogue of the random binary signal wave occurring in communication theory in which the starting time of a pulse is a random variable, uniformly distributed over the duration of the pulse\*. The duration of transmittance pulses must be multiples of  $\ell$ . The correlation function of the process  $\{\tau(x,y)\}$  can be readily shown to be

$$\phi_{\tau}(\alpha, \beta) = t_0(1 - t_0) \left(1 - \frac{|\alpha|}{\ell}\right) \left(1 - \frac{|\beta|}{\ell}\right) \quad \begin{matrix} |\alpha| < \ell \\ |\beta| < \ell \end{matrix}$$

$$\phi_{\tau}(\alpha, \beta) = 0 \quad \text{otherwise} \quad (4.2-2)$$

and the associated power spectrum  $w_{\tau}(u,v)$  is given by

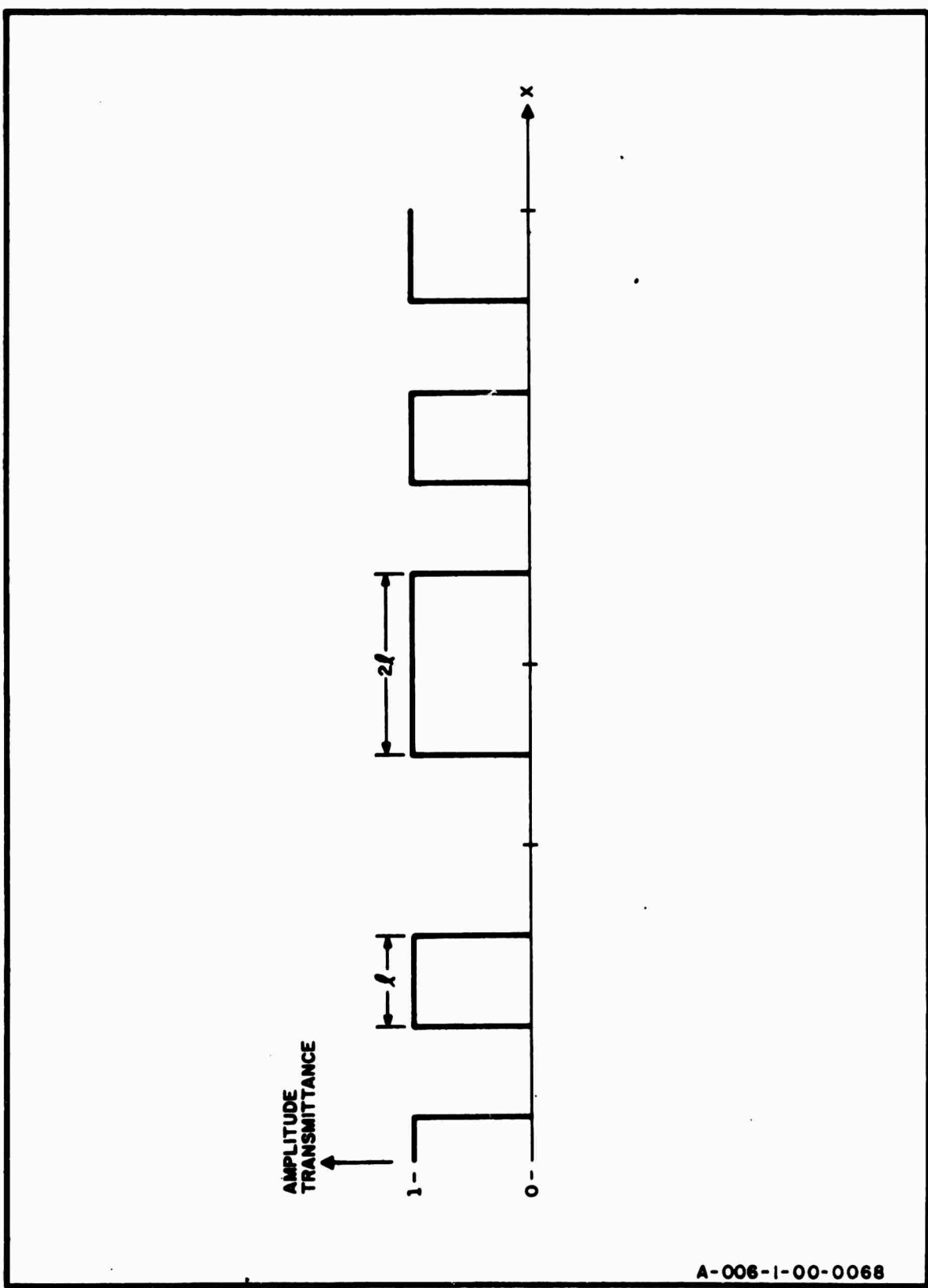
$$w_{\tau}(u,v) = \pi^2 t_0(1 - t_0) \left(\frac{\sin \pi u \ell}{\pi u \ell}\right)^2 \left(\frac{\sin \pi v \ell}{\pi v \ell}\right)^2 \quad (4.2-3)$$

where  $u$  and  $v$  are spatial frequencies. For  $u$  and  $v$  fixed,  $w_{\tau}(u,v)$  has a maximum at  $t_0 = .5$ . At frequencies given by  $u = n/\ell$  and  $v = k/\ell$  where  $n = 1, 2, \dots$ , and  $k = 1, 2, \dots$ ,  $w_{\tau}(u,v)$  is zero.

From Eq. (4.2-2) it can be seen that  $\phi_{\tau}(\alpha, \beta)$  is an even function of both its arguments. However, since the covariance function is not a function of  $(\alpha^2 + \beta^2)^{\frac{1}{2}}$ , the process is not isotropic. Although the random checkerboard model is not a very realistic model of granularity, it has been used in signal-to-noise predictions for holographic systems (Goodman, 1967) and also in entropy and granularity studies (O'Neill, 1958). The random checkerboard model has also been proposed as a standard of granularity, against which the granularity of real films could be compared (Fry, 1963).

---

\* See for example Schwarz and Friedland, 1965.



A-006-1-00-0068

FIG. 4.2-2 THEORETICAL POINT APERTURE MICRODENSITOMETER TRACE OF RANDOM CHECKERBOARD MODEL OF FILM GRAINS

## B. THE OVERLAPPING CIRCULAR GRAIN MODEL (OCG)

The initial treatment of the transmittance and auto-correlation function of this model was given by Picinbono (Picinbono 1955) who, in deriving the autocorrelation function, assumed that an exposed grain is completely opaque while the unexposed grain and the emulsion were completely transparent. Savelli (Savelli 1958) extended Picinbono's treatment to allow for greater than zero transmittances for exposed grains and less than unity transmittances for the unexposed grains. However, since an exposed grain is essentially a particle of silver which is opaque in the visible light region, it is reasonable to assume that the transmittance of an exposed grain is always zero.

The basic OCG model is based on the following assumptions: (1) the grains are circular and the centers of these circles fall at random on a plane as independent events; (2) the grain centers are Poisson distributed in the sense that the probability that there are  $n$  grains in an area  $A$  is given by

$$P_n(A) = \frac{\bar{n}^n e^{-\bar{n}}}{n!} \quad (4.2-4)$$

where  $\bar{n}$  is the expected number of grains in  $A$ ; and (3) the grain sizes are random variables with a distribution law

$$P(\ell) = \text{Prob } (L \leq \ell)$$

where  $L$  is a random variable denoting the grain radius. The factors governing grain development are the same as in the random checkerboard model.

Subject to assumptions (1) through (2), it can be shown (Picinbono 1955) that

$$t_o = \langle t(x,y) \rangle = e^{-2\pi d} \int_0^\infty [1 - p(r)] r dr \quad (4.2-5)$$

where  $d$  = average number of grains per unit area. The correlation function for this model,  $\phi_t(\alpha, \beta)$ , can be shown to equal (Picinbono 1955)

$$\begin{aligned} \phi_t(\alpha, \beta) &= \langle t(x,y) t(x+\alpha, y+\beta) \rangle = \phi_t(\rho), \text{ where} \\ \rho &= (\alpha^2 + \beta^2)^{\frac{1}{2}} \\ &= \exp \left[ -4d \left( \pi \int_0^{\rho/2} (1 - p(r)) r dr \right. \right. \\ &\quad \left. \left. + \int_{\rho/2}^{\infty} (\pi - \cos^{-1} \rho/2r) (1 - p(r)) r dr \right) \right] \end{aligned} \quad (4.2-6)$$

By Eq. (2.2-6) it can be seen that the OCG model has isotropic statistics. In the special case where all the grain are assumed to have the same radius  $\ell_o$ , there results (Fig. 4-2-3)

$$\begin{aligned} p(r) &= 0 & r < \ell_o \\ p(r) &= 1 & r \geq \ell_o \end{aligned} \quad (4.2-7)$$

so that

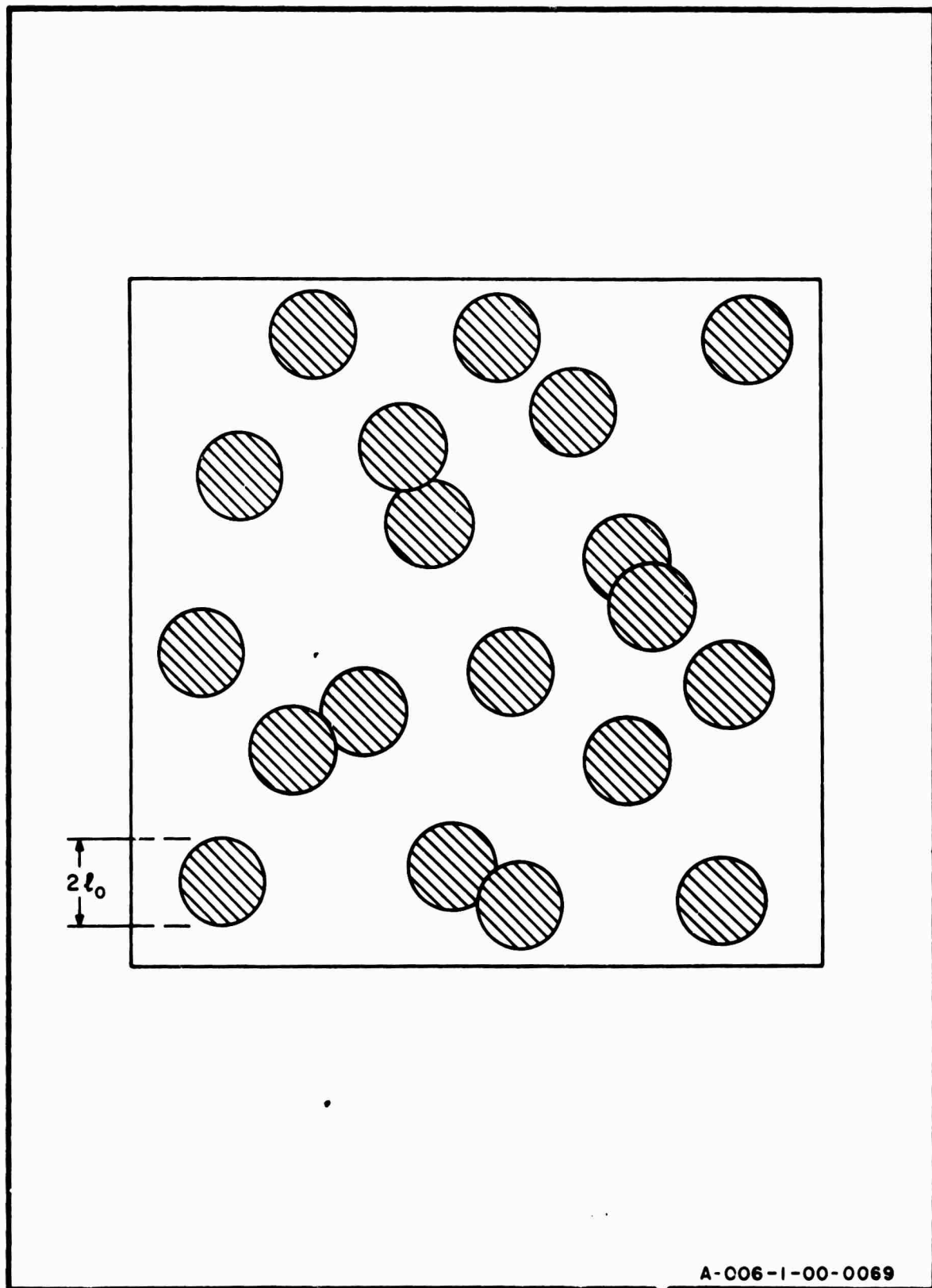
$$t_o = e^{-\pi \ell_o^2 d} \quad (4.2-8)$$

The autocorrelation function for this special case is

$$\begin{aligned} \phi_t(\rho) &= e^{-2\pi \ell_o^2 d} = t_o^2 & \rho > 2\ell_o \\ \phi_t(\rho) &= t_o^2 e^{\pi \ell_o^2 d} F(\rho/2\ell_o) & \rho \leq 2\ell_o \end{aligned} \quad (4.2-9)$$

where

$$\begin{aligned} F(\rho/2\ell_o) &= 2/\pi \left[ (\cos^{-1} (\rho/2\ell_o) - \rho/2\ell_o \sqrt{1 - (\rho/2\ell_o)^2}) \right] \\ &= 0 \quad \text{otherwise} \end{aligned} \quad (4.2-10)$$



A-006-1-00-0069

FIG. 4.2-3 OVERLAPPING CIRCULAR-GRAIN MODEL OF PHOTOGRAPHIC FILM.

The covariance,  $\phi_{\tau}(\alpha, \beta)$ , is given by

$$\phi_{\tau}(\alpha, \beta) = \langle \tau(x, y) \tau(x+\alpha, y+\beta) \rangle = \phi_{\tau}(\rho) \quad (4.2-11)$$

and

$$\phi_{\tau}(\rho) = t_o^2 \begin{bmatrix} t_o^{-F(\rho/2t_o)} & -1 \\ 0 & \leq \rho \leq 2t_o \\ 0 & \text{otherwise} \end{bmatrix} \quad (4.2-12)$$

When the unexposed portions of the film have a transmittance  $h$ , where  $h$  is not necessarily unity, then the previous results are modified to

$$t_o = \langle t(x, y) \rangle = h e^{-\pi t_o^2 d} \quad (4.2-13)$$

and

$$\phi_{\tau}(\rho) = t_o^2 \left[ \left( \frac{h}{t_o} \right)^{F(\rho/2t_o)} - 1 \right] \quad (4.2-14)$$

where  $F(\rho/2t_o)$  is as defined earlier.

The power spectra  $W(u, v)$  of this model is given by

$$\begin{aligned} W(u, v) &= \int_0^{2\pi} \int_0^\infty \phi_{\tau}(\rho) e^{-j2\pi w\rho \cos(\Omega-\rho)} \rho d\rho d\Omega \\ &= 2\pi \int_0^\infty \phi_{\tau}(\rho) J_o(2\pi w\rho) \rho d\rho \quad (4.2-15) \\ &= W(w) \end{aligned}$$

where  $w = (u^2 + v^2)^{\frac{1}{2}}$ .

The normalized power spectra, defined by

$$W_n(w) = \frac{w^2}{8\pi t_o^2} \quad (4.2-16)$$

has been numerically integrated and is shown in Fig. 4.2-4 as a function of the dimensionless variable  $X = w t_o$  with  $t_o/h$  as a parameter. The Picinbono model is obtained when  $h = 1$ .

This model, like the random checkerboard model, has a covariance function which is zero for intervals greater than the grain diameter. The relative power spectra, at dc, of the checkerboard and OCG model are shown in Fig. 4.2-5,\* as a function of amplitude transmittance.

#### 4.3 MODELS FOR TOTAL FILM NOISE

The complex transmittance of uniformly exposed film is a stochastic quantity that describes the joint effect on coherent light of film granularity and variations in the optical path length through the cross section of the film. In writing for the complex transmittance at a point  $(x,y)$

$$R(x,y) = t(x,y) e^{j\psi(x,y)} \quad \langle t(x,y) \rangle = t_o \\ \langle R(x,y) \rangle = R_o \quad (4.3-1)$$

the amplitude transmittance  $t(x,y)$  is primarily a consequence of the granularity of the film emulsion, and  $\psi(x,y)$  is due to non-uniformities in the thickness of the film and the refractive index of the emulsion. Attempts to assess the relative contribution of these two factors to the phase noise process  $\{\psi(x,y)\}$  have shown that the major cause of phase deterioration of coherent light as it passes through film is the random variation in film thickness (Ingalls 1960).

\* No significance should be attached to the difference in heights between the two curves.

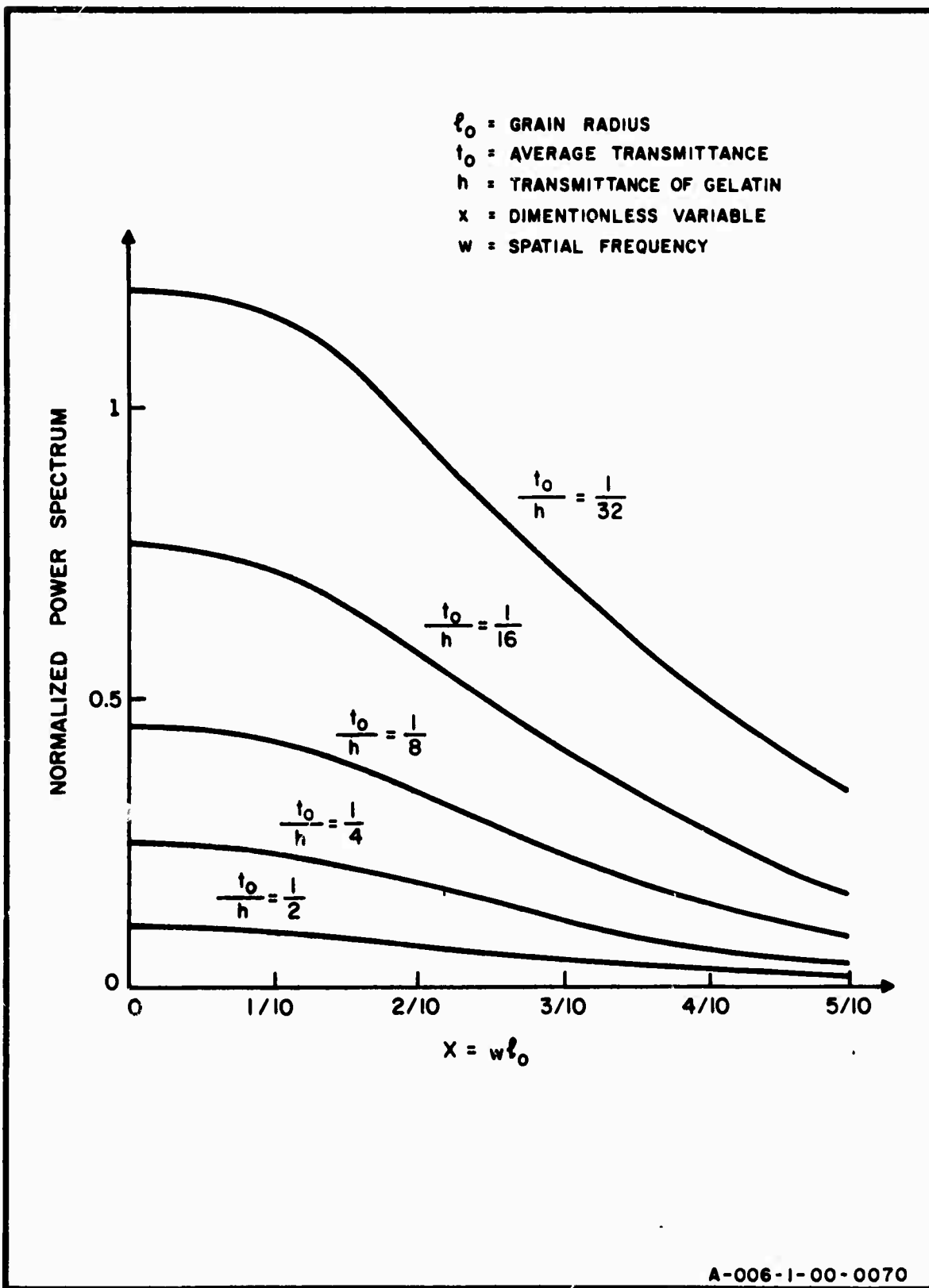


FIG. 4.2-4 THE NORMALIZED POWER SPECTRUM OF GRAIN NOISE AS COMPUTED FOR THE OVERLAPPING CIRCULAR-GRAIN MODEL. ( ADAPTED FROM SAVELLI 1958 )

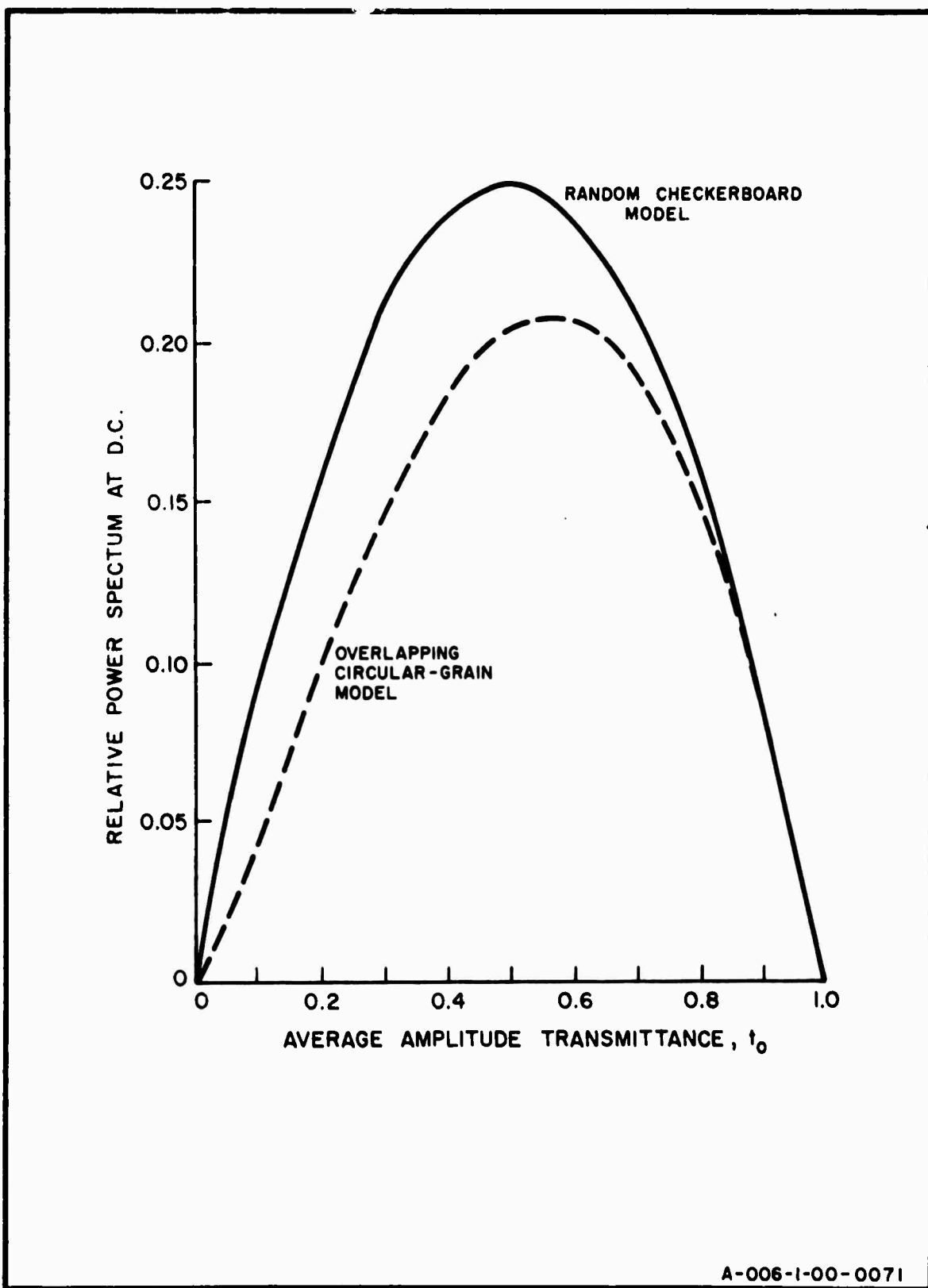


FIG. 4.2-5 VARIATION OF POWER SPECTRUM AT ZERO SPATIAL FREQUENCY WITH AVERAGE AMPLITUDE TRANSMITTANCE. (ADAPTED FROM GOODMAN 1967)

In attempting to construct stochastic models for the complex transmittance of uniformly exposed film, it is of primary importance to determine whether  $\{t(x,y)\}$  and  $\{\psi(x,y)\}$  can be considered as independent processes. Although it would appear that surface corrugations of the emulsion have little to do with film amplitude transmittance, there is in fact evidence to suggest that these are not independent phenomena. For example, it has been found that when developed film has been immersed in an aqueous solution, the more highly dense (low transmittance) areas dry more quickly than regions of low density (high transmittance) and thus, while drying, pull the moist and flexible low-density regions with them. The resulting shift in the emulsion which is both parallel and normal to the plane of the emulsion is called the gelatin effect. The changes in the thickness of the emulsion layer are visible in relief on the surface (James and Higgins 1960). Thus, the relieving is a function of transmittance and in dealing with deterministic transmittance variations such as images, the phase and amplitude transmittance cannot be adjudged to be independent quantities. It has been suggested that the phase modulation that results from relieving can be described by a complex transmittance with a phase dependence that is linearly proportional to the relative transmittance at that point (Leith 1962).

When considering the random properties of uniformly exposed film, however, the average deterministic relieving is zero and inhomogeneities in film thickness are probably more likely a reflection of the film manufacturing process. In any case, the relieving at any point on the film is the sum of the pulling forces of many clumps of grains, randomly situated and exerting their forces in random directions. For these reasons, it may be reasonable to assume a simplified model of the complex transmittance of uniformly exposed film consisting of the independent processes  $\{t(x,y)\}$  and  $\{\psi(x,y)\}$  with  $\{\psi(x,y)\}$

a wide-sense stationary, Gaussian process. The assumption of a Gaussian process allows, in principle at least, the covariance of the process  $\{\theta(x,y)\} = \{e^{j\psi(x,y)}\}$  to be computed in terms of the moments of  $\{\psi(x,y)\}$ . This follows from the fact that the density functions of all orders are determined by the covariances of all pairs of random variables and no higher-order moments are needed. Under these assumptions, the correlation function of the process  $\{R(x,y)\}$  is given by

$$\phi_R(\alpha, \beta) = \phi_T(\alpha, \beta) + t_0^{-2} e^{-(\sigma^2 - \phi_\psi(\alpha, \beta))} \quad (4.3-2)$$

and  $\sigma^2 = \phi_\psi(0,0)$ . The covariance function of  $\{r(x,y)\}$  is given by

$$\phi_r(\alpha, \beta) = \phi_R(\alpha, \beta) - |R_0|^2 \quad (4.3-3)$$

where  $R_0 = \langle R(x,y) \rangle = t_0 e^{-(1/2)\sigma^2}$ , a result that follows from the formula for the characteristic function of a Gaussian variate\*. When the phase errors are small, such as they might be when the liquid gate is slightly mismatched to the film, the exponential can be expanded into a Taylor series:

$$e^{-(\sigma^2 - \phi_\psi(\alpha, \beta))} \approx 1 - \sigma^2 + \phi_\psi(\alpha, \beta) \sigma^2 \ll 1 \quad (4.3-4)$$

and the diffraction system of Fig. 2.4-1 will produce an average relative light intensity in the  $(u,v)$  plane given by

$$\langle I(u,v) \rangle \approx t_0^{-2}(1 - \sigma^2) LW \operatorname{sinc}^2 uL \operatorname{sinc}^2 vW + w_r(u,v) \quad (4.3-5)$$

where it has been assumed that all significant correlation intervals are very small compared with the dimensions  $L, W$ .

---

\* See for example Schwarz and Friedland, 1965.

Since  $\sigma^2$  is small, the amount of light energy scattered away from the zero-order light through phase errors is small and the attenuation is essentially caused by the factor  $t_0^{-\sigma^2}$ . When the phase angles are large,  $\sigma^2 \gg 1$ , the average light intensity is given by

$$\langle I(u,v) \rangle \approx t_0^{-\sigma^2} LW \operatorname{sinc}^2 uL \operatorname{sinc}^2 vW + w_r(u,v) \quad (4.3-6)$$

Clearly in this case, a great deal of energy has been scattered away from the zero order into the power spectrum of the complex process  $\{r(x,y)\}$ .

Rowe has dealt with the problem of phasefront deterioration of coherent light by lenses with large random imperfections (Rowe 1966). The imperfections are assumed to create phase errors with stationary, isotropic Gaussian statistics. This problem is similar to the problem of random aperture errors on antenna radiation patterns first treated by Ruze (Ruze 1952). One would expect the average back-focal plane light intensity distribution in a coherent optical system to be very similar in the two cases of phasefront deterioration by film followed by a very good lens or phasefront deterioration by a poor lens alone if the statistics in the two cases were the same. Rowe considered typical examples of both differentiable and non-differentiable processes. If the covariance is assumed to be of a type

$$\phi_\psi(\rho) = \sigma^2 e^{-c^2\rho^2} \quad \rho = (\alpha^2 + \beta^2)^{1/2} \quad (4.3-7)$$

corresponding to a differentiable random process, the associated power spectrum,  $w_\psi(w)$ , is

$$w_\psi(w) = \sigma^2 (\pi/c^2) e^{-(\pi w/c)^2} \quad w = (u^2 + v^2)^{1/2} \quad (4.3-8)$$

and if the covariance is of the type

$$\phi_{\psi}(r) = \sigma^2 e^{-c|r|} \quad (4.3-9)$$

corresponding to a non-differentiable process, the associated power spectrum is

$$W_{\psi}(w) = \sigma^2 \frac{2\pi/c^2}{[1 + (\frac{2\pi w}{c})^2]^{3/2}} \quad (4.3-10)$$

The covariance of the zero-mean process  $\theta(x,y)$  associated with the process  $\psi(x,y)$  is

$$\phi_{\theta}(x,y) = \langle e^{j[\psi(x+\alpha, y+\beta) - \psi(x,y)]} \rangle = e^{-\sigma^2} \quad (4.3-11)$$

If the process  $\{\psi(x,y)\}$  has a covariance given by Eq. (4.3-7), the power spectrum of  $\{\theta(x,y)\}$  is approximately given by (4.3-12)

$$W_{\theta}(w) = \pi (\frac{2}{\sigma})^2 e^{-(2\pi w/\sigma)^2} \quad (4.3-12)$$

while if the process  $\{\psi(x,y)\}$  has a covariance given by Eq. (4.3-9), the power spectrum of  $\{\theta(x,y)\}$  is approximately given by

$$W_{\theta}(w) = \frac{2\pi/m^2}{[1 + (\frac{2\pi w}{m})^2]^{3/2}} \quad (4.3-13)$$

In Eqs. (4.3-12) and (4.3-13):

$$\sigma'^2 = \langle |\frac{\partial \psi(x,y)}{\partial x}|^2 + |\frac{\partial \psi(x,y)}{\partial y}|^2 \rangle$$

$m$  = the initial slope of  $\phi_{\psi}(r)$

$$c = \frac{\sigma^2}{2\sigma} \text{ for Eq. (4.3-7)}$$

$$c = \frac{m}{\sigma^2} \text{ for Eq. (4.3-8)}$$

The power spectrum of the random process  $\{r_o(x,y)\}$  in either case, subject only to independence between  $\{t(x)\}$  and  $\{\psi(x)\}$  is

$$w_r(w) = e^{-\sigma^2} w_\tau(w) + t_0^2 w_\theta(w) + w_\tau(w)*w_\theta(w) \quad (4.3-14)$$

It is to be emphasized that the spectra  $w_\theta(w)$  given by Eqs. (4.3-12) and (4.3-13) are approximate. Truncated versions of  $\phi_\theta(\rho)$  ( $\rho$  small) were used in their computation. Nevertheless these spectra serve as a first approximation to the problem.

## 5. VARIANCE OF POWER SPECTRUM ESTIMATE

In this chapter, the variance of the power spectral density estimate is derived. A real, wide-sense stationary, Gaussian process is assumed. The estimate occurs in the form of a light intensity in the  $(u,v)$  plane of the two-dimensional optical system shown in Fig. 2.4-2. The assumption of a Gaussian law when the process is a random transmittance, as it must be when spectral density estimates are made by diffraction, is somewhat unrealistic since by definition, transmittances must be confined to values greater than zero and less than unity. However, in the case of film grain noise, microdensitometer traces bear out the fact that the transmittance deviations about the mean are in good agreement with the Gaussian probability density [Mees and James (5) 1966].

The results derived in Sec. 5.2 are exact for rectangular or diamond-shaped apertures. The form of the solution when the aperture is large suggests that the results may be used as guides for other apertures with comparable resolution and area.

### 5.1 FORMULA FOR THE VARIANCE

Consider the Gaussian process  $\{t(x,y)\}$  with mean value  $t_0$  for which the estimated spectrum is  $I(u,v)$ . Then for a rectangular aperture of area  $A = LW$ , the estimated apparent spectrum is

$$I(u,v) = I(u,v) - t_0^2 H(u,v) \quad (5.1-1)$$

and the mean and variance are given by

$$\langle \mathcal{W} (u, v) \rangle = \tilde{w}(u, v) \equiv w(u, v) * h(u, v) \quad (5.1-2)$$

$$\text{var } (\mathcal{W} (u, v)) = \tilde{w}^2 (u, v) + F^2 (u, v) + 2t_o^2 h(u, v) [F(u, v) \\ + \tilde{w}(u, v)] \quad (5.1-3)$$

where

$I(u, v)$  = total relative light intensity

$H(u, v)$  = system function for a rectangular aperture

$$= LW \operatorname{sinc}^2 uL \operatorname{sinc}^2 vW$$

$$F(u, v) = LW \int_{-\infty}^{+\infty} \int_{-\infty}^{+\infty} w(\xi, \eta) \operatorname{sinc} (u+\xi)L \operatorname{sinc} (u-\xi)L$$

$$. \operatorname{sinc} (v-\eta)W \operatorname{sinc} (v+\eta)W d\xi d\eta$$

$\tilde{w}(u, v)$  = apparent or biased spectrum

$$= \int_{-\infty}^{+\infty} \int_{-\infty}^{+\infty} w(\xi, \eta) \operatorname{sinc}^2 (u-\xi)L \operatorname{sinc}^2 (v-\eta)W d\xi d\eta$$

## 5.2 DERIVATION OF EQUATION (5.1-3)

The relative light intensity  $I(u, v)$  is defined by

$$I(u, v) = \frac{1}{LW} \int_{-L/2}^{L/2} \int_{-L/2}^{L/2} \int_{-W/2}^{W/2} \int_{-W/2}^{W/2} t_1 t_2 e^{-j2\pi(u(x_1 - x_2) + v(y_1 - y_2))} \\ d x_1 d x_2 d y_1 d y_2 \quad (5.2-1)$$

where

$$t_i = t(x_i, y_i)$$

$$i = 1, 2, \dots$$

The square of  $I(u, v)$  is

$$I^2(u, v) = \left(\frac{1}{LW}\right)^2 \underbrace{\int \dots \int}_{\text{8 times}} t_1 t_2 t_3 t_4 e^{-j2\pi(u(x_1-x_2+x_3-x_4)+v(y_1-y_2+y_3-y_4))} \prod_{i=1}^4 dx_i dy_i \quad (5.2-2)$$

To evaluate  $\langle I^2(u, v) \rangle$  it is required to obtain  $\langle t_1 t_2 t_3 t_4 \rangle$ . Observe that

$$\begin{aligned} t_1 t_2 t_3 t_4 &= t_o^4 + t_o^3 \sum_{i=1}^4 \tau_i + t_o^2 \sum_{i=1}^3 \sum_{j>i}^4 \tau_i \tau_j \\ &\quad + t_o \sum_{i=1}^2 \sum_{j>i}^3 \sum_{k>j}^4 \tau_i \tau_j \tau_k + \tau_1 \tau_2 \tau_3 \tau_4 \end{aligned} \quad (5.2-3)$$

The  $\tau_j$ 's are Gaussian variates with zero mean. Hence

$$\begin{aligned} \langle \tau_1 \tau_2 \tau_3 \tau_4 \rangle &= \phi_{12} \phi_{34} + \phi_{13} \phi_{24} + \phi_{14} \phi_{23} \\ \langle \tau_i \tau_j \tau_k \rangle &= 0 \end{aligned} \quad (5.2-4)$$

(See for example, Miller 1964.)

In Eq. (5.2-4)  $\phi_{ij} \equiv \langle \tau(x_i, y_i) \tau(x_j, y_j) \rangle$ . It follows that

$$\begin{aligned} \langle t_1 t_2 t_3 t_4 \rangle &= t_o^4 + t_o^2 (\phi_{12} + \phi_{13} + \phi_{14} + \phi_{23} \\ &\quad + \phi_{24} + \phi_{34}) + \phi_{12} \phi_{34} + \phi_{13} \phi_{24} + \phi_{14} \phi_{23} \end{aligned} \quad (5.2-5)$$

It is convenient to write

$$I^2(u,v) = I_1 + t_o^2 \sum_{i=1}^6 I_{2i} + \sum_{i=1}^3 I_{3i} \quad (5.2-6)$$

where the  $I_{ij}$ 's are the contributions of integrals involving the covariances and  $I_1$  is the contribution of the  $t_o^2$  term. Consider the contribution of  $I_{31}$ ,  $I_{32}$ , and  $I_{33}$ . For  $I_{31}$  there results

$$\begin{aligned} I_{31} &= \left(\frac{1}{LW}\right)^2 \underbrace{\int \dots \int}_{8 \text{ times}} \phi_{12} \phi_{34} e^{-j2\pi(u(x_1-x_2+x_3-x_4) + v(y_1-y_2+y_3-y_4))} \\ &\quad \cdot \prod_{i=1}^4 dx_i dy_i \\ &= \left(\frac{1}{LW}\right) \underbrace{\int \dots \int}_{4 \text{ times}} \phi_{12} e^{-j2\pi(u(x_1-x_2) + v(y_1-y_2))} dx_1 dx_2 dy_1 dy_2 \\ &\quad \cdot \left(\frac{1}{LW}\right) \underbrace{\int \dots \int}_{4 \text{ times}} \phi_{34} e^{-j2\pi[u(x_3-x_4) + v(y_3-y_4)]} dx_3 dx_4 dy_3 dy_4 \end{aligned} \quad (5.2-7)$$

By Eq. (2.4-14), each integral is  $\langle I_n'(u,v) \rangle / [J/\lambda^2 f^2] \equiv \tilde{W}(u,v)$ . Hence  $I_{31} = \tilde{W}^2(u,v)$ . The contribution of  $I_{33}$  which involves  $\phi_{14} \phi_{23}$  is also  $\tilde{W}^2(u,v)$ . For  $I_{32}$ , there results

$$\begin{aligned} I_{32} &= \left(\frac{1}{LW}\right) \underbrace{\int \dots \int}_{4 \text{ times}} \phi_{13} e^{-j2\pi[u(x_1+x_3) + v(y_1+y_3)]} \\ &\quad \cdot dx_1 dx_3 dy_1 dy_3 \\ &\quad \cdot \left(\frac{1}{LW}\right) \underbrace{\int \dots \int}_{4 \text{ times}} \phi_{24} e^{j2\pi[u(x_2+x_4) + v(y_2+y_4)]} dx_2 dx_4 dy_2 dy_4 \end{aligned} \quad (5.2-8)$$

which may be written as

$$I_{32} = I'_{32} I''_{32} \quad (5.2-9)$$

where the primed quantities are the two integrals involved in the product. Consider  $I'_{32}$ , given by

$$I'_{32} = \frac{1}{LW} \int_{-L/2}^{L/2} \int_{-L/2}^{L/2} \int_{-W/2}^{W/2} \int_{-W/2}^{W/2} \phi(x_1 - x_3, y_1 - y_3) \cdot e^{-j2\pi[u(x_1 + x_3) + v(y_1 + y_3)]} dx_1 dx_3 dy_1 dy_3 \quad (5.2-10)$$

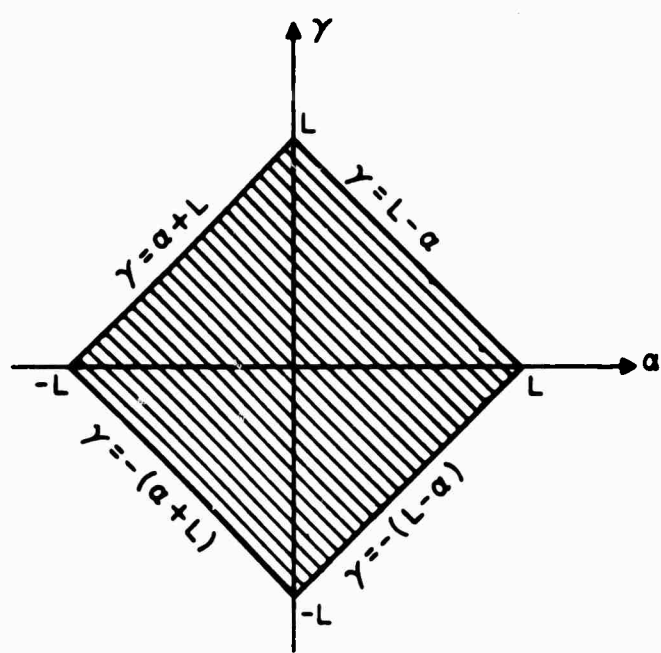
This integral can be simplified by considering the transformation

$$\begin{aligned} \alpha &= x_1 - x_3 \\ \beta &= y_1 - y_3 \\ \gamma &= x_1 + x_3 \\ \delta &= y_1 + y_3 \end{aligned} \quad (5.2.11)$$

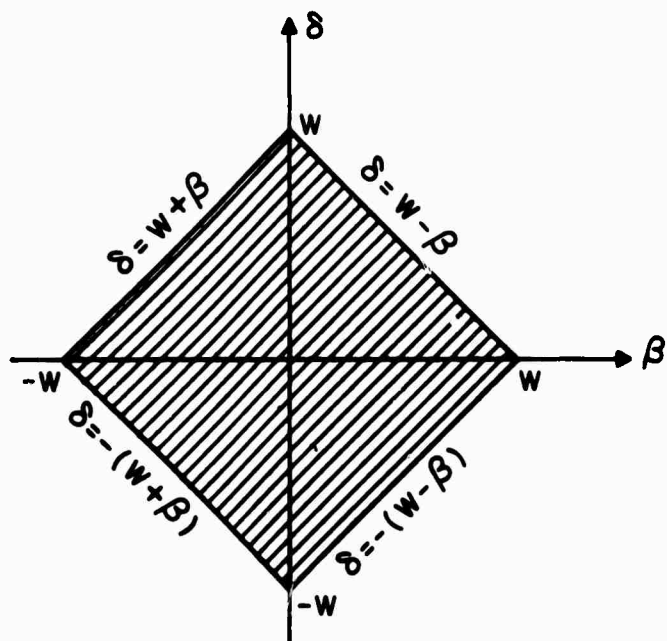
which has a Jacobian  $J(\frac{\alpha, \beta, \gamma, \delta}{x_1, x_3, y_1, y_3}) = 4$ . The field of integration is shown in Fig. 5.2-1. It is bounded by

$$\begin{array}{lll} -(L+\alpha) \leq \gamma \leq L + \alpha & -L \leq \alpha \leq 0 \\ -(L-\alpha) \leq \gamma \leq L - \alpha & L > \alpha > 0 \\ -(W+\beta) \leq \delta \leq W + \beta & -W \leq \beta \leq 0 \\ -(W-\beta) \leq \delta \leq W - \beta & W > \beta > 0 \end{array} \quad (5.2.12)$$

The result of using this transformation is



a) FIELD OF INTEGRATION IN  $\alpha$ - $\gamma$  PLANE



b) FIELD OF INTEGRATION IN  $\beta$ - $\delta$  PLANE

A-006-1-00-0072

FIG.5.2-1 DIAGRAM SHOWING THE FIELD OF INTEGRATION FOR EQ. (5.2-10)  
WITH THE TRANSFORMATION OF EQ.(5.2-II)

$$I'_{32} = \frac{1}{4} \left( \frac{1}{LW} \right) \int_{-L}^L \int_{-W}^W \phi(\alpha, \beta) \frac{\sin 2\pi u(L - |\alpha|)}{\pi u} \cdot \frac{\sin 2\pi v(W - |\beta|)}{\pi v} d\alpha d\beta \quad (5.2-13)$$

Since  $I'_{32}$  is an even function of  $u$  and  $v$ ,  $I''_{32} = I'_{32}$ .  $F(u, v)$  and  $I_{32} = F^2(u, v)$ . The function  $F(u, v)$  can be written as follows

$$F(u, v) = \frac{1}{4} \left( \frac{1}{LW} \right) \int_{-\infty}^{\infty} \int_{-\infty}^{\infty} d\xi d\eta W(\xi, \eta) \int_{-L}^L \frac{\sin 2\pi u(L - |\alpha|)}{\pi u} e^{j2\pi \xi \alpha} d\alpha \cdot \int_{-W}^W \frac{\sin 2\pi v(W - |\beta|)}{\pi v} e^{j2\pi \eta \beta} d\beta \quad (5.2-14)$$

where use was made of the relation

$$\phi(\alpha, \beta) = \int_{-\infty}^{\infty} \int_{-\infty}^{\infty} W(\xi, \eta) e^{j2\pi(\xi\alpha + \eta\beta)} d\xi d\eta. \quad (5.2-15)$$

The integrals

$$f_L(u, \xi) = \frac{1}{\pi u} \int_{-L}^L \sin 2\pi u (L - |\alpha|) e^{j2\pi \xi \alpha} d\alpha \quad (5.2-16)$$

$$f_W(v, \eta) = \frac{1}{\pi v} \int_{-W}^W \sin 2\pi v (W - |\beta|) e^{j2\pi \eta \beta} d\beta$$

can be written, after some tedious but straightforward algebra, as

$$f_L(u, \xi) = 2L^2 \operatorname{sinc}(u + \xi)L \operatorname{sinc}(u - \xi)L \quad (5.2-17)$$

$$f_W(v, \eta) = 2W^2 \operatorname{sinc}(v + \eta)W \operatorname{sinc}(v - \eta)W.$$

Hence

$$F(u,v) = LW \int_{-\infty}^{\infty} \int_{-\infty}^{\infty} W(t, \eta) \operatorname{sinc}(u+t)L \operatorname{sinc}(u-t)L \\ \cdot \sin(v-\eta)W \operatorname{sinc}(v+\eta)W dt d\eta \quad (5.2-18)$$

Observe that, when  $L$  is large, the product  $\operatorname{sinc}(u+t)L \operatorname{sinc}(u-t)L$  is small for any value of  $u$  except those near the origin (see Fig. 5.2-2), because the overlap occurs in the "tails" of the sinc functions. When  $L$  becomes very large, (a similar argument holds for  $W$ ) the amount of overlap becomes a vanishingly small and

$$\lim_{W,L \rightarrow \infty} F(u,v) = 0 \quad u,v \text{ not zero} \quad (5.2-19)$$

The exception occurs at the origin; there

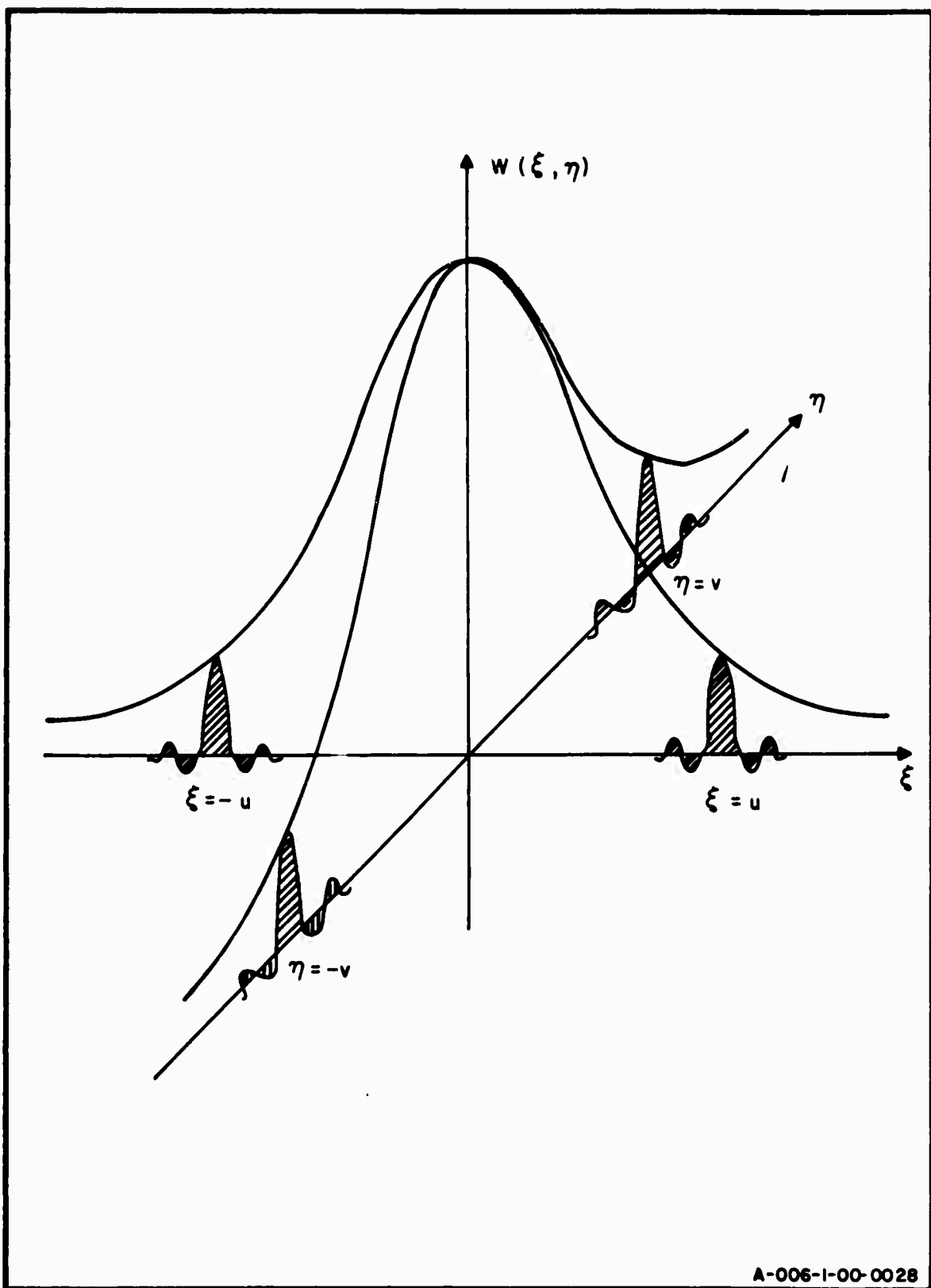
$$F(0,0) = LW \int_{-\infty}^{\infty} \int_{-\infty}^{\infty} W(t, \eta) \operatorname{sinc}^2(t)L \operatorname{sinc}^2(\eta)W dt d\eta \quad (5.2-20)$$

for which

$$\lim_{W,L \rightarrow \infty} F(0,0) = W(0,0) \quad (5.2-21)$$

The total contribution of the last three terms in Eq. (5.2-2) is  $2\tilde{W}^2(u,v) + F^2(u,v)$ .

Consider now the second summation in Eq. (5.2-6). There are two types of terms - those where the arguments of the covariance and the exponents contain the difference of the variables of integration and those where the exponent contains the sum while the covariance contains the difference. There



A-006-I-00-0028

FIG. 5.2-2 THE INTEGRAND OF EQUATION (5.2-18)

are four terms of the first type and two of the second. Each of the four terms where the arguments agree, contributes an amount

$$I_{21} = \frac{t_0^2}{(LW)^2} \underbrace{\int \dots \int}_{4 \text{ times}} \phi(x_1 - x_2, y_1 - y_2) e^{-j2\pi[u(x_1 - x_2) + v(y_1 - y_2)]} dx_1 dx_2 dy_1 dy_2 \cdot \left| \int_{-L/2}^{L/2} e^{-j2\pi ux} dx \right|^2 \cdot \left| \int_{-W/2}^{W/2} e^{-j2\pi vy} dy \right|^2 \quad (5.2-22)$$

$$= I_{23} = I_{24} = I_{26}$$

$$= t_0^2 \tilde{W}(u, v) H(u, v).$$

The two remaining terms involve the covariances  $\phi_{13}$  and  $\phi_{24}$  whose arguments do not agree with their respective exponents. Thus,

$$I_{22} = I_{25} = \frac{t_0^2}{(LW)^2} \underbrace{\int \dots \int}_{4 \text{ times}} \phi(x_1 - x_3, y_1 - y_3) e^{-j2\pi[u(x_1 + x_3) + v(y_1 + y_3)]} dx_1 dx_3 dy_1 dy_3 \cdot \left| \int_{-L/2}^{L/2} e^{-j2\pi ux} dx \right|^2 \left| \int_{-W/2}^{W/2} e^{-j2\pi vy} dy \right|^2 \quad (5.2-23)$$

$$= t_0^2 F(u, v) H(u, v) \quad (5.2-24)$$

$I_1$ , which involves only the constant  $t_0^4$ , is given by

$$I_1 = t_0^4 H^2(u, v). \quad (5.2-25)$$

Summing all the contributions gives

$$\begin{aligned} \langle I^2(u,v) \rangle &= (t_o^2 H(u,v) + \tilde{w}(u,v))^2 + \tilde{w}^2(u,v) + F^2(u,v) \\ &\quad + 2t_o^2 H(u,v) [F(u,v) + \tilde{w}(u,v)] \end{aligned} \quad (5.2-26)$$

The variance of  $\tilde{w}(u,v)$  is given by

$$\begin{aligned} \text{var } (\tilde{w}(u,v)) &= \langle \tilde{w}(u,v)^2 \rangle - \langle \tilde{w}(u,v) \rangle^2 \\ &= \langle (I(u,v) - t_o^2 H(u,v))^2 \rangle - \tilde{w}^2(u,v) \\ &\quad - \tilde{w}^2(u,v) + F^2(u,v) + 2t_o^2 H(u,v) \\ &\quad \cdot [F(u,v) + \tilde{w}(u,v)]. \end{aligned} \quad (5.2-27)$$

For large apertures,  $\text{var } (\tilde{w})$  is given to a good approximation by (except at the origin)

$$\text{var } (\tilde{w}(u,v)) \approx \tilde{w}^2(u,v) \quad (5.2-28)$$

a result which follows from the argument leading to Eq. (5.2-19) and from the fact that  $H(u,v)$  is very small away from the origin for large apertures. The variability of  $\tilde{w}(u,v)$  is quite pronounced since

$$\frac{\text{var } (\tilde{w})}{\langle \tilde{w} \rangle^2} \approx \frac{\tilde{w}^2(u,v)}{\tilde{w}^2(u,v)} = 1 \quad (5.2-29)$$

## 6. EXPERIMENTAL TECHNIQUES AND APPARATUS

The feasibility of reliable spectral density measurements by diffraction is borne out by the theoretical considerations of the earlier chapters. The results of chap. 4 provide a basis against which experimental results can be compared. Such experimental results are given in chap. 7. The present chapter is a discussion of the laboratory apparatus and procedures used to obtain the experimental data.

The first section gives a brief description of the experimental apparatus used for obtaining spectral density measurements. Section 6.2 describes the basic measuring procedure and its advantage over more direct methods. Section 6.3 summarizes the techniques by which various film noise parameters can be measured. Section 6.4 describes the use of contoured apertures and aperture functions to achieve "desirable" zero-order diffraction patterns since intense, spatially distributed, zero-order diffraction levels preclude the measurement of power spectra. Finally, Sec. 6.5 contains a description of a magnification technique by which low-noise spectra can be enhanced.

### 6.1 DESCRIPTION OF MEASUREMENT EQUIPMENT

The spectral density measurements were performed on the coherent optical system shown schematically in Fig. 6.1-1 . The same basic system has been extensively described in the thesis of J. Minkoff (Minkoff 1967). A brief description of the system, together with some peripheral equipment is provided here.

The basic system consisted of a granite bench upon which was mounted a He-Ne (6328 Å) laser, spatial filters, collimating

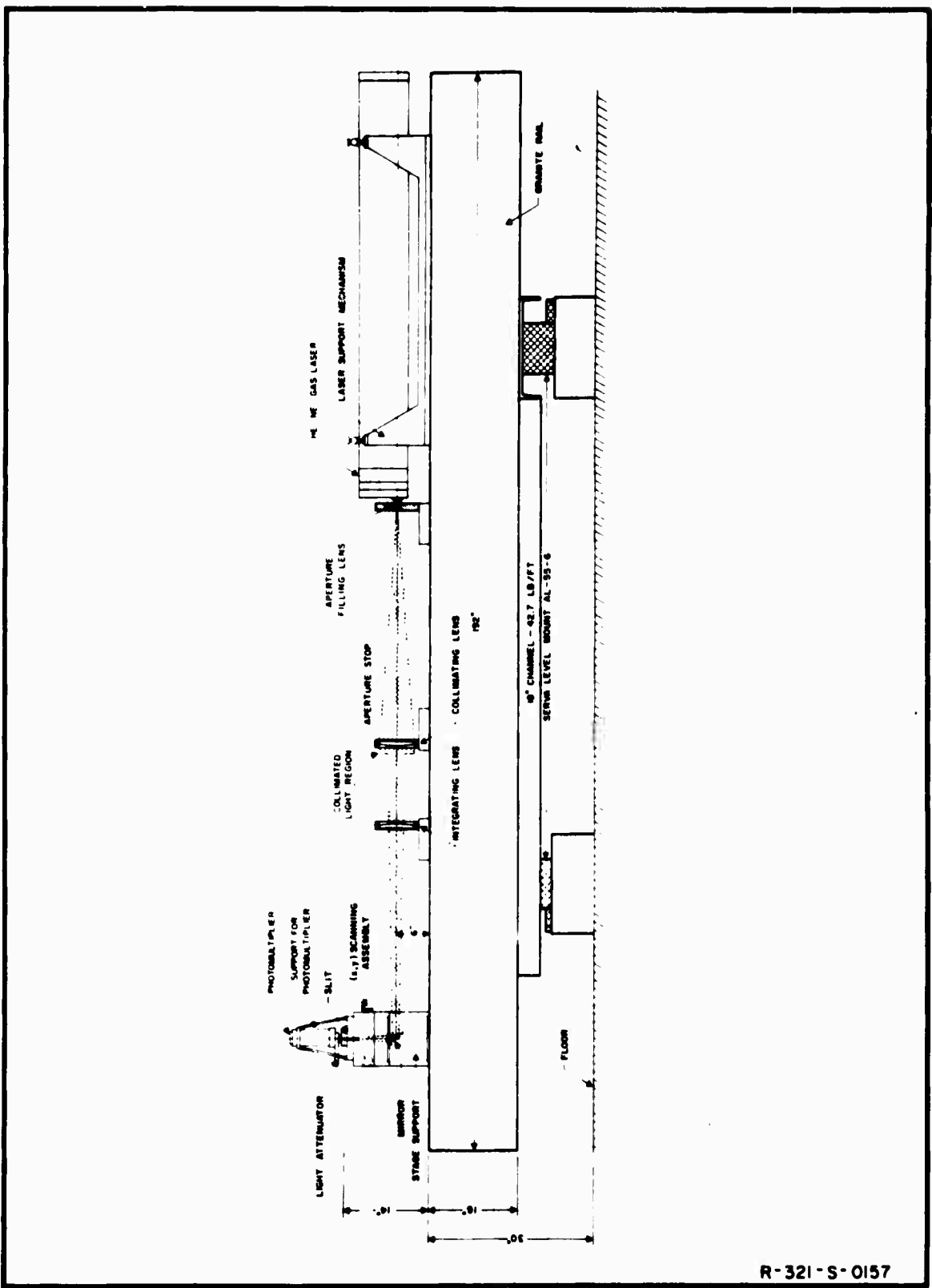


FIG. 6.1-1 SCHEMATIC DIAGRAM OF COHERENT OPTICAL SYSTEM

and integrating lenses, a scanning assembly and a photomultiplier tube. The output of the photomultiplier tube fed an (x,y) recorder through an amplifier which could be operated in a linear or logarithmic mode. All the optical components and light beams were shielded against extraneous light, dust, and air currents by cylindrical-bellow light shields and light-tight boxes. As an added precaution, all unnecessary lights were turned off during the actual experiments.

The optical bench was 16 ft x 18 in. x 18 in. with a steel base mounted in tripod fashion on air-operated, self-regulated damping mounts. The top surface of the bench was ground to a flatness of  $\pm 0.0001$  in. A T-shaped slot was machined into the bench to accommodate the optical components. One surface of this slot provided a reference surface for the components and was machined to a flatness of .001 in. The actual system showing the laser, bellows, etc., is shown in Fig. 6.1-2 .

The laser provided a 1.8-mm diameter vertically polarized beam. This beam was focused by a spreading lens (microscope objective) onto a  $20\mu$  pinhole serving as a spatial low-pass filter (Fig. 6.1-3 ). Beyond the pinhole, the beam spread sufficiently to cover the entire collimating lens. The location of the pinhole in transverse directions was controlled by a set of positioning screws and the axial location was controlled by positioning a barrel-type pinhole mount along the optic axis (Fig. 6.1-4 ). The pinhole was positioned at the focal point of the objective in a way that would allow uniform illumination to appear across the entire collimating lens aperture.

The data sample was located in the region between the collimating and integrating lenses - the so-called collimated region. The sample was rigidly held between two optically flat glass pieces and mounted on a rotary table which provided six



1. Granite Optical Table
2. Laser Light Source
3. Mount for Spreader-Lens Assembly
4. Bellows Light-Shields
5. Light-Shield over Collimated Region  
(Location of Modulator)
6. Light-Shield for XY-Scanning Mechanism
7. Laser Power-Supply
8. Readout and Photomultiplier-Supply Electronics

Fig. 6.1-2 Coherent Optical System

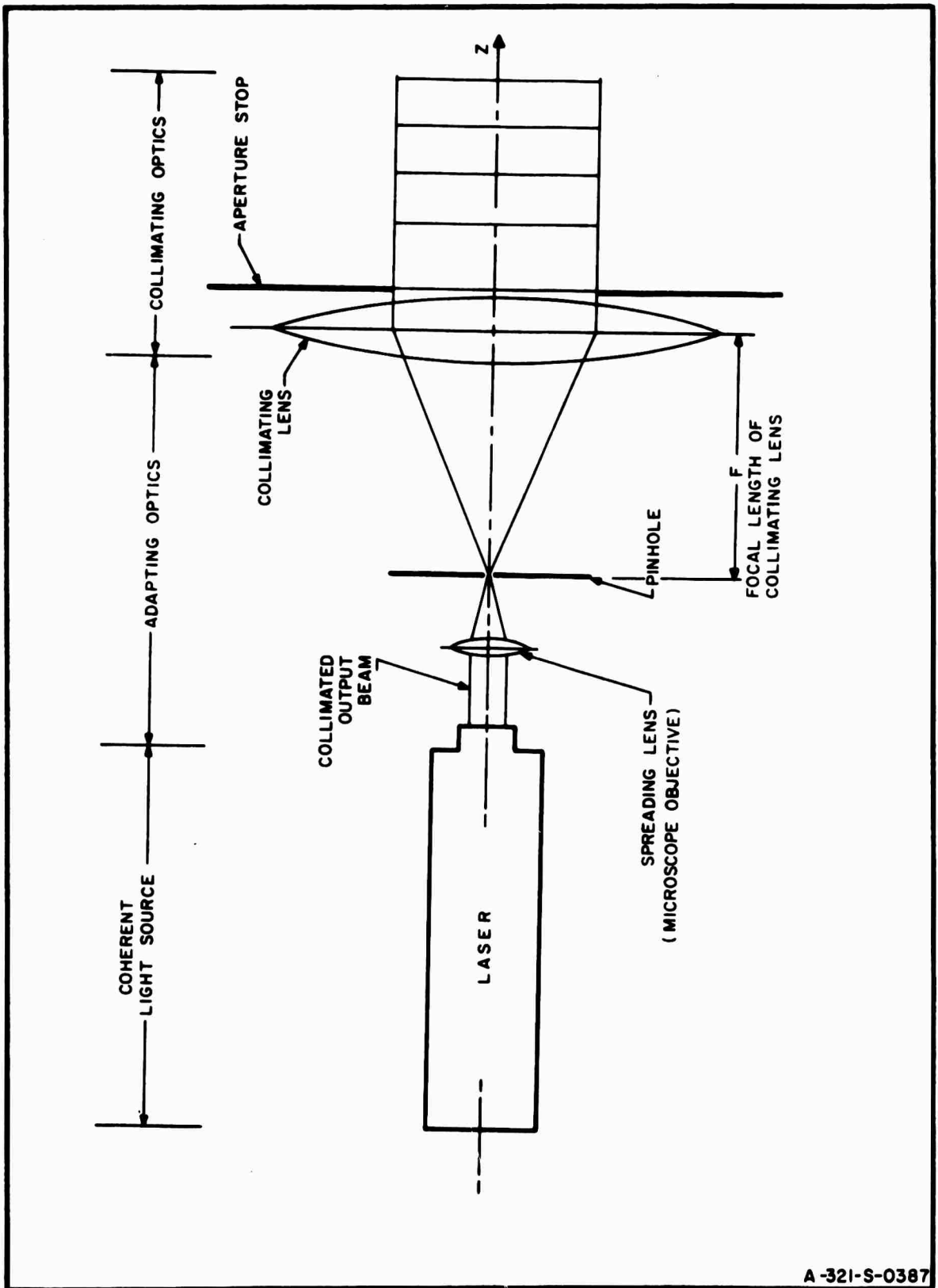
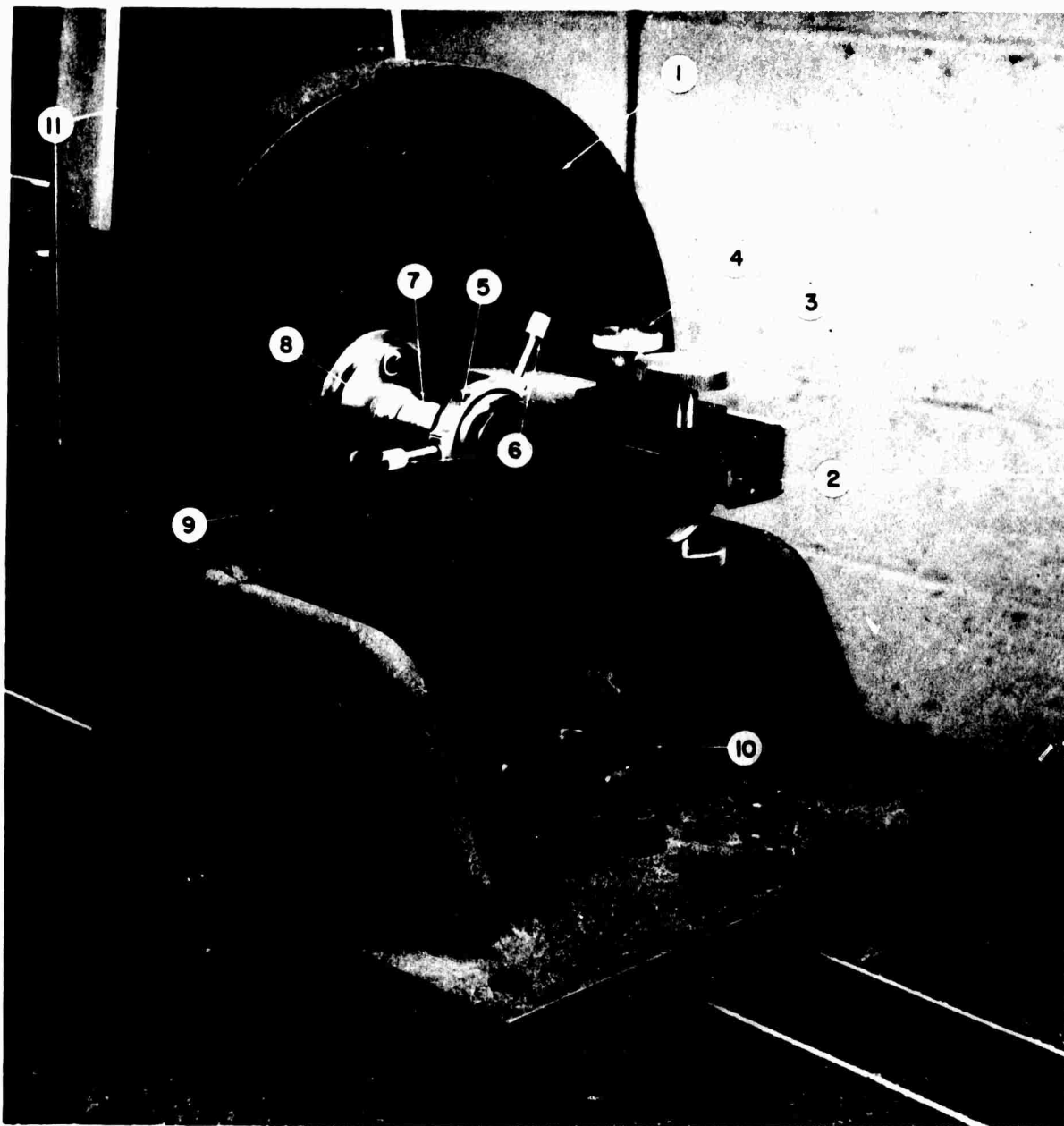


FIG. 6.1-3 FILTERING AND COLLIMATION OF LASER BEAM



1. Lens Mount
2. Microscope-Barrel Assembly
3. Coarse Focusing Adjustment
4. Fine Focusing Adjustment
5. Pinhole Assembly
6. Pinhole Positioning Screws
7. Microscope Objective Lens
8. Objective-Lens Holder
9. Spreader-Lens-Assembly Mounting Plate
10. Lens-Mount Locking Knob
11. Mounting-Plate Adjustment Screws

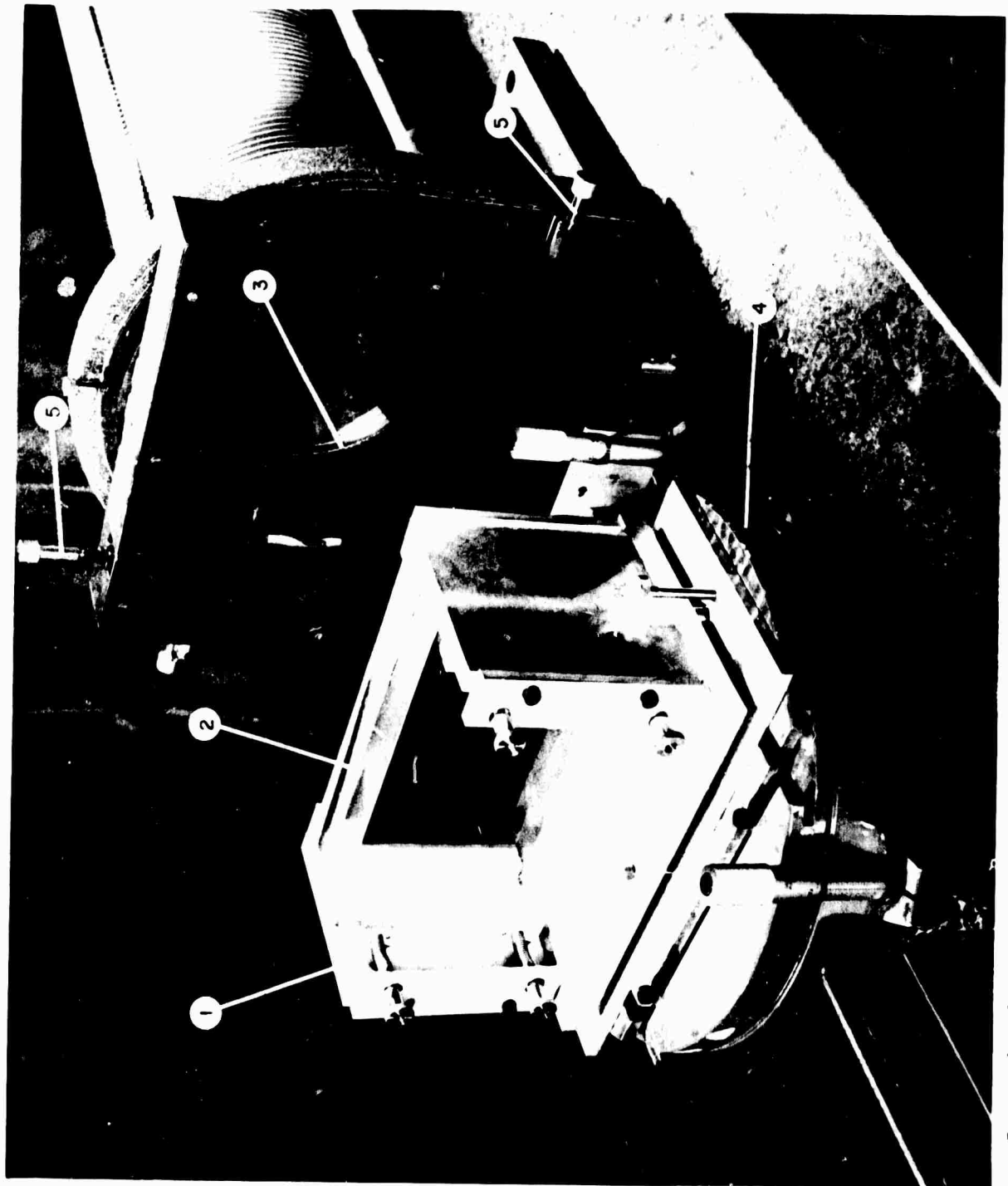
Fig. 6.1-4 Spreader-Lens Assembly

degrees of freedom for precise positioning. The aperture stop was located immediately after the collimating lens and was interchanged according to the type of apodisation used (Sec. 6.3). The phase-eliminating liquid gate [ see Fig. 4.1-1] was located in the collimated region and is shown in Fig. 6.1-5 with the film sample in place. The light transmitted by the sample was then focused on the  $x'y'$  plane by the integrating lens and detected with the scanning mechanism shown in Figs. 6.1-7 and 6.1-7 . Scanning was possible in two orthogonal directions and it was possible to allow any size scanning slit to be mounted on the scanning assembly. Between the scanning slit and the photomultiplier tube were located adjustable neutral-density filters to limit the peak intensity of light entering the photomultiplier. By adjusting the neutral density filters, the light level at the photomultiplier was held nearly constant despite the varying optical densities of the various samples. The entire scanning mechanism was housed in a light-tight box. System alignment was accomplished using an auto-collimator telescope shown in Fig. 6.1-6 .

The transmittance of the sample was measured by an automatic recording microdensitometer (Joyce Ltd., Model MK 111C) shown in Fig. 6.1-8 . The microdensitometer provided a voltage proportional to optical density, which is related to intensity transmittance by

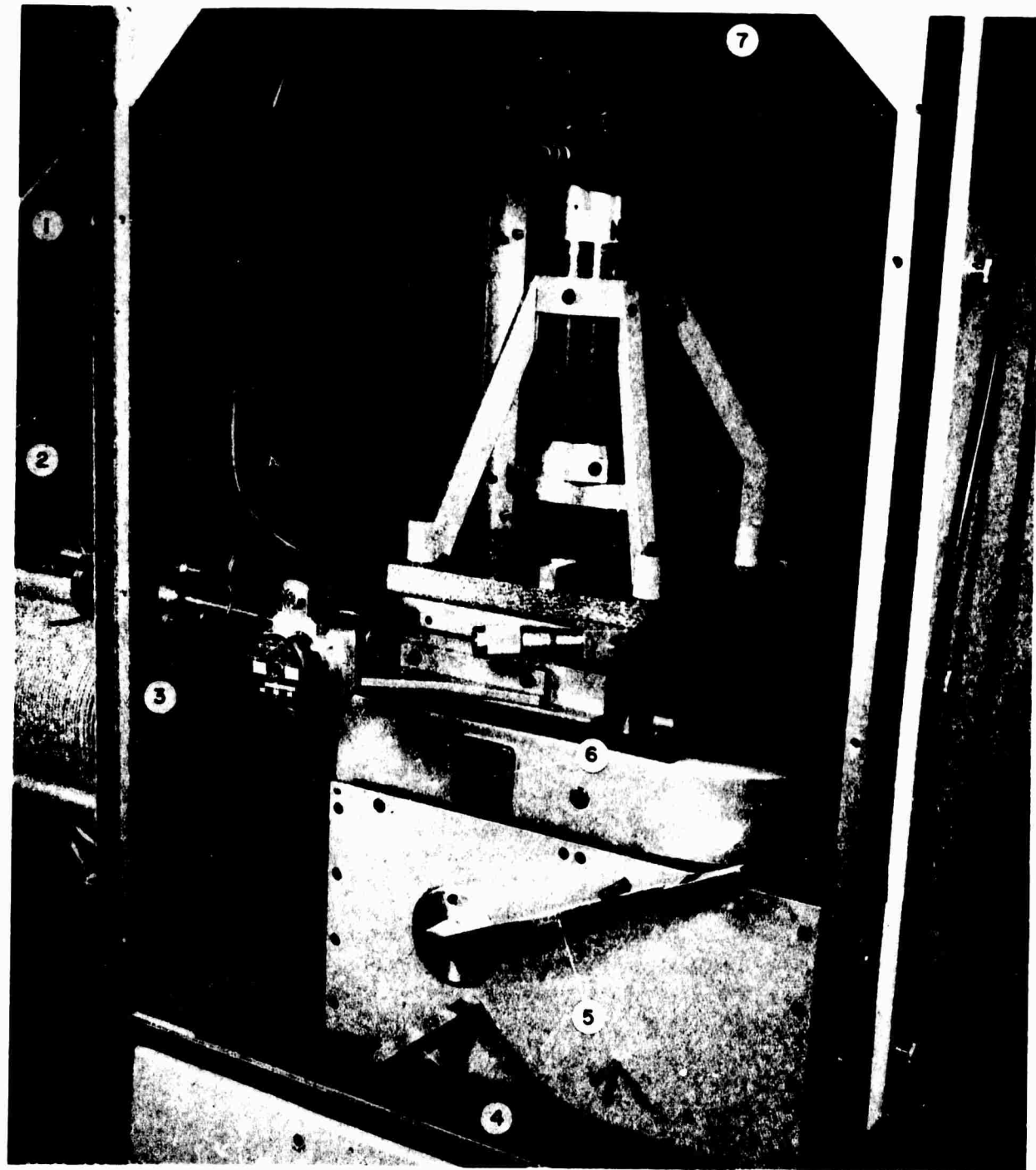
$$\text{Density} = -\log_{10} T$$

The square root of  $T$  is denoted as the average amplitude transmittance  $T_A$  but for reasons given in Sec. 6-3, the amplitude transmittance obtained by incoherent illumination



1. Liquid Gate
2. Film Sample
3. Adjustable Diamond Aperture
4. Rotary Table with Controls
5. Aperture Controls

Fig. 6.1-5 Gate and collimated Region



1. Light Shield
2. Slit-Traversing Knob
3. Traversing-Mechanism Connecting Shaft
4. Pellicle-Assembly Support Bar
5. Mirror-Position Lever
6. Window for Pellicle Assembly
7. Photomultiplier Voltage Divider Unit

Fig. 6.1-6 Scanning-Mechanism Assembly

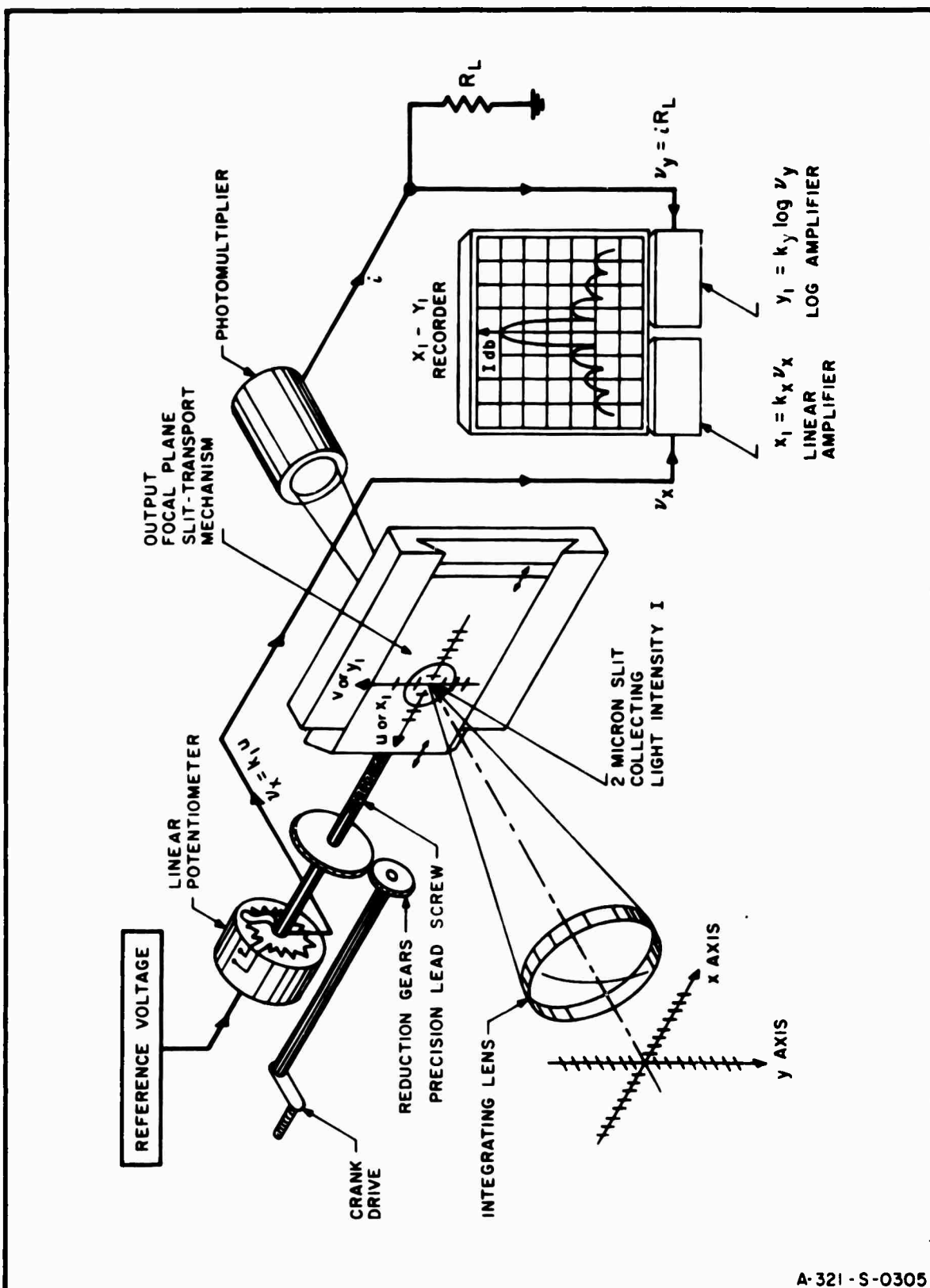
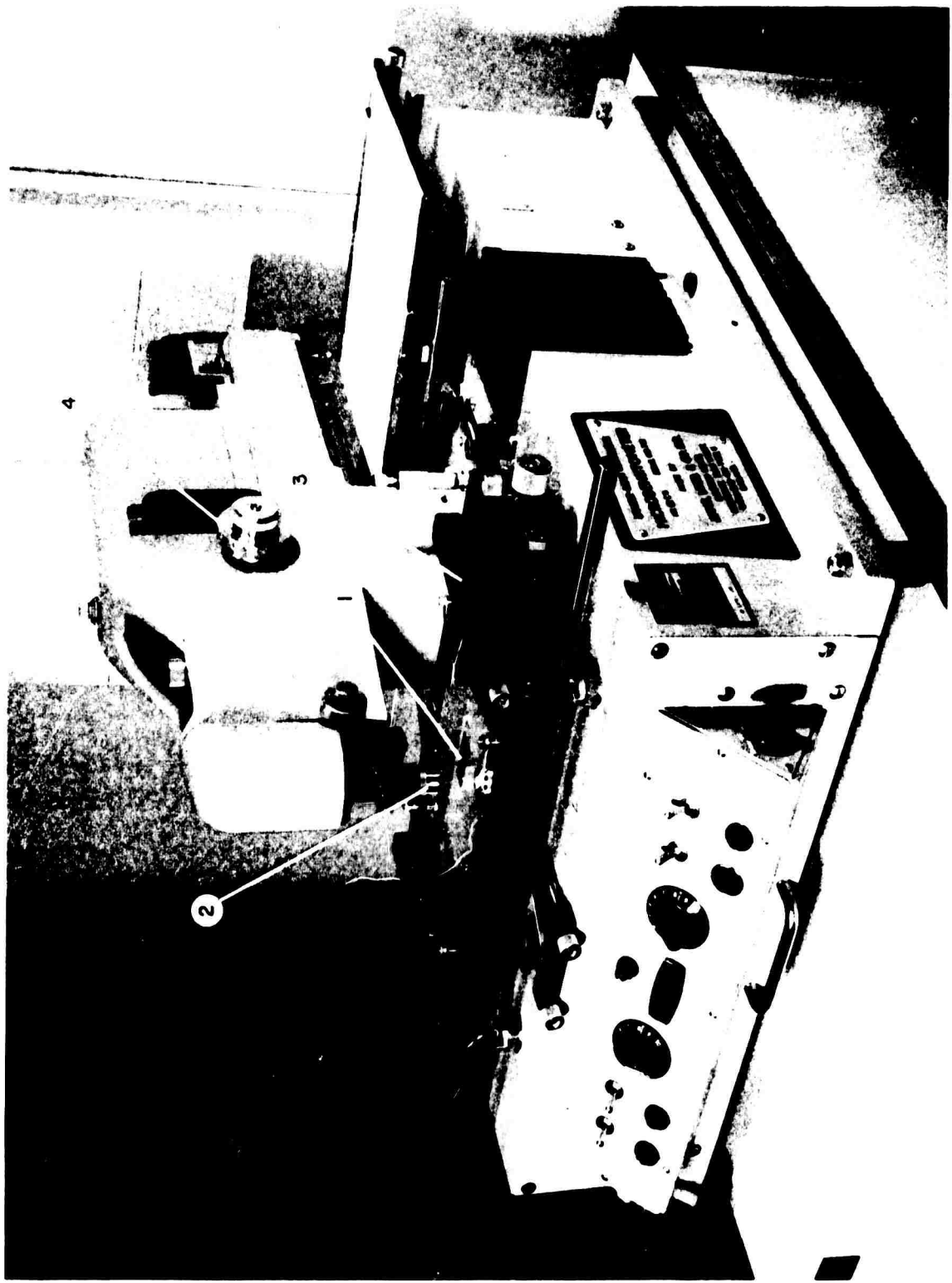


FIG 6.1-7 SCHEMATIC REPRESENTATION OF SYSTEM FOR MEASUREMENT BACK-FOCAL PLANE LIGHT INTENSITY



1. Sample
2. Objective
3. Movable Table
4. Aperture Control

Fig. 6.1-8 Automatic Recording Microdensitometer

was not assigned the same symbol as the transmittance measured with the laser. Microdensitometer traces were used to determine the uniformity of film exposure (Fig. 6-1-9).

In some cases, grain structure of film samples were altered by magnification. Magnification was done by two separate means, both involving incoherent illumination. Low-resolution magnification was obtained with a Wollensak "Raptar" F/4.5, 50-mm focal length lens. High resolution was obtained with an American Optical "Fluorestar" microscope, Cat. No. L1OTU-FDW. The microscope, power supply, and exciter are shown in Fig. 6.1-10.

## 6.2 MEASUREMENT TECHNIQUE AND CALIBRATION

In this section, the basic measurement technique is described. A rectangular aperture of area  $LW$  is assumed. If  $L=W$  the results can be applied to a diamond aperture of the same area provided that scanning is then along the line  $u=v$ . For the analysis that follows, it is sufficient to deal only with the relative light intensity  $I(u,v)$ , so that the factor  $J^2/(\lambda f)^2$  of Eq. (2.4-13) will not appear in any of the equations.

The zero-order light diffraction pattern of a rectangular aperture of length  $L$  and width  $W$  is given by

$$I^{(0)}(u,v) = H(u,v) \quad (6.2-1)$$

where  $H(u,v) = LW \operatorname{sinc}^2 uL \cdot \operatorname{sinc}^2 vW$ . When the same system is loaded with an object of average complex transmittance  $R_o$  the resulting average diffraction intensity is

$$\begin{aligned} \langle I(u,v) \rangle &= |R_o|^2 H(u,v) + \tilde{W}(u,v) \\ \tilde{W}(u,v) &= W(u,v) * H(u,v) \\ &\equiv \text{apparent spectrum.} \end{aligned} \quad (6.2-2)$$



(A)



(B)

KODAK 2479 FILM;  
AVERAGE INTENSITY TRANSMITTANCE,  $T_I = 0.28$

A-006-I-00-0019

FIG. 6.1-9 INTENSITY TRANSMITTANCE MEASUREMENTS WITH A  
MICRODENSITOMETER. (A) 10 MICRON SLIT; (B) 50  
MICRON SLIT.



1. Power Supply
2. Camera
3. Camera Adapter
4. Mercury-Xenon Light Source
5. Trinocular Microscope
6. Film Sample

Fig. 6.1-10

Microscope and Camera Assembly

If the system is unloaded and a point scanning slit is temporarily assumed, the output of the log amplifier, when the slit is at  $(u, v)$ , will produce a displacement on the recorder given by

$$C_1(u, v) = 10 \log H(u, v)$$

where the logarithm is to base 10. When the sample is inserted into the system, the displacement will be

$$C_2(u, v) = 10 \log [H(u, v) |R_o|^2 + \tilde{w}(u, v)]$$

If the recorder is now offset by a displacement  $\Delta_{db}$  so that  $C_2(0, 0) + \Delta_{db} = C_1(0, 0)$  then it follows that ( $\Delta_{db} \equiv 10 \log \Delta$ )

$$\begin{aligned} 10 \log [\Delta |R_o|^2 LW + \tilde{w}(0, 0)] &= 10 \log LW \\ &\equiv C_2'(0, 0) \end{aligned} \quad (6.2-3)$$

If  $LW |R_o|^2 \gg \tilde{w}(0, 0)$ , a condition which is easily met in most cases, then to a high degree of accuracy,

$$\Delta = |R_o|^{-2} \quad (6.2-4)$$

To get an idea of the relative magnitude of these quantities, assume that  $\tilde{w}(u, v) \approx w(u, v)$  and that the random checkerboard representation of film grain noise is used in an estimate of  $w(0, 0)$ . Then from Sec. 4.2

$$w(0, 0) = \ell^2 t_o (1 - t_o)$$

where  $\ell^2$  = the area of a grain and  $t_o$  is the average transmittance of the sample. Assume the following typical values

$$\begin{aligned}
 t_o &= .5 \\
 l &= 10 \text{ microns} \\
 w &= L = 50 \text{ mm}
 \end{aligned}$$

Then  $w(0,0)$  is 74 db below the peak of the zero-order light and the approximation in Eq. (6.2-4) is justified.

The two traces,  $C_1(u,v)$  and  $C_2'(u,v)$ , thus obtained have the following properties. The addition of  $\Delta_{db}$  effectively compensates for the average density of the film without affecting the power spectrum which results from transmittance fluctuations about the average. If the sample were noiseless, the traces would coincide at all spatial frequencies. Since the sample is not noiseless, the curve  $C_2'(u,v)$  will be above  $C_1(u,v)$ . Suppose that the scanning is done along the  $u$ -axis ( $v = 0$ ) and there exists a frequency  $u_o$  such that for  $u > u_o$ ,  $C_2'(u_o,0) > C_1(u_o,0) + 10$  db; then the error in interpreting  $C_2'(u,0)$  as  $10 \log W(u,0) + 10 \log |R_o|^2$  is 11% or less. This technique has the very strong advantage of avoiding any kind of operation on the data except compensating for  $|R_o|^2$ . This means that the presence of unwanted noise such as might be contributed by random lens errors, scattering from mirrors, etc., which add significantly to the zero-order light away from the origin, (Fig. 6.2-1), does not upset the validity of the measurement, since the power spectral light component must be a factor of 9 or more above the diffracted light of the unloaded system before it is interpreted as such. Fig. 6.2-2 summarizes the measurement procedure. Smoothed light patterns are shown as they would appear through a slit of nonzero area.

A disadvantage of this procedure is that the spectrum  $\tilde{W}(u,v)$  may not become observable in the sense of the 10-db criteria of the previous paragraph until the zero-order light is relatively small, which may occur at fairly high frequencies.

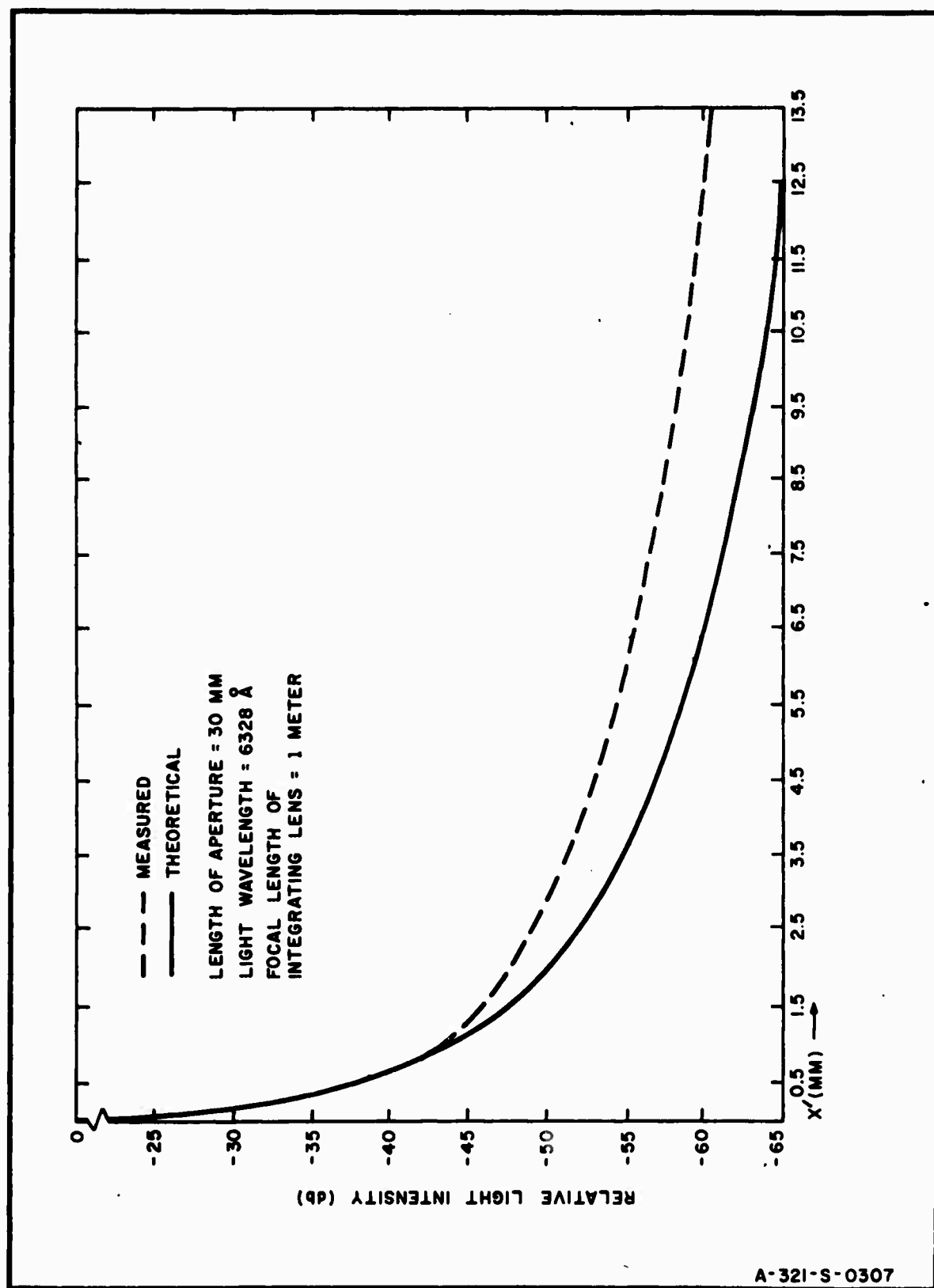


FIG. 6.2-1 SCATTERED-LIGHT LEVEL OF OPTICAL SYSTEM

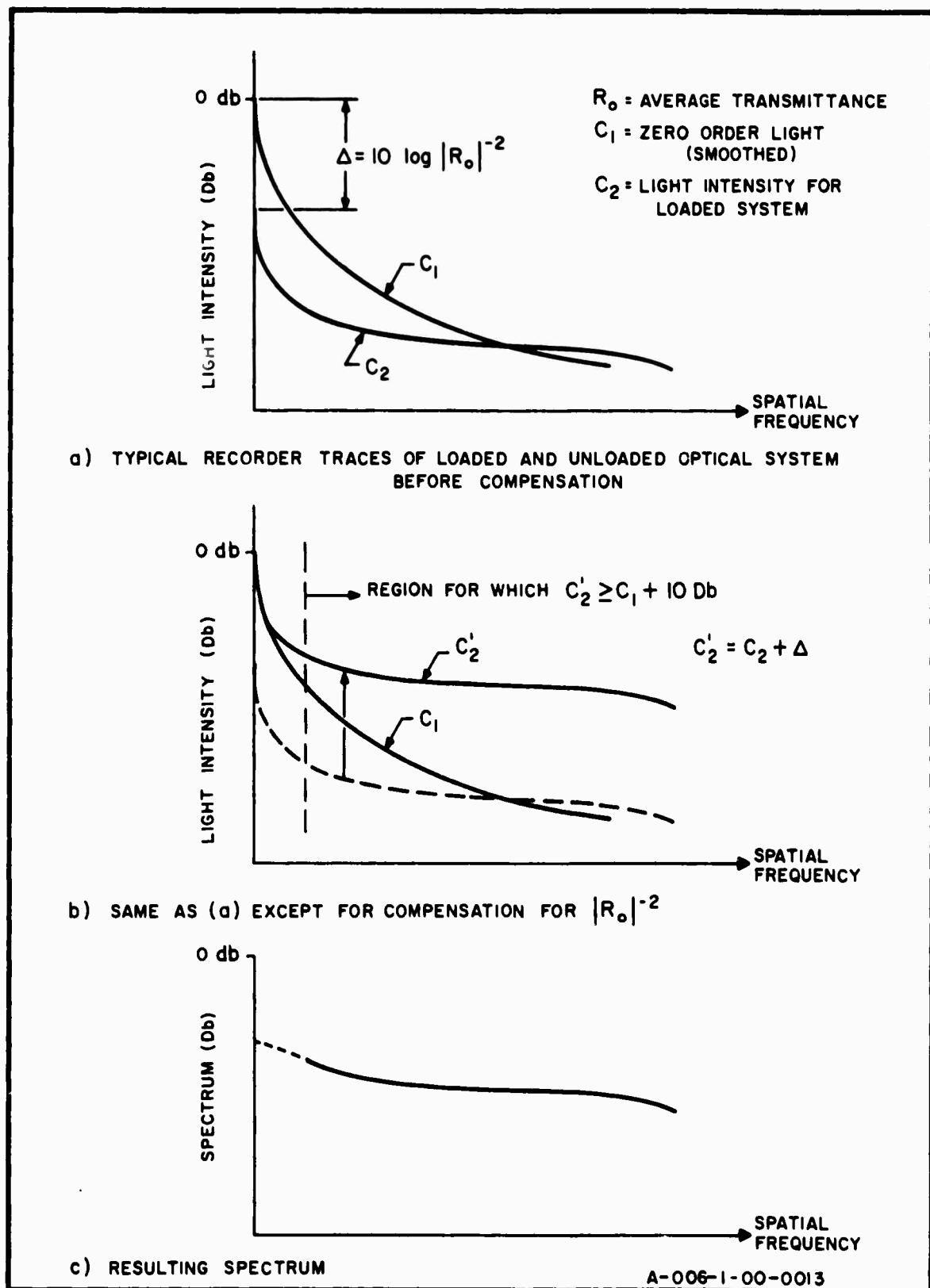


FIG. 6.2-2 ILLUSTRATING POWER SPECTRUM MEASUREMENT TECHNIQUE

For example, an estimate may be obtained by taking the random checkerboard configuration as a model of film grain noise and assuming diffraction by a rectangular aperture of area  $LW$  for which the DC value of the power spectrum will be 10 db above the zero-order intensity at spatial frequencies satisfying

$$t_o(1 - t_o) \lambda^2 \geq \frac{9LW t_o^2}{(\pi u L)^2}$$

which for the numbers previously chosen gives

$$\begin{aligned} u &> 100 \text{ cycles/mm for } \lambda = 10\mu \\ u &> 10 \text{ cycles/mm for } \lambda = 100\mu \end{aligned}$$

The discussion so far has assumed a point scanning slit and that  $\tilde{W}(u,v)$  and not its estimate was available in the  $(u,v)$  plane. For calibration purposes, the effect of slit area must be taken into account. The slit is chosen large enough to reduce the variability of the estimate so that repeated experimental runs yield the same result, and not so large as to smooth variations in the power spectrum. In measuring the grain noise of film, the slit may be several times the width of the main lobe of the zero-order diffraction pattern. If, simultaneously, the variation in the power spectrum over the frequency span of the slit is sufficiently small to enable the spectrum to be approximated by its value at the center frequency of the slit filter, then the calibration of the spectrum is straightforward as will now be shown.

From Eq. (3.6-5), the light observed through a slit of area  $A_s$ , described by the filter function  $\gamma(u',v')$  is

$$I_o(u,v) = \frac{(\lambda f)^2}{A_s} \int_{-\infty}^{\infty} \int_{-\infty}^{\infty} I(u',v') g(u-u',v-v') du' dv' \quad (6.2-5)$$

The observed zero-order light at the origin is then

$$I_o^{(0)}(0,0) = \frac{(\lambda f)^2}{A_s} \int_{-\infty}^{\infty} \int_{-\infty}^{\infty} H(u', v') g(-u', -v') du' dv' \quad (6.2-6)$$

With the assumptions of the preceding paragraph, there results

$$I_o^{(0)}(0,0) \approx \frac{(\lambda f)^2}{A_s} \quad (6.2-7)$$

The observed apparent spectrum at the origin is given by

$$\begin{aligned} \tilde{w}_o(0,0) &= \frac{(\lambda f)^2}{A_s} \int_{-\infty}^{+\infty} \int_{-\infty}^{+\infty} \tilde{w}(u', v') g(-u', v') du' dv' \\ &\approx \frac{(\lambda f)^2}{A_s} \tilde{w}(0,0) \int_{-\infty}^{+\infty} \int_{-\infty}^{+\infty} g(u', v') du' dv' \\ &\approx w(0,0) \end{aligned} \quad (6.2-8)$$

If the measurement is properly designed, then  $\tilde{w}(0,0) \approx w(0,0)$ . Following the measurement procedure outlined in this section, assume that the extrapolated value of the curve  $C_2'(u,0)$ , (Fig. 6.2-2) is  $-r$  db below the peak zero-order light. Then it follows that the suitable calibration in the case of grain noise is

$$10 \log \frac{t_o^{-2} w(0,0)}{(\lambda f)^2 / A_s} = -r \quad (6.2-9)$$

or

$$w(0,0) = \frac{(\lambda f)^2}{A_s} t_o^{-2} 10^{-r/10} \quad (6.2-10)$$

Eq. (6.2-10) is then the proper calibration for the spectrum. Observe that the spectrum has units of meter<sup>2</sup>. From Eq. (6.2-9), it may be seen that the ratio of power spectral to zero-order light at the origin depends on the parameters  $\lambda$ ,  $f$  and  $A_s$ ; since  $A_s$  is usually determined by other considerations (Sec. 3.6) and  $\lambda$  is the wavelength of the coherent source and is therefore fixed, improvement in this ratio can best be achieved by using lenses with short focal lengths.

From the discussion so far, it can be seen that a central problem in spectral measurements by diffraction is the observation of the spectral component of light in the presence of the strong zero-order diffraction of the aperture. Measurements of the spectrum at the origin, where the zero-order is a maximum, cannot be made unless phase-grating type aperture functions are used (Sec. 6.5). In general, with the origin excluded, it is desirable to use a large aperture which, in addition to adding to the resolution capability of the system, would concentrate the zero-order light in the vicinity of the origin while reducing the envelope of the sidelobes. The envelope of the relative diffraction pattern of a square aperture is the curve connecting the local maxima of the function  $H(u,v)$  and is given by

$$Z(u,v) = \left( \frac{1}{\pi u L} \right)^2 \left( \frac{1}{\pi v W} \right)^2 LW \quad u,v \neq 0$$

which decreases as  $(LW)^{-1}$ . Apodisation by aperture shaping can be used to reduce the envelope even further. This is discussed in Sec. 6.4.

### 6.3 DETERMINATION OF FILM NOISE PARAMETERS

The purpose of this section is to show how various film-noise parameters can be determined experimentally.

(a) Measurement of Intensity Transmittance of Film

The intensity transmittance of a film sample, denoted by  $T(x,y)$  is the ratio of the transmitted to incident light intensity at the point  $(x,y)$ . Sample traces of  $\{T(x,y)\}$  can be obtained with the microdensitometer described in Sec. 6.1. When the microdensitometer is used with a large scanning aperture, the traces will have few fluctuations and essentially furnish the average value of  $\{T(x,y)\} = T_0$ . When a small scanning aperture is used, the resulting trace furnishes qualitative information regarding the grain noise of the film.

It should be noted that the square root of  $T_0$  is not the average amplitude transmittance  $t_0$ , defined as the average magnitude of the ratio of transmitted to incident amplitude despite the tendency for some authors to ignore the distinction (Kozma 1966). The inequality can be demonstrated as follows. Since

$$T(x,y) = \frac{I_T(x,y)}{I_I(x,y)} = \left| \frac{E_T(x,y)}{E_I(x,y)} \right|^2 = t^2(x,y)$$

it follows that

$$T_0 = \langle T(x,y) \rangle = t_0^2 + \sigma_\tau^2$$

where  $\sigma_\tau^2 = \langle (t(x,y) - t_0)^2 \rangle$ . Hence  $t_0 \neq T_0^{\frac{1}{2}}$ . If  $t_0$  and  $t_0^2$  can be measured with sufficient accuracy, the above relation provides a scheme by which  $\sigma_\tau^2$  could be determined. Experiments have shown, however, that the measured values of  $T_0$  obtained with a microdensitometer are not reliable enough to provide an accurate value of  $\sigma_\tau^2$ .

Sample functions of intensity transmittance can be used to test the uniformity of film transmittance. Uneven exposures result in systematic transmittance variations [i.e.,  $T_0 = T_0(x,y)$ ] which can easily be observed in the sample function.

(b) Measurement of the Magnitude of the Average Complex Transmittance,  $|R_o|$

The complex transmittance is defined by Eq. (2.1-5); the magnitude of the average complex transmittance can be measured with the coherent optical system shown in Fig. 6.1-2 by measuring the attenuation in the peak zero-order light when the sample is inserted in the collimated region. In this measurement no liquid gate is used. It is seen from Eqs. (6.2-1) and (6.2-2) that if  $\tilde{w}(0,0)$  is neglected, the ratio of  $\langle I(0,0) \rangle$  to  $I^{(0)}(0,0)$  is  $|R_o|^2$ .

(c) Measurement of the Average (Coherent) Amplitude Transmittance,  $t_o$

The amplitude transmittance  $t_o$  is measured by the same technique used to measure  $|R_o|$  except that the film sample is immersed in a matched liquid gate which has the effect of negating phase noise. In this case  $R_o = t_o$  and the attenuation in the peak zero-order light when the film sample is in the system is  $t_o^2$ .

(d) Determination of the Variance of the Random Phase Process  $\{\psi(x,y)\}$

When the processes,  $\{t(x,y)\}$  and  $\{\psi(x,y)\}$  are considered independent and  $\{\psi(x,y)\}$  is a wide-sense, zero-mean Gaussian process, then

$$\langle R(x,y) \rangle \equiv R_o = t_o e^{-(1/2)\sigma_\psi^2} \quad [\text{Sec. 4.3, Eq. (4.3-3)}].$$

where

$$\sigma_\psi^2 = \text{the variance of } \{\psi(x,y)\}$$

Under these conditions, a graph of  $R_o$  vs  $t_o$  should be a straight line with slope  $m = e^{-(1/2)\sigma_\psi^2}$ . Hence  $\sigma_\psi^2$  can be obtained from  $\sigma_\psi^2 = 2 \ln 1/m$

(e) Determination of the Isotropic Statistics of Film Noise

If film noise is isotropic, the power spectrum is a function of the frequency  $w$  where  $w = (u^2 + v^2)^{\frac{1}{2}}$ . In this case, the power spectrum is an even function of spatial frequencies and depends only on the distance from the origin of the spatial frequency plane. In general, when the noise is anisotropic, the two-dimensional power spectrum will not be an even function of frequency as discussed in Sec. 2.3 and will not be a symmetric function of its arguments. Hence, anisotropic noise can be detected experimentally by observing asymmetric spectra about the origin or unequal spectra along different orthogonal axes.

(f) Variations of the Power Spectrum with Transmittance

Both the random checkerboard and overlapping circular grain model predict a maximum in the power spectrum of grain noise in the vicinity of  $t_o \approx 0.5$ . Following the procedure outlined in Sec. 6.2, this can be verified experimentally by obtaining the spectra at fixed spatial frequencies for a large number of film samples with varying transparencies. The variation of the spectrum of the total noise with  $R_o$  can be obtained with the same procedure, provided that the liquid gate is not used.

(g) Measurements by Magnification

Under certain conditions, magnification can be used to obtain the spectra of low noise films and the frequency response of optical systems. This technique is discussed further in Sec. 6.5.

#### 6.4 REDUCTION OF ZERO-ORDER SIDELOBES BY APERTURE SHAPING

The reduction of the zero order light, a problem of central importance in spectral measurements by diffraction,

can be accomplished, in principle at least, in two ways. The most direct way is to decrease the dimensions of the aperture diffraction pattern by increasing the transverse dimensions of the aperture. However, in practice, the aperture is usually already as large as can be, being limited by the size of the lens, the uniformity of the collimated beam, and the off-axis capability of the optical system.

Much study and literature have been devoted to the other method, which suppresses the zero-order light by "apodisation" (Jacquinot and Roizen-Doazzier 1966), by which is meant the application of pupil or aperture functions with sidelobe-suppressing properties. Sidelobe reduction is usually achieved at the expense of main-lobe broadening, which has the effect of diminishing the resolving power of the system.

The pupil function can be generated by an aperture with uniform (unity) transmission together with a suitable contour or by an absorbing filter of appropriate transmission with a "normal" contour. The latter technique offers the advantage of not confining the desired effect to any one or, at most, a few particular directions in the frequency plane as is characteristic of apodising by contour shaping. However, the construction of accurate absorbing filters is in itself a difficult task since great care must be taken to avoid filter-generated noise. The other possibility - apodisation by aperture shaping - avoids this problem, providing the contour is reasonably constructed, as is not difficult in practice.

When contoured apertures are used, the power spectrum should be measured along a direction of apodisation. If the random process has isotropic statistics, the measurement of the spectrum in any direction is sufficient to obtain second moment information about the process; if the process is not isotropic,

then rotating the sample with respect to the aperture will effectively allow the measurement of the power spectrum along different directions.

It will now be shown how apodisation by aperture shaping is possible. The diffraction amplitude of an aperture of area  $A$  with uniform, unity transmission, is given by

$$E_f(u,v) = K \iint_A e^{-j2\pi(ux+vy)} dx dy \quad (6.4-1)$$

where the constant  $K$  required for energy conservation is of no interest in this discussion and is therefore set equal to one.

When the diffraction intensity of a square aperture of side  $D$  is scanned by a point aperture along  $v = 0$ , the intensity is

$$I_f(u,v) = D^4 \left( \frac{\sin \pi u D}{\pi u D} \right)^2 \quad (6.4-2)$$

The envelope is proportional to  $(\pi u D)^{-2}$  and decreases at the rate of  $\sim 6$  db/octave. A diamond aperture with the same area produces a diffraction intensity with an envelope function proportional to  $(\pi u D)^{-4}$  which decreases at 12 db/octave. The diffraction pattern of a diamond aperture can be obtained by scanning the diffraction pattern of a square aperture along the line  $u = v$ . The diamond aperture was the first and simplest example of apodisation along a special direction (Couder and Jacquinot 1939). An adjustable diamond aperture constructed for the experiment is shown in Fig. 6.1-5.

The diffraction pattern resulting from an aperture with contour

$$\begin{aligned} y &\pm 1/2 c(x) & -a/2 < x < a/2 \\ 0 &\text{ otherwise} & (6.4-3) \end{aligned}$$

is given by

$$E_f(u, v) = \int_{-a/2}^{a/2} e^{-j2\pi ux} dx \int_{-C(x)/2}^{C(x)/2} e^{-j2\pi vy} dy$$

which gives, along the u-axis

$$E_f(u, 0) = \int_{-a/2}^{a/2} C(x) e^{-j2\pi ux} dx \quad (6.4-4)$$

This is the one-dimensional Fourier transform of  $C(x)$  over the interval  $[-a/2, a/2]$ . Complete sidelobe elimination can be achieved with the Gaussian aperture defined by

$$y = D e^{-x^2/2\sigma^2} \quad -\infty < x < \infty \quad (6.4-5)$$

which gives a diffraction amplitude of the form  $e^{-2(\pi u\sigma)^2}$ . The diffraction patterns of square, diamond, and Gaussian apertures of equal area are shown in Fig. 6.4-1. In practice, the aperture must always be of finite extent and the diffraction pattern is then:

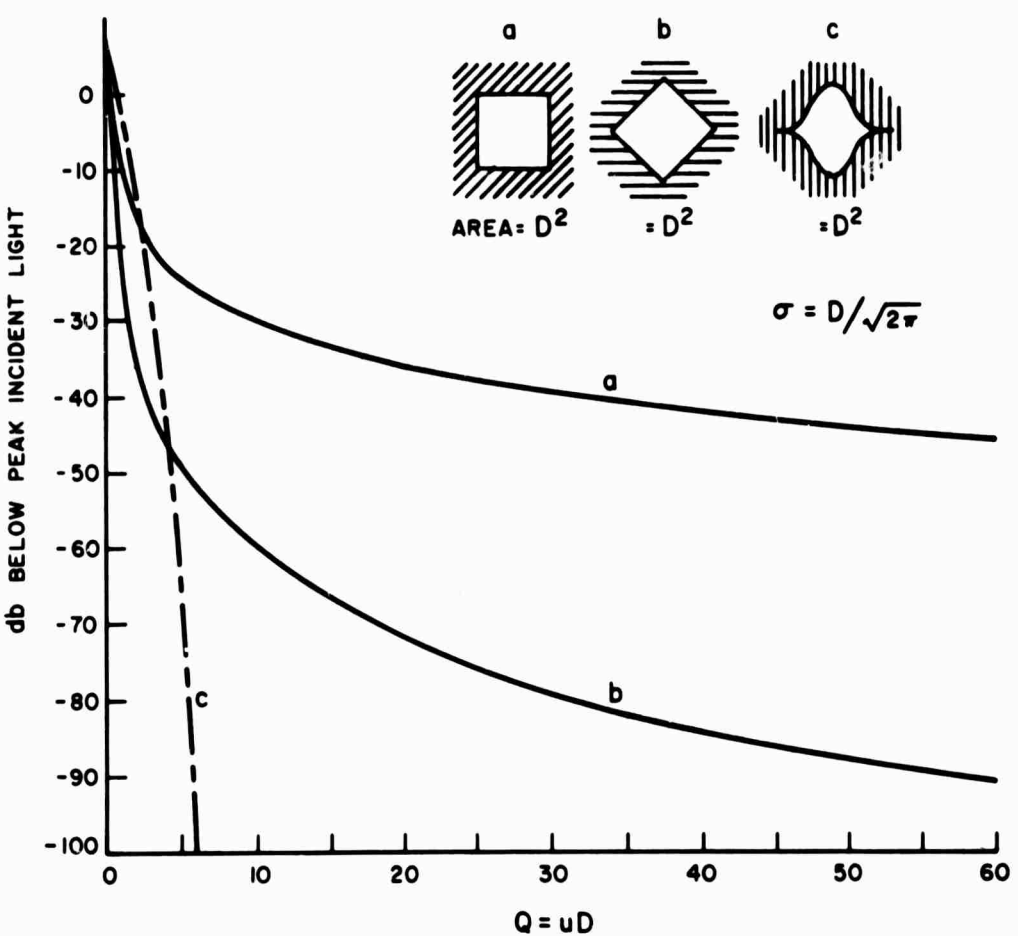
$$\begin{aligned} E_f(u, 0) &= \int_{-\infty}^{+\infty} e^{-x^2/2\sigma^2} \text{rect } x/a e^{-j2\pi ux} dx \\ &= S(u) * a \text{sinc ua} \end{aligned} \quad (6.4-6)$$

where

$$S(u) = \sqrt{2\pi} \sigma D e^{-2(\pi u\sigma)^2}$$

Gaussian apertures used in the experiment are shown in Fig. 6.4-2. The widths are approximately  $3\sigma$ .

In practice, aperture shaping does not provide a complete solution to the zero-order light suppression problem. First of all, the source light at the origin remains unaffected

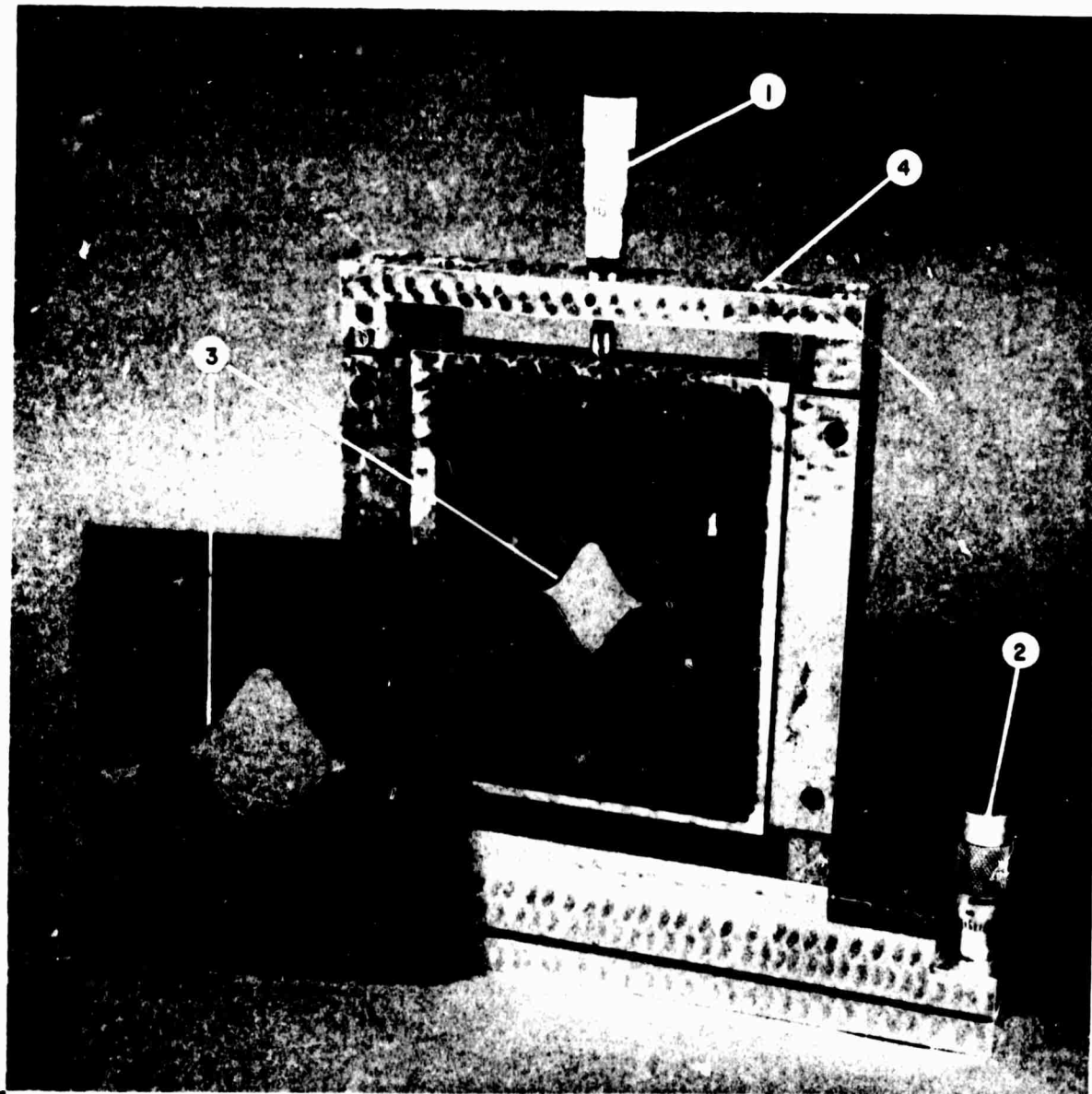


u = SPATIAL FREQUENCY

$D^2$  = AREA OF APERTURES

A-006-1-00-0008

FIG. 6.4-1 ENVELOPE OF DIFFRACTION PATTERNS FOR THREE APERTURES  
(THEORETICAL)



1. Vertical Control
2. Rotational Control
3. 30 mm and 50 mm Gaussian Apertures
4. Holder

**Fig. 6.4-2      Gaussian Apertures for Sidelobe  
                  Suppression**

and may be many orders of magnitude above the spectral light component, thus prohibiting its measurement at or near zero frequency.\* Also, apodisation cannot compensate for light scattered by random imperfections in the lenses. Regardless of the care and precision with which contoured apertures are constructed, the light levels in the diffraction pattern cannot be reduced further than the basic scattering level of the optical system. For the system described in Sec. 6.1, this level was found to be of the order of 70-80 db below the peak incident light for the largest off-axis scan displacements of interest.

#### 6.5 USE OF MAGNIFICATION IN POWER SPECTRA MEASUREMENTS

There are certain situations where it is desirable to magnify the film grains before attempting to measure the power spectrum by diffraction. For example, it may be difficult, if not impossible to measure the spectrum of low-noise film in which the grains are too small to scatter sufficient light that can be distinguished from the zero order. Even if the film is such that the spectrum of its noise can be measured, the off-axis capability of the optical system may preclude the observation of the spectrum at high spatial frequencies. From Eq. (2.4-2) it can be seen that high spatial frequencies correspond to large transverse displacements in the frequency plane which result from large diffraction angles. The response of most lenses becomes poorer for large diffraction angles and hence this mode of operation should be avoided.

It is shown in this section that if the film grains of a sample are magnified and transferred to low-noise film, the spectrum of the magnified grains can often be easily obtained by diffraction and after suitable calibration can be interpreted as the spectrum which would have been produced by unmagnified grains. Magnification also effectively "compresses" the frequency axis so that much higher spatial frequency components of the original spectrum can be observed.

---

\* See Appendix B

The above advantages accrue provided that the magnification is done without distortion. In practice, the elimination of all distortion is not possible. However, the use of precision lenses with large numerical apertures can minimize the distortion as will now be shown.

Consider first "ideal" magnification. This involves changing all dimensions by the magnification factor  $K$  so that a grain of radius  $r_o$  now has radius  $Kr_o$ . The amplitude transmittance  $t(x,y)$  of the original process is assumed to have mean value  $t_o$  which does not change through magnification provided that the magnified sample contains a very large number of grains. That the mean value remains the same follows from the observation that the ratio of opaque to total area is the same before and after magnification. If the covariance of the original process  $\{\tau(x,y)\} = \{t(x,y) - t_o\}$  is  $\psi_\tau(\alpha, \beta)$ , then the covariance of the new process  $\{\tau'(x,y)\}$  (Fig. 6.5-1) is

$$\psi_{\tau'}(\alpha, \beta) = \psi_\tau(\alpha/K, \beta/K) \quad (6.5-1)$$

and the power spectrum of  $\{\tau'(x,y)\}$  is given by

$$\begin{aligned} W_{\tau'}(u, v) &= \int_{-\infty}^{+\infty} \int_{-\infty}^{+\infty} \psi_{\tau'}(\alpha, \beta) e^{-j2\pi(u\alpha+v\beta)} d\alpha, d\beta \\ &= K^2 \int_{-\infty}^{\infty} \int_{-\infty}^{\infty} \psi_\tau(\alpha, \beta) e^{-j2\pi(u\alpha+v\beta)K} d\alpha, d\beta \\ &= K^2 W(Ku, Kv). \end{aligned} \quad (6.5-2)$$

and may be many orders of magnitude above the spectral light component, thus prohibiting its measurement at or near zero frequency.\* Also, apodisation cannot compensate for light scattered by random imperfections in the lenses. Regardless of the care and precision with which contoured apertures are constructed, the light levels in the diffraction pattern cannot be reduced further than the basic scattering level of the optical system. For the system described in Sec. 6.1, this level was found to be of the order of 70-80 db below the peak incident light for the largest off-axis scan displacements of interest.

#### 6.5 USE OF MAGNIFICATION IN POWER SPECTRA MEASUREMENTS

There are certain situations where it is desirable to magnify the film grains before attempting to measure the power spectrum by diffraction. For example, it may be difficult, if not impossible to measure the spectrum of low-noise film in which the grains are too small to scatter sufficient light that can be distinguished from the zero order. Even if the film is such that the spectrum of its noise can be measured, the off-axis capability of the optical system may preclude the observation of the spectrum at high spatial frequencies. From Eq. (2.4-2) it can be seen that high spatial frequencies correspond to large transverse displacements in the frequency plane which result from large diffraction angles. The response of most lenses becomes poorer for large diffraction angles and hence this mode of operation should be avoided.

It is shown in this section that if the film grains of a sample are magnified and transferred to low-noise film, the spectrum of the magnified grains can often be easily obtained by diffraction and after suitable calibration can be interpreted as the spectrum which would have been produced by unmagnified grains. Magnification also effectively "compresses" the frequency axis so that much higher spatial frequency components of the original spectrum can be observed.

---

\* See Appendix B

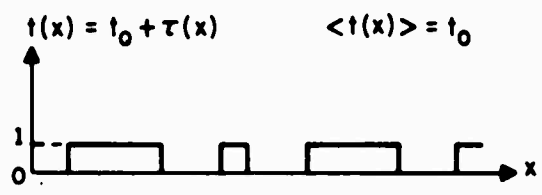
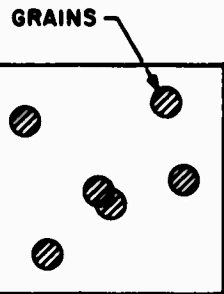
The above advantages accrue provided that the magnification is done without distortion. In practice, the elimination of all distortion is not possible. However, the use of precision lenses with large numerical apertures can minimize the distortion as will now be shown.

Consider first "ideal" magnification. This involves changing all dimensions by the magnification factor  $K$  so that a grain of radius  $r_0$  now has radius  $Kr_0$ . The amplitude transmittance  $t(x,y)$  of the original process is assumed to have mean value  $t_0$  which does not change through magnification provided that the magnified sample contains a very large number of grains. That the mean value remains the same follows from the observation that the ratio of opaque to total area is the same before and after magnification. If the covariance of the original process  $\{\tau(x,y)\} = \{t(x,y) - t_0\}$  is  $\phi_{\tau}(\alpha, \beta)$ , then the covariance of the new process  $\{\tau'(x,y)\}$  (Fig. 6.5-1) is

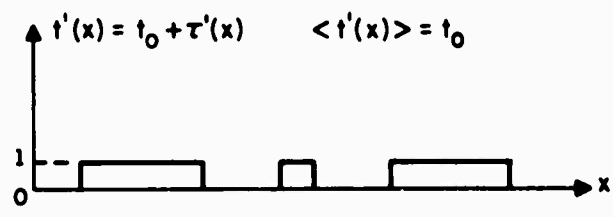
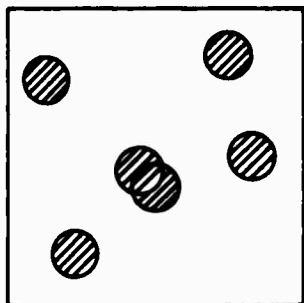
$$\phi_{\tau'}(\alpha, \beta) = \phi_{\tau}(\alpha/K, \beta/K) \quad (6.5-1)$$

and the power spectrum of  $\{\tau'(x,y)\}$  is given by

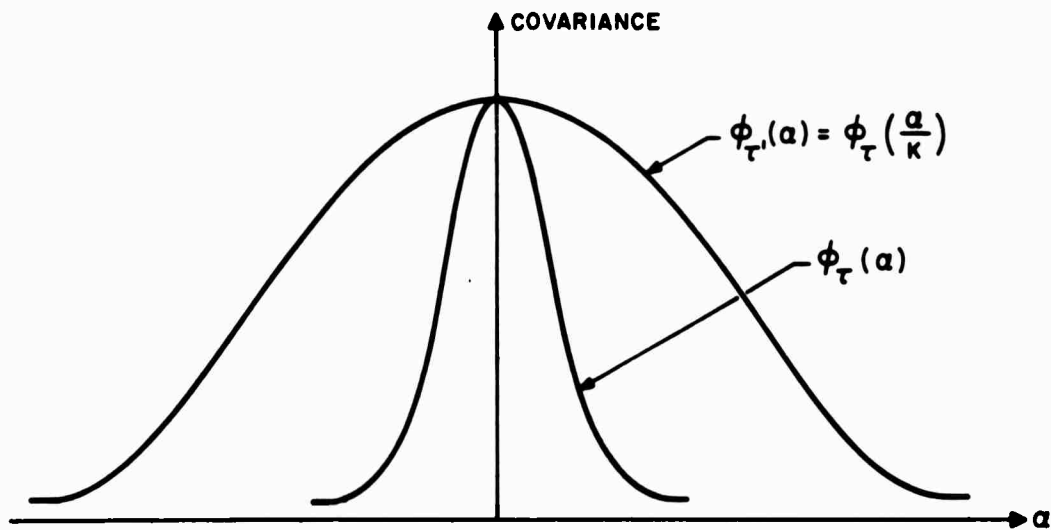
$$\begin{aligned} W_{\tau'}(u, v) &= \int_{-\infty}^{+\infty} \int_{-\infty}^{+\infty} \phi_{\tau'}(\alpha, \beta) e^{-j2\pi(u\alpha+v\beta)} d\alpha, d\beta \\ &= K^2 \int_{-\infty}^{+\infty} \int_{-\infty}^{+\infty} \phi_{\tau}(\alpha, \beta) e^{-j2\pi(u\alpha+v\beta)K} d\alpha, d\beta \\ &= K^2 W(Ku, Kv). \end{aligned} \quad (6.5-2)$$



a) FILM SAMPLE WITH TYPICAL TRANSMITTANCE TRACE



b) SAMPLE AND TRANSMITTANCE TRACE AFTER MAGNIFICATION BY K.



A-006-1-00-0009

FIG. 6.5-1 THE EFFECT OF LINEAR MAGNIFICATION

Hence, the magnification produces a power spectrum that is  $K^2$  times as large at the origin as the original spectrum and  $K^{-1}$  times as narrow. The total power in the two processes are the same since

$$\int_{-\infty}^{\infty} \int_{-\infty}^{\infty} W_{\tau'}(u, v) du dv = \int_{-\infty}^{\infty} \int_{-\infty}^{\infty} W_{\tau}(u, v) du dv \quad (6.5-3)$$

which follows from Eq. (6.5-1).

When magnification is done by a real optical system, the frequency response characteristics of the lenses must be taken into account. It has been shown (Hopkins 1955, Born and Wolf 1964) that the maximum frequency that an optical imaging system can transmit is a function of the width of the aperture, the wavelength and type (coherent or incoherent) of illumination and the location of the image plane. For incoherent illumination, the frequency response of an optical system is the Fourier transform of the transmission function  $B_I(x_1 - x_o, y_1 - y_o)$  defined as the distribution of light intensity in the image plane at  $(x_1, y_1)$  due to a point source of unit strength in the object plane at  $(x_o, y_o)$ . By superposition, the imaging can be described by the convolution

$$I_1(x_1, y_1) = \int_{-\infty}^{\infty} \int_{-\infty}^{\infty} B_I(x_1 - x_o, y_1 - y_o) I_o(x_o, y_o) dx_o dy_o \quad (6.5-4)$$

where

$I_1(x_1, y_1)$  = light intensity at  $(x_1, y_1)$   
in the image plane.

$I_o(x_o, y_o)$  = light intensity at  $(x_o, y_o)$   
in the object plane.

A similar relation holds for coherent systems, namely,

$$E_1(x_1, y_1) = \int_{-\infty}^{\infty} \int_{-\infty}^{\infty} B_C(x_1 - x_0, y_1 - y_0) E_0(x_0, y_0) dx_0 dy_0 \quad (6.5-5)$$

where

$E_1(x_1, y_1)$  = complex light amplitude in the image plane at  $(x_1, y_1)$

$E_0(x_0, y_0)$  = complex light amplitude in the object plane at  $(x_0, y_0)$

$B_C(x_1 - x_0, y_1 - y_0)$  complex amplitude distribution in the image plane due to a point source of unit amplitude and zero phase in the object plane.

In this case, the frequency response is the Fourier transform of  $B_C(x, y)$ . Denoting by  $b_I(u, v)$  and  $b_C(u, v)$  the frequency response characteristics of incoherent and coherent systems, Hopkins has shown that for aberration-free systems,  $b_I(u, v)$  is proportional to the self-correlation of the aperture function and  $b_C(u, v)$  is equal to the aperture function. For a circular aperture of diameter  $d$ , the aperture function  $G(x, y)$  is given by

$$\begin{aligned} G(x, y) &= 1 & x^2 + y^2 &< d^2/4 \\ &= 0 & \text{otherwise} \end{aligned}$$

For coherent illumination, all frequency pairs  $(u, v)$  such that ( $\lambda$  = wavelength of radiation,  $R$  = radius of the Gaussian reference sphere, i.e.  $\sim$  the distance from the aperture to the image plane)

$$u^2 + v^2 > \left(\frac{d}{2\lambda R}\right)^2$$

will not be transmitted. When the illumination is incoherent all frequency pairs such that

$$u^2 + v^2 \leq \left(\frac{d}{\lambda R}\right)^2$$

will not be transmitted, and the frequency response is not uniform as shown in Fig. 6.5-2.

In order to derive the conditions under which power spectra can be magnified with high fidelity by imaging, consider the incoherent optical system shown schematically in Fig. 6.5-3. The optical system denoted by  $L$  can be a microscope or an ordinary lens such as those used in the experiments of this thesis. Assume the coordinates in image and object planes are normalized so that the magnification is unity. If the intensity of the source is unity, it follows from Eq. (6.5-4), that if  $T(\xi, \eta)$  denotes the intensity transmittance of the object  $O$ , and  $b_T(\alpha, \beta) = \langle T(\xi, \eta) T(\xi+\alpha, \eta+\beta) \rangle$  then the light in plane  $P$  is given by

$$I_P(x, y) = \int_{-\infty}^{\infty} \int_{-\infty}^{\infty} T(\xi, \eta) b_I(x-\xi, y-\eta) d\xi d\eta \quad (6.5-6)$$

and

$$w_T^{(P)}(u, v) = |b_I(u, v)|^2 w_T(u, v) \quad (6.5-7)$$

where

$w_T^{(P)}(u, v)$  = the power spectrum of the imaged process in plane  $P$

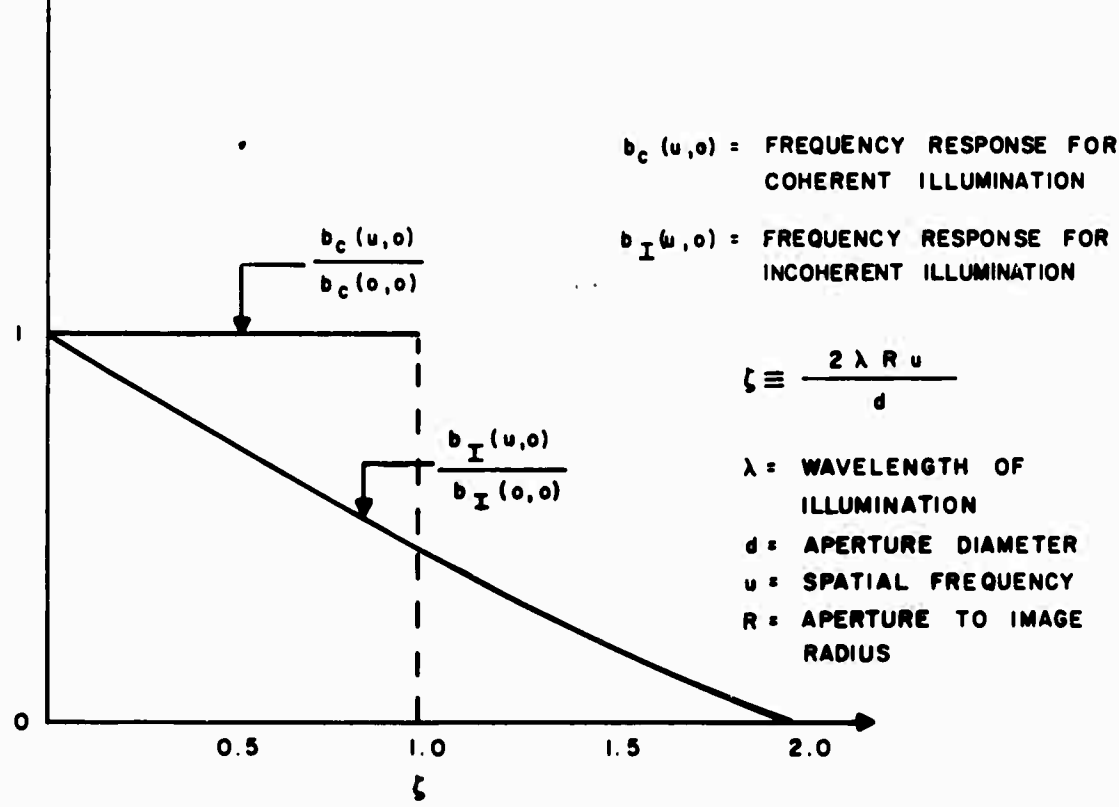
$$w_T(u, v) = F\{\phi_T(\alpha, \beta)\}$$

$F\{\cdot\}$  = Fourier transform of  $\{\cdot\}$ .

Eq. (6.5-1) involves intensity spectra. The intensity spectrum will be equal to the amplitude spectra if the sample functions of the intensity and amplitude transmittances are equal such

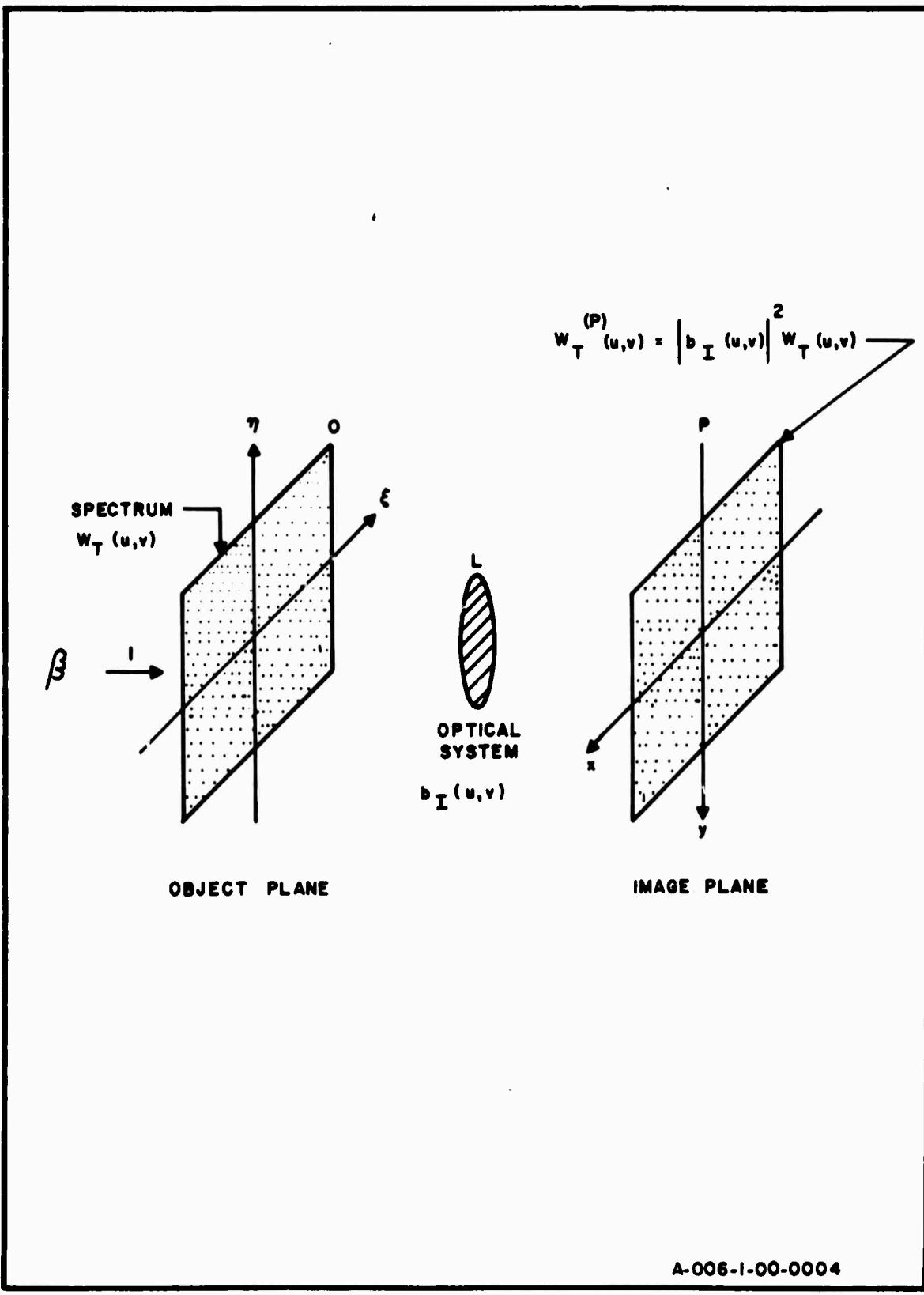
---

A similar relation holds for coherent systems namely  $w_t^{(P)}(u, v) = |b_c(u, v)|^2 w_t(u, v)$ , where  $w_t(u, v)$  is the power spectrum of the amplitude transmittance.  $b_I$  is the self-correlation function of  $b_c$  (Born and Wolf 1964).



A-006-1-00-0003

FIG. 6.5-2 NORMALIZED FREQUENCY RESPONSES FOR  
SYSTEMS FREE OF GEOMETRICAL ABERRATIONS  
(HOPKINS, 1952; BORN AND WOLF, 1964)



A-006-1-00-0004

FIG. 6.5-3 IMAGING OF GRANULARITY THROUGH AN INCOHERENT OPTICAL SYSTEM

as in the random checkerboard and overlapping circular-grain models.

It can be seen from Eq. (6.6-7), that high-fidelity imaging of spectra requires that  $|b_I(u,v)|^2$  be nearly constant over the frequencies that  $w_T(u,v)$  has significant amplitude. If  $w_T(u,v)$  is flat, or nearly so, over all the frequencies for which  $b_I(u,v)$  is not zero, the transferred spectrum will be proportional to  $|b_I(u,v)|^2$  so that the magnitude of the frequency response can be measured by measuring the magnified spectrum.

For the experiments, two magnification schemes were employed. High resolution, wide band magnification was obtained with the "Fluorestar" microscope shown in Fig. 6.1-10. An indication of the frequency performance of a high-quality microscope is its resolving power which is often specified in terms of the numerical aperture (N.A.); the N.A. can be expressed as

$$N.A. = \frac{\text{objective diameter}}{2 \times \text{focus}} = \frac{d}{2f}$$

The theoretical cut-off frequency for an aberration-free objective is

$$w_c = d/\sqrt{f} = 2 N.A. / \lambda \quad w = \sqrt{u^2 + v^2}$$

Depending on the magnification used, the microscope objectives used in these experiments had values of  $w_c$  that ranged from  $w_c = 1850$  cycles/mm (N.A. = .5) to  $w_c = 4600$  cycles/mm (N.A. = 1.25). These values were adequate for observing the power spectrum of film noise at frequencies not above several hundred cycles/mm.

Low resolution magnification was obtained with an inexpensive commercial enlarging lens, operated in white light (see Sec. 6.1). When this lens was used for magnification, the resulting spectra were significantly distorted by the frequency response of the lens.

## 7. EXPERIMENTAL RESULTS

This chapter contains the results of the experimental phase of the research. The experiments that were performed can be broadly classified into three categories. In the first (Sec. 7.1-7.2) are those experiments designed to verify the theoretical conclusions regarding the influence of system parameters on spectral density measurements. Included in this group are the determinations of the effects of the liquid gate, aperture sizes and shapes, and scanning slit widths. The second category (Sec. 7.3-7.4) contains experiments concerned with the measurement of film noise and related subjects. Comparisons between measured spectra and the spectra of several mathematical models of granularity are furnished. A posteriori discussions are provided in the several instances where the results were not anticipated. The last (Sec. 7.5) category contains those experiments related to magnification and the measurement of the frequency response of optical systems.

### 7.1 REDUCTION OF FILM NOISE WITH A LIQUID GATE

The contention made in earlier chapters regarding the reduction of film-scattered light by the use of a liquid gate was experimentally verified by several workers (Thiry 1963, Leith 1962). In practice, the choice of liquid which furnishes the optimum refractive index can be made by using an interferometer in the collimated region and observing the interference fringes or by examining the structure of the diffraction pattern with the film sample in place. The second technique is decidedly preferable since the diffraction pattern is extremely sensitive to phase errors in the coherent beam.

Under the condition of optimum match, the chief contributor to the scattered light is the film grain noise which, being much smaller than the phase noise, would not be expected to distort the diffraction pattern by a significant degree. Hence little difference should be discerned between the diffraction patterns of the loaded and unloaded systems.

In Fig. 7.1-1 the diffraction pattern of a carefully aligned, coherent optical system is shown. The parameters of the optical system in this case were:  $f_c$  = focal length of lens : 1 meter,  $\lambda = 6328 \text{ \AA}$ ,  $d$  = length of rectangular aperture  $\approx 34 \text{ mm}$ . The null-to-null width of the main lobe is  $\approx 37 \text{ \mu}$  which is  $2f/d$ . The distortion in the zero-order when film is placed in the collimated region (Fig. 2.4-2) is clearly seen in Fig. 7.1-2 for which no liquid gate was used. When a liquid gate is used with a mismatched liquid, the diffraction pattern still suffers serious deterioration as can be seen from Fig. 7.1-3. Here the refractive index,  $n$ , of the liquid was 1.5 while the best average value of  $n$  for the film was 1.610. When this value of  $n$  was used, the diffraction pattern was very nearly the symmetrical pattern of Fig. 7.1-1 except for the slight attenuation of the peak of the zero-order component, a consequence of the optical density of the film. The diffraction pattern is shown in Fig. 7.1-4.

## 7.2 EXPERIMENTAL DETERMINATION OF THE EFFECTS OF THE APERTURE AND SCANNING FILTER

It was shown in Sec. 3.2 that the apparent spectrum is the convolution of the true spectrum and the aperture function  $H(u,v)$ , defined for a rectangular aperture of dimensions  $L, W$ , by Eq. (3.2-2). The apparent spectrum is a biased estimate of the true spectrum and the bias [Eq. (3.4-11)] can be seen to depend on the dimensions  $L$  and  $W$  of the aperture.

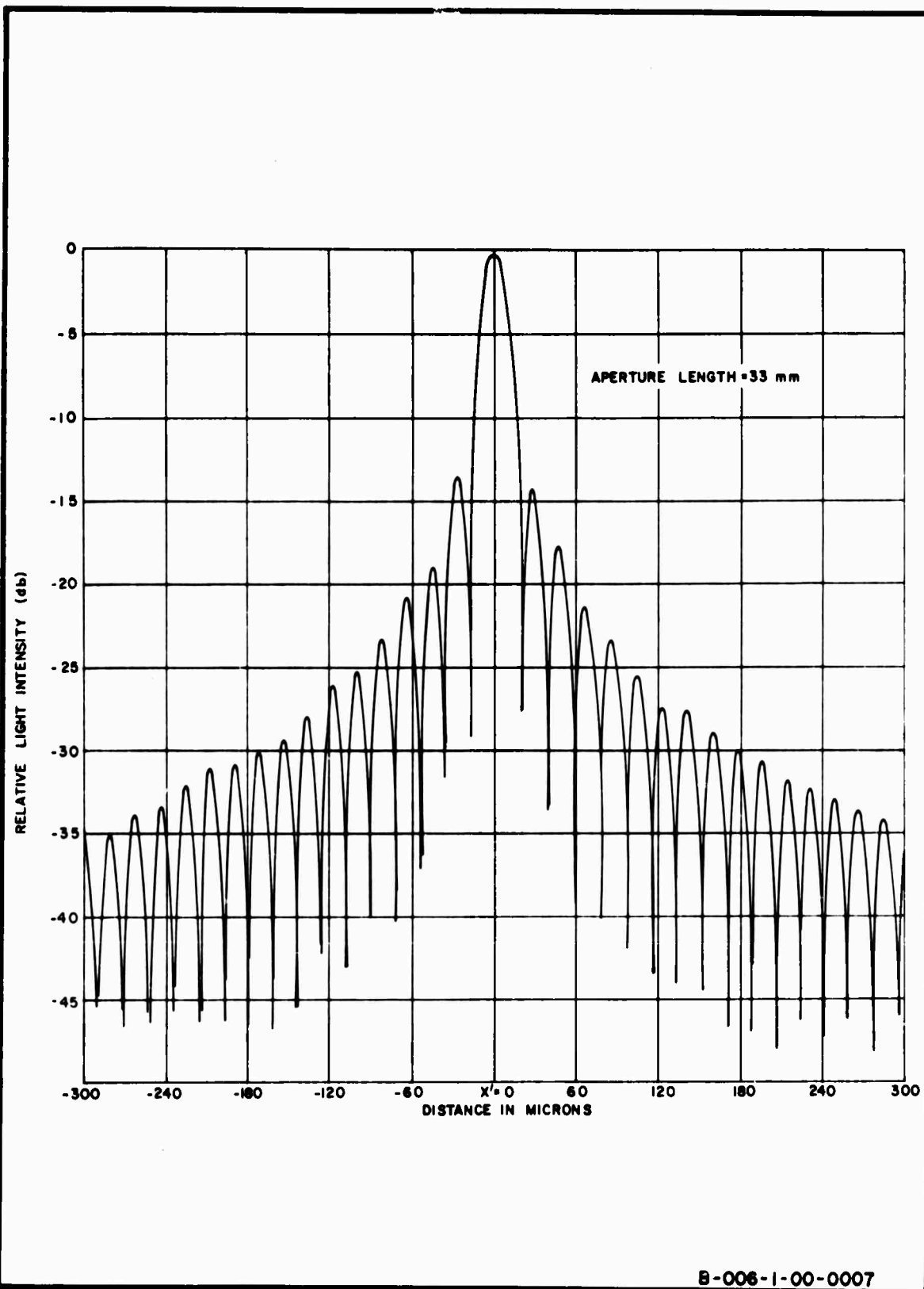


FIG. 7.1-1 FOCAL-PLANE LIGHT INTENSITY DISTRIBUTION  
ALONG  $X'$  AXIS FOR CLEAR (UNLOADED) SYSTEM

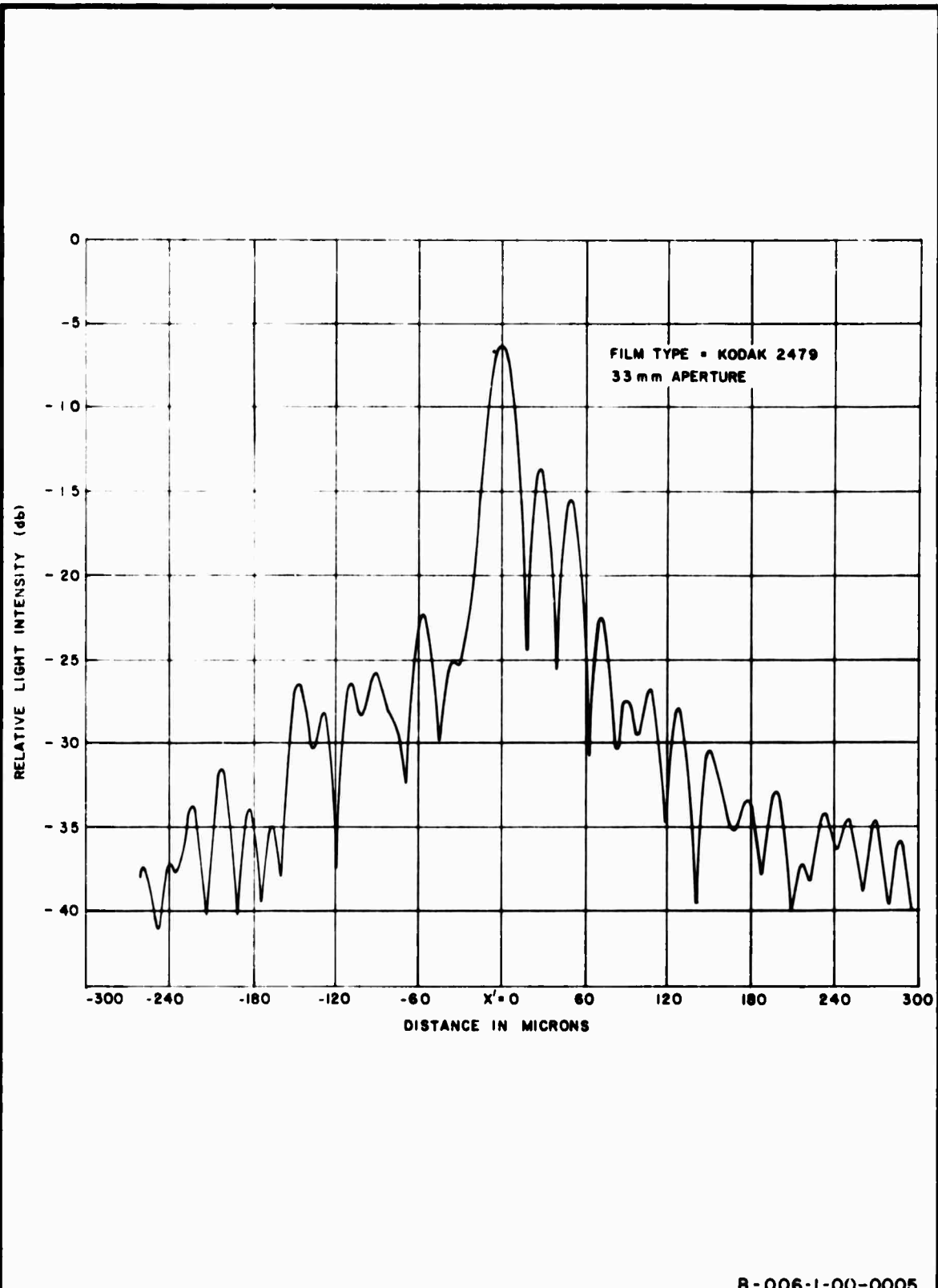


FIG. 7.1-2 FOCAL-PLANE LIGHT INTENSITY DISTRIBUTION ALONG  $X'$  AXIS WHEN SYSTEM IS LOADED WITH FILM WITHOUT PHASE COMPENSATION

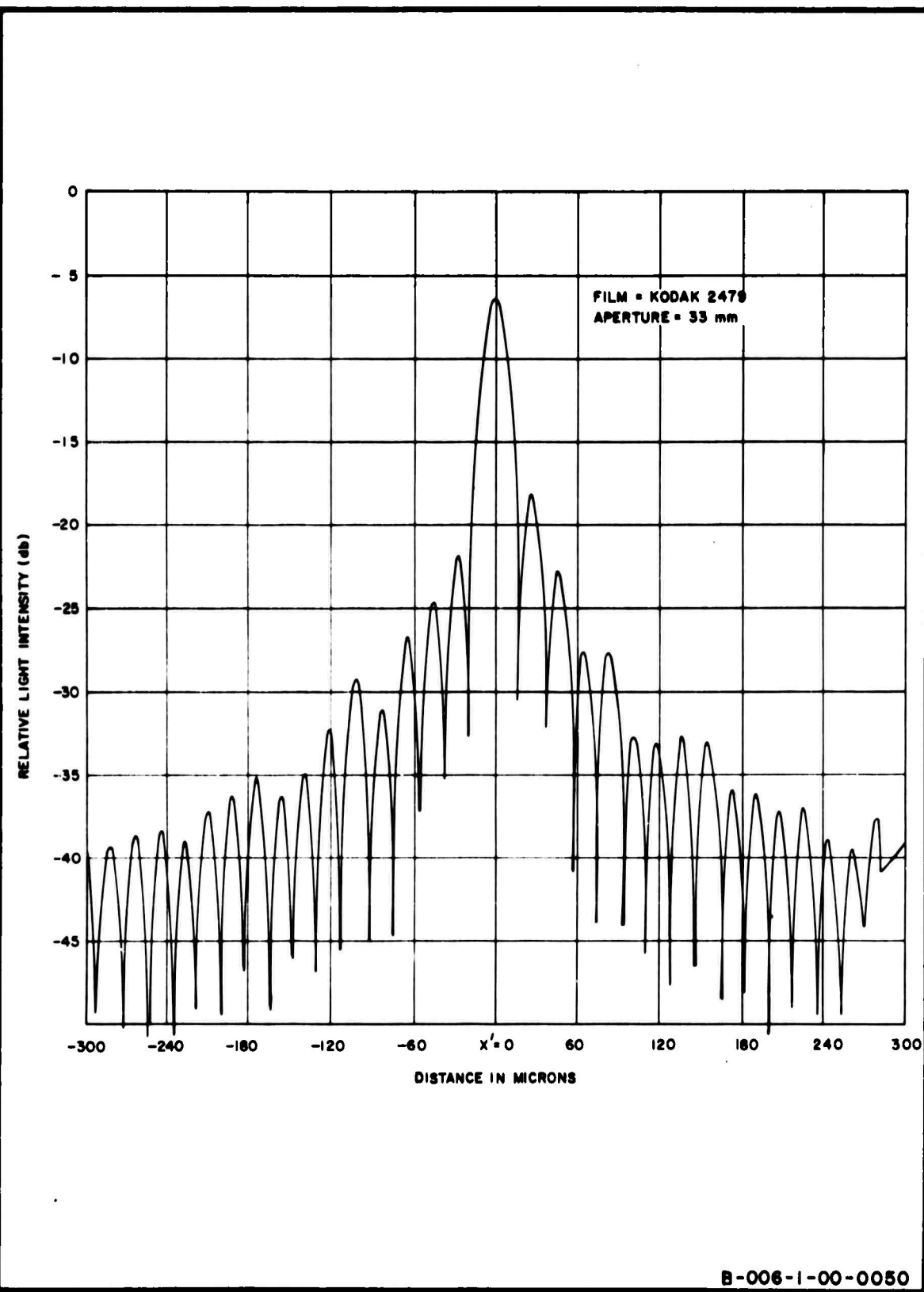
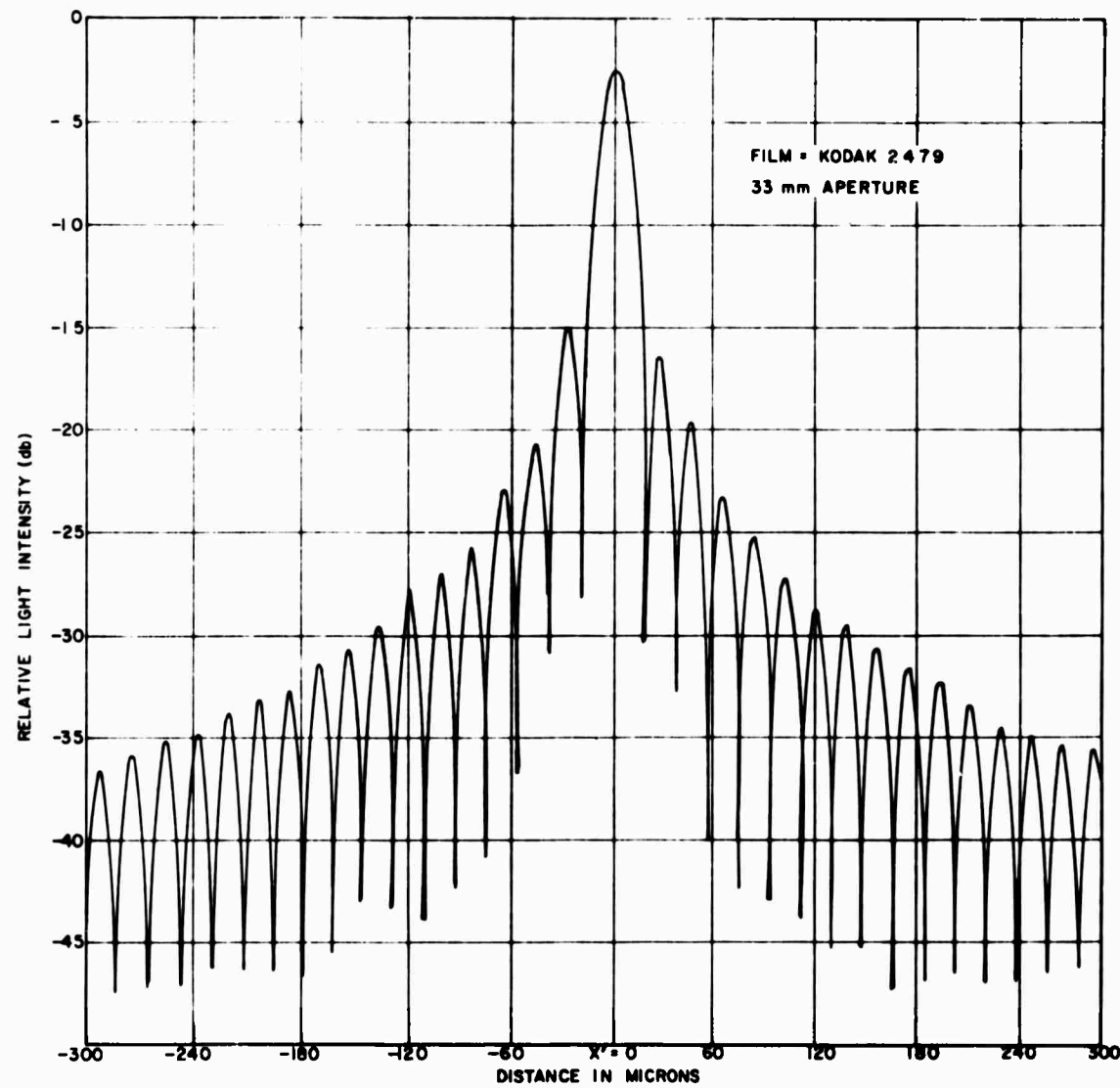


FIG. 7.1-3 FOCAL-PLANE LIGHT INTENSITY DISTRIBUTION  
ALONG X' AXIS WHEN SYSTEM IS LOADED WITH  
FILM WITH PARTIAL PHASE COMPENSATION



B-006-1-00-0049

FIG. 7.1-4 FOCAL-PLANE LIGHT INTENSITY DISTRIBUTION  
ALONG X' AXIS WHEN SYSTEM IS LOADED WITH FILM  
WITH OPTIMUM PHASE COMPENSATION

-143-

The bias error varies inversely with the size of the aperture, becoming zero when the aperture is infinitely large [Eq. (3.2-7)]. Figure 7.2-1 shows the effect of different aperture sizes and shapes on the measured spectrum. It can be seen that the four apertures listed in Table 7.2-1 furnished, despite minor differences, essentially similar results at most frequencies despite radical differences in size and shape. The results demonstrate the earlier contention that when the aperture dimensions are large compared with the largest significant correlation intervals, the measured spectral estimates are relatively independent of the aperture and reflect a fundamental property of the film.

TABLE 7.2-1

SHAPE	WIDTH OF SIDE OR BASE (mm)	AREA (mm <sup>2</sup> )
Gaussian	30	400
Diamond	30	900
Gaussian	50	1100
Diamond	50	2500

It will be remembered from Sec. 3.2 that when the averaging over frequency is confined to a single point as in Eq. (3.2-7), the bias is zero. The best approximation to Eq. (3.2-7) is achieved with the 50-mm diamond aperture which furnished a maximum half-power bandwidth of  $1.27 \times 10^{-2}$  cycles/mm.

The slight variations that exist among the spectra in Fig. 7.2-1 relate to two different phenomena which will presently be discussed. The decrease at high spatial frequencies in the apparent spectra obtained with the three smaller apertures is the attenuation due to the phenomenon called vignetting (Born and Wolf 1964). Vignetting occurs when the diffraction

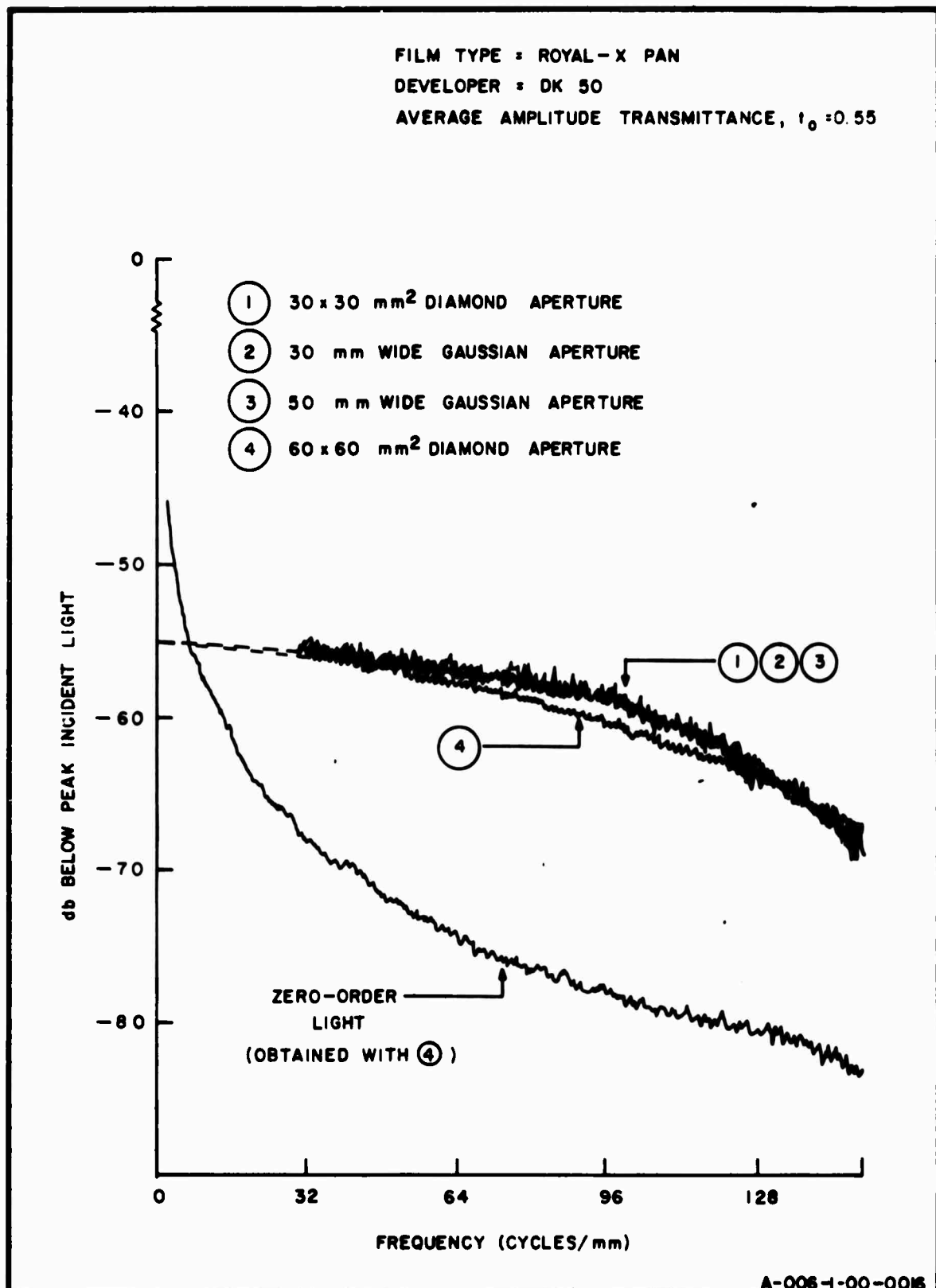


FIG. 7.2-1 EFFECT OF APERTURE SHAPES ON THE MEASUREMENT OF THE POWER SPECTRUM OF GRAIN NOISE

angles are sufficiently large to force some rays to miss the lens. When the object which generates the angular diffraction modes is placed near the lens, the vignetting is reduced or eliminated. Slight vignetting is also present in the apparent spectrum furnished by the largest aperture. In this case the vignetting appears at lower frequencies. In the extreme case when the aperture is as large as the lens, vignetting will be present for all spatial frequencies except DC.

The second discernible difference in Fig. 7.2-1 is the decrease in variability that results when the largest aperture is used. The relation between the aperture size and the variance of the estimated power spectrum was determined for rectangular and diamond apertures, in Chap. 5 under the assumptions of wide-sense stationary, Gaussian statistics. The key result was Eq. (5.1-3) which can be rewritten as

$$\text{var}(\hat{W}(u,v)) = \tilde{W}^2(u,v) + F^2(u,v) + t_o^2 H(u,v) G(u,v) \quad (7.2-1)$$

where

$$\tilde{W}(u,v) = \text{apparent spectrum}$$

$$= W(u,v) * H(u,v)$$

$$H(u,v) = LW \text{ sinc}^2 uL \text{ sinc}^2 vW$$

$$F(u,v) = LW \int_{-\infty}^{\infty} \int_{-\infty}^{\infty} W(\xi,\eta) \text{ sinc}(u+\xi)L \text{ sinc}(u-\xi)L \cdot \text{ sinc}(v-\eta)W \text{ sinc}(v+\eta)W d\xi d\eta$$

$$t_o = \text{average amplitude transmittance}$$

$$G(u,v) = LW \int_{-\infty}^{\infty} \int_{-\infty}^{\infty} W(\xi,\eta) \cdot \left[ \text{ sinc}(u+\xi)L \text{ sinc}(v+\eta)W + \text{ sinc}(u-\xi)L \text{ sinc}(v-\eta)W \right]^2 d\xi d\eta$$

The functions  $H$ ,  $G$  and  $F$  are positive for all  $u$ ,  $v$ ,  $L$ ,  $W$  and have envelopes that decrease uniformly with increasing aperture size. For large apertures, all the terms except for  $\tilde{W}^2(u,v)$  become insignificant away from the origin. Hence, on the basis of Eq. (7.2-1), less variability is expected in the estimate when a large aperture is used as opposed to a smaller one. Figure 7.2-2 shows more explicitly the influence of aperture size on the variability of the measured spectrum. The extrapolated spectrum (dashed lines) corresponds to the region where the zero-order light was too intense for an accurate measurement of the spectrum. Fig. 7.2-2 also illustrates, as predicted by Eq. (7.2-1) that the envelope of the variance decreases with increasing frequency.

The result of Chap. 5 shows that for a rectangular aperture, the ratio of the variance of the estimated spectrum to its square mean cannot be made less than unity. However, additional smoothing is provided by the scanning filter.

The action of the scanning filter was discussed in Sec. 3.6 and illustrated in Fig. 3.6-1. The smoothing of the high frequency components in the spectrum by the scanning filter is shown in Fig. 7.2-3. In this experiment, a 4" diameter lens with a focal length of  $f = .4$  meters was used. Both filters shown in Fig. 7.2-3 had diameters well within the range of reasonable values established by the criterion of Eq. (3.6-7) which for this case was  $5\mu < d < 250\mu$ . As can be seen the  $120\mu$  diameter slit furnished a uniformly smoother spectrum over the entire frequency band of interest than the  $50\mu$  slit.

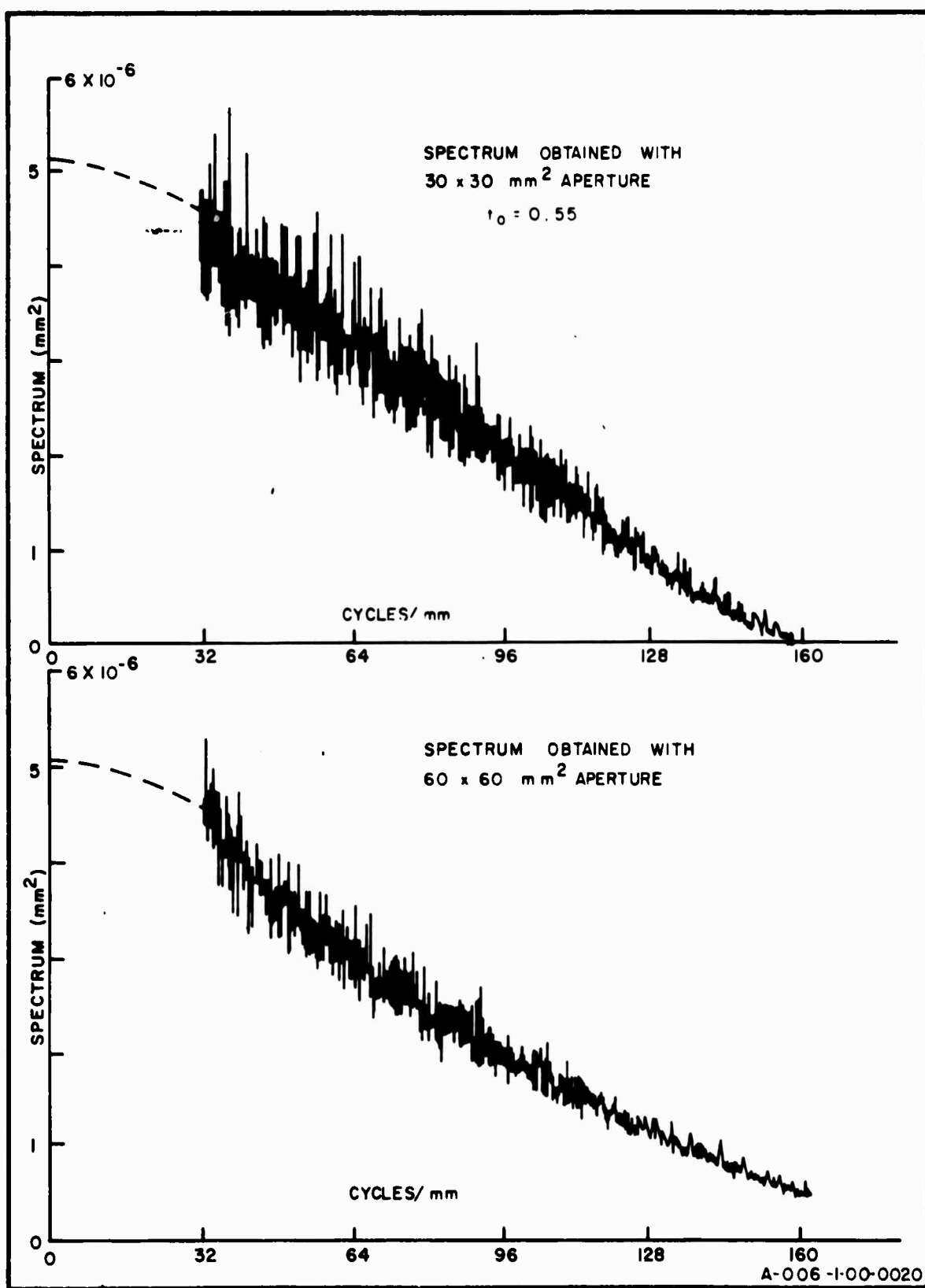


FIG 7.2-2 INFLUENCE OF APERTURE ON POWER SPECTRUM MEASURE-  
 MENT FILM TYPE IS ROYAL-X PAN DEVELOPED IN  
 -148- DK-50. SCANNING FILTER IS  $50 \mu$  DIAMETER PINHOLE.

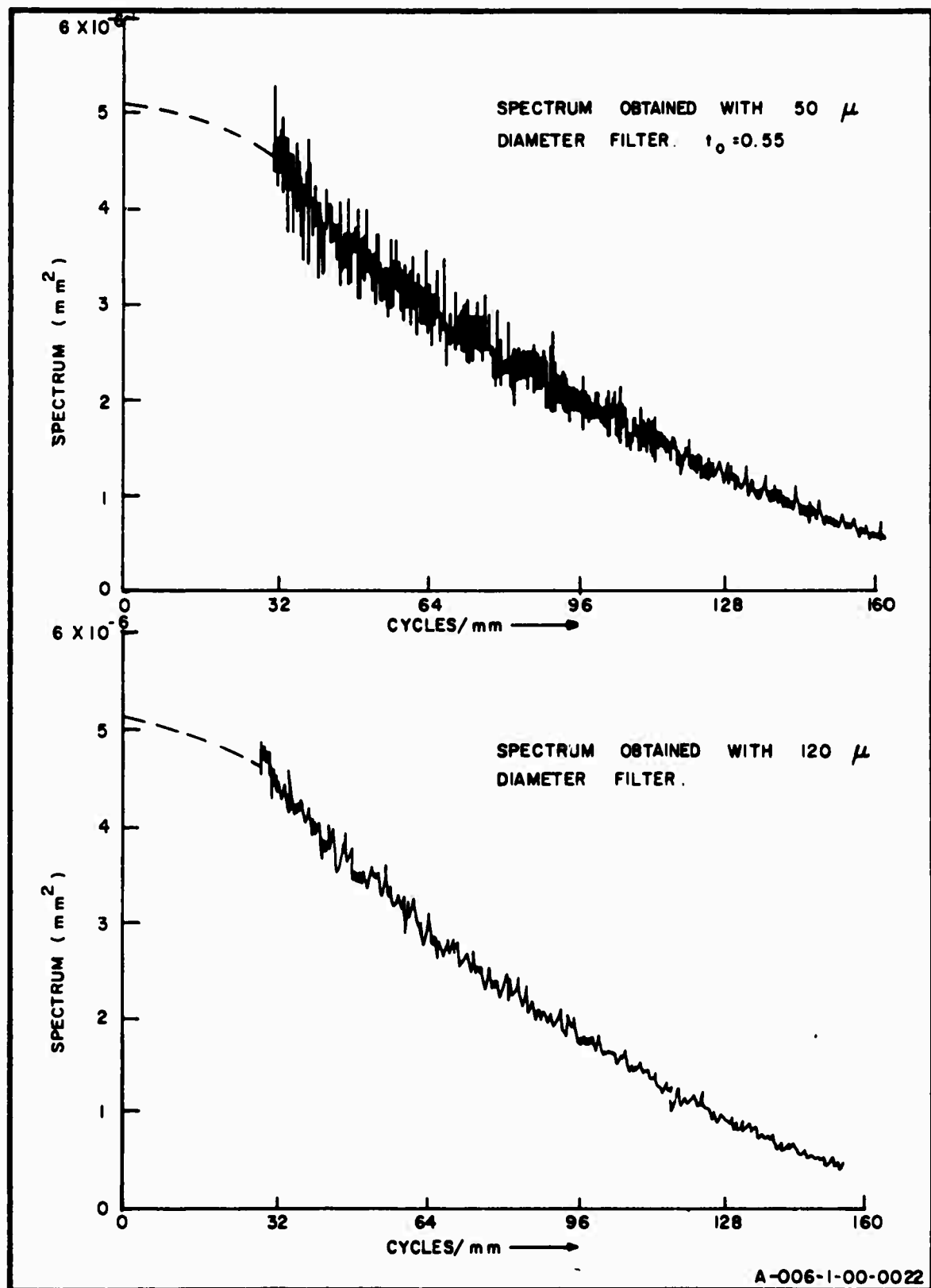


FIG. 7.2-3 INFLUENCE OF SCANNING FILTER ON POWER SPECTRUM  
MEASUREMENT. FILM TYPE IS ROYAL-X PAN DEVELOPED  
IN DK-50. APERTURE IS  $60 \times 60 \text{ mm}^2$  DIAMOND -140-

### 7.3 MEASUREMENTS OF THE SPECTRA OF FILM GRAIN NOISE

The procedure described in Sec. 6.2 was used to obtain the spectra of several common, commercially available films. The important characteristics of these films are summarized in Table 7.3-1.\*

TABLE 7.3-1

	<u>2475</u>	<u>2479</u>	<u>ROYAL X-PAN</u>
ASA Speed	800 (fast)	400 (medium)	1000-1200 (fast)
Resolving Power	Low < 55 cpm**	Medium 69-95 cpm	Low < 55 cpm
Granularity Class	Coarse	Coarse-medium	Coarse
Special Properties	Extended sensitivity to red light	Panchromatic	

Three developers\*\*\* were used: Kodak DK-50, D-19 and Dektol.

---

\* Data obtained from Kodak Tech Bits, 1966, No. 2. Also Kodak Reference Handbook, No. 1.

\*\* Cycles per millimeter.

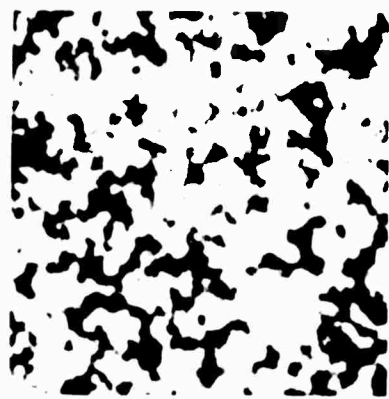
\*\*\* The developing agent is a chemical compound which reduces silver ions to metallic silver. The basic reaction equation is  $\text{Ag}^+ + e \rightarrow \text{Ag}$ . A condition that any developer must fulfill is that it must reduce exposed silver halide grains at a higher rate than the unexposed grains. Other conditions that a developer must satisfy are (1) it must be soluble in water or in an alkaline solution, (2) be reasonably stable and resistant to aerial oxidation, (3) yield soluble oxidation products, and (4) be non-toxic. The developer makes visible the latent image on the film after exposure. The hypo on the other hand, stops the development process and fixes permanently the visible image. The mechanism of the formation of the latent image was explained by the theory of R. W. Gurney and N. F. Mott, (1938) who formulated what is now known as the Gurney-Mott principle.

The latter is what is known as a paper developer and is normally not used with the processing of negatives. D-19 is a high contrast developer usually applied for 10 minutes at 68°F. DK-50 is a medium grain producing, moderately fast, very popular developer used in the same way as D-19. The Dektol developer was applied for 3 minutes at 72°. According to Kodak authorities, the use of Dektol with negatives would result in grainy transparencies. It was of interest to determine whether the diffraction method could discern the difference between film treated with Dektol and a recommended developer. It is for this reason that Dektol was used.

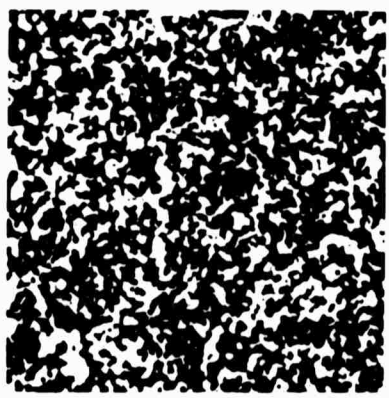
Figure 7.3-1 are photomicrographs of the grain structure of Kodak 2476 film developed in D-19 at three different levels of magnification. To obtain these photographs, the equipment shown in Fig. 6.1-10 was used. The choice of film is incidental. The clumping of grains is evident by the chain-like aggregates of silver which extend in some cases to 40 or more microns. These aggregates can be much larger than the actual exposed silver halide crystals.

The spectra discussed in the subsequent paragraphs were calibrated by using Eq. (6.2-10), and extrapolating the spectrum back to the origin. It will be remembered that the measurement of the spectrum near the origin is difficult to make because of the presence of the strong zero-order light. Thus, the extrapolated spectrum corresponds to the region where the difference between the zero-order and the scattered light was less than 10 db.

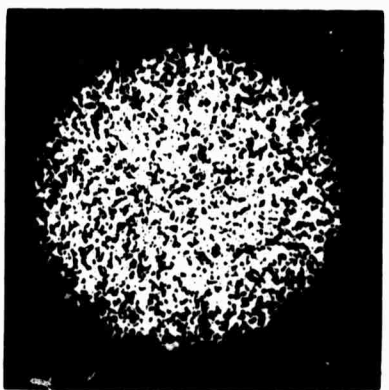
Figures 7.3-2 to 7.3.5 are actual retraces of experimentally obtained spectra of the films listed in Table (7.3-1). Superimposed on each graph are the theoretical spectra predicted by the overlapping circular grain (OCG), the random checkerboard (RC) and the modified overlapping circular grain (MOCG) models. Each film sample was carefully tested with a microdensitometer



A) Magnification = 130X



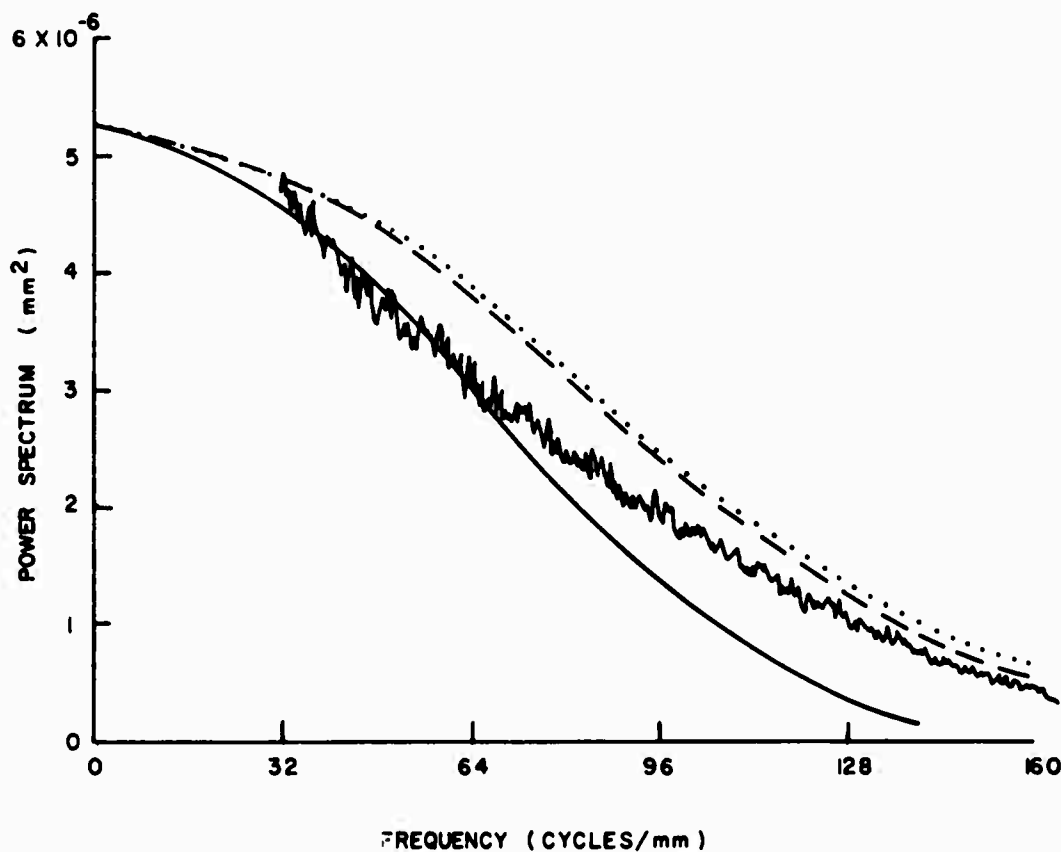
B) Magnification = 650X



C) Magnification = 1300X

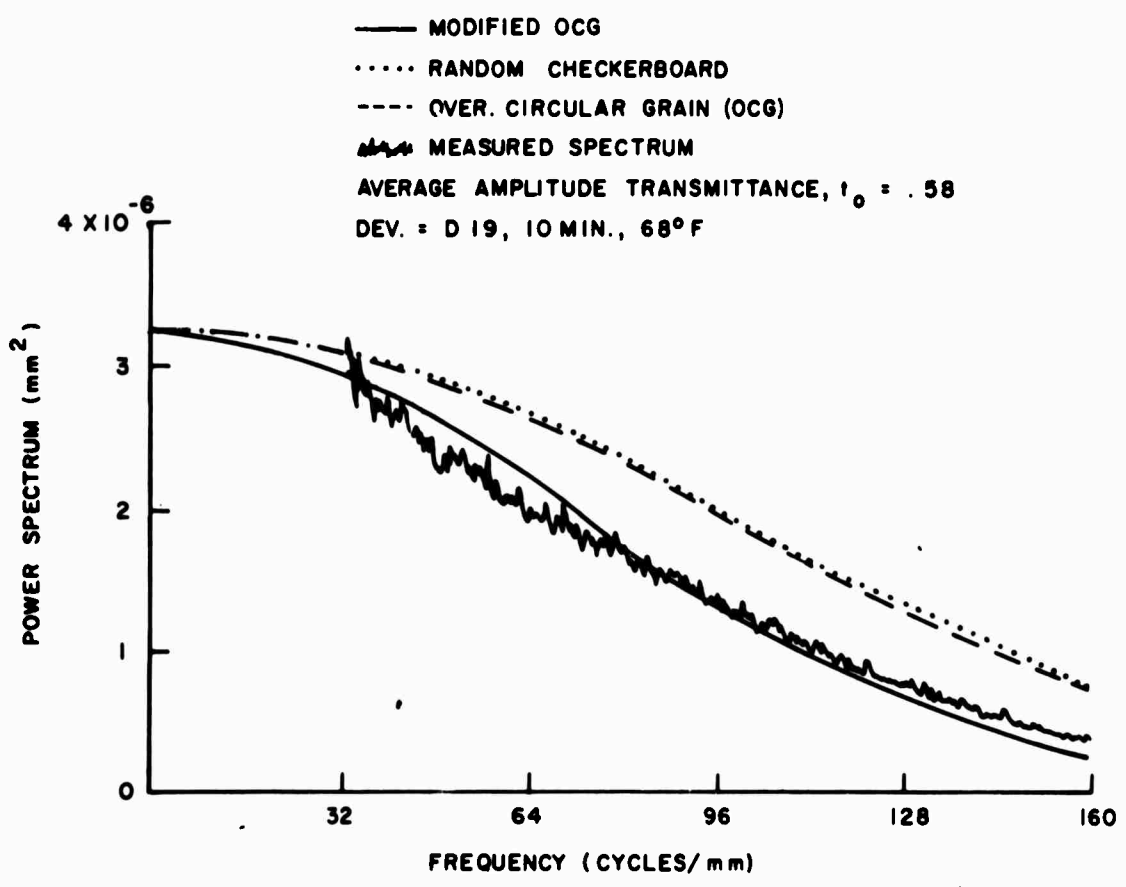
Fig. 7.3-1      **Grain Structure of Film (Kodak 2496)**  
Viewed at Three Levels of Magnification

————— MODIFIED OCG  
 ..... RANDOM CHECKERBOARD  
 - - - OVERLAPPING CIRCULAR GRAIN (OCG)  
 ~~~~~ MEASURED SPECTRUM  
 AMP. TRANSMITTANCE,  $t_0 = 0.55$   
 DEV. = DK 50, 5 MIN.,  $68^\circ$



A-006-1-00-0023

FIG. 7.3-2 POWER SPECTRUM OF GRAIN NOISE OF ROYAL-X PAN  
COMPARED WITH THEORETICAL MODELS



A-006-1-00-0043

FIG. 7.3-3 POWER SPECTRUM OF GRAIN NOISE OF KODAK 2479 FILM COMPARED WITH THEORETICAL MODELS

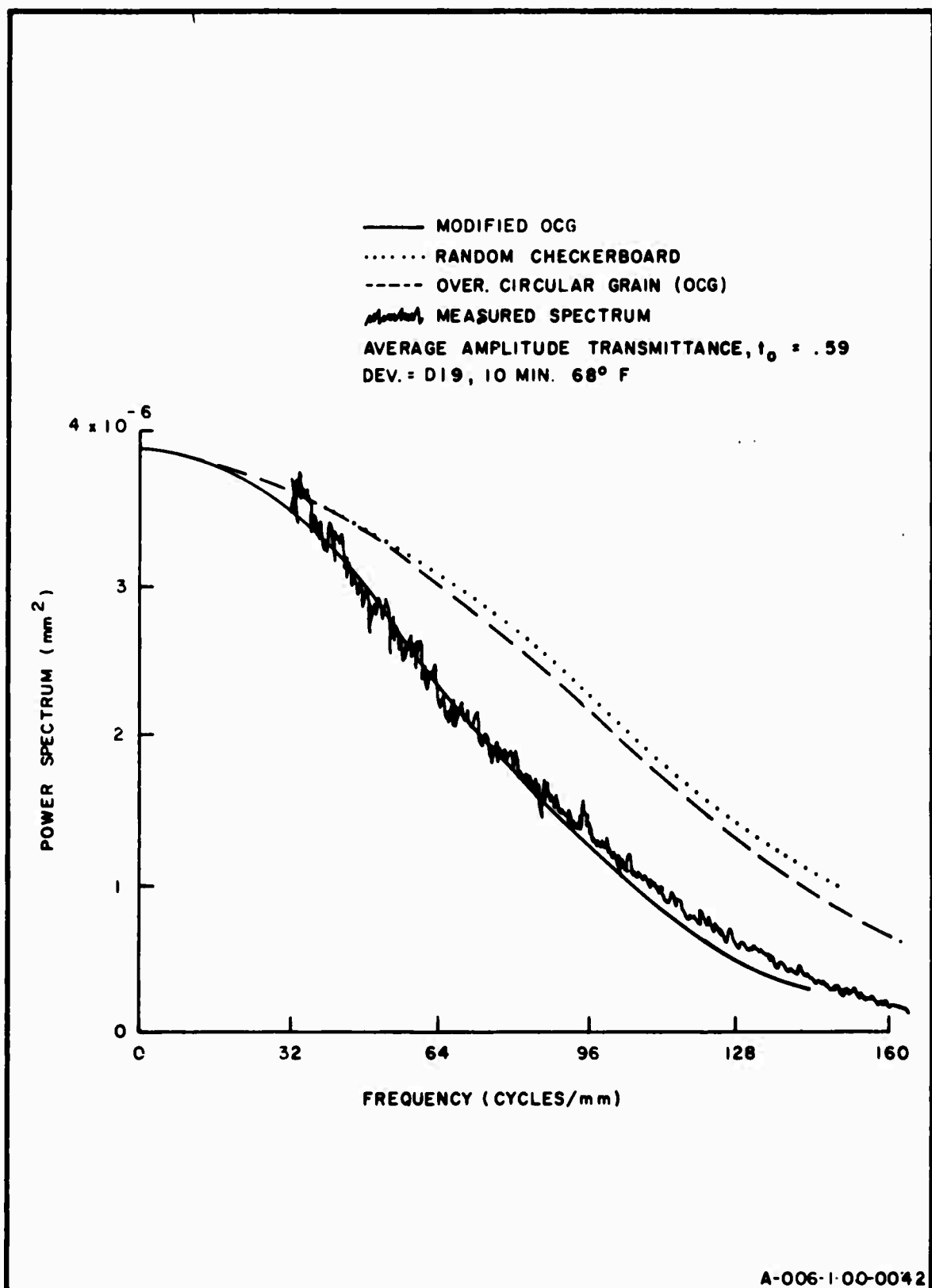
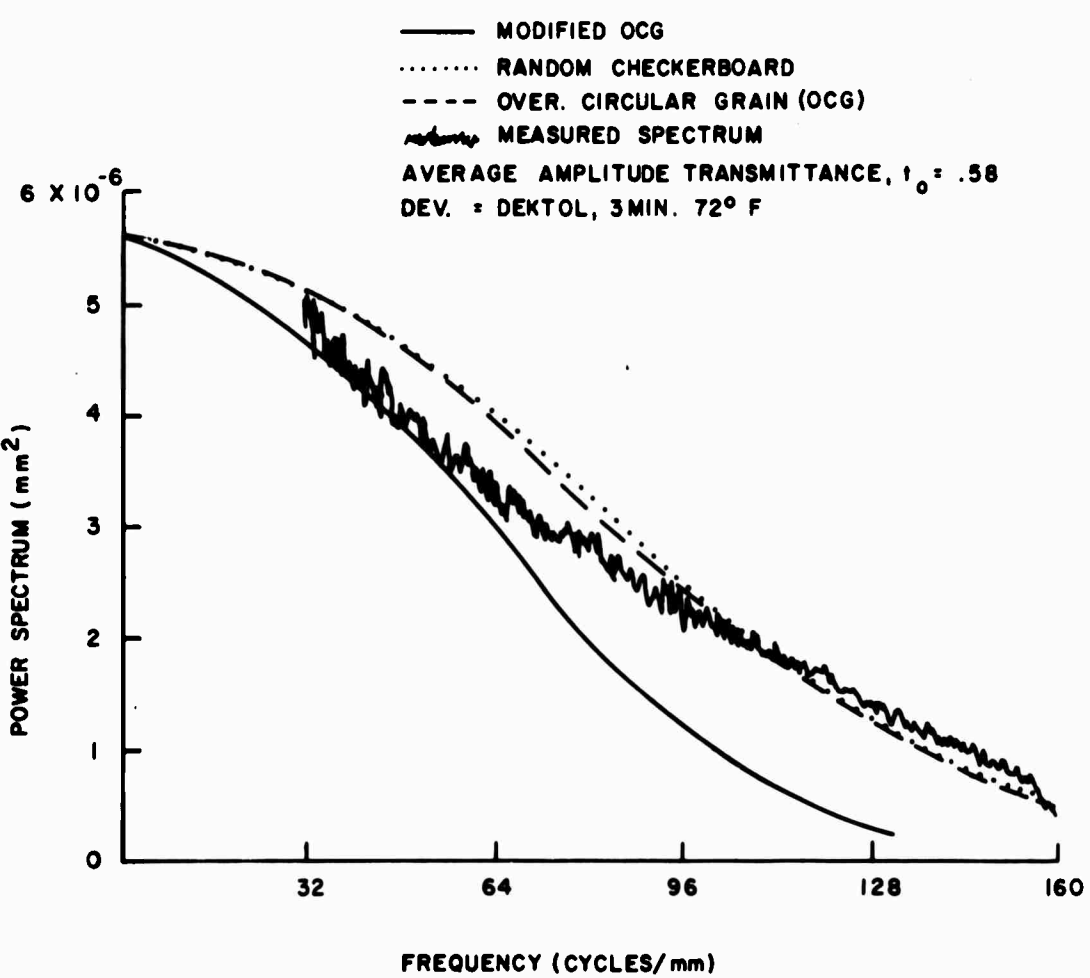


FIG. 7.3-4 POWER SPECTRUM OF GRAIN NOISE OF KODAK 2475  
DEVELOPED IN D-19, COMPARED WITH THEORETICAL MODELS



A-006-1-00-0077

FIG. 7.3-5 POWER SPECTRUM OF GRAIN NOISE OF KODAK 2475 (DEKTOL) COMPARED WITH THEORETICAL MODELS

to insure that the noise was isotropic. The theoretical curves do not represent "best fit" curves in any sense. The parameters used for the theoretical models were obtained by independent measurements. For example, in order to specify the spectrum of the RC model as given by Eq. (4.2-3), it is necessary to specify  $w_{\tau}(0,0)$  and the grain size  $\ell$ . Since  $w_{\tau}(0,0)$  is estimated by extrapolating the experimental spectrum and  $t_o$  is measured independently,  $\ell$  can be calculated from

$$\ell = \left( \frac{w_{\tau}(0,0)}{t_o (1-t_o)} \right)^{1/2} . \quad (7.3-1)$$

By this procedure, the theoretical spectra and the extrapolated spectra were made to coincide at the origin. For the OCG model, numerical integration of Eq. (4.2-15) was required. From Eqs. (4.2-14) and (4.2-15), it can be seen that the power spectrum depends on the parameters  $t_o$ ,  $h$  and  $\ell_o$  where  $\ell_o$  is the mean grain radius and  $h$  is the transmittance of the gelatin (Sec. 4.2). For  $h = 1$  and  $t_o$  measured independently by the procedure in Sec. 6.3 (part c),  $\ell_o$  can be determined by numerically computing the normalized spectrum  $w_n(0)$ , which does not depend on  $\ell_o$ , and using Eq. (4.2-16):

$$\ell_o = \frac{1}{8\pi t_o^2} \left( \frac{w(0)}{w_n(0)} \right)^{1/2} . \quad (7.3-2)$$

With  $\ell_o$  computed as above, the power spectrum for the OCG model can be computed for all other frequencies. The parameter  $d$ , which is the average number of grains per unit area, can be determined from Eq. (4.2-9).

The modified overlapping circular-grain model (MOCG) results when the effect of the transmittance of the gelatin,  $h$ , is considered

(Savelli 1958). A very good estimation of  $h$  can be made by measuring the transmittance of unexposed film, i.e., film freshly removed from the pack without prior exposure to light. However, despite precautions to the contrary, there will always be some unavoidable exposure partly due to photon leakage into the emulsion. For the MOCG model,  $l_0$  is computed from Eq. (7.3-2) but Eq. (4.2-13) with  $h$  as measured by the procedure of Sec. 6.3 (part c) is used for computing  $d$ .

Of the three models, the MOCG gave the best fit to the measured spectrum, particularly at lower frequencies. The RC and simplified OCG models furnished curves which were not significantly different even though the latter is the more realistic. The simplified OCG model is less convenient to use since numerical integration is required for computing its power spectrum. The RC spectrum was used with  $v = 0$  (Eq. 4.2-3) which corresponds to a specific grain "alignment" in the film plane. This rather artificial situation is a consequence of trying to fit isotropic models, and hence the problem of grain alignment is not relevant. Another advantage of these models is that, unlike the RC model, they do not predict nulls at frequencies which are multiples of the inverse grain sizes.

The RC and OCG models yielded power spectra which were larger than the MOCG and the measured spectra at most frequencies. This behavior is a consequence of the larger variance of these models which, because the variance is the integral of the power spectrum, tended to produce larger spectra.

Table 7.3-2 summarizes some of the principal data extracted from Figs. 7.3-2 through 7.3-5. The data listed in Table 7.3-2 are in good agreement with the film properties listed in Table 7.3-1. The known coarsest film of the set (Royal-X Pan, when the other films are used with their normal developers) can be seen to have the largest grains while the known finest film

TABLE I.3-ε

| Film and Developer | Measured Transmittance, $t_0$ | Grain Area Microns |      |          | No. of Grains mm <sup>-2</sup><br>In Thousands |      |          |
|--------------------|-------------------------------|--------------------|------|----------|------------------------------------------------|------|----------|
|                    |                               | OCG                | RC   | MOD. OCG | OCG                                            | RC   | MOD. OCG |
| Royal-X Pan DK-50  | 0.55                          | 24.6               | 21.2 | 20.5     | 20.1                                           | 21.2 | 20.1     |
| 2479 D-19          | 0.58                          | 15.2               | 13.5 | 26.4     | 35.8                                           | 31   | 12.1     |
| 2475 D-19          | 0.59                          | 16.1               | 16   | 34.2     | 29.2                                           | 25.6 | 8.9      |
| 2475 Dektol        | 0.58                          | 26.4               | 23.4 | 47.6     | 20.6                                           | 18   | 6.8      |

of the set (Kodak 2479) had the smallest grains and the largest grain density. The data reveal a well-known property of fast films (Mees and James 1966), namely, that such films have large grains and low grain densities.

It was of interest to determine why the various models furnished different results. For example, for every film and developer combination, the estimated grain size computed from the RC model is smaller than the corresponding grain sizes computed from the OCG models. Equally apparent is the discrepancy between the two models with respect to the computed grain density. In every case, this figure is largest when computed by the OCG model and smallest for the MOCG model.

The theoretical justification for these differences can be found by considering the properties of the RC and OCG models. First, in all three models, it is assumed that there is no variability in the opacity of exposed grains and that an exposed grain has zero transmittance. Thus, in the OCG model, the fact that two exposed grains may overlap does not further reduce the transmittance of a point in the overlapped region. Second, since the random checkerboard model does not provide for overlapping, it follows that the total opaque area is simply the number of exposed grains multiplied by the grain size - a result not true for the OCG models. For the latter, the developed grains do not remove clear area equal to their size because some grains overlap. Hence, for a given transmittance, the nature of the OCG models requires that a greater amount of silver be deposited than in the RC model. This greater silver deposit can result from a greater number of developed grains, larger grains, or both.

The large grain areas and low grain densities supplied by the MOCG model are a consequence of the additional parameter  $h$ , which must be determined before the model is completely specified. Comparing Eq. (4.2-1) with Eq. (4.2-8) it is seen that since  $h$

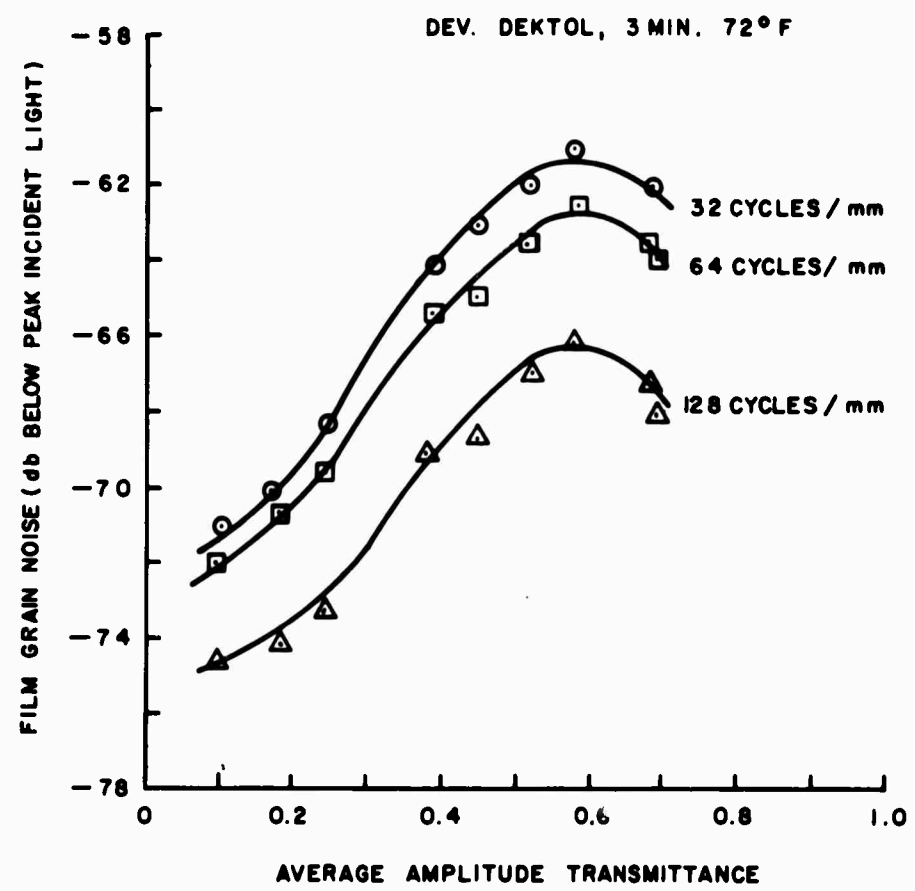
is less than unity, less silver (fewer grains) must be exposed for the same value of  $t_o$  than in the OCG model. This accounts for the low densities recorded for the MOCG model.

Experimental evidence is given later in this section to show that grain sizes decrease with decreasing transmittance over a wide transmittance range. Since the MOCG model can be regarded (except for a multiplicative constant) as the ordinary OCG model with equivalent transmittance  $t'_o = \frac{t_o}{h}$  and since  $t'_o > t_o$ , the larger grain sizes furnished by the MOCG model are not surprising in view of the above.

The last two columns of Table 7.3-2 refer to data obtained on Kodak 2475 film samples treated with different developers. The recommended developer in this case is D-19 while the Dektol (deemed unsuitable for 2475) was expected to yield a grainy transparency. The results corroborated this. Using the MOCG model as a basis, the Dektol developer produced grains 40% larger than the D-19. With the OCG and RC models, the increases were equally significant at 46%.

When the spectrum of grain noise is plotted vs  $t_o$ , the RC model predicts a maximum in the vicinity of  $t_o \approx 0.5$  while from Fig. 4.2-5, the peak for the OCG is shifted to the left near  $t_o = 0.57$ . Figure 7.3-6 shows the variation of the actual spectrum as a function of  $t_o$  for several different frequencies. In each case, the peak occurred at approximately the value of  $t_o \approx 0.6$ , although the peak value decreased with increasing frequency. This is predicted by both the OCG and RC models - for the latter, at least until the first null. All the film samples used in this experiment were developed in Dektol for 3 minutes at 72°F. Figure 7.3-7 shows the variation of the extrapolated spectrum with  $t_o$  at the origin [see Fig. 4.2-5.]

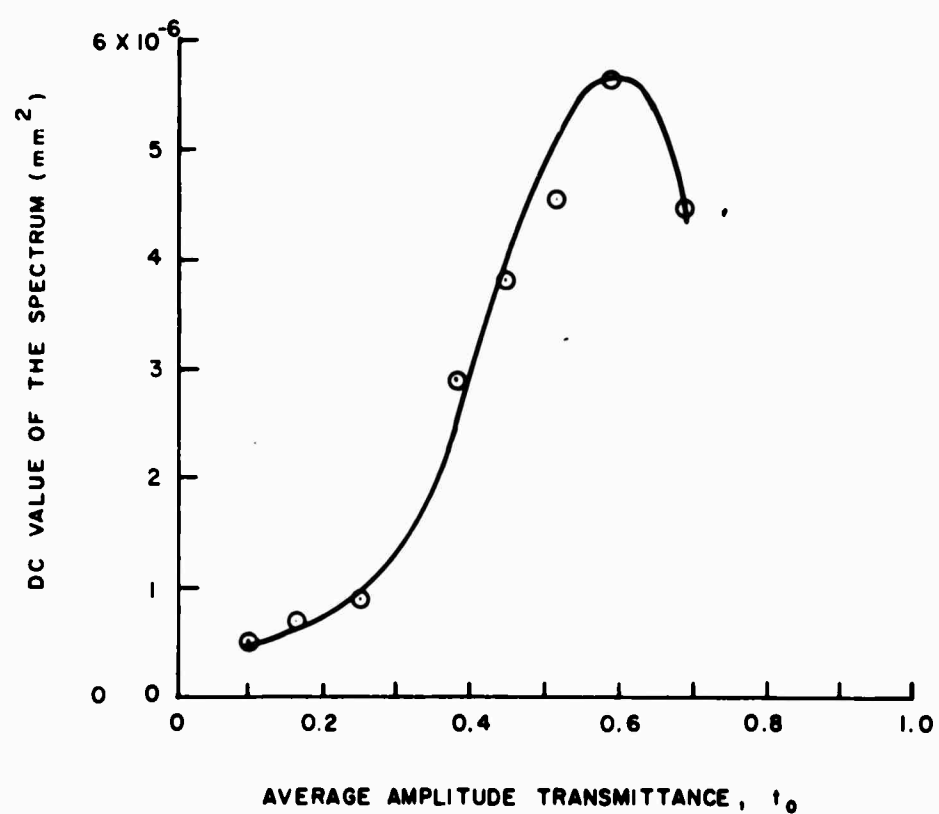
The variation of grain noise with transmittance was determined for still another sequence of transparencies which were



A-006-1-00-0054

FIG. 7.3-6 VARIATION OF GRAIN NOISE WITH AMPLITUDE TRANSMITTANCE FOR KODAK 2475

FILM TYPE = KODAK 2475  
DEV. = DEKTOL, 3 MIN. 72° F



A-006-1-00-0056

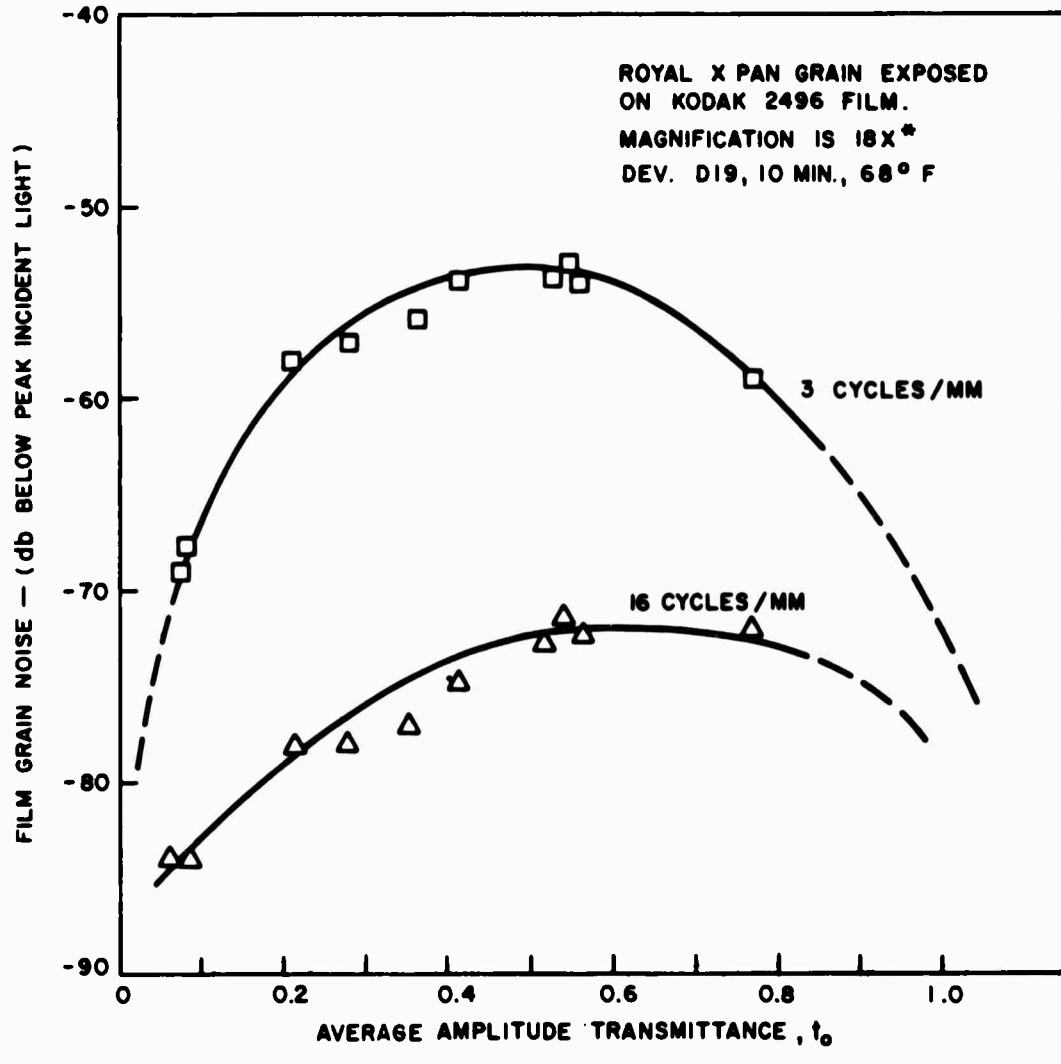
FIG. 7.3-7 VARIATION OF SPECTRUM AT DC WITH  $t_0$ ,  
(EXTRAPOLATED FROM MEASUREMENTS)

obtained by imaging Royal X-Pan grain on low noise Kodak 2496 film with magnification of 18x. Although these samples were generated for another purpose, their use in this case proved advantageous because the magnified grains furnished a very strong scattered light level, thus enabling the observation of the spectrum at much lower frequencies without the need for extrapolation. The results are shown in Fig. 7.3-8, where it can be seen that the film noise again peaked near  $t_0 \approx 0.6$ , although at 16 cycles/mm the peak was found to be quite broad.

When the grain sizes were computed from the theoretical models and the extrapolated spectra, it was found that the average grain area decreased with decreasing transmittance until a minimum was reached beyond which, for still lower transmittances, the grain size increased (Fig. 7.3-9). The decrease in grain size with decreased transmittance, that is, with increased exposure, was first observed, but not explained, by M. Savelli (Savelli 1958).

The two regions on either side of the minimum reflect separate phenomena. The negative-slope region can be explained by considering Silberstein's quantum theory of exposure. According to Eq. (4.1-1), for an emulsion of equally sensitive grains, the large grains will have a higher probability of absorbing the necessary number of photons required for development than the small grains. Hence, for low exposure levels, the large grains will develop first and the average grain size will be high. For example, if  $m$  and  $\epsilon$  are unity in Eq. (4.1-1), the probability of exposure is

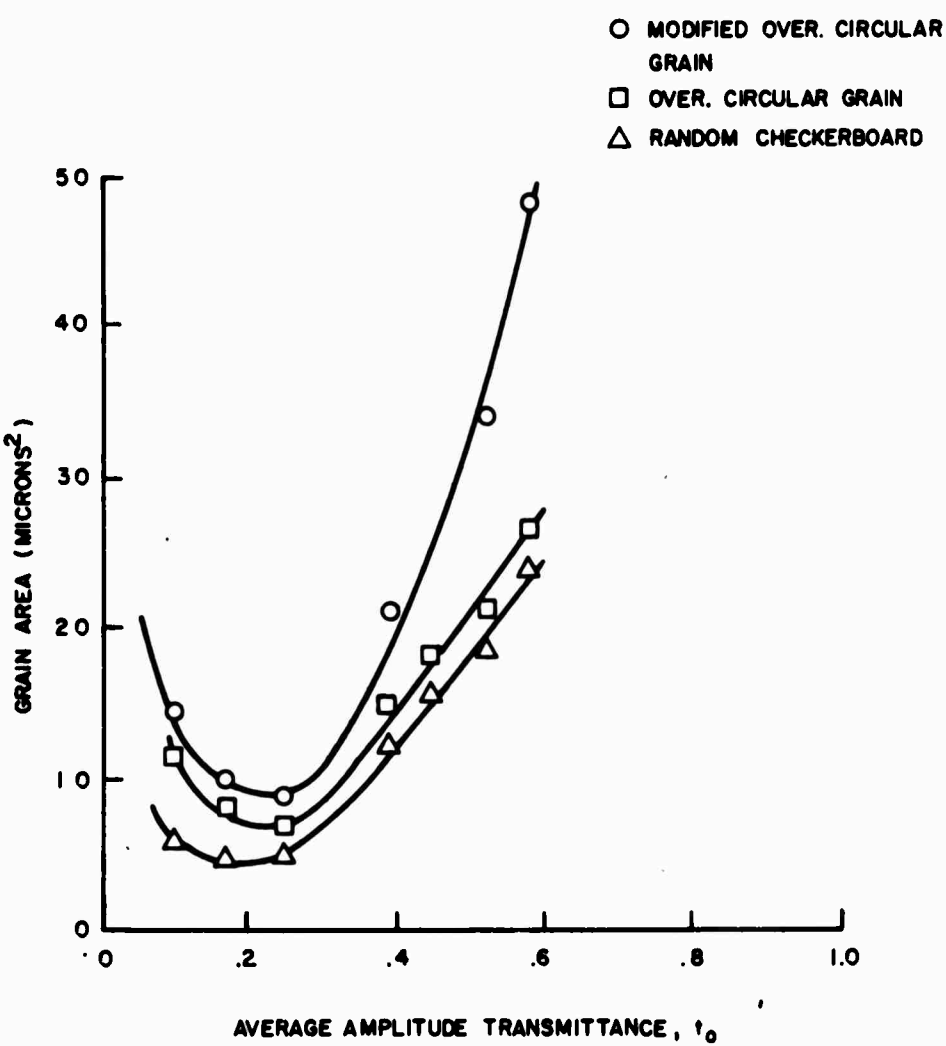
$$P(t=0) = 1 - \exp\left(-\frac{E_{TA}q}{h\omega}\right)$$



\* MAGNIFICATION OBTAINED WITH WOLLENSAK  
"RAPTAR" ENLARGING LENS (F/4.5, 50 mm)

A-006-1-00-0052

FIG. 7. 3-8 VARIATION OF GRAIN NOISE WITH AMPLITUDE TRANSMITTANCE,  $t_0$   
FOR ROYAL X-PAN GRAIN EXPOSED ON KODAK 2496 FILM



A-006-1-00-0073

FIG. 7.3-9 VARIATION OF GRAIN SIZES WITH AMPLITUDE TRANSMITTANCE (KODAK 2475, DEKTOL)

where  $A_g$  is grain area and  $E_T$  is the incident energy density (the other terms are defined in Sec. 4.1). This equation shows that for low exposure levels, the probability of exposure varies approximately linearly with area.

As the exposure becomes more intense, the probability that smaller grains will develop increases and the development of large grains becomes exhausted. Thus, the average grain size is reduced. This process continues until significant grain clumping begins to form. As mentioned in Sec. 4, these clumps are principally due to the phenomenon of grain exposure by contact (Mees and James 1966) and are not accounted for in Silberstein's theory. It should also be remembered that with increased exposure, development spreads to the grains in the deeper layers beneath the surface so that clumping occurs throughout the gelatin. The projection of these clumps on a plane produces large, contiguous opaque shadings which increase with increasing exposure. These shadings are the equivalent grains sensed by the models. It is of interest to note that all the theoretical models furnish the two regions reflecting these separate phenomena and that the minimum for all three occurs at the same  $t_o$ .

Small grains are associated with high resolving power. For Kodak 2475 developed in Dektol, the minimum grain area occurs near  $t_o = 0.25$ . That a given film could have its resolving power depend on exposure was discovered by M. Levy (Mees and James 1966). Levy found that for certain aerial films, the maximum resolution occurs at exposure levels corresponding to an average amplitude transmittance of  $t_o \approx 0.34$ .

One advantage in making spectral density measurements by diffraction is the possibility of obtaining two-sided spectra by simply scanning in the back focal plane on either side of the origin. Such two-sided spectra are shown in Fig. 7.3-10 ;the

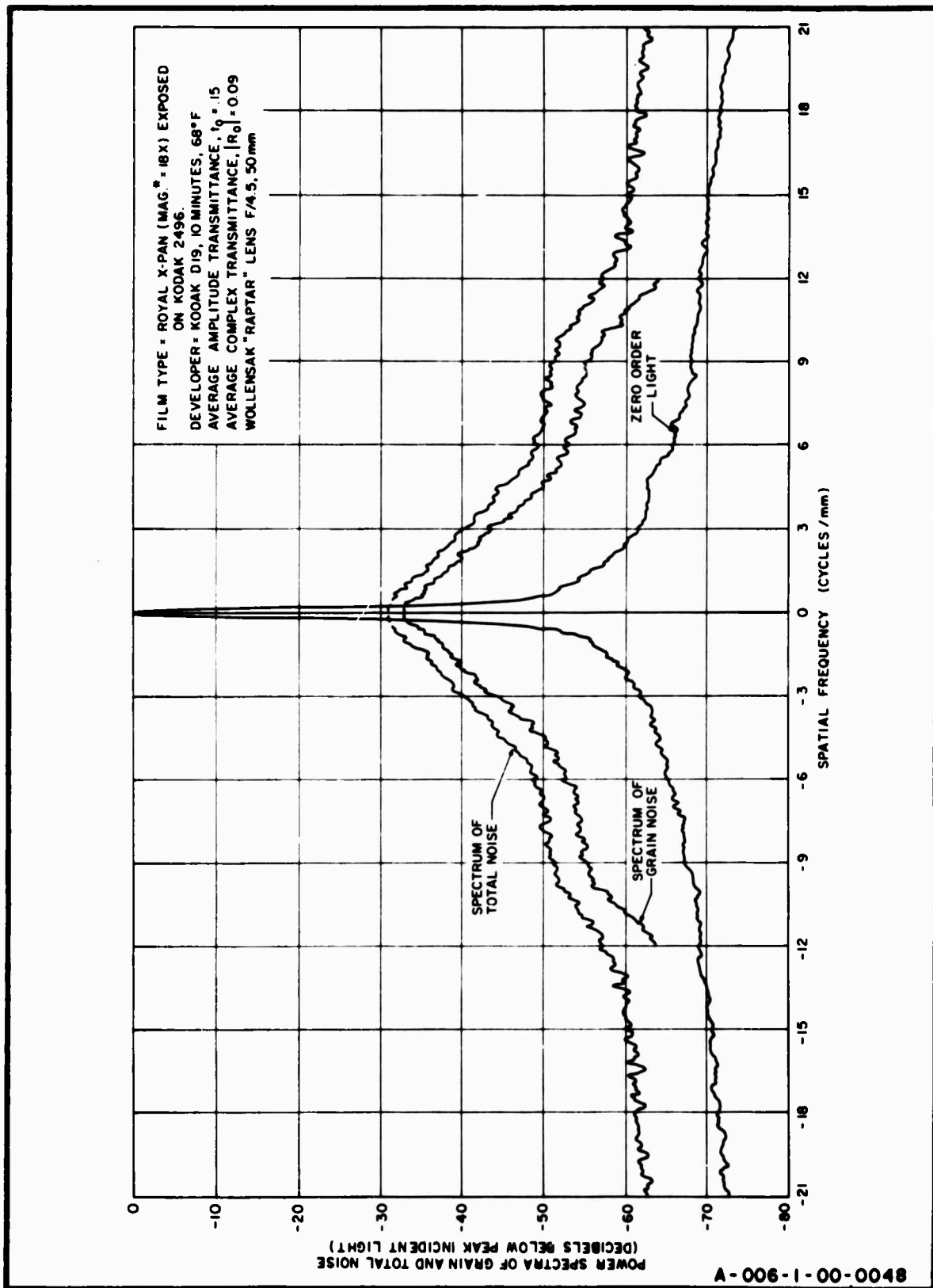


FIG. 7.3-10 TWO-SIDED POWER SPECTRUM OF ISOTROPIC NOISE

film in this case was magnified Royal-X Pan imaged on 2496. The unusual structure is partly a reflection of the imaging optics. The evenness about the origin and the repeatability along orthogonal axes is a characteristic of isotropic noise, which requires that the spectrum be an even and symmetric function of the orthogonal spatial frequencies  $(u, v)$ . An example of nonisotropic noise is the condition of granularity "streaking", which is characterized by pronounced, parallel transmittance variations in some specific direction. Streaking can be detected from microdensitometer traces. Such traces and the spectrum of the resulting noise are shown in Fig. 7.3-11.

#### 7.4 MEASUREMENTS OF THE SPECTRA OF TOTAL FILM NOISE

The scattered light that results in the Fourier plane when film is not immersed in a liquid gate was shown earlier to be an estimate of the power spectrum of the process  $\{R(x, y)\}$ . The random variable describing the complex transmittance  $R(x, y)$  defined in terms of  $t(x, y)$  and  $\psi(x, y)$  by Eq. (4.3-1) is reduced to the amplitude transmittance  $t(x, y)$  when phase correction is provided by way of a liquid gate matched to the refractive index of the film.

When the magnitude of  $R_o = \langle R(x, y) \rangle$  was plotted vs the average amplitude transmittance  $t_o$ , a linear relationship was observed over wide transmittance variations, excluding very low transmittances. If the model of Sec. 4.3 is applied, namely, the assumptions of independence between  $\{\psi(x, y)\}$  and  $\{t(x, y)\}$  and Gaussian statistics for the former, then the theoretical relationship between  $R_o$  and  $t_o$  is given by  $R_o = t_o \exp(-\sigma_\psi^2/2)$ , which is a line with constant slope that furnishes the variance of the phase noise [Sec. 6.3, part (d)].

To see if the  $R_o$  vs  $t_o$  relation given above was valid for commercial film, two sets of transparencies were tested: Kodak 2496 developed in D-19 and Kodak 2475 developed in Dektol. The

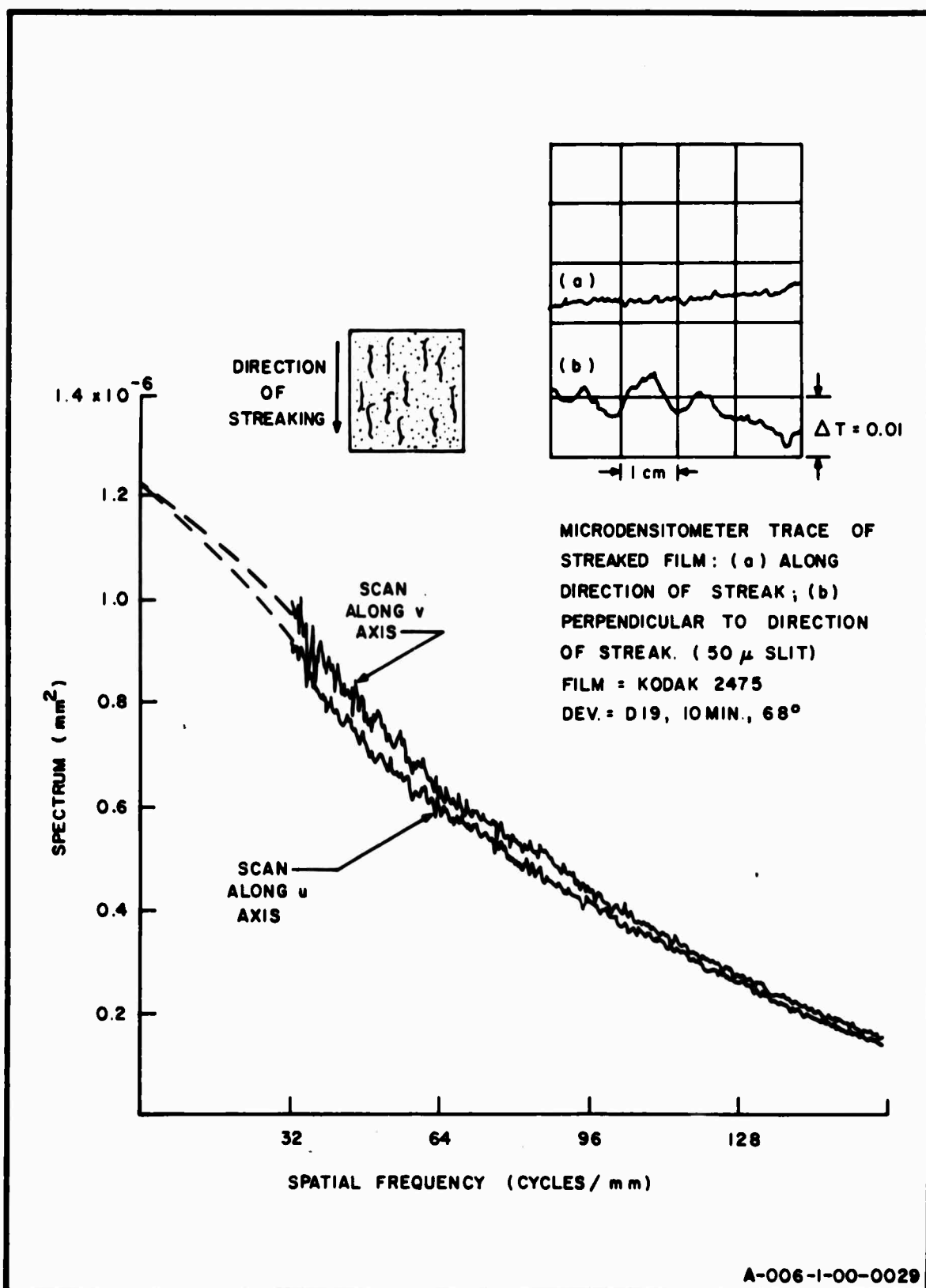


FIG. 7.3-II POWER SPECTRA OF NON-ISOTROPIC GRAIN NOISE.

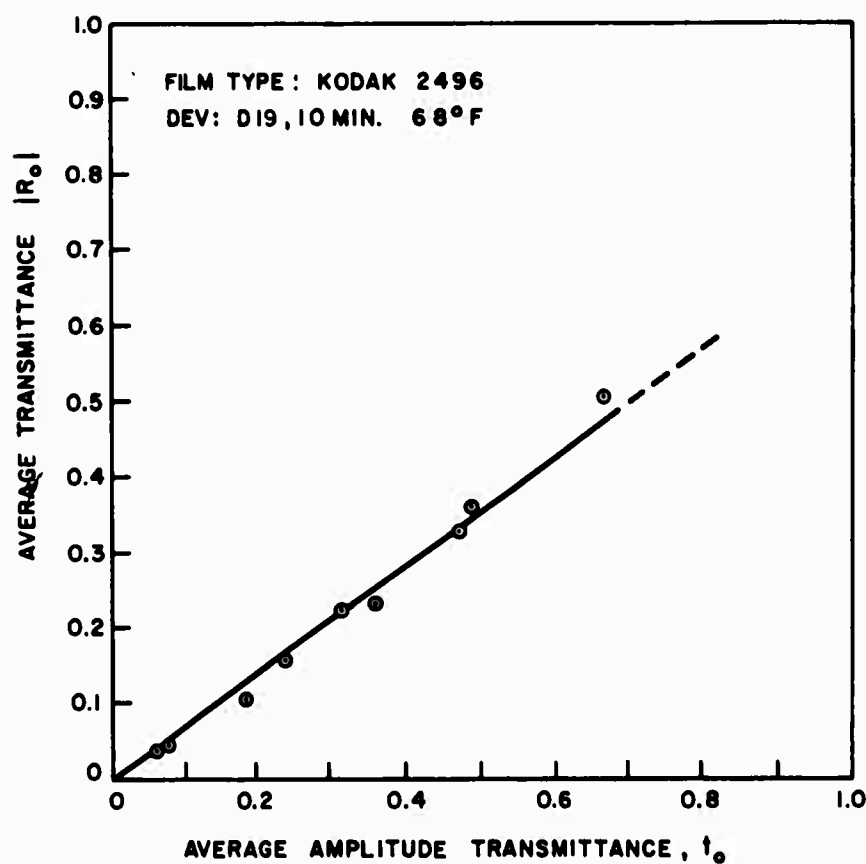
two films had radically different properties. Kodak 2496 is a high resolution, low noise film with a "Fine" granularity rating while Kodak 2475, particularly when treated with Dektol, is a fast, coarse film (see Tables 7.3-1 and 7.3-2). When optical path lengths were considered, however, the two films were more similar in that both had the same clear, fast drying backing and same 4-mil gray Estar base. The results are shown in Figs. 7.4-1 and 7.4-2. It can be seen that the two curves have nearly the same slope over the central values of  $t_o$ , strongly pointing to the fact that, in this case,  $\sigma_\psi$  is essentially a measure of the base and backing and not of developer and granularity. Table 7.4-1 summarizes the results of this experiment.

TABLE 7.4-1

| FILM AND DEVELOPER | MEASURED<br>$\sigma_\psi$ | RMS THICKNESS DEVIATION  | RMS OPTICAL PATH* LENGTH DEVIATION |
|--------------------|---------------------------|--------------------------|------------------------------------|
| 2479<br>D-19       | .836 rad                  | $1.38 \times 10^{-4}$ mm | $0.84 \times 10^{-4}$ mm           |
| 2475<br>Dektol     | .844 rad                  | $1.40 \times 10^{-4}$ mm | $0.85 \times 10^{-4}$ mm           |

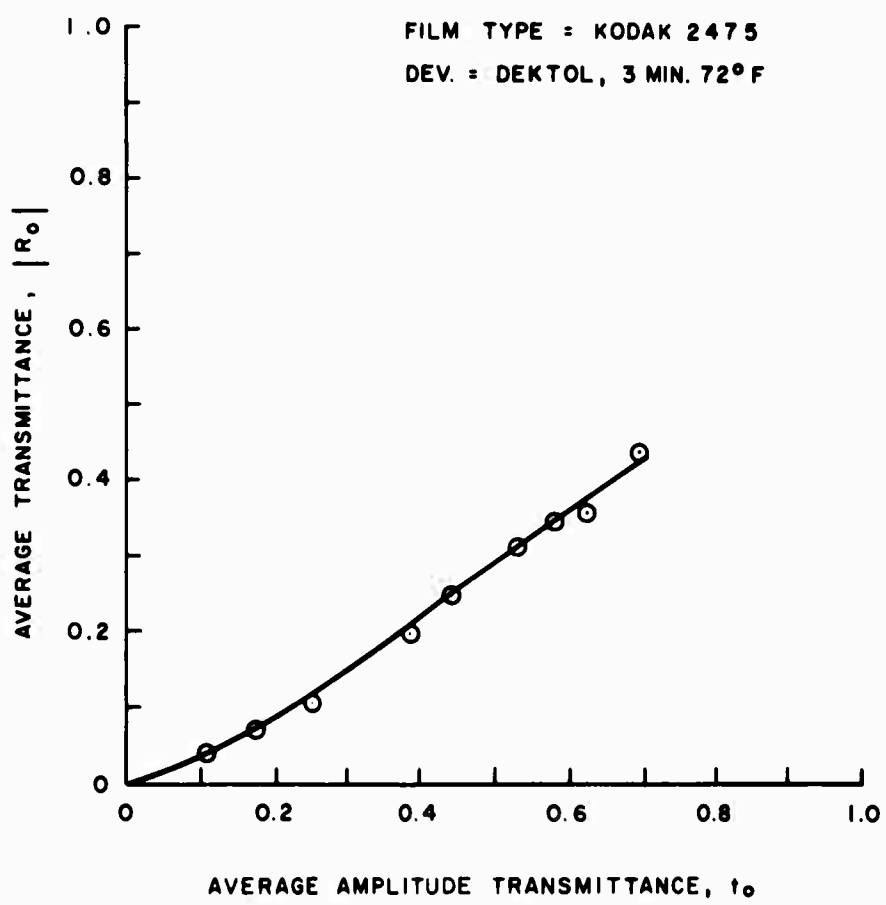
Measurements indicated that the total noise spectrum was considerably larger at low frequencies than the spectrum of grain noise alone. This was expected after obtaining the diffraction patterns shown in Figs. 7.1-2 and 7.1-4, where it can be seen that the effect of the grain noise on the zero-order light was hardly discernible [Fig. (7.1-4)] while the effect of the total noise on the zero-order [Fig. (7.1-1)] was clearly evident.

\* For film in a vacuum or air.



A-006-1-00-0051

FIG. 7.4-1 EXPERIMENTAL RELATIONSHIP BETWEEN THE REAL AND COMPLEX TRANSMITTANCE OF FILM



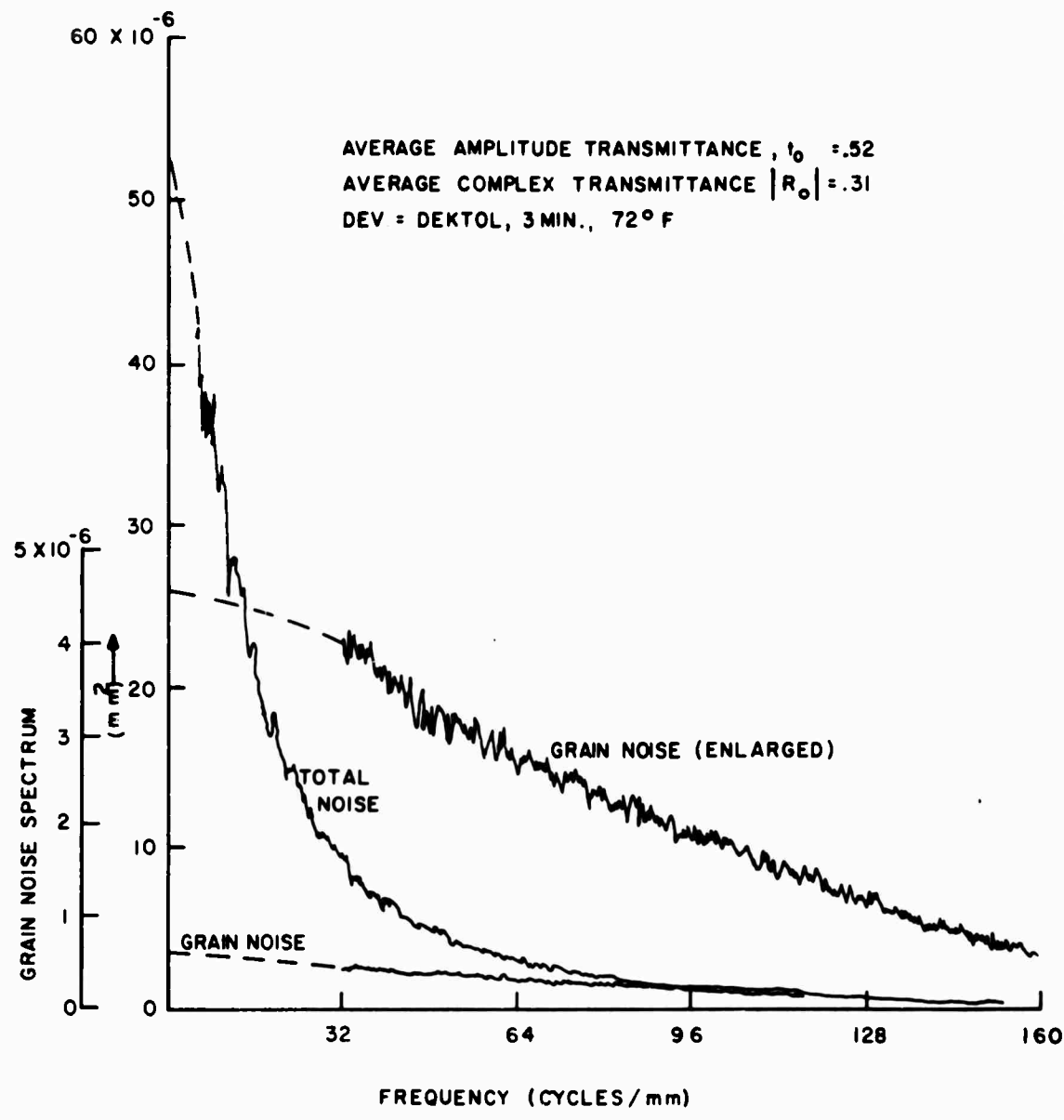
A - 006 - 1 - 00 - 0053

FIG. 7.4-2 EXPERIMENTAL RELATIONSHIP BETWEEN REAL AND COMPLEX TRANSMITTANCE OF FILM

Figures 7.4-3 through 7.4-5 are experimentally obtained spectra of total film noise. Unlike the behavior of grain noise, the spectrum of the total noise is peaked near the origin and falls off very rapidly for higher frequencies. In Fig. 7.4-3 spectral densities of the grain and total noise are compared. An enlarged view of the grain noise is provided. Calibration of the total noise spectrum was effected by using Eq. (6.2-10) with  $|R_o|^2$  substituted for  $t_o^2$ . It can be seen that the spectrum of the total noise is nearly an order of magnitude above the grain noise. The large total noise spectrum enabled its measurement near the origin, and little interpolation was required. The low-frequency nature of the total noise spectrum can be illustrated by observing that the spectrum decreases to half of its maximum value, which is at the origin, at a frequency  $\sim 16$  cycles/mm, whereas the half-maximum of the grain noise does not appear until 80 cycles/mm. These results imply that the phase-related process  $\{\eta(x,y) = e^{j\psi(x,y)}\}$  is a low-frequency phenomenon.

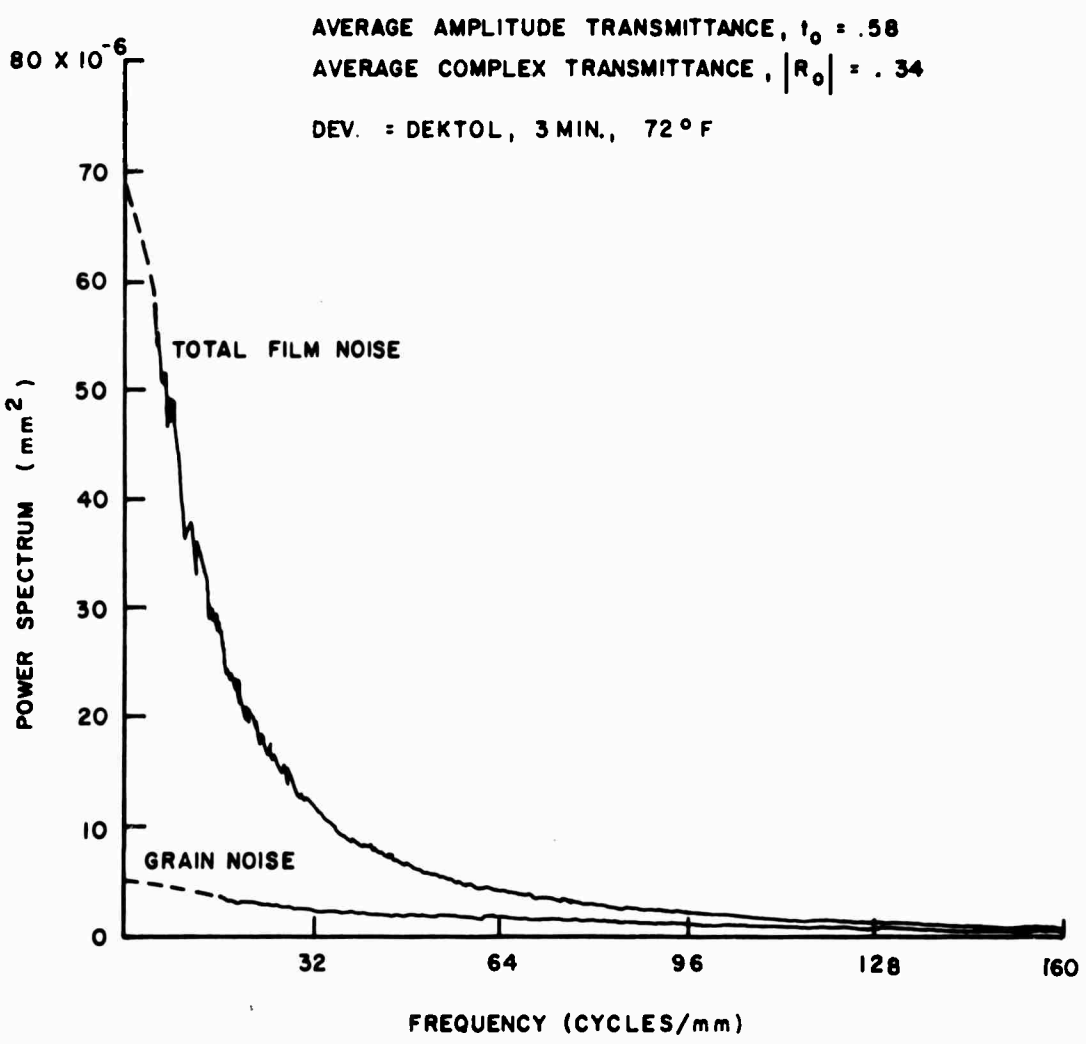
Equation (4.3-14), which was derived on the basis of the previous assumptions of independence between  $\{\psi(x,y)\}$  and  $\{t(x,y)\}$ , and the normality of  $\{\psi(x,y)\}$ , predicts that the spectrum of the total noise will vary approximately with  $t_o^2$  provided that  $t_o$  is not too small and that the related phase spectrum  $w_\eta(w)$  is the dominant term. The spectrum in Fig. 7.4-4 was obtained for a sample of Kodak 2475 (Dektol) with transmittance  $t_o = 0.58$ . Comparing the spectra of Fig. 7.4-3 and 7.4-4, it is seen that the ratio of the square of the transmittances (1.24) closely follows the ratio of the peaks of total noise spectra (1.29).

Examination of Eq. (4.3-14) shows that the spectrum of the total noise is the sum of attenuated versions of the spectra of grain noise and related phase noise and their convolution product. Under the conditions of small  $t_o$ , large  $\sigma_\psi$ , and



A-006-1-00-0078

FIG. 7.4-3 POWER SPECTRUM OF TOTAL NOISE COMPARED WITH GRAIN NOISE (KODAK 2475)



A-006-1-00-0076

FIG. 7.4-4 POWER SPECTRUM OF TOTAL FILM NOISE AT PEAK GRAIN NOISE (KODAK 2475)

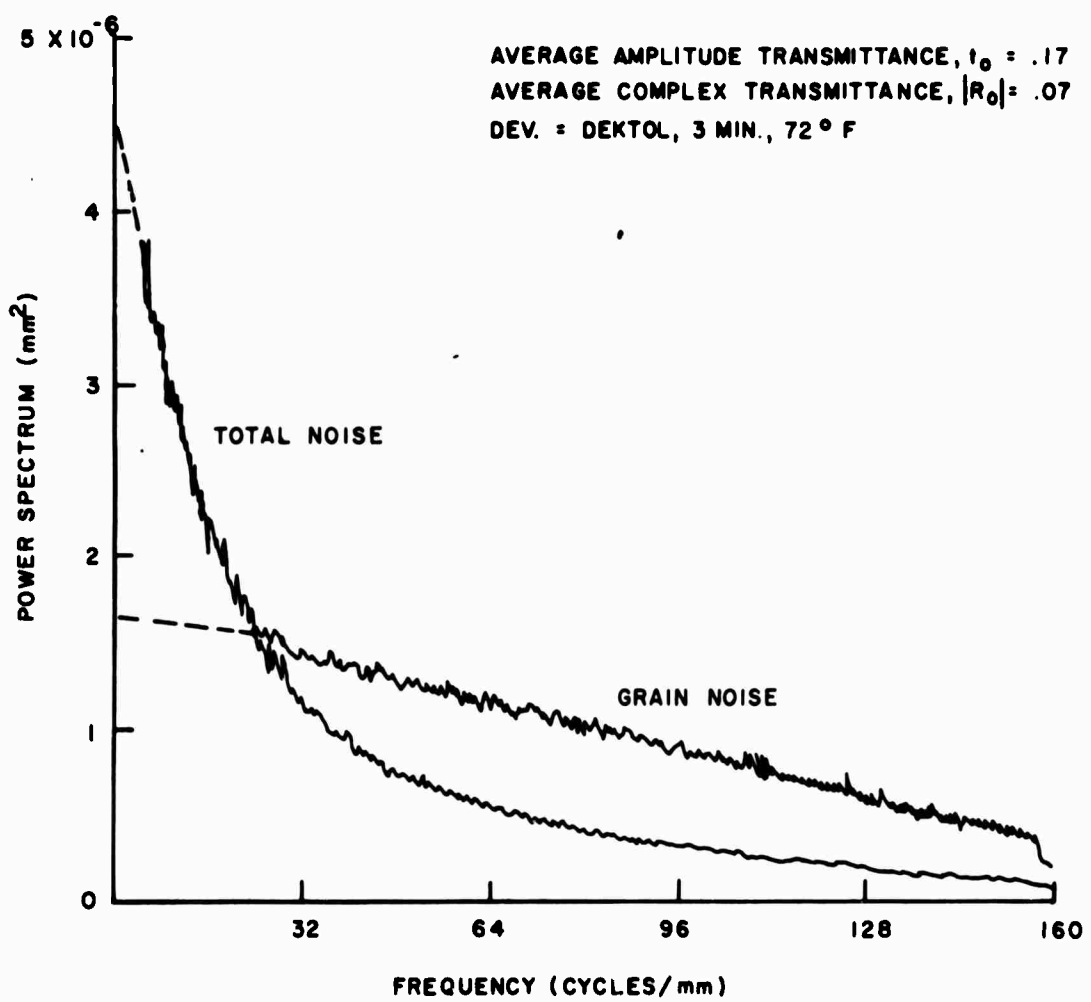
sufficiently high frequency, the spectrum of the total noise may have a smaller amplitude than the grain-noise spectrum.

The situation where  $w_r(w) < w_t(w)$  was experimentally observed (Fig. 7.4-5) for a Kodak 2475 sample with low transmittance. The prediction and interpretation of the results in Fig. 7.4-5 in the light of Eq. (4.3-14) is however not completely valid since the  $|R_o|$  vs  $t_o$  curve for Kodak 2475 developed in Dektol undergoes a departure from linearity at low transmittances, thus violating the assumption of complete independence between  $\{\psi(x,y)\}$  and  $\{t(x,y)\}$  upon which Eq. (4.3-14) was derived.

## 7.5 SPECTRA OF MAGNIFIED GRAIN NOISE AND FREQUENCY RESPONSE OF OPTICAL SYSTEMS

The discussion in Sec. 6.5 indicates that, based on the theoretical considerations leading up to Eqs. (6.5-2) and (6.5-7), magnification and imaging techniques can be used to obtain the extended spectra of grain noise and the frequency response of optical systems. Because of a limitation in the availability of laboratory apparatus, the results in this section were obtained using procedures which were not ideal. Hence, these results are intended more to illustrate feasibility than to provide refined data.

Ideally, imaging, magnification, and spectral analysis should be performed simultaneously as spatially sequential operations on the optical bench comprising the coherent optical system. The available laboratory equipment did not permit this, and it was necessary to adopt a procedure which involved doing the imaging on a separate, incoherent system, storing the image on low-noise film, and then transferring the film to the coherent optical system to measure the spectrum. A major disadvantage of storing the image on film results from the interaction of the film's own granularity with the imaged granularity. In view of



A-006-1-00-0055

FIG. 7.4-5 ANOMALOUS BEHAVIOR OF DENSE FILM (KODAK 2475)

the analysis given in Appendix A, it is unclear whether or not the spectrum of the granularity simply adds to the spectrum of the granularity of the storage medium as some authors propose (Doerner 1952). However, in the present case, the image was stored on Kodak 2496 film which, insured that the magnified granularity would exercise a dominant role. Kodak 2496 is a high-resolution (136-225 cycles/mm), low-noise film suitable for applications where grain noise has to be kept small. A second serious disadvantage results from the use of incoherent illumination systems. This is discussed in greater detail below. The reader is reminded, however, that these problems are a consequence of the procedure that was used and could be eliminated by using an all-coherent optical system.

In order to determine experimentally the frequency response of the "Raptar" commercial enlarger lens described in Sec. 6.1, the following procedure was used. The log spectrum of the film storing the imaged magnified granularity of Royal X-Pan was superimposed on the original log spectrum of the Royal X-Pan after calibrating the frequency axis according to Eq. (6.5-2), that is, the frequencies associated with the magnified spectrum were multiplied by the magnification factor. The log spectra were made to coincide at the origin, thereby normalizing the frequency response with respect to its value at the origin. Away from the origin, a separation that increased with frequency was observed between the log spectra. The interpretation of this separation, in the light of the imaging theory summarized in Sec. 6.5, is as follows:

The imaging of granularity in incoherent light produced an intensity in the image plane given by (Eq. 6.5-6)

$$I_p(x, y) = \int_{-\infty}^{\infty} \int_{-\infty}^{\infty} T(\xi, \eta) B_I(x - \xi, y - \eta) d\xi d\eta$$

When film is placed in the image plane, it is possible by proper control of exposure and development to generate an amplitude transmittance variation proportional to the light intensity.

Hence,

$$t^{(p)}(x,y) = K I_p(x,y) \quad (7.5-1)$$

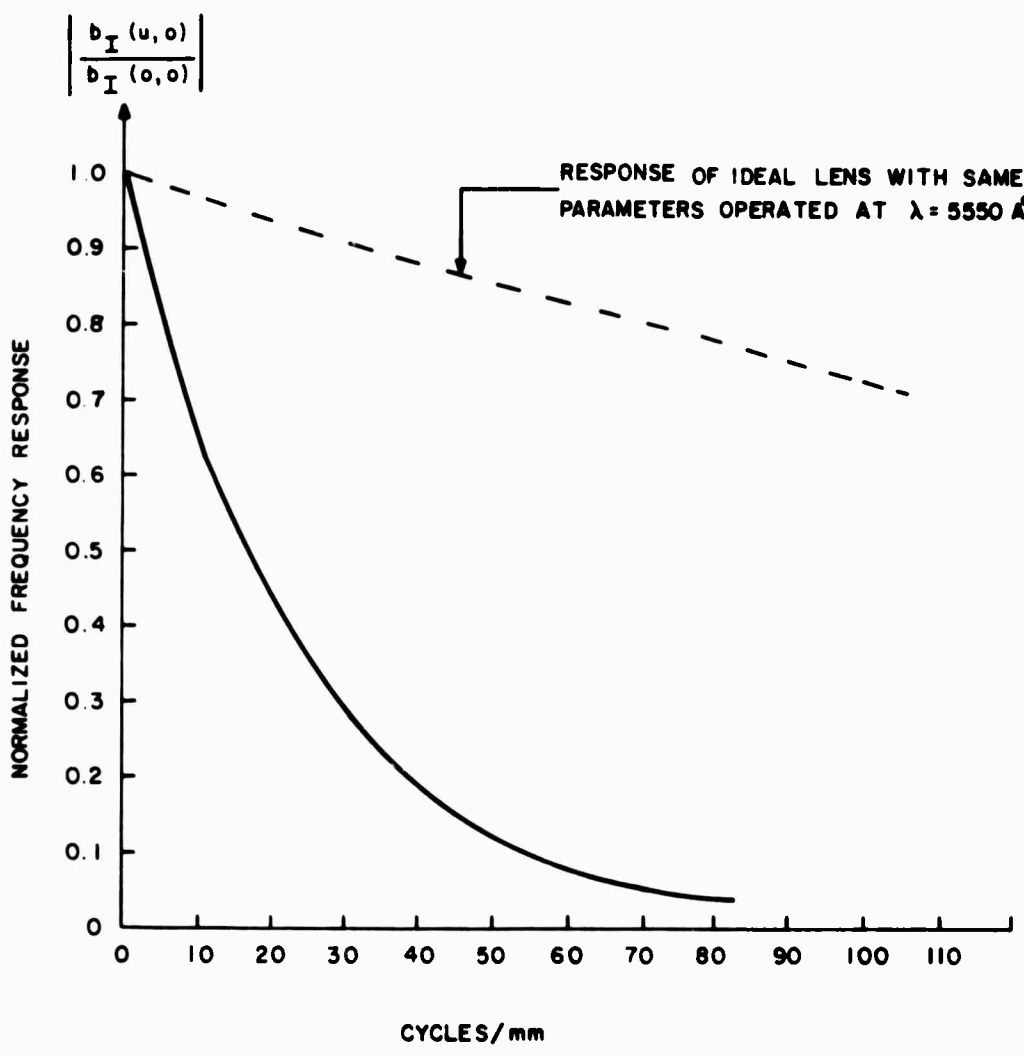
where  $K$  is the constant of proportionality. It follows from Eqs. (7.5-1) and (6.5-6) that

$$\phi_t^{(p)}(\alpha, \beta) = K^2 \phi_T(\alpha, \beta) * G(\alpha, \beta) \quad (7.5-2)$$

where  $G(\alpha, \beta)$  is the self-correlation function of the transmission function  $B_I(x,y)$ , and  $\phi_T$  and  $\phi_t$  are the autocorrelation functions of the intensity and amplitude transmissions. The Fourier transform of Eq. (7.5-2) yields

$$w_t^{(p)}(u,v) = K w_T(u,v) | b_I(u,v) |^2 \quad (7.5-3)$$

which establishes the proper relationship between the spectrum of the print and the spectrum of the original sample. However, knowledge of the granularity structure of the original sample was in the form of  $w_t(u,v)$  and not  $w_T(u,v)$ . Hence, the observed difference between the two log spectra can be interpreted as  $\log | b_I(u,v) |$  provided that any point on the film is in a dichotomous state - either opaque or transparent. This condition implies that the amplitude and intensity spectra are the same. Figure 7.5-1 shows the normalized average frequency response of the lens obtained by this procedure. The term average is used because (a) white light was used for illumination during imaging and (b) most of the lens surface, as opposed to the axial region alone, was used for image formation.

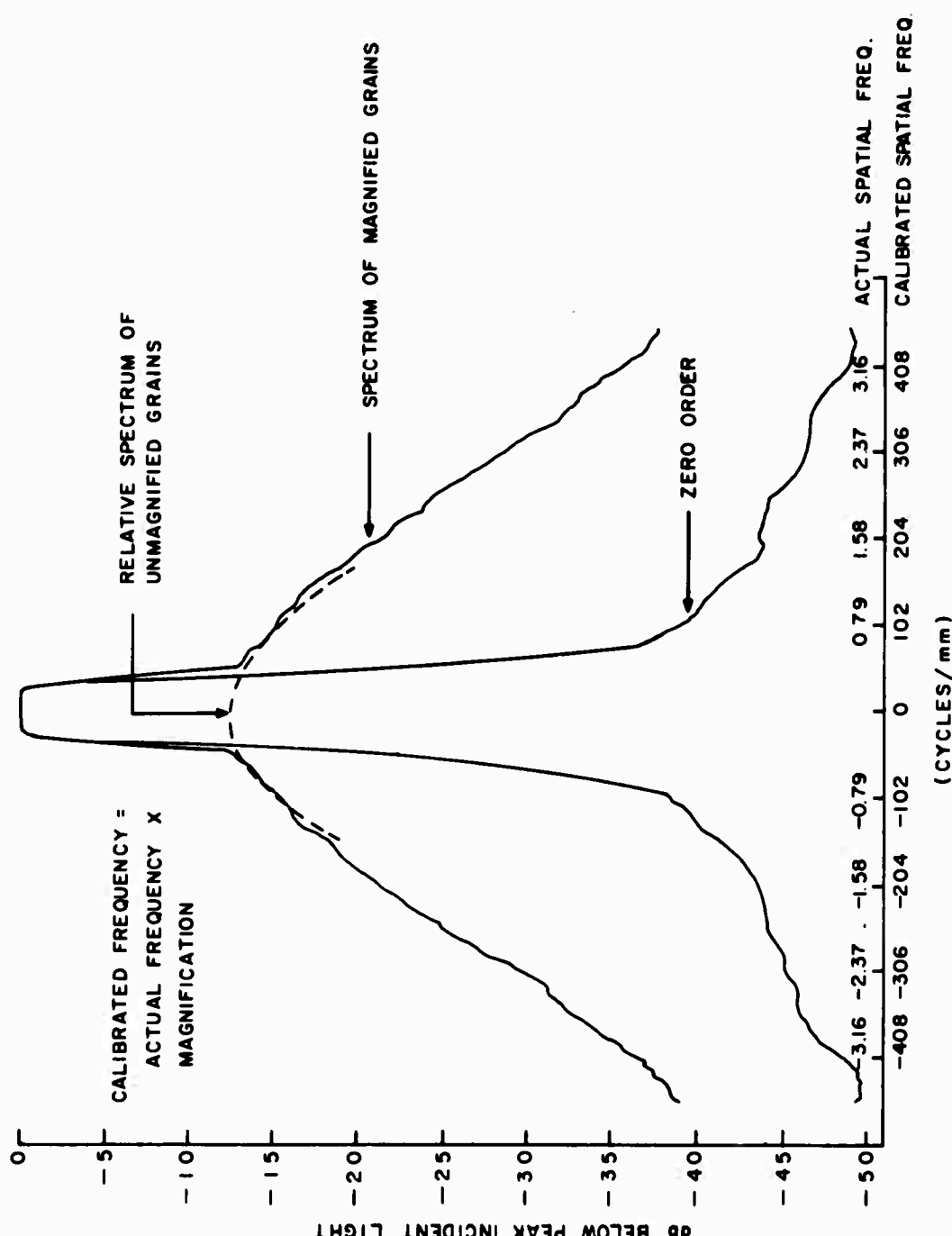


LENS PARAMETERS  
F/4.5, 50 mm FOCAL LENGTH

A-006-1-00-0015

FIG 7.5-1 MEASURED AVERAGE FREQUENCY RESPONSE OF WOLLENSAK "RAPTAR" ENLARGING LENS USED IN WHITE LIGHT

When it is desired to obtain the extended-frequency spectrum accurately by magnification, the imaging optics must have a frequency response which is flat over the frequency interval of interest. The "Fluorestar" microscope, described in Sec. 6.1 was used for high-resolution imaging. In this case, the attenuation of the microscope optics was negligible as can be seen in Fig. 7.5-2 . The cut-off frequency (the maximum spatial frequency transmitted by the lens) was 1850 cycles per millimeter corresponding to an N.A. (for definition see Sec. 6.5) of 0.5 and a wavelength of 5400 Å. The magnification was measured by a precision stage micrometer and was found to be 130X. The film type and developer was Kodak 2479 developed in D-19. When the original spectrum was superimposed on the spectrum of the magnified grains so that the two coincided at the origin, excellent coincidence resulted at low frequencies although a slight drooping-off occurred in the spectrum of the unmagnified grains at higher frequencies due to off-axis vignetting. The spectrum of the magnified grains is not affected by off-axis attenuation because the actual diffraction angles are very small. For example, at a spatial frequency of 1.58 cycles per mm., corresponding to a calibrated frequency of 204 cycles per mm., the diffraction angle is  $1.58 \times .6328 \times 10^{-3} = 10^{-3}$  radians = .057 degrees. Hence, magnification offers the advantage of observing the spectrum at high spatial frequencies without exceeding the off-axis capability of most lenses. The extended spectrum shown in Fig. 7.5-2 shows that at frequencies above ~ 150 cycles/mm, the spectrum of grain noise can be approximated with high accuracy by a negative exponential. In this particular case, the high-frequency spectrum is proportional to  $\exp(-16.2 \times 10^{-3} |w|)$ .



A-006-1-00-0032

**FIG. 7.5-2 SPECTRUM OF GRANULARITY MAGNIFIED 130X  
COMPARED WITH SPECTRUM OF ORIGINAL GRANULARITY  
(KODAK 2479 DEVELOPED IN D19)**

APPENDIX A  
FILM GRAIN NOISE IN THE PRESENCE  
OF SIGNAL

This appendix represents an attempt to determine the nature of film grain noise in the presence of signal. Using the random checkerboard model (Chap. 4, Sec. 2) as a basis, it is shown that grain noise in the presence of signal cannot be considered as additive or multiplicative noise.

The transmittance fluctuation about the mean transmittance  $t_o$  is defined by

$$\tau(x,y) = t(x,y) - t_o$$

where  $t(x,y)$  is a random variable denoting the transmittance at  $(x,y)$ . It is assumed that a developed grain is opaque to light [ $t(x,y) = 0$ ] while an undeveloped grain is completely transparent [ $t(x,y) = 1$ ]. The relative phase of the transmitted light is undisturbed in passing through the medium.

The correlation function for this model is given by Eq. (4.2-2)

$$\begin{aligned}\phi_{\tau\tau}(x_1, x_2, y_1, y_2) &= \phi_{\tau\tau}(x_2 - x_1, y_2 - y_1) \\ &= t_o(1 - t_o) \left(1 - \frac{|x_2 - x_1|}{\ell}\right) \left(1 - \frac{|y_2 - y_1|}{\ell}\right) \\ &\quad |x_2 - x_1|, |y_2 - y_1| \leq \ell \\ &= 0 \quad \text{otherwise}\end{aligned}\tag{A-1}$$

Assume now that a bipolar transmittance representing the signal  $s(x,y)$  is present. If all correlation intervals and observations are restricted to the  $x$ -axis ( $y = 0$ ), then the analysis can be made conveniently one-dimensional with  $\phi_{TT}(x,0) \equiv \phi_{TT}(x)$ ,  $s(x,0) \equiv s(x)$  and  $t(x,0) \equiv t(x)$ . If the operating point is confined in the linear region of the transmittance-exposure characteristic of the film, then the ensemble average of the transmittance at  $(x,0)$  is  $s(x) + t_0$ . Denoting by  $p_{ij}$  the probability that  $t(x_1) = i$  and  $t(x_2) = j$ , it follows that

$$\phi_{TT}(x_1, x_2) \equiv \langle t(x_1) t(x_2) \rangle = \sum_0^1 \sum_0^1 ij p_{ij} = p_{11} \quad (A-2)$$

where  $\langle \rangle$  denotes ensemble average.

If  $B$  is a random variable that denotes the coordinate of the start of the cell (Fig. A-1) that contains  $x_1$  ( $x_2 \geq x_1$ ) and  $B$  is assumed uniformly distributed in the interval  $(x_1 - \ell, x_1)$ , then the distribution function of  $B$  is

$$\begin{aligned} F_B(x) &= 0 & x < x_1 - \ell \\ F_B(x) &= \frac{x}{\ell} - \frac{x_1 - \ell}{\ell} & x_1 - \ell < x < x_1 \\ F_B(x) &= 1 & x \geq x_1 \end{aligned} \quad (A-3)$$

where

$$F_B(x) = \text{Prob } \{B \leq x\}$$

Now

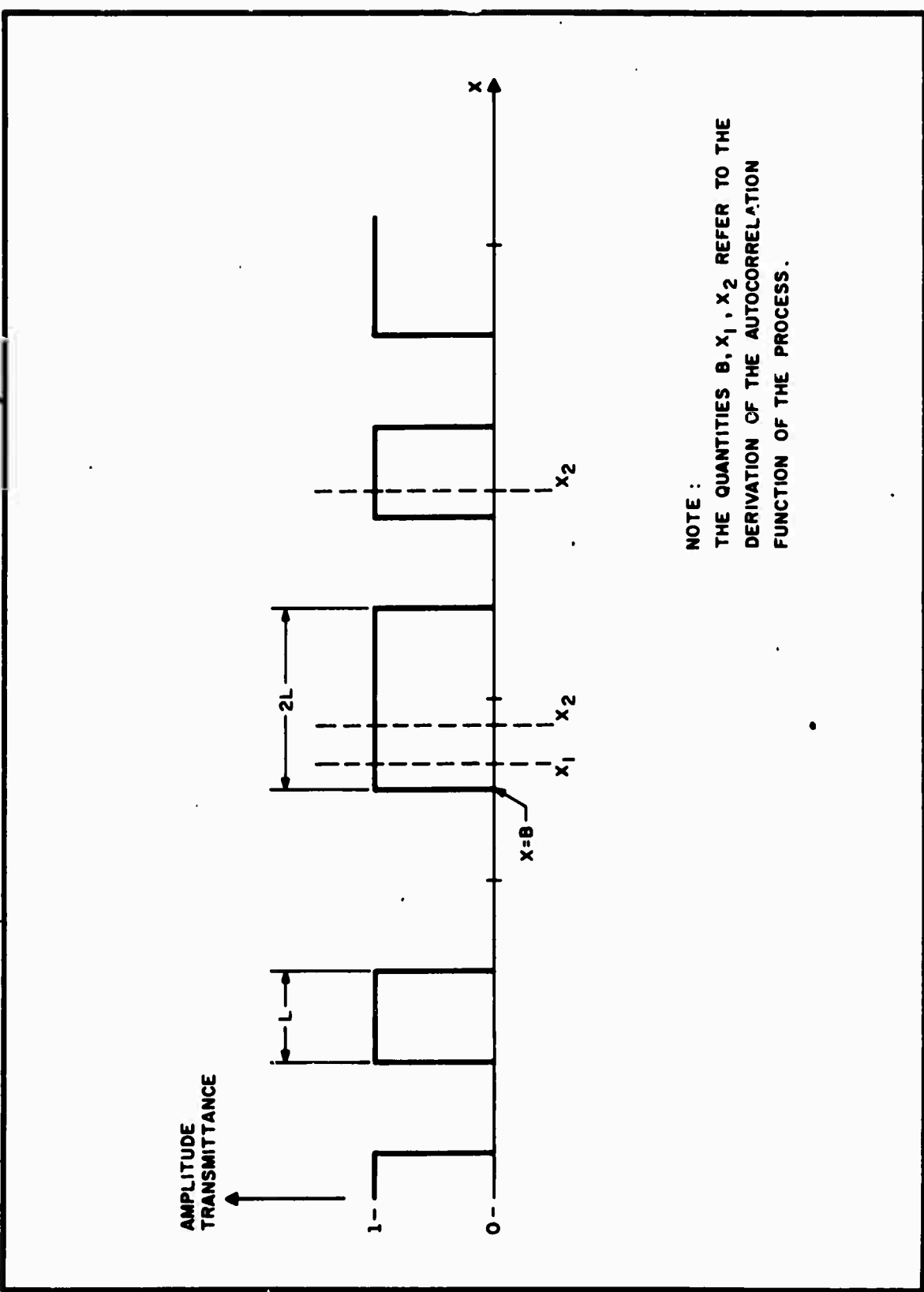


FIG. A-1 THEORETICAL POINT APERTURE MICRODENSITOMETER TRACE OF RANDOM CHECKERBOARD MODEL OF FILM GRAINS

$$\begin{aligned}
\phi_{tt}(x_1, x_2) &= \text{Prob} \left\{ t(x_2) = 1 \mid t(x_1) = 1 \right\} \cdot \text{Prob} \left\{ t(x_1) = 1 \right\} \\
&= (\text{Prob} \left\{ x_2 < B + \ell \right\} + \text{Prob} \left\{ x_2 > B + \ell \right\} \\
&\quad \cdot \text{Prob} \left\{ t(x_2) = 1 \right\}) \text{Prob} \left\{ t(x_1) = 1 \right\} \\
&= (1 - F_B(x_2 - \ell) + F_B(x_2 - \ell)(t_o + s(x_2))) \\
&\quad \cdot (t_o + s(x_1))
\end{aligned}$$

Hence from Eq. (A-3) it follows that for  $x_2 > x_1$

$$\begin{aligned}
\phi_{tt}(x_1, x_2) &= (t_o + s(x_1)) \left( 1 - \frac{x_2 - x_1}{\ell} + \frac{x_2 - x_1}{\ell} (t_o + s(x_2)) \right) \\
&\quad 0 < x_2 - x_1 \leq \ell \\
&= (t_o + s(x_1)) (t_o + s(x_2)) \quad x_2 - x_1 > \ell
\end{aligned} \tag{A-4}$$

The autocorrelation function for both cases,  $x_2 > x_1$  and  $x_2 < x_1$ , can be conveniently written as

$$\begin{aligned}
\phi_{tt}(x_1, x_2) &= \left( t_o + s(\min(x_1, x_2)) \right) \left( 1 - \frac{|x_2 - x_1|}{\ell} \right. \\
&\quad \left. + \frac{|x_2 - x_1|}{\ell} (t_o + s(\max(x_1, x_2))) \right) \\
&\quad |x_2 - x_1| \leq \ell \\
&= (t_c + s(x_1)) (t_o + s(x_2)) \quad |x_2 - x_1| > \ell
\end{aligned} \tag{A-5}$$

Consider now the following mathematical model which includes both additive and multiplicative noise in a representation of transmittance in the presence of signal:

$$t'(x) = t_0 + s(x) + \mu\tau(x) + \lambda s(x)\tau'(x) \quad (A-6)$$

where  $\mu$  and  $\lambda$  are adjustable constants and  $\tau(x)$  and  $\tau'(x)$  are zero-mean signal-uncorrelated additive and multiplicative noise components respectively. Then

$$\langle t'(x) \rangle = t_0 + s(x) \quad (A-7)$$

$$\begin{aligned} \phi_{tt'} &= t_0^2 + t_0(s(x_1) + s(x_2)) + s(x_1)s(x_2) \\ &\quad + \mu^2\phi_{\tau\tau}(x_1, x_2) + \mu\lambda\phi_{\tau'\tau}(x_1, x_2)s(x_1) \\ &\quad + \mu\lambda s(x_2)\phi_{\tau\tau}(x_1, x_2) + \lambda^2 s(x_1)s(x_2)\phi_{\tau'\tau'}(x_1, x_2) \end{aligned} \quad (A-8)$$

where

$$\phi_{\tau\tau}(x_1, x_2) = \langle \tau(x_1) \tau(x_2) \rangle$$

$$\phi_{\tau\tau'}(x_1, x_2) = \langle \tau(x_1) \tau'(x_2) \rangle$$

$$\phi_{\tau'\tau'}(x_1, x_2) = \langle \tau'(x_1) \tau'(x_2) \rangle$$

In order for  $\phi_{tt}(x_1, x_2)$  of Eq. (A-5) to be the correlation function for the process  $t'(x)$ , it is required to find a set of values for  $\mu$  and  $\lambda$  such that  $\phi_{tt}(x_1, x_2) = \phi_{tt'}(x_1, x_2)$ . In looking for such numbers, the following restrictions that apply to  $t'(x)$  must not be violated:

- (i)  $t'(x)$  must be real
- (ii)  $\phi_{\tau' \tau'}(0,0) > 0$
- (iii)  $\phi_{\tau \tau}(x_1, x_2) = t_o(1 - t_o) \left( 1 - \frac{|x_2 - x_1|}{\lambda} \right)$

Restrictions (i) - (iii) preclude finding real values of  $\alpha$  and  $\lambda$  such that  $\phi_{tt}(x_1, x_2) = \phi_{t't'}(x_1, x_2)$ . For example in attempting to equate Eq. (A-8) with Eq. (A-4), it is found that  $\lambda^2 = -1$ , thus violating (i). Hence to the extent that the random checkerboard model represents film granularity, film-grain noise cannot be resolved into signal-uncorrelated independent additive and multiplicative noise processes.

APPENDIX B  
SUPPRESSION OF THE ZERO-ORDER  
LIGHT AT DC

The contoured apertures discussed in Sec. 6.4 are not adequate for measuring the power spectrum at zero spatial frequency because their diffraction patterns do not have nulls at the origin. A diffraction pattern with a null at DC can be obtained with an aperture function of odd symmetry along one or more axes. For example, consider a one-dimensional system with odd aperture function  $g(x)$ . Let the aperture width be  $D$ . Then the diffraction amplitude is proportional to

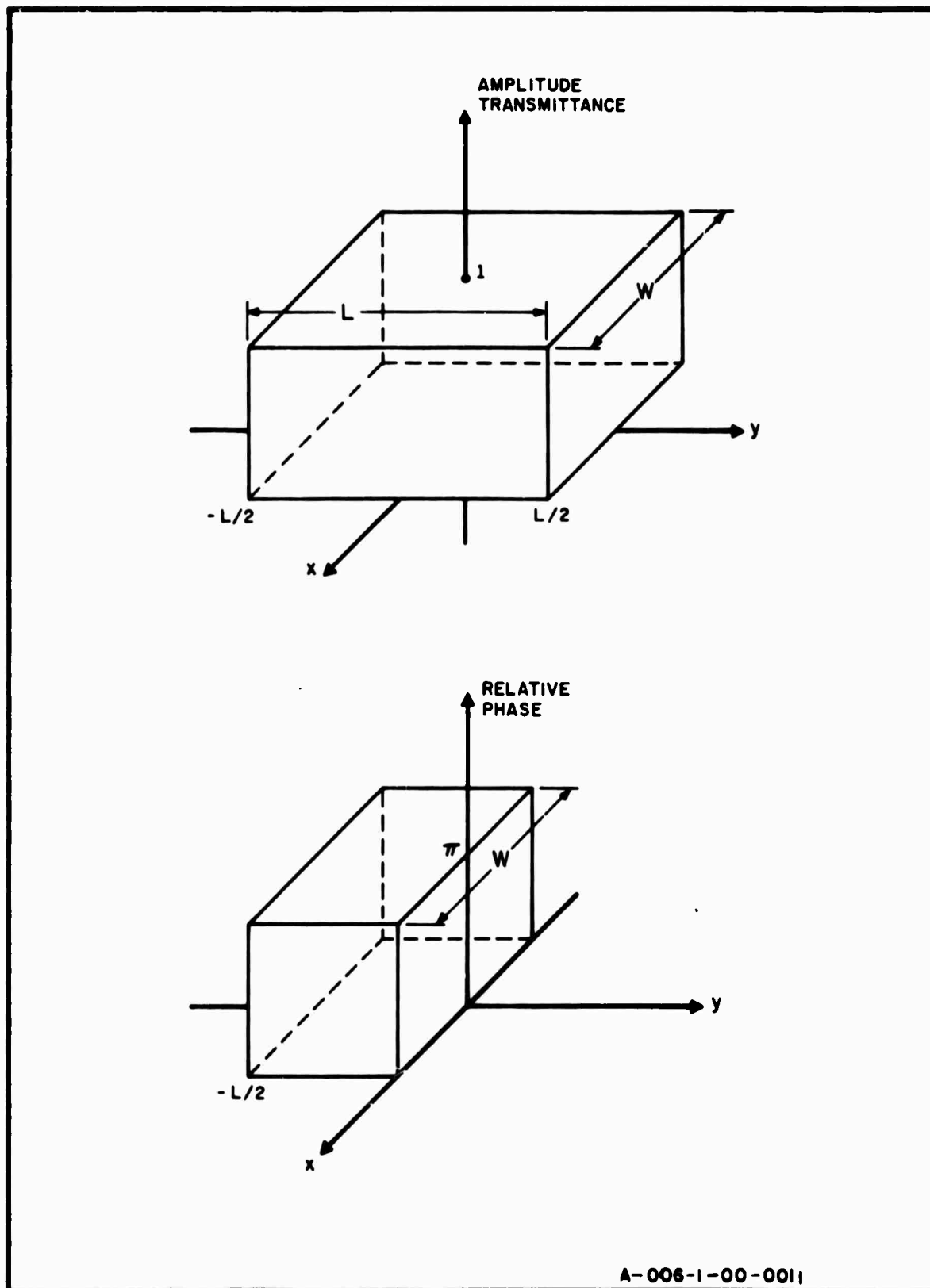
$$E(u) = \int_{-D/2}^{D/2} g(x) e^{-j2\pi ux} dx = -j \int_{-D/2}^{D/2} g(x) \sin 2\pi ux dx \quad (B-1)$$

which is zero at the origin.

One of the simplest aperture functions which has this property is the half-wave plate shown in Fig. B-1. The half-wave plate is a one-cycle phase grating and produces a relative diffraction intensity given by

$$H_H(u,v) = LW \operatorname{sinc}^2 \frac{uL}{2} \operatorname{sinc}^2 vw \sin^2 \frac{\pi uL}{2} \quad (B-2)$$

which is shown in Fig. B-2. The sidelobe response is shown in Fig. B-3. When the half-wave plate is used in spectral density measurements, there is a loss in resolution in the measurement of the spectrum along the frequency axis parallel to the direction of the phase grating. However, the loss of resolution will generally not be serious enough to affect the measurement of ordinary film noise.



A-006-1-00-0011

FIG. B-1 HALF-WAVE RETARDATION PLATE : AMPLITUDE AND PHASE CHARACTERISTICS

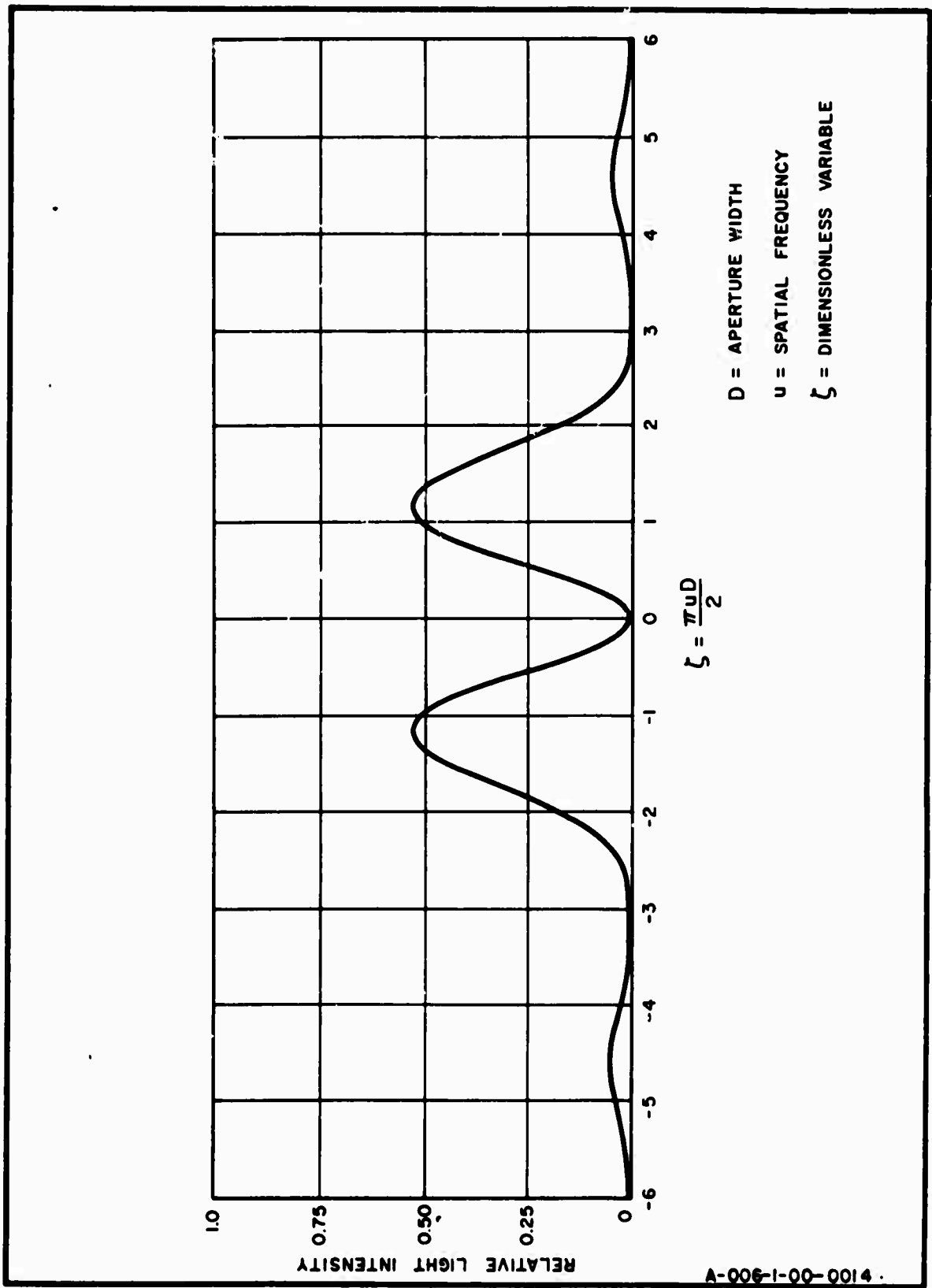


FIG. B-2 DIFFRACTION PATTERN OF HALF-WAVE RETARDATION PLATE.  
(THEORETICAL)

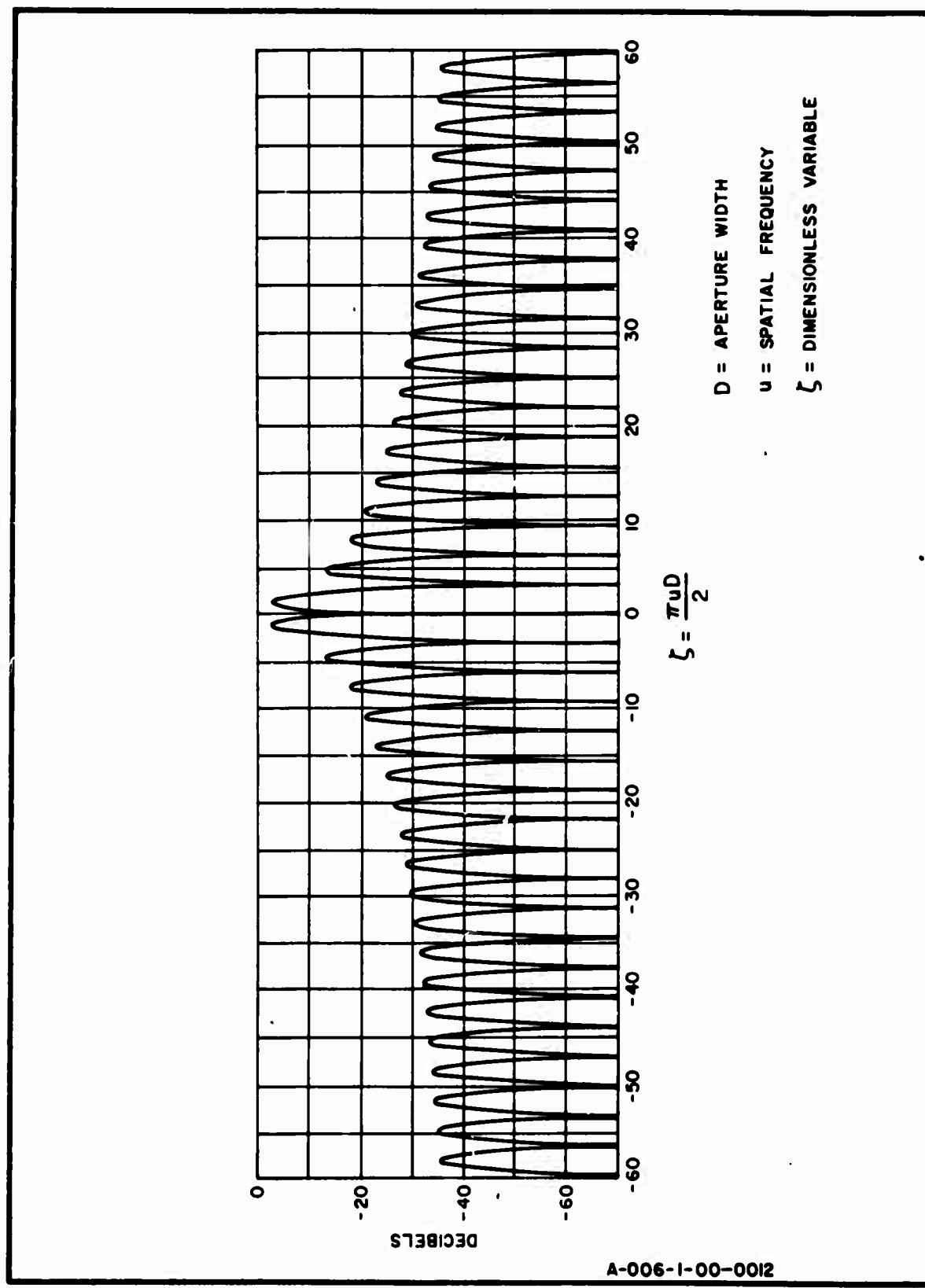


FIG. B-3 LOG DIFFRACTION PATTERN OF HALF-WAVE RETARDATION PLATE.  
(THEORETICAL.)

When the half-wave plate is used, the apparent spectrum  $\tilde{w}(u, v)$  is given by

$$\begin{aligned}
 \tilde{w}(u, v) = & \frac{1}{LW} \int_{-W/2}^{W/2} \int_{-W/2}^{W/2} dy d\eta \int_0^{L/2} \int_0^{L/2} f(x-\xi, y-\eta, u, v) dx d\xi \\
 & + \int_{-L/2}^0 \int_{-L/2}^0 f(x-\xi, y-\eta, u, v) dx d\xi \\
 & - \int_{-L/2}^0 \int_0^{L/2} f(x-\xi, y-\eta, u, v) dx d\xi \\
 & - \int_0^{L/2} \int_{-L/2}^0 f(x-\xi, y-\eta, u, v) dx d\xi
 \end{aligned} \tag{B-3}$$

where

$$f(x-\xi, y-\eta, u, v) \equiv h(x-\xi, y-\eta) e^{-j2\pi[u(x-\xi) + v(y-\eta)]}.$$

With the transformation

$$\begin{aligned}
 \alpha &= x-\xi \\
 \beta &= y-\eta \\
 \gamma &= x \\
 \delta &= y
 \end{aligned}$$

Eq. (B-3) may be written as

$$\tilde{w}(u, v) = \int_{-\infty}^{\infty} \int_{-\infty}^{\infty} \phi(\alpha, \beta) h_H(\alpha, \beta) e^{-j2\pi(u\alpha+v\beta)} d\alpha d\beta \tag{B-4}$$

where  $h_H(\alpha, \beta) = h_H(\alpha, 0) h_H(0, \beta)$  and is shown in Fig. B-4. From Eq. (B-4), the apparent covariance  $\tilde{\phi}(\alpha, \beta)$  is

$$\tilde{\phi}(\alpha, \beta) = h_H(\alpha, \beta) \phi(\alpha, \beta) \tag{B-5}$$

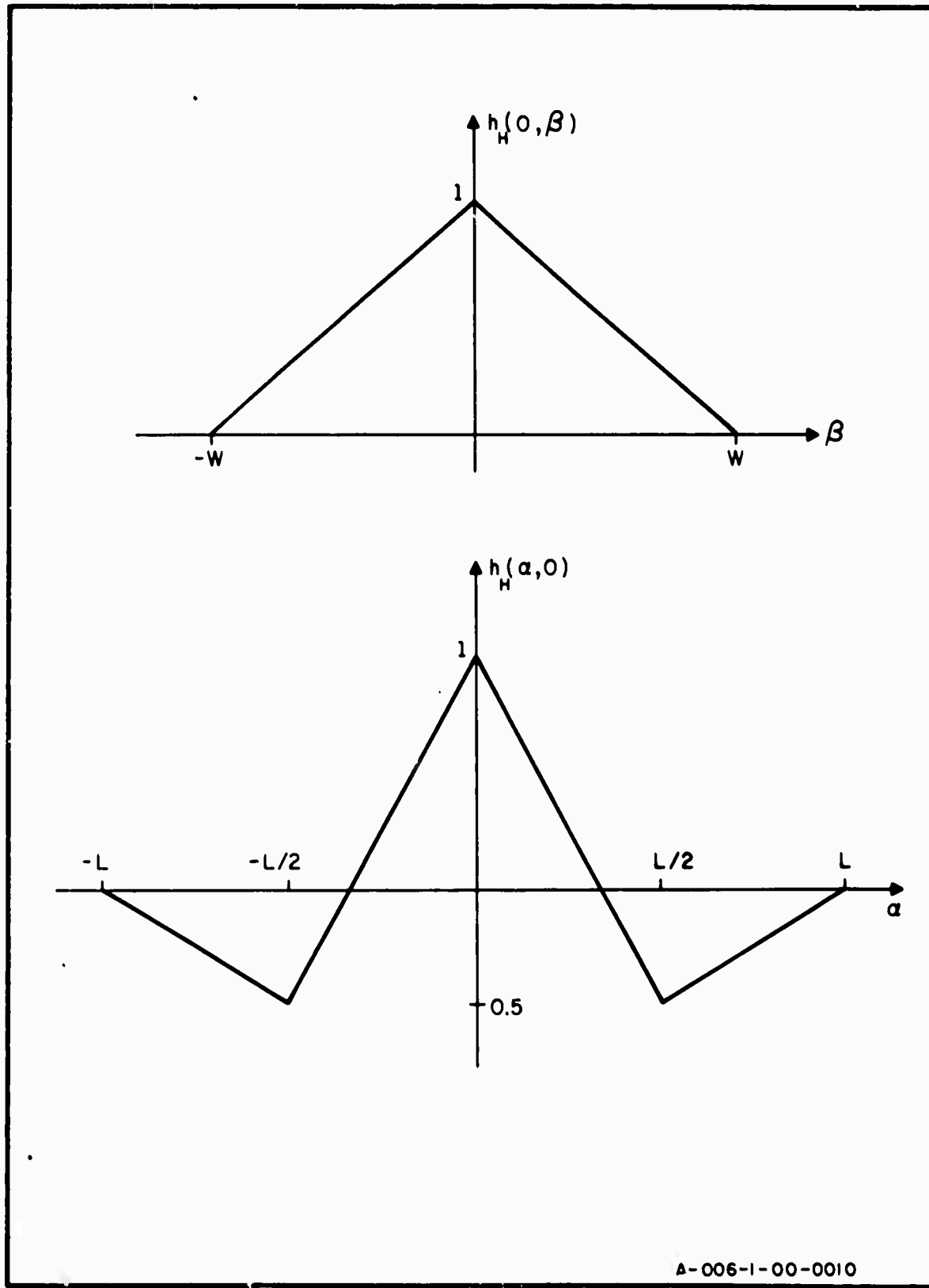


FIG. B-4 SELF-CORRELATION FUNCTION OF HALF-WAVE PLATE OF AREA  
 $A = LW$ .

where  $\hat{C}(\alpha, \beta)$  is the true covariance of the process. It is evident that for a square aperture with side  $D$ , there will be greater distortion of the covariance for correlation intervals in the direction of the phase grating, due to the steeper slope and phase reversal property of  $h_H(\alpha, 0)$ . This distortion, when viewed in the frequency domain, is equivalent to averaging  $w(\xi, \eta)$  over frequency with weights proportional to  $H_H(u-\xi, v-\eta) = D^2 \text{sinc}^2(u-\xi)D/2 \text{sinc}^2(v-\eta)D \sin^2 \pi(u-\xi)D/2$ . Observe that the weight given to  $w(\xi, \eta)$  at  $\xi = u$  is zero, which is quite the opposite of what the ideal aperture, which would give infinite weight, would do. The significant averaging over frequency extends over the two lobes on either side of  $\xi = u$  which furnish a null-to-null width in frequency of  $4D^{-1}$ . For an ordinary rectangular aperture of the same width, the significant averaging over frequency is restricted to the main lobe of the diffraction pattern which has a null-to-null width of  $2D^{-1}$ .

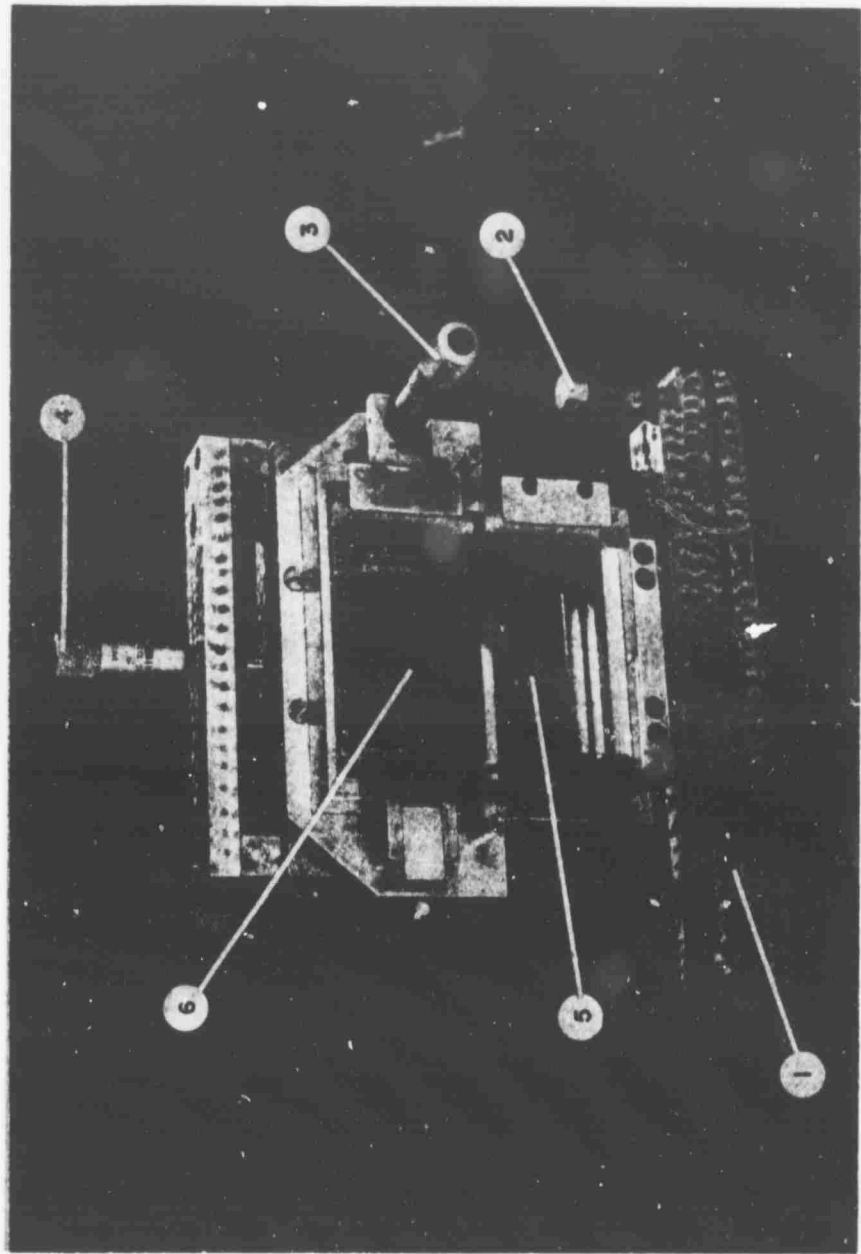
The loss of resolution inherent with the use of the half-wave plate is not serious provided that  $D/2$  is much larger than the largest significant correlation interval of interest. In the measurement of ordinary film noise, the correlation intervals are, at most, of the order of hundreds of microns while  $D$  may be several centimeters.

From a theoretical viewpoint, the half-wave plate is a solution to the problem of zero-order elimination at the origin. However, from a practical viewpoint there are very serious design problems to overcome. For example, if the phase difference is accomplished by using clear glass plates of different thicknesses, the required thickness difference between the two halves is  $\lambda/2(n-1)$  which, for  $\lambda = 6328 \text{ \AA}$  and a typical value of  $n = 1.6$ , is  $\sim 5.2 \times 10^{-4} \text{ mm}$  - a value difficult to maintain to high tolerance over a large area. The tolerance and parallelism requirements to achieve a deep null are very severe. Even if such a null were furnished there would remain the difficulty of measuring

$\tilde{W}(0,0)$  with a very narrow pinhole or slit in order not to lose the null by averaging over the sides of the adjacent zero-order lobes. That is, the width of the slit must be confined to frequencies for which the zero-order light is essentially insignificant compared with the power spectrum. Only in this way will the null be preserved. However, this leads to a third problem: Since the averaging effect of the slit is confined to a very narrow band of frequencies, the estimate of the power spectrum will be inherently unreliable because of very little smoothing over frequency. Smoothing could be improved by increasing the length of the slit, but this would cause loss of resolution.

An interesting technique for achieving the required phase shift between the two halves of the aperture while avoiding the problems associated with the use of plates of different thicknesses is to use two plates of equal thickness (i.e., a single plate cut in two) and then rotate one plate with respect to the other. Such a device was built in the laboratory specifically for zero-order cancellation in power spectra measurements and is shown in Fig. B-5. The principle of operation can be explained as follows. The lower plate is fixed and positioned for normal incidence. Rotation of the upper plate about an axis orthogonal to the optic axis changes the angle of incidence for the collimated beam and hence the optical path length. It is not hard to show that in order to obtain a  $180^\circ$  phase difference between the waves of the upper and lower plates, the upper plate must be rotated through an angle  $\theta$  where  $\theta$  can be obtained from

$$\frac{\lambda}{2d} = \frac{n - \cos(\theta - \theta')}{\cos \theta'} - n+1$$



1. Mount
2. Tilt Control
3. Optical Path Length Control
4. Vertical Control
5. Fixed Plate
6. Movable Plate

Fig. B-5 Laboratory Built Half-Wave Phase Grating

where       $\alpha' = \sin^{-1} \left( \frac{\sin \theta}{n} \right)$   
 n = refractive index of the glass plate  
 d = thickness of the plate  
 $\lambda$  = wavelength of radiation

When the angles are small, as they usually are,  $\sin \theta \approx \theta$ ,  $\cos \theta \approx 1 - \theta^2/2!$  so that

$$\theta = \left( \frac{\lambda}{d(n-1)} \right)^{\frac{1}{2}} n \quad (B-6)$$

For the grating used,  $d = 1.8$  cm,  $n = 1.515$  and  $\theta \approx 0.7$  deg. This order of sensitivity was easily controlled with a micrometer as shown.

The diffraction pattern furnished by the actual half-wave plate (Fig. B-6) corresponded closely to the theoretical diffraction pattern shown in Fig. B-2. The two-dimensional diffraction pattern was observed in the Fourier plane and recorded on film through the use of a microscope objective which imaged the magnified diffraction pattern on the back-plate of a camera. Figures B-7 and B-8 show the diffraction patterns for square and diamond apertures; the null at the center is clearly visible and its orientation can be seen to be unaffected by a rotation of the aperture. The orientation of the null depends only on the positioning of the glass plates in the collimated region.

To obtain the DC value of the spectrum from the diffraction pattern furnished by the half-wave plate, it is not possible to use the formula given in Eq. (6.2-10) because in the present case the slit is not used to smooth the zero-order light; in fact, in order to take advantage of the null at the origin, the equivalent bandwidth of the slit in the direction parallel to scan must be much smaller than  $2(\pi D)^{-1}$  where D is the length of a side of the square aperture. In other words the slit is required to distort the diffraction pattern as little as possible.

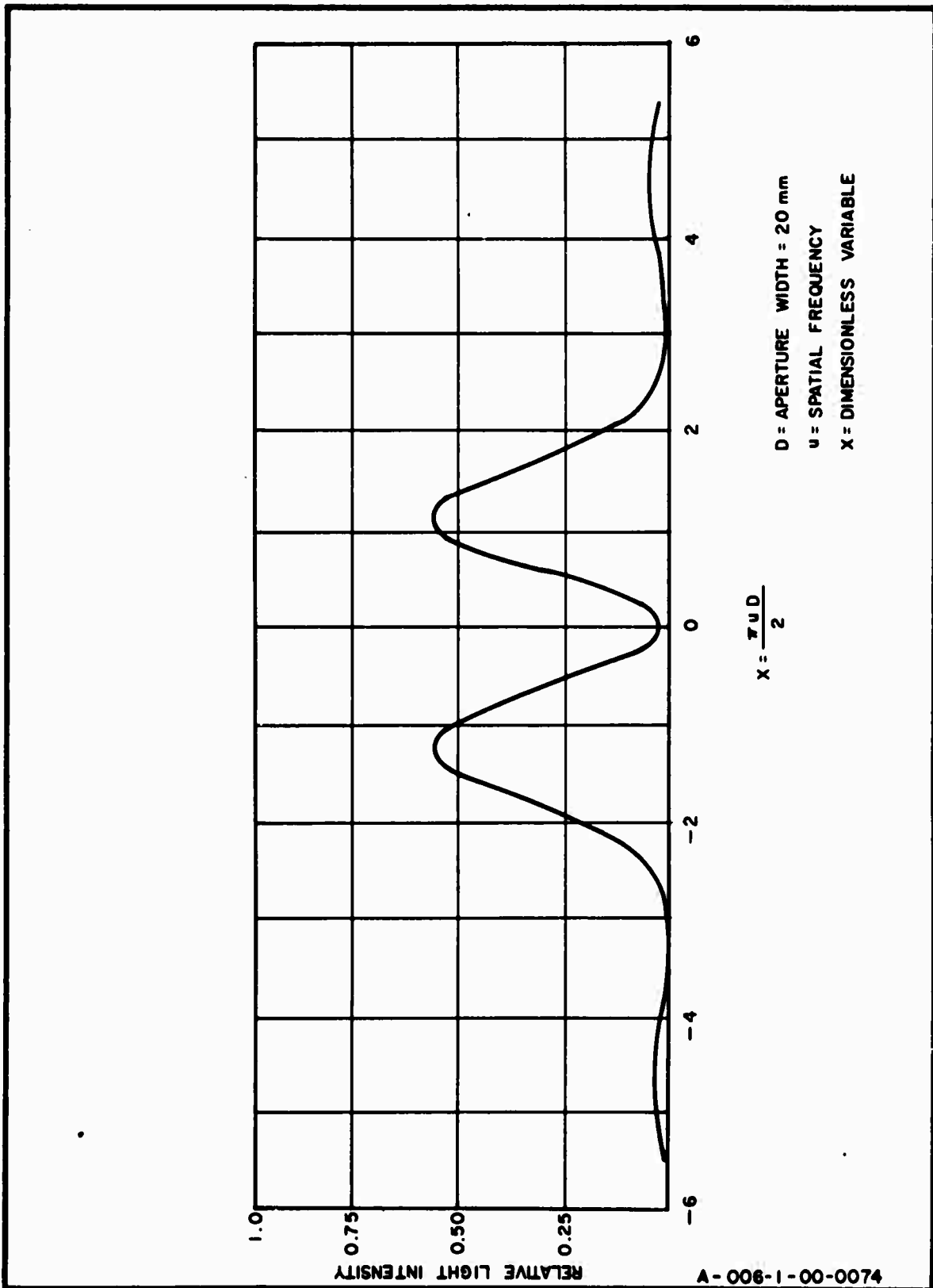
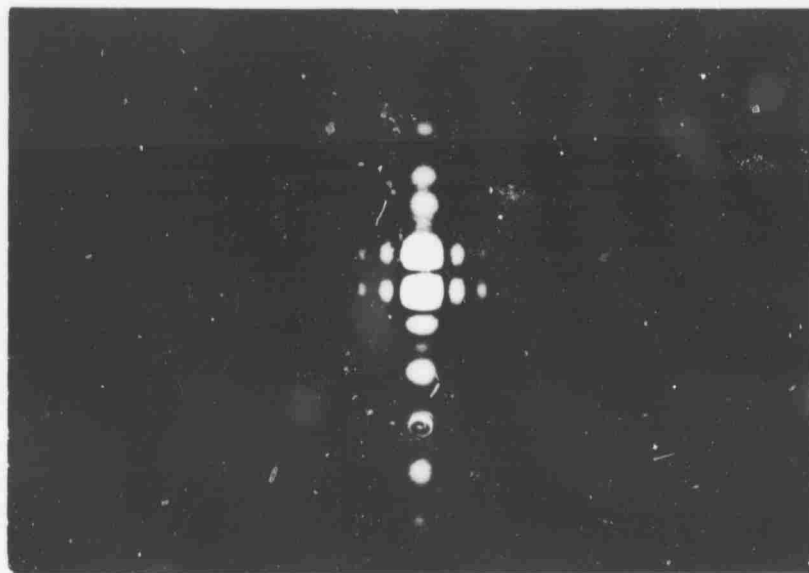


FIG. B-6 EXPERIMENTALLY OBTAINED DIFFRACTION PATTERN OF HALF-WAVE PLATE (COMPARE WITH FIG. B-2)

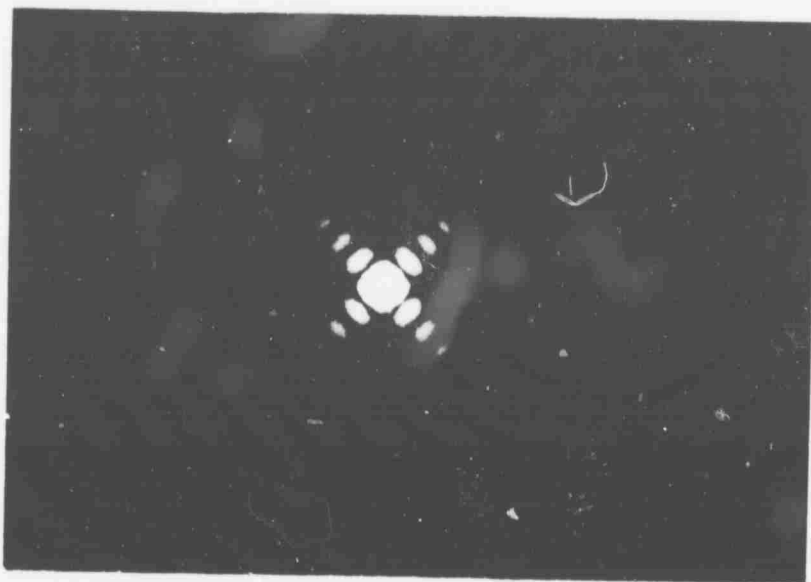


- A) Diffraction Pattern of  $10 \times 10 \text{ mm}^2$  Square Aperture.  
Width of Main Lobe is 127 Microns. Diffraction Pattern Corresponds to  $\text{sinc}^2 uD \text{ sinc}^2 vD$ .

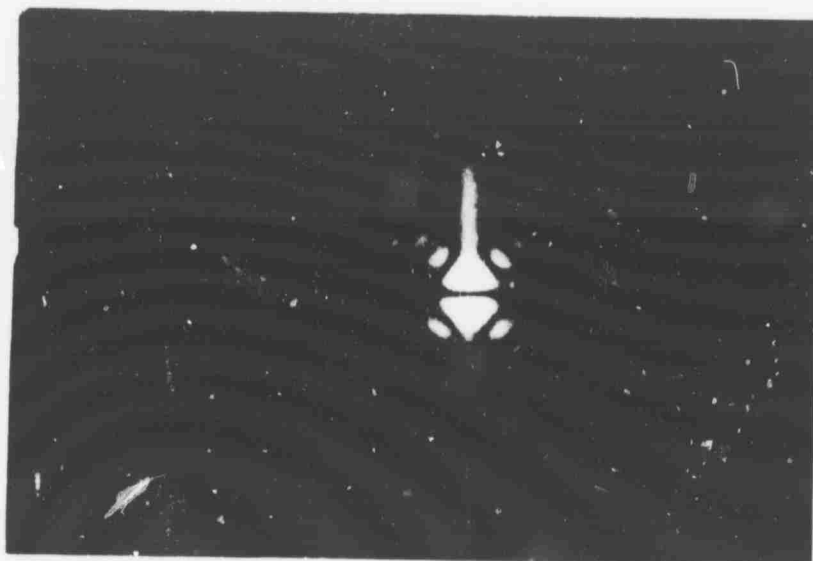


- B) Diffraction Pattern of  $10 \times 10 \text{ mm}^2$  Square Aperture.  
Width of Main Lobe is 127 Microns. Diffraction Pattern Corresponds to  $\text{sinc}^2 uD \text{ sinc}^2 vD$  with Phase Grating in Place. Null is Clearly Seen at Center.

Fig. B-7 Fourier Plane Photographs Illustrating Use of Phase Grating with a Square Aperture



A) Diffraction Pattern of  $10 \times 10 \text{ mm}^2$   
Diamond Aperture



B) Diffraction Pattern of  $10 \times 10 \text{ mm}^2$   
Diamond Aperture with Phase Grating  
in Place.

Fig. B-8 Fourier Plane Photographs Illustrating  
Use of Phase Grating with a Diamond  
Aperture

The calibration technique for extracting the DC value of the spectrum can be derived as follows.

From Eqs. (B-2) and (6.2-5). the x-y recorder when operating in the log mode will produce a record  $R_1$  given by

$$R_1 = 10 \log (\lambda f)^2 A_s^{-1} H_H(u,v) * g(u,v) \quad (B-7)$$

where

$$\lambda = 6328 \text{ \AA}$$

$f$  = focal length of lens

$A_s$  = slit area

$H_H(u,v)$  is given by Eq. (B-2)

$g(u,v)$  is given by Eq. (3.6-6),

when the system is devoid of film. When the film sample is placed in the collimated region, the recorder will then produce a record,  $R_2$ , given by

$$R_2 = 10 \log (\lambda f)^2 A_s^{-1} g(u,v) * \left( t_o^2 H_H(u,v) + \tilde{w}_\tau(u,v) \right)$$

where  $\tilde{w}_\tau(u,v)$  is the apparent spectrum. If the y axis of the recorder is displaced by an amount  $K$  so that the two records are made to coincide at the peaks of the diffraction patterns (i.e.,  $v = 0$   $u \approx .75^{-1} \equiv u_o$ ), then the mathematical equivalent of this procedure can be written as

$$\begin{aligned} & 10 \log (\lambda f)^2 A_s^{-1} g(u,v) * \left[ t_o^2 H_H(u,v) + w_\tau(u,v) \right] + K \\ &= 10 \log (\lambda f)^2 A_s^{-1} H_H(u,v) * g(u,v) \quad \left| \begin{array}{l} u = u_o \\ v = 0 \end{array} \right. \end{aligned}$$

Except when  $t_o^2$  is much smaller than unity it can be assumed with little error that

$$t_o^2 H_H(u, v) * g(u, v) \gg w_\tau(u, v) * g(u, v) \quad \left| \begin{array}{l} u = u_o \\ v = 0 \end{array} \right. \quad (B-8)$$

so that to a good approximation  $K = \log t_o^{-2}$ . Hence superposing the two diffraction patterns is equivalent to compensating for the nonzero density of the film. If the film were noiseless, the compensation for  $t_o^2$  would enable the two diffraction patterns to overlap completely. When there is no overlap, the difference between the diffraction patterns after compensation is a measure of the film noise.

Assume that at the origin there exists a displacement  $\Delta$  between the two records. Then  $\Delta$  is given by

$$\Delta = 10 \log (\lambda f)^2 A_s^{-1} g(u, v) * \left( H_H(u, v) + t_o^{-2} w_\tau(u, v) \right) - 10 \log (\lambda f)^2 A_s^{-1} g(u, v) H_H(u, v) * g(u, v) \quad \left| \begin{array}{l} u = 0 \\ v = 0 \end{array} \right. \quad (B-8)$$

If the slit is properly chosen and the aperture is sufficiently large, then to a good approximation

$$\frac{(\lambda f)^2}{A_s} \tilde{w}_\tau(u, v) * g(u, v) \quad \left| \begin{array}{l} u = 0 \\ v = 0 \end{array} \right. \approx \tilde{w}_\tau(0, 0)$$

and, from Eq. (B-8)

$$w_\tau(0, 0) \approx \frac{t_o^2 (\lambda f)^2}{A_s} \left( 10^{\frac{\Delta}{10}} - 1 \right) H_H(u, v) * g(u, v) \quad \left| \begin{array}{l} u = 0 \\ v = 0 \end{array} \right. \quad (B-9)$$

If the slit is rectangular with area  $A_s = \ell d$  with  $\ell \gg (\lambda f)(\pi D)^{-1}$  and  $\ell \gg d$ , then

$$H(u, v) * g(u, v) \Big|_{\begin{array}{l} u=0 \\ v=0 \end{array}} = \frac{d}{2\lambda f} \int_{-\frac{d}{2\lambda f}}^{\frac{d}{2\lambda f}} \sin c^2 \frac{\xi D}{2} \sin^2 \frac{\pi \xi D}{2} d\xi \int_{-\frac{l}{2\lambda f}}^{\frac{l}{2\lambda f}} \sin c^2 \eta D d\eta \approx \frac{2}{\pi} \Psi \left( \frac{\pi Dd}{4\lambda f} \right)$$

where

$$\Psi(N) = \int_{-N}^N \frac{\sin^4 \theta}{\theta^2} d\theta \quad (\text{see Table B-1}).$$

Hence, Eq. (B-9) may be written as

$$w_\tau(0,0) \approx \frac{t_o^2(\lambda f)^2}{A_s} \left( 10^{\frac{\Delta}{10}} - 1 \right) \frac{2}{\pi} \Psi \left( \frac{\pi Dd}{4\lambda f} \right) \quad (\text{B-10})$$

The procedure and theory discussed above was applied to measuring the spectrum of Kodak 2479 film developed in D-19. The parameters of the system and film were:  $t_o^2 = 0.31$ ,  $f = 1 \text{ m}$ ,  $\lambda = 6328 \text{ \AA}$ , aperture  $D = 30 \text{ mm}$ , and slit length  $l = 1 \text{ mm}$ . The nominal slit width  $d$  was  $1 \mu$  but an experiment\* indicated  $d = 1.5 \mu$  was more likely. Also the diffraction pattern of the real half-wave plate was not quite as given by Eq. (B-2) because there existed a narrow obscuration between the plates whose effect was to furnish a pattern described by

$$H_H(u, v) = (D-\delta)^2 \operatorname{sinc}^2 \frac{u}{2}(D-\delta) \sin^2 \frac{\pi u}{2}(D+\delta)$$

---

\* The ratio of the zero-order peak-to-null in the absence of film was 27 db. This number is a function of the slit width, which in this case would have to be  $1.5 \mu$ . A  $1 \mu$  slit would furnish a 30-db peak-to-null ratio.

TABLE B-1

| <u>N</u>      | <u><math>\psi(N)</math></u> |
|---------------|-----------------------------|
| .30000000,-01 | .17993507,-04               |
| .31000000,-01 | .19853020,-04               |
| .32000000,-01 | .21836373,-04               |
| .33000000,-01 | .23947545,-04               |
| .34000000,-01 | .26190530,-04               |
| .35000000,-01 | .28569305,-04               |
| .36000000,-01 | .31087852,-04               |
| .37000000,-01 | .33750140,-04               |
| .38000000,-01 | .36560176,-04               |
| .39000000,-01 | .39521900,-04               |
| .40000000,-01 | .42639320,-04               |
| .41000000,-01 | .45916393,-04               |
| .42000000,-01 | .49357103,-04               |
| .43000000,-01 | .52965413,-04               |
| .44000000,-01 | .56745300,-04               |
| .45000000,-01 | .60700680,-04               |
| .46000000,-01 | .64835643,-04               |
| .47000000,-01 | .69154053,-04               |
| .48000000,-01 | .73659946,-04               |
| .49000000,-01 | .78357220,-04               |
| .50000000,-01 | .83249880,-04               |
| .51000000,-01 | .88341903,-04               |
| .52000000,-01 | .93637163,-04               |
| .53000000,-01 | .99139700,-04               |
| .54000000,-01 | .10485346,-03               |
| .55000000,-01 | .11078234,-03               |
| .56000000,-01 | .11693036,-03               |
| .57000000,-01 | .12330144,-03               |
| .58000000,-01 | .12989956,-03               |
| .59000000,-01 | .13672862,-03               |
| .60000000,-01 | .14379257,-03               |
| .61000000,-01 | .15109540,-03               |
| .62000000,-01 | .15864102,-03               |
| .63000000,-01 | .16643335,-03               |
| .64000000,-01 | .17447638,-03               |
| .65000000,-01 | .18277393,-03               |
| .66000000,-01 | .19133011,-03               |
| .67000000,-01 | .20014872,-03               |
| .68000000,-01 | .20923375,-03               |
| .69000000,-01 | .21858908,-03               |
| .70000000,-01 | .22821867,-03               |

With  $D = 30$  mm and  $\delta$  measured as 0.6 mm, the effect of the obscuration on the null of the diffraction pattern was negligible.

The experimental results (see Fig. B-9) yielded a value of  $w_T(0,0)$  which was much larger than the extrapolated grain noise spectra of Sec. 7.3. The increase was sufficiently large to cause serious doubt as to whether the experimental technique did indeed furnish the DC value of the grain-noise spectrum. The results raised the suspicion that despite the careful attempts to reduce the phase noise with a liquid of matching refractive index, the residual phase noise at the origin played a dominant role. To test this assertion, a sample of 2479 film was developed under identical circumstances except for being bleached\*, and tested for noise at DC. The grain noise of bleached film is negligible, and any significant noise observed at the origin must be attributed to phase noise. The results are shown in Fig. B-10 and strongly imply that the grain noise at the origin cannot be measured in the presence of the residual phase noise of the film.

The results of Sec. 7.4 demonstrated that the noise associated with the random phases of film was a peaked, low-frequency process. The use of a liquid gate is an effective means of eliminating most of the phase noise except for variations in the refractive index of the gelatin which, it seems, cannot be disregarded when attempting a grain-noise measurement of the origin. The results of Figs. B-9 and B-10 demonstrated that the grain noise must indeed be very small, as witnessed by the insignificant change in  $\Delta$  under circumstances that either include or negate the granularity. The measurement of grain noise at the origin requires a technique by which the phase noise is rendered insignificant. Under such circumstances,

---

\* A process that removes the exposed silver grains in the emulsion, thus in effect rendering the film transparent and grain-free.

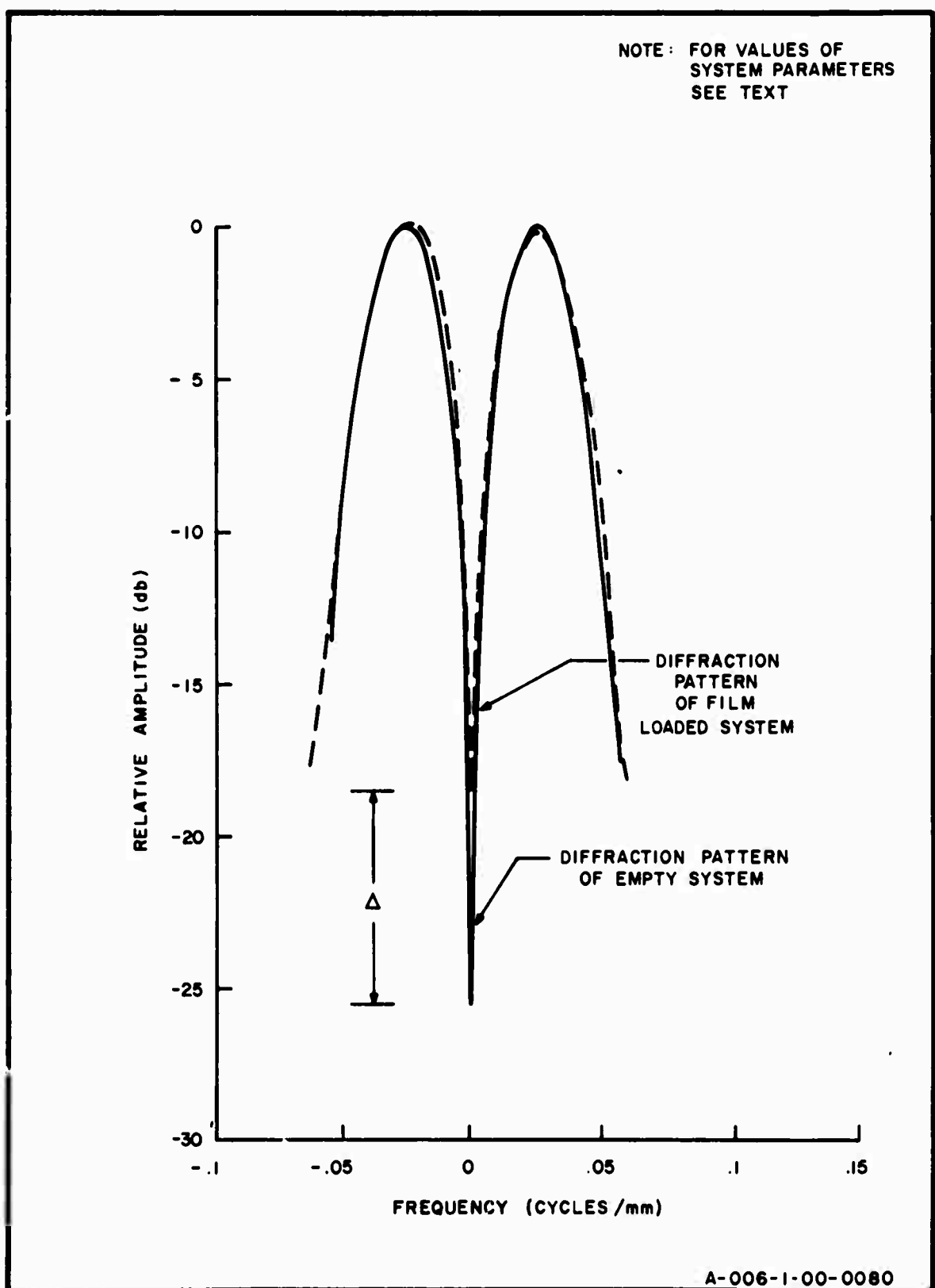
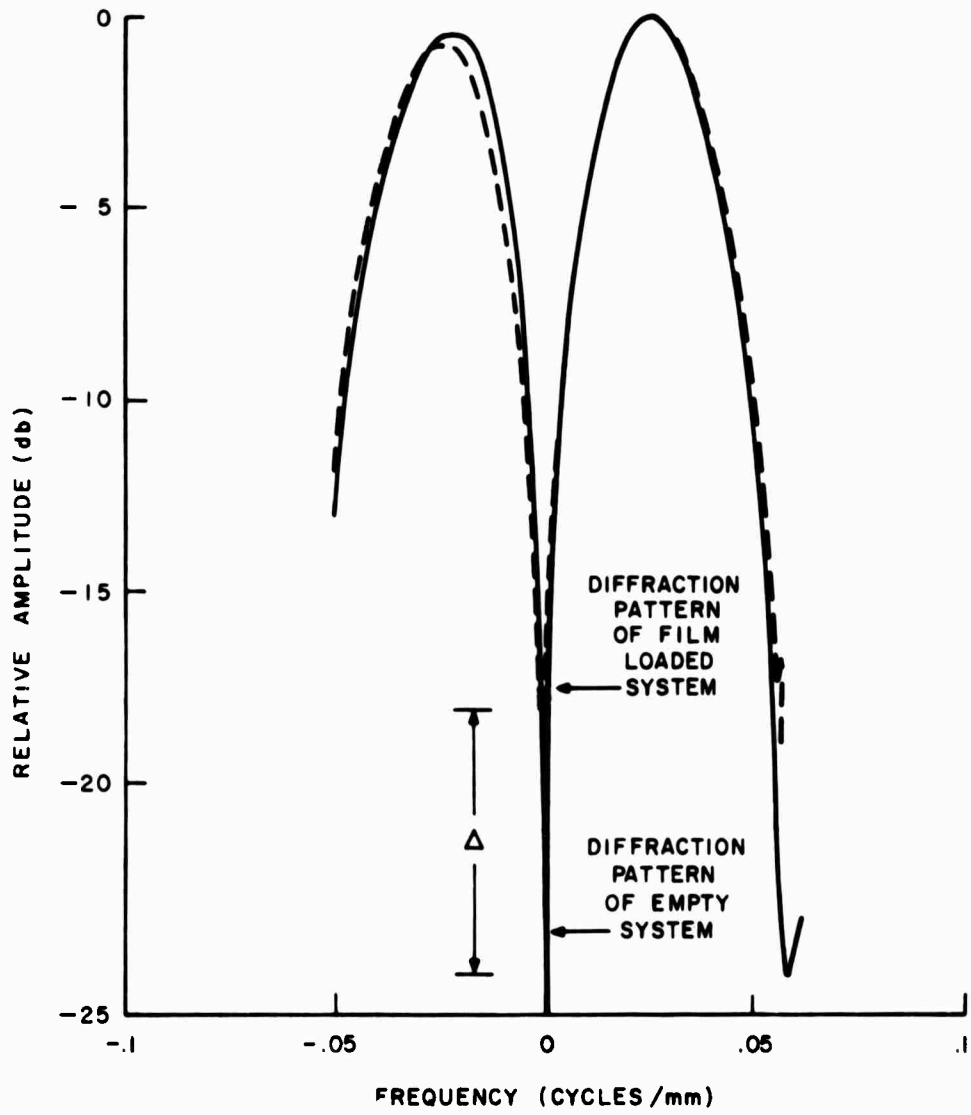


FIG. B-9 MEASUREMENT OF NOISE AT ORIGIN OF KODAK 2479  
DEVELOPED IN D-19

NOTE: FOR VALUES OF  
SYSTEM PARAMETERS  
SEE TEXT.



A-006-1-00-0079

FIG. B-10 MEASUREMENT OF FILM NOISE AT ORIGIN OF BLEACHED KODAK 2479

the half-wave plate could be used to advantage for the measurement of spectra in the presence of a zero-order light that is several orders of magnitude above the spectra to be measured. The excellent correspondence between the theoretical and actual performances of the half-wave plate establishes it as a valuable tool for spectral analysis.

## REFERENCES

- Blackman, R.B., and Tukey, J.W., The Measurement of Power Spectra, Dover, New York, 1958.
- Born, M., and Wolf, E., Principles of Optics, Pergamon Press, New York, 1964.
- Burckhardt, C.B., "Storage Capacity of an Optically Formed Spatial Filter for Character Recognition," Applied Optics, Vol. 6, August 1967.
- Couder, A., and Jacquinot, P., Comptes Rendus, Vol. 208, p.1639.
- Cutrona, L.J., et al., "Optical Data Processing and Filtering Systems," IRE Trans. on Information Theory, Vol. IT-6, 1960, pp. 386-400.
- Doerner, E.C., "Wiener-Spectrum Analysis of Photographic Granularity," J. Opt. Soc. Am., Vol. 52, 1962.
- Dolph, C.L., "A Current Distribution for Broadside Arrays which Optimizes the Relationship Between Beam Width and Sidelobe Level," Proc. IRE, 34, pp. 225-348, 1946.
- Felgett, P.B., "Concerning Photographic Grain, Signal-to-Noise Ratio and Information," J. Opt. Soc. Am., Vol. 43, 1953.
- Fry, G.F., "Coarseness of Photographic Grain," J. Opt. Soc. Am., Vol. 53, March 1963.
- Gabor, D., "A New Microscopic Principle" Nature, No. 4098, May 1948.
- Gabor, D., "Microscopy by Reconstructed Wave Fronts," Proc. Phys. Soc., Vol. 64, June 1951.
- Goodman, J.W., "Film Grain Noise in Wavefront Reconstruction Imaging," J. Opt. Soc. Am., Vol. 57, April 1967.
- Higgins, G.C., and Stultz, K.F., "Experimental Study of rms Granularity as a Function of Scanning-Spot Size," J. Opt. Soc. Am., Vol. 49, Sept. 1959.

Hopkins, H.H., "On the Diffraction Theory of Optical Images," Proc. Roy. Soc., A. p. 231, 1955.

Ingalls, A.L., "The Effect of Film Thickness Variations on Coherent Light," Phot. Sci. and Eng., Vol. 4, May-June 1960.

Jacquinot, P., and Roizen-Dossier, "Apodisation," published in Progress in Optics, Vol. II, H. Wolf, ed., North-Holland Publishing Co., Amsterdam, 1966.

Jahnke, E. and Emde, F., Table of Functions, Dover, New York, 1945.

James, T.H., and Higgins, G.C., Fundamentals of Photographic Theory, 2nd Ed., Morgan and Morgan, New York, 1960.

Jones, R.C., "New Method of Describing and Measuring the Granularity of Photographic Materials," J. Opt. Soc. Am., Vol. 45, October 1955.

Kozma, A., "Photographic Recording of Spatially Modulated Coherent Light," J. Opt. Soc. Am., Vol. 56, April 1966.

Lambert, L.B., "Electro-Optical Signal Processors for Array Antennas," Technical Report T-1/321, Electronics Research Laboratories, Columbia University, New York, May 2, 1965.

Leith, E.N., "Photographic Film as an Element of a Coherent Optical System," Phot. Sci. and Eng., Vol. 6, No. 2, 1962.

Marriage, A., and Pitts, E., "Relation Between Granularity and Autocorrelation," J. Opt. Soc. Am., Vol. 46, Dec. 1956.

Mees, C.E.K., and James, T.H., The Theory of the Photographic Process, MacMillan Co., New York, 1966.

- (1) Dunham, T., in Ber. VIII Intern. Wiss u. Angen. Phot., Dresden, 1931, J. Eggest and A. von Biebler, eds., J.A. Barth, Leipzig, 1937, p. 287.
- (2) Bricout, P., Comptes Rendus, Vol. 197, 1933, p. 1202.
- (3) van Kreveld, A., Photo. J., Vol. 74, (N.S.) 58, p. 590.
- (4) Debot, R., Research (London), Vol. 2, p. 139, 1949.

- (5) Selwyn, E.W.H., Phot. J. Vol. 75, p. 571, 1935;  
ibid., Vol. 82, p. 208, 1942.
- (6) Hansen, G., and Keck, P.H., Z. Wiss. Phot., Vol. 37,  
p. 86, 99, 1938.
- Miller, K.S., Multidimensional Gaussian Distributions, Wiley,  
New York, 1944.
- Minkoff, J., Wideband Amorphous-Solid Debye-Sears Light Modula-  
tors for Array-Antenna Processors, Ph.D Thesis, Electrical  
Engineering Dept., Columbia University, New York, 1967.
- O'Neill, E.L., "Graininess and Entropy," J. Opt. Soc. Am.,  
Vol. 48, December 1958.
- O'Neill, E.L., Introduction to Statistical Optics, Addison-  
Wesley, Reading, Mass., 1963.
- Picinbono, B., Comptes Rendus, Vol. 240, p. 2206, 1955.
- Rowe, H.E., "Lenses with Random Imperfections," Internal  
Technical Memo, No. 20564, Bell Telephone Labs.,  
August 1965.
- Ruze, J., "The Effect of Aperture Errors on the Antenna  
Radiation Pattern," Nuovo Cimento, No. 3, 1952.
- Savelli, M., Comptes Rendus, Vol. 246, p. 3605, 1958.
- Schwarz, R.J., and Friedland, B., Linear Systems, McGraw-Hill,  
New York, 1965.
- Shack, R.V., et al., "Spectrometer for Optical Image Analy-  
sis," J. Opt. Soc. Am., Vol. 51, p. 481, 1961.
- Silberstein, L., "Quantum Theory of Photographic Exposure,"  
Phi. Mag., Vol. 44, 1922.
- Silberstein, L., "On the Number of Quanta Required for the  
Developability of a Silver Halide Grain," J. Opt. Soc.  
Am., Vol. 31, May 1941.
- Sneddon, I.N., Fourier Transforms, McGraw-Hill, New York,  
1951.
- Steel, B., "Granularity," Visual, Vol. 4, No. 1, 1966.
- Stroke, G.W., An Introduction to Coherent Optics and Holo-  
graphy, Academic Press, New York, London, 1966.
- Thiry, H., "Power Spectrum of Granularity as Determined by  
Diffraction," Jour. Phot. Science, Vol. 11, 1963.

Titchmarsh, E.C., Introduction to the Theory of Fourier Integrals, Clarendon, Oxford, 1937.

Trivelli, A.P.H., and Righter, L., "Preliminary Investigations on Silberstein's Theory, Phil. Mag., Vol. 44, 1922.

Zweig, H.J., "Autocorrelation and Granularity: Part I. Theory," J. Opt. Soc. Am., Vol. 46, Oct. 1956.

Zweig, H.J., "Autocorrelation and Granularity: Part II. Results," J. Opt. Soc. Am., Vol. 46, Oct. 1956.